

TRAPPED ION CYCLOTRON RESONANCE STUDIES
OF ION-MOLECULE REACTIONS

Thesis by
Terrance Brian McMahon

In Partial Fulfillment of the Requirements
For the Degree of
Doctor of Philosophy

California Institute of Technology
Pasadena, California

1973

(Submitted August 31, 1973)

ACKNOWLEDGEMENTS

So many people contribute in such a variety of ways to one's graduate education that it is difficult to adequately acknowledge all of them.

Foremost, I wish to thank my advisor, Jack Beauchamp, who has provided inspiration, advice and insight during my stay at Caltech. Any chemical acumen I may have acquired is due in large measure to him. In addition, both Jack and Diane Beauchamp must be thanked for many good times outside the lab.

During my early days at Caltech, David Holtz was extremely helpful, providing much good advice on laboratory techniques.

All the members of the Beauchamp group, past and present, are warmly thanked for many stimulating discussions. The warm fellowship these people provided made Noyes basement an enjoyable place to work. In particular, Peter Miasek is thanked for being both a good friend and good counsel. The ideas we exchanged over "just one beer" were legion.

My wife, Mary Lynn, has patiently and lovingly typed this thesis and, in addition, drew many of the figures. In spite of my ill humor and bad writing, she has survived the ordeal, contrary to others' speculation. She is thanked for making the completion of this thesis both possible and much more meaningful to me.

I would also like to thank the many friends I have made at Caltech for making life here very enjoyable. The many trips to the beach and mountains provided often much needed diversions.

Lastly, I would like to thank the National Research Council of Canada for supplying support for three of my four years here. I would also like to thank Caltech for supplying tuition for all but my last year. Caltech's decision to require me to pay tuition for my final year was a needless exercise in frustration for all concerned.

TABLE OF CONTENTS

<u>Chapter</u>		<u>Page</u>
I	Introduction	1
II	Ion Motion in Ion Cyclotron Resonance	
	Experiments	7
	A. Introduction	7
	B. Ion Motion in Drift Mode	7
	1. Analysis of Electrostatic Fields	7
	2. Drift Motion	11
	3. Variation of Transit Time with Magnetic Field Strength	21
	4. Variation of Transit Time with Drift Voltages	24
	5. Variation of Transit Time with Trapping Voltage	31
	6. Effects of Ion Energy on Transit Time	36
	7. Variation of Ion Transit Time with Pressure	36
	C. Ion Motion in Trapped-Ion Mode	38
	1. General Description of the Method	38
	2. Description of Fields and Ion Motion	39
III	Design, Construction and Operation of a Trapped-Ion Cyclotron Resonance Spectrometer	57

<u>Chapter</u>	<u>Page</u>
A. Introduction	57
B. Mechanical Modifications to the ICR Cell	57
C. Electronic Design	58
1. Ion Trapping Circuitry	58
2. Electron Energy Pulsing Circuitry	66
3. Trapping Voltage Circuitry	70
4. Radio Frequency Pulse Circuitry	75
D. Pressure Measurement	79
E. Data Collection and Analysis	85
F. Effect of Trapping Voltage on Rate Constants	
G. Error Limits on Rate Constants	98
IV Trapped Ion Cyclotron Resonance Studies of Symmetric Charge and Proton Transfer Processes	101
A. Molecular Resonant Charge Transfer	101
B. Symmetric Charge Exchange Reactions	111
1. Nitrogen, Carbon Monoxide and Carbon Dioxide	111
2. Methyl Bromide	134
C. Symmetric Proton Transfer Reactions	141
1. Hydrogen	141
2. Methane	157
3. Ammonia	168
4. Methyl Chloride	173

<u>Chapter</u>		<u>Page</u>
V	Kinetics of Symmetric Proton Transfer Reactions in Alcohols and Amines. De-Excitation Mechanisms in Equilibrium Studies of Gas Phase Basicities and Structures of Proton Bound Dimer Intermediates	186
	A. Introduction	186
	B. Methylamine	188
	C. Dimethylamine	197
	D. Methanol	203
	E. Ethanol	212
	F. Discussion	212
	G. Conclusions	222
VI	Trapped Ion Cyclotron Resonance Investigations of Equilibria of Organic Ions	228
	A. Gas Phase Ion Molecule Equilibria	228
	B. Proton Transfer Equilibria. Gas Phase Basicities and Acidities	234
	1. Proton Affinities	234
	2. Gas Phase Acidities	243
	C. Fluoride Transfer Equilibria. Carbonium Ion Stabilities	247
VII	Gas Phase Ion Chemistry of Trimethylene Oxide. Unimolecular Decomposition of Excited Inter- mediates in Ion-Molecule Reactions	295
	A. Introduction	295

<u>Chapter</u>	<u>Page</u>
B. Ion-Molecule Reactions of Trimethylene Oxide	296
C. Unimolecular Decomposition of Chemically Activated Trimethylene Oxide	316
Appendix	323

ABSTRACT

Techniques and instrumentation have been developed which permit trapping of ions in the source region of an ion cyclotron resonance cell. These techniques have been used to determine rates of ion-molecule reactions and to observe gas phase ion-molecule equilibria.

The rate constants of a number of symmetric charge exchange and proton transfer reactions in simple molecules have been determined and related to theoretical models of ion-molecule reaction. In addition, the role of a symmetric reaction in competition with exothermic reaction channels has been discussed.

The rates of symmetric proton and deuteron transfer in a number of simple alkyl alcohols and amines have also been obtained. These reactions have been related to de-excitation mechanisms of excited ions.

Gas phase ion-molecule equilibria have been examined to obtain substituent effects on such properties as gas phase basicity, acidity and carbonium ion stabilities.

Finally, the ion-molecule reactions of a cyclic ether, trimethylene oxide, have been examined to illustrate the wide range of information available through ion cyclotron resonance experiments.

CHAPTER I

Introduction

In the relatively few years since its inception, ion cyclotron resonance spectroscopy (ICR) has emerged as one of the most versatile techniques for the study of gas phase ion-molecule reactions. Using double resonance (1) and ion-ejection experiments (2), complex reaction sequences and product distributions may be readily obtained. In addition, useful information regarding thermochemical properties such as gas phase basicities and acidities (3) in the absence of complicating solvation phenomena have led to fundamental insights into substituent effects and the role of solvents in organic reactions in solution. These and other incursions into physical organic chemistry have shown that ion cyclotron resonance spectroscopy is a vital tool for the understanding of reactivities of organic ions.

Of fundamental importance, however, in the characterization of any reacting system is the determination of reaction rate constants. Equations to calculate ICR peak intensities from power absorption equations have been formulated and rate constants extracted from them by approximate methods and analysis involving iterative computer solution (4-6). These methods are cumbersome, however, and can be accurately applied only to the simplest of ion-molecule reaction sequences.

Recently, a number of diverse mass spectrometric techniques have been developed for the determination of ion-molecule reaction rate constants. Among the most successful of these have been methods involving examination of relative ion abundances as a function of reaction time. Several of these methods employ electric or combinations of electric and magnetic fields to trap ions for controlled periods of time. For example, Harrison et al. (7) have shown that the negative space charge of a low energy, high intensity electron beam can be used to trap positive ions in a conventional mass spectrometer.

This is similar to an apparatus developed by Tal'roze (8) where ions are trapped in a cylindrical region by a wire biased at lower voltage than the cylinder walls and running through the center along the longitudinal axis of the cylinder. It was shown that ions execute rosette motion about the wire with a low probability for actually striking the wire. This technique has the advantage over that of Harrison in that it is capable of trapping both positive and negative ions.

More recently, in this laboratory, a trapped ion source has been designed for use with a quadrupole mass spectrometer (9). Ions formed by a pulsed electron beam are trapped in a cylindrical region by the combined action of electric and magnetic fields. After the desired reaction time, ions are ejected from the source through a series of collimating

lenses into the mass spectrometer.

The above techniques suffer from the disadvantage that ions are formed in regions of relatively high electric field and hence have excessive amounts of kinetic energy. It is in general of much more interest to examine the rate constants for reactions of thermal energy ions.

An advantage inherent in ICR experiments is that ions are formed in a region of low electric field and have near thermal energies. Wobschall has described a method for trapping ions for periods up to one millisecond in an ICR spectrometer of solenoidal design (10). More recently, McIver (11,12) has demonstrated that a trapped ion analyzer cell based on the trapping action of electric and magnetic fields is a valuable tool for determination of ion-molecule reaction rates. The simple analysis required to relate reaction rate constants to the variation of ion abundance with time obviates the difficult task of calculating ICR rate constants by iterative computer solution to the ICR power absorption equations. This increased ease of calculation makes the variation of ion abundance with time far more amenable to determination of reaction rate constants by the more conventional study of variation of ion abundance with pressure. However, the conventional ICR cell remains well-suited to routine aspects of gas phase ion chemistry. These include examination of elastic collisions by collision broadening of the absorption line (13,14), identification

of reaction sequences in double resonance experiments (1), determination of product distributions using source and trapping ion ejection techniques (2), study of variation of rates with ion kinetic energy (15-17), observation of collisional stabilization of excited intermediates in ion-molecule reactions (18,19), and the routine recording of mass spectra without mass discrimination (3). While it is possible to perform many of these experiments using the trapped ion analyzer all described by McIver, the conventional drift cell offers distinct advantages in most applications, primarily in terms of operational simplicity. It was desirable, therefore, to modify the conventional ICR cell in such a manner as to permit its convenient use in both drift and trapped-ion modes. The fruits of that endeavor are the subject of this thesis.

REFERENCES

1. L. R. Anders, J. L. Beauchamp, R. C. Dunbar and J. D. Baldeschwieler, J. Chem. Phys. 45, 1062 (1966).
2. J. L. Beauchamp and J. T. Armstrong, Rev. Sci. Instrum. 40, 123 (1969).
3. J. L. Beauchamp, Ann. Rev. Phys. Chem. 22, 527 (1971).
4. S. E. Buttrill, Jr., J. Chem. Phys. 50, 4125 (1969).
5. A. G. Marshall and S. E. Buttrill, Jr., J. Chem. Phys. 52, 2752 (1970).
6. M. B. Comisarow, J. Chem. Phys. 55, 205 (1971).
7. A. A. Herod and A. G. Harrison, Int. J. Mass Spectrom. Ion Phys. 4, 415 (1970).
8. V. L. Tal'roze and G. V. Karachevtsev, "Ion-Molecule Reactions," in Advances in Mass Spectrometry (W. L. Mead, ed.), Vol. 3, Institute of Petroleum, London (1966)
9. P. G. Miasek, Ph.D. Thesis, California Institute of Technology, 1973.
10. R. A. Fluegge and D. Wobschall, Cornell Aeronautical Laboratory, U. S. Government Res. Develop. Rep. 69, 63 (1969).
11. R. T. McIver, Jr., Rev. Sci. Instrum. 41, 555 (1970).
12. R. T. McIver, Jr. and R. C. Dunbar, Int. J. Mass Spectrom. Ion Phys. 7, 471 (1971).
13. J. L. Beauchamp, J. Chem. Phys. 46, 1231 (1967).
14. D. P. Ridge, Ph.D. Thesis, California Institute of

Technology, 1973.

15. L. R. Anders, J. Phys. Chem. 73, 469 (1969).
16. R. P. Clow and J. A. Futrell, Int. J. Mass Spectrom. Ion Phys. 4, 165 (1970).
17. W. T. Huntress, Jr., M. M. Mosesman, and D. D. Elleman, J. Chem. Phys. 54, 843 (1971).
18. M. T. Bowers, D. D. Elleman, and J. L. Beauchamp, J. Phys. Chem. 72, 3599 (1968).
19. T. A. Lehman, T. A. Elwood, J. T. Bursey and J. L. Beauchamp, J. Amer. Chem. Soc. 93, 2108 (1971).

CHAPTER II

Ion Motion in Ion Cyclotron Resonance Experiments

A. Introduction

In order to extract quantitative rate data from ion cyclotron resonance experiments, it is necessary to understand ion motion under the combined effects of electric and magnetic fields. Classical electrodynamic theory can be applied to the configurations of electric and magnetic fields appropriate for both conventional drift and trapped-ion ICR experiments and provide a means of understanding the factors governing ion motion (1). In the conventional drift mode of operation the combined effects of magnetic field and potentials applied to the drift and trapping plates on the transit time of ions through the apparatus can be investigated and used to obtain accurate reaction times (2). In trapped-ion mode (3,4) the electric and magnetic forces governing ion trapping can be determined and used to advantage in design of trapped-ion cells and in execution of experiments requiring a knowledge of distribution of ions in the trapping region.

B. Ion Motion in Drift Mode

1. Analysis of Electrostatic Fields

Deauchamp and Armstrong have presented an analysis of the electrostatic fields for ICR cells with equally spaced

trapping and drift plates (5). Greater homogeneity for the drift field is obtained by decreasing the spacing between drift plates relative to the spacing between the trapping plates.

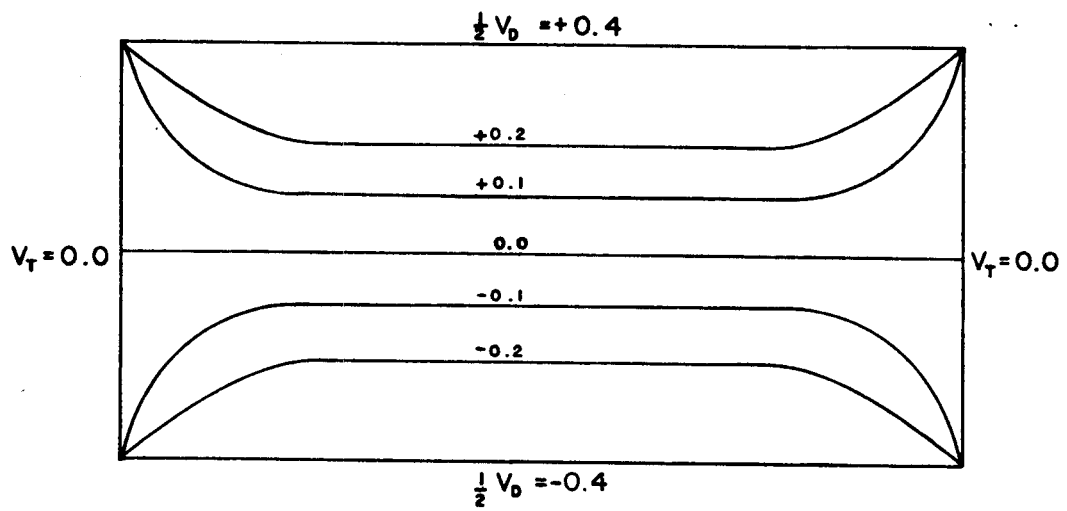
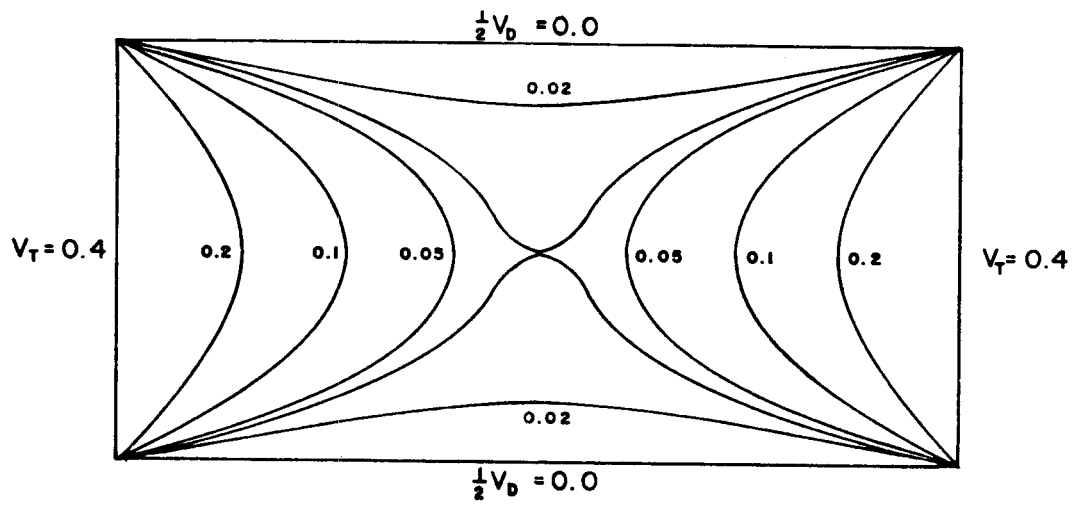
Equipotentials of the electrostatic fields in this type of "flat" cell have been determined both by applying appropriate voltages to silver electrodes painted on uniform resistance paper in accordance with the geometry of the flat cell and by an exact solution of Laplace's equation. With no applied drift voltages, a typical set of equipotentials arising from the trapping and drift voltages applied alone are illustrated in Fig. 1. In order to describe the effects of potentials applied to the drift and trapping electrodes on ion motion, it is useful to parameterize the electrostatic fields in the cell. Following Beauchamp and Armstrong (5) the equipotentials shown in Fig. 1, which arise from the trapping voltage, can be approximated by an asymmetric quadrupolar field of the general form

$$V = V_0 + Az^2 - Bx^2, \quad (1)$$

where V_0 is the potential at the center of the cell and the constants A and B are chosen to best match the boundary conditions. The origin of the coordinate system is taken at the center of the cell midway between the trapping and drift electrodes. A detailed solution to the electrostatic field equations gives $V \cong 0.11 V_T$. If d is the spacing between the trapping plates, and Eq. (1) is to satisfy the

Figure 1

Equipotentials obtained from an exact solution to Laplaces equation for separately applied trapping and drift voltages. The view shown represents a cross section in the xz plane.



boundary conditions at both $x = 0$, $z = \pm d/2$ and $z = 0$,

$x = \pm d/4$, then $A \cong 3.52$, $B \cong 1.76$ and

$$V = V_T \left[0.11 + \frac{1.76}{d^2} (2z^2 - x^2) \right] \quad (2)$$

The drift voltages are assumed to give rise to an idealized set of equipotentials appropriate to a parallel plate capacitor with

$$V = \frac{2x V_D}{d}, \quad (3)$$

where V_D is the drift voltage applied across the ICR cell. For reasons discussed in detail below, this voltage is nominally divided between the top and bottom plates of the cell. A set of equipotentials for typical experimental values of combined drift and trapping voltages are shown in Fig. 2.

2. Drift Motion

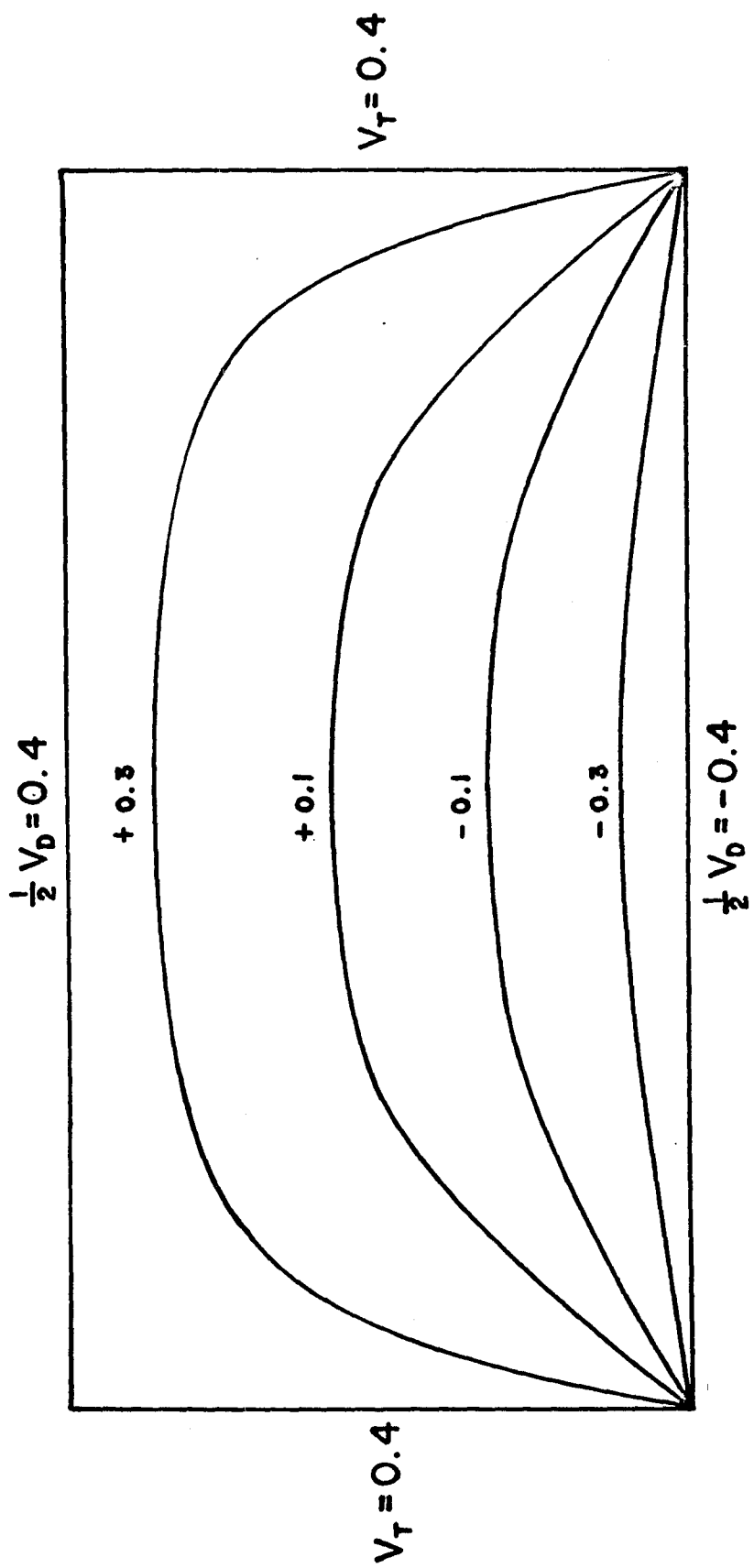
The trajectory of a particle of charge q and mass m subject to the combined action of an electric field, E , and magnetic field, H , can be determined from the solution of Eq. (4).

$$m \frac{dv}{dt} = q \left(E + \frac{v \times H}{c} \right). \quad (4)$$

In the absence of an applied electric field, the ion moves in a circular orbit in the plane perpendicular to H at the cyclotron frequency, $\omega_c = qH/mc$. Addition of a constant electric field gives rise to a net drift motion given by

Figure 2

Equipotentials for a typical experimental combination of trapping and drift voltages. Note that the trapping and drift characteristics are maintained in the combined fields.



$$v_D = \frac{cE \times H}{H^2}, \quad (5)$$

which will be in a direction perpendicular to both E and H . In executing this drift motion, the center of the ion orbit will remain on an equipotential of the applied electric field.

Combining the potentials given by Eqs. (2) and (3) gives

$$E = -\nabla V = \left(\frac{3.52 \times V_T}{d^2} - \frac{2V_D}{d} \right) i - \frac{7.04z}{d^2} k \quad (6)$$

from which we have

$$v_D = \left(\frac{3.52 \times V_T}{d^2} - \frac{2V_D}{d} \right) \frac{c}{H} j. \quad (7)$$

In the more normal experimental situation, different voltages are applied to the source and resonance regions of the ICR cell. If we let V_{DS} and V_{DR} be the drift voltages in each region, respectively, then the corresponding drift velocities are

$$v_{DS} = \frac{2c V_{DS}}{Hd} - \frac{3.52 \times c V_T}{Hd^2} \quad (8)$$

and

$$v_{DR} = \frac{2cV_{DR}}{Hd} - \frac{3.52 \times cV_T}{Hd^2} \quad (9)$$

in the negative y direction. If ℓ_1 and ℓ_2 are the distances from the electron beam to the beginning and end of the

resonance region, respectively, then

$$\tau = \frac{\ell_1}{v_{DS}} \quad (10)$$

and

$$\tau' = \frac{\ell_1}{v_{DS}} + \left(\frac{\ell_2 - \ell_1}{v_{DR}} \right). \quad (11)$$

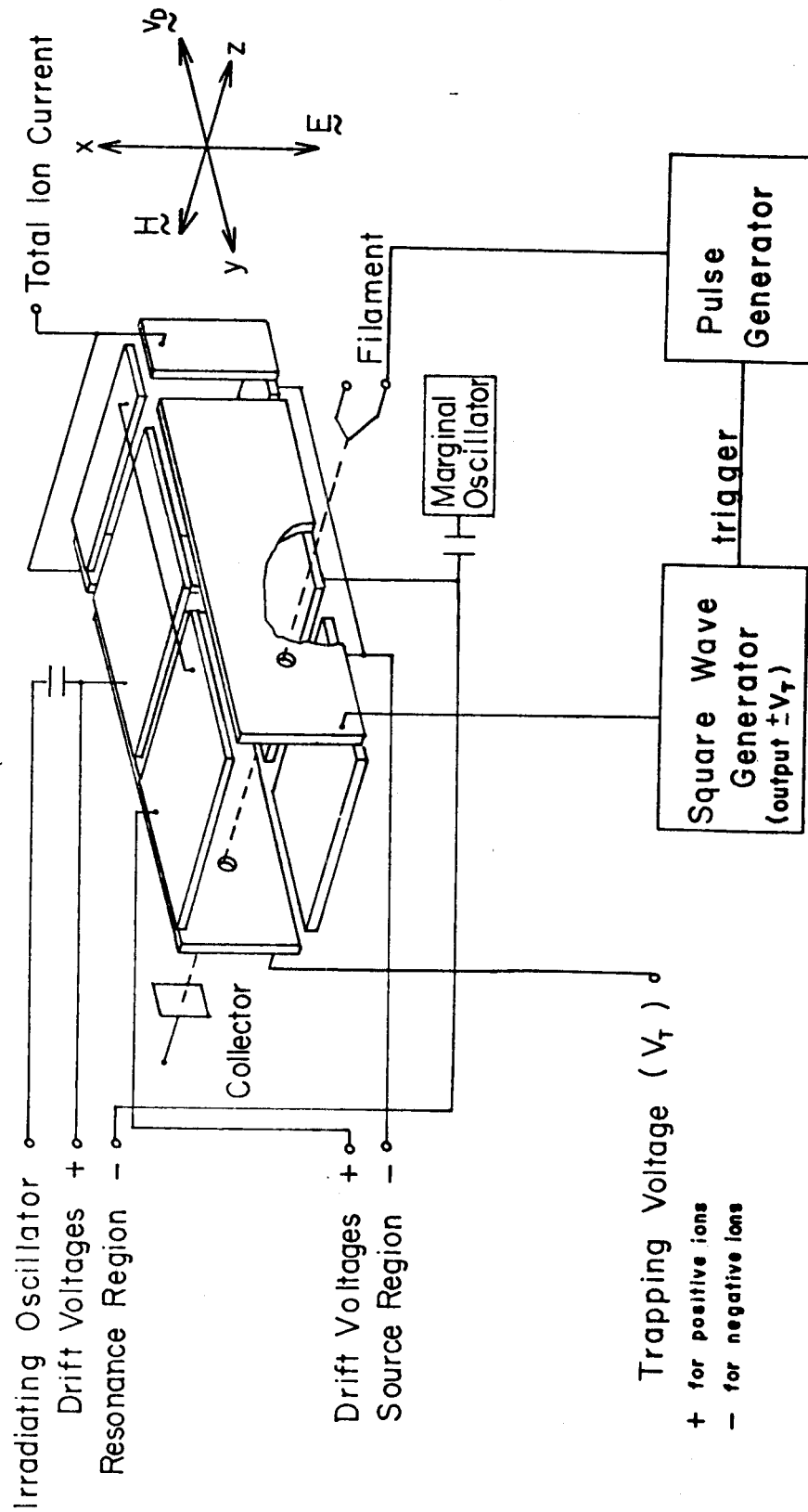
where τ is the time the ions enter the resonance region and τ' is the time the ions leave the resonance region of the ICR cell.

It should be noted that the drift velocity is predicted to be independent of trapping voltage only if the ions remain in the center of the cell in the plane defined by $x = 0$. This is accomplished by balancing the drift voltages applied to the source and resonance regions so as to match the equipotentials in the center of the cell at the interface between the two regions. If the equipotentials are mismatched the ions will move out of the $x = 0$ plane as they enter the resonance region.

In order to experimentally verify the predicted ion transit times a technique was devised to measure them and simultaneously obtain dispersion in transit times of ions from the electron beam to the ion current monitor (2). Modifications required to perform these experiments are shown in Fig. 3. A Hewlett-Packard HP-3300 Function Generator generates a square wave of variable frequency and amplitude which is applied to one trapping plate of the ICR

Figure 3

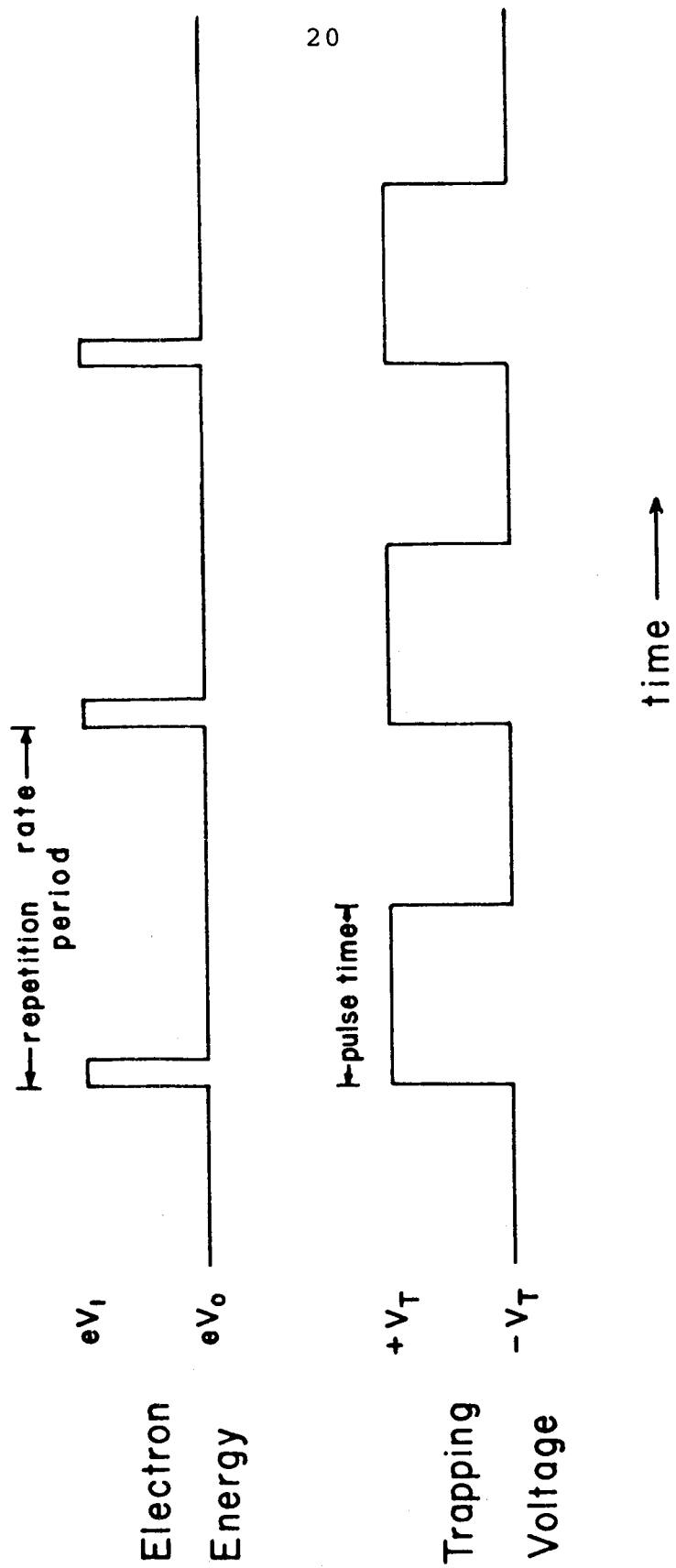
Cutaway view of the ICR cell including a block diagram showing the modifications required to perform transit time experiments.



cell. The opposite trapping plate is held at a fixed potential equal to the square wave maximum voltage. The positive slope of the square wave is used to trigger a Tektronix Type 161 pulse generator, providing a negative pulse of variable duration and magnitude which is applied to the filament to generate ions by switching the electron energy above the ionization threshold. In the present experiment the trapping plate was pulsed between ± 0.40 V for times in the millisecond region corresponding to the ion transit times. The electron energy was pulsed from 10 to 43 eV for a duration of approximately 50 μsec . The trapping time is determined by the positive half-cycle of the square wave, measured directly to ± 1.0 μsec with a Heath Universal Digital Instruments Model EU-805. The pulse sequence is illustrated in Fig. 4. The pulse times represent the on period of the square wave, which is equal to one-half the repetition rate period. Determination of transit times follows in a straightforward manner. An ion current is registered only if the trapping voltage remains on long enough for ions to reach the monitor. This technique is the simplest method for determining transit times. Difficulties are encountered in measuring the dispersion in arrival times since the ion current decreases inversely with trapping pulse width when the ion transit time is exceeded. To measure dispersion in arrival times, an alternate pulsing scheme was devised in which the

Figure 4

Pulse sequence for transit time measurements. The electron energy is switched from below the ionization threshold (eV) to above (eV) to generate a pulse of ions. The pulse time defines the time during which ions are trapped in the cell. An ion current is registered if this exceeds the drift time through the cell.



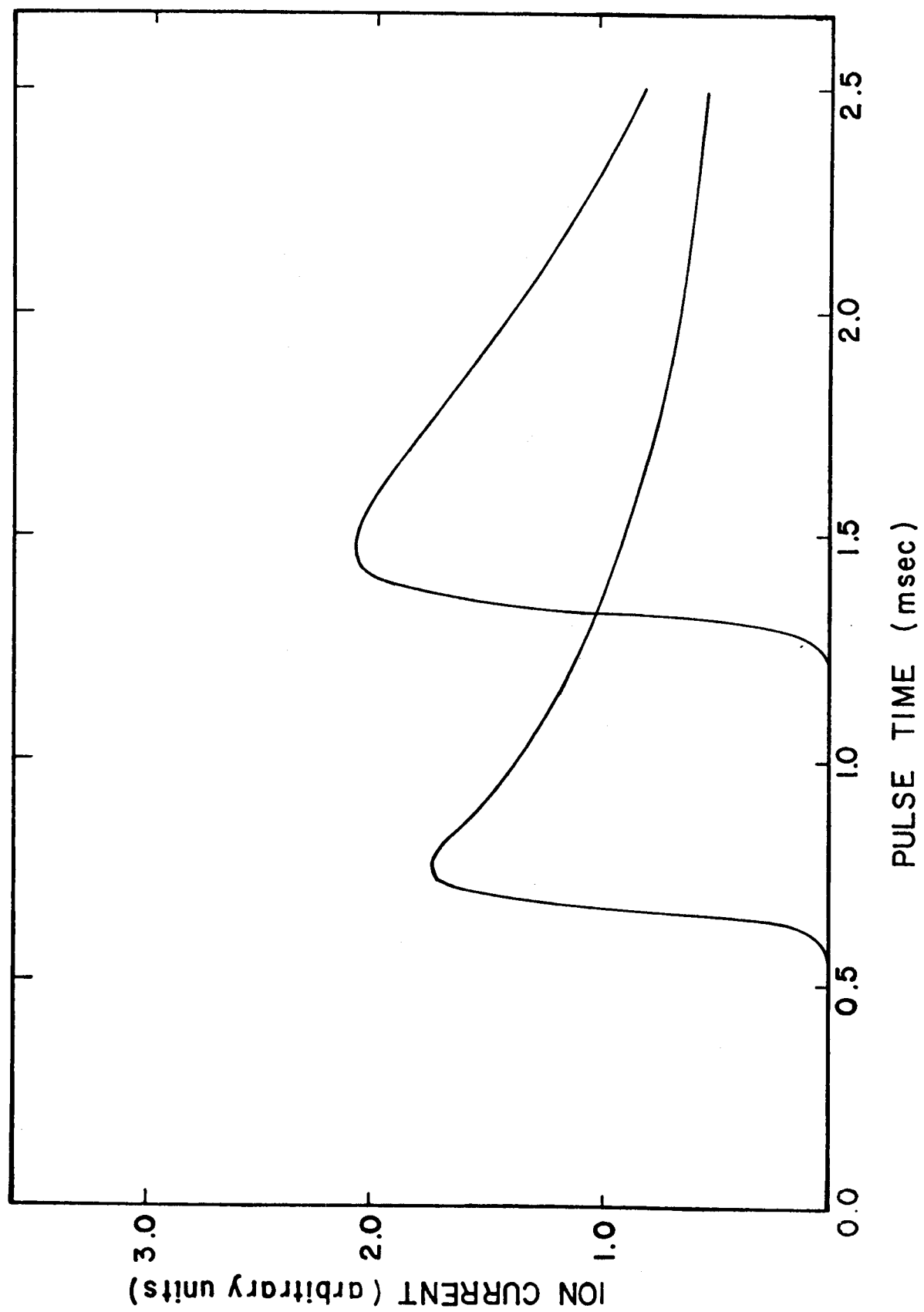
repetition rate period, determined by the square wave generator, remains fixed at a period longer than the transit time. One of the trapping plates is held at a constant positive potential and the other is switched from this potential to a negative value after a suitable delay time, using a Tektronix Type 161 pulse generator. Only if the delay period exceeds the transit time is an ion current registered. Referring to Fig. 4, this pulse sequence involves operation at a fixed repetition rate with a variable pulse time.

3. Variation of Transit Time with Magnetic Field Strength

The variation of ion current with pulse time using the simpler pulsed trapping method is illustrated in Fig. 5 for N_2^+ at a pressure of approximately 10^{-5} torr and magnetic fields at 2.5 and 5.0 kG. The time at which the first ions arrive at the monitor was taken to be that time for which an ion current is first detectable. The maximum ion current gives the time at which the last ions formed in the electron beam pulse arrive at the electrometer. The mean arrival time of the ions is taken as that time at which the ion current attains one-half its maximum value. Assuming ion velocities in the range of 10^{-4} to 10^{-5} cm/sec we estimate that after they leave the resonance region it requires approximately 10 to 40 μ sec for the ions to move to the side plates of the cell in the collector region (in which

Figure 5

Variation of ion current (N_2^+) with duration of pulse applied to the trapping plates, using the simpler pulsing method described in the text. Magnetic field strengths of 2.5 and 5.0 kilogauss were employed, the latter corresponding to the longer transit time. Other conditions were $V_{DR} = V_{DS} = V_T = 0.4$ volts. Maximum ion currents of 10^{-11} A were recorded.



no trapping voltage is applied). This error in transit time measurement is approximately canceled by the 50 μ sec delay in formation of ions, at the electron beam following the turning on of the trapping.

The variation of ion current with trapping pulse time for the second pulsing scheme described above exhibits the expected step function behavior as shown in Fig. 6. The dispersion in ion transit times can be determined from the derivative of this curve, obtained by numerical analysis. The observed dispersion in transit times is small, about 100 μ sec, as determined by the full width at half height of the derivative curve displayed in Fig. 6. The spread in ion production and collection times contribute to this measured dispersion.

In Fig. 7 the experimental variation of ion transit time with magnetic field strength is compared with that calculated from Eq. (11) for ions at the center of the cell ($x = 0$). The agreement is excellent for the range of magnetic fields tenable with our instrument (0-14 kg).

4. Variation of Transit Time with Drift Voltages

The variation of ion transit times with simultaneous variation of the drift voltages in the source and resonance regions is shown in Fig. 8. The line represents calculated transit times. As is evident, agreement is good for the full range of electric field strengths.

A simple transposition of Eqs. (10) and (11) gives

Figure 6

Variation of ion current (N_2^+) with duration of pulse applied to the trapping plates using a fixed duty cycle for ion formation. The derivative of the ion current with respect to pulse time was determined by fitting a polynomial to the experimental curve at the indicated points. This derivative curve details the dispersion in transit times. Other conditions were the same as Fig. 5 with $H = 5.0$ kilogauss.

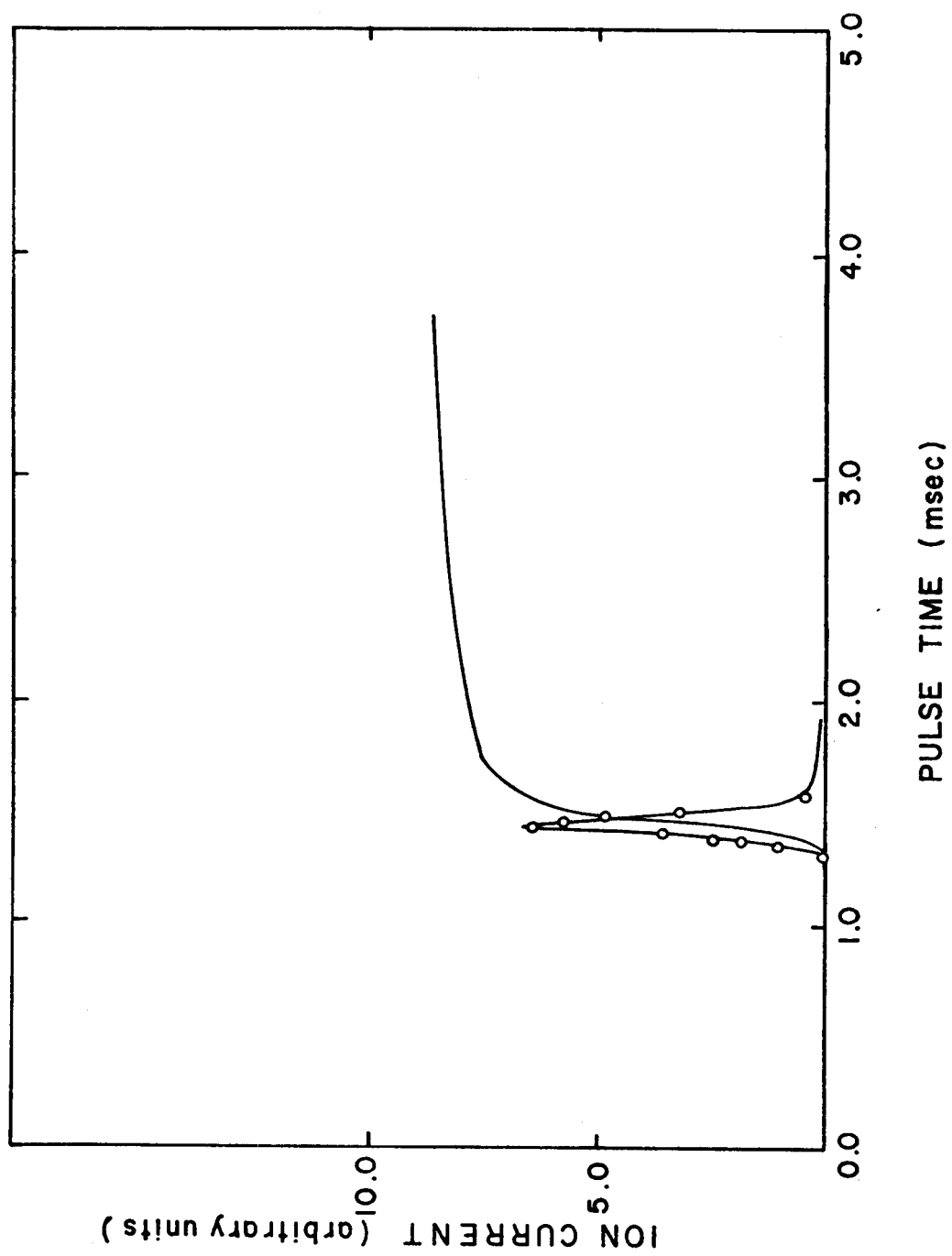


Figure 7

Variation of ion transit time with magnetic field strength. The points represent experimentally determined mean ion transit times. The line indicates the calculated times using Eq. (11) in the text. Other conditions were $V_{DR} = V_{DS} = V_T = 0.4$ volts.

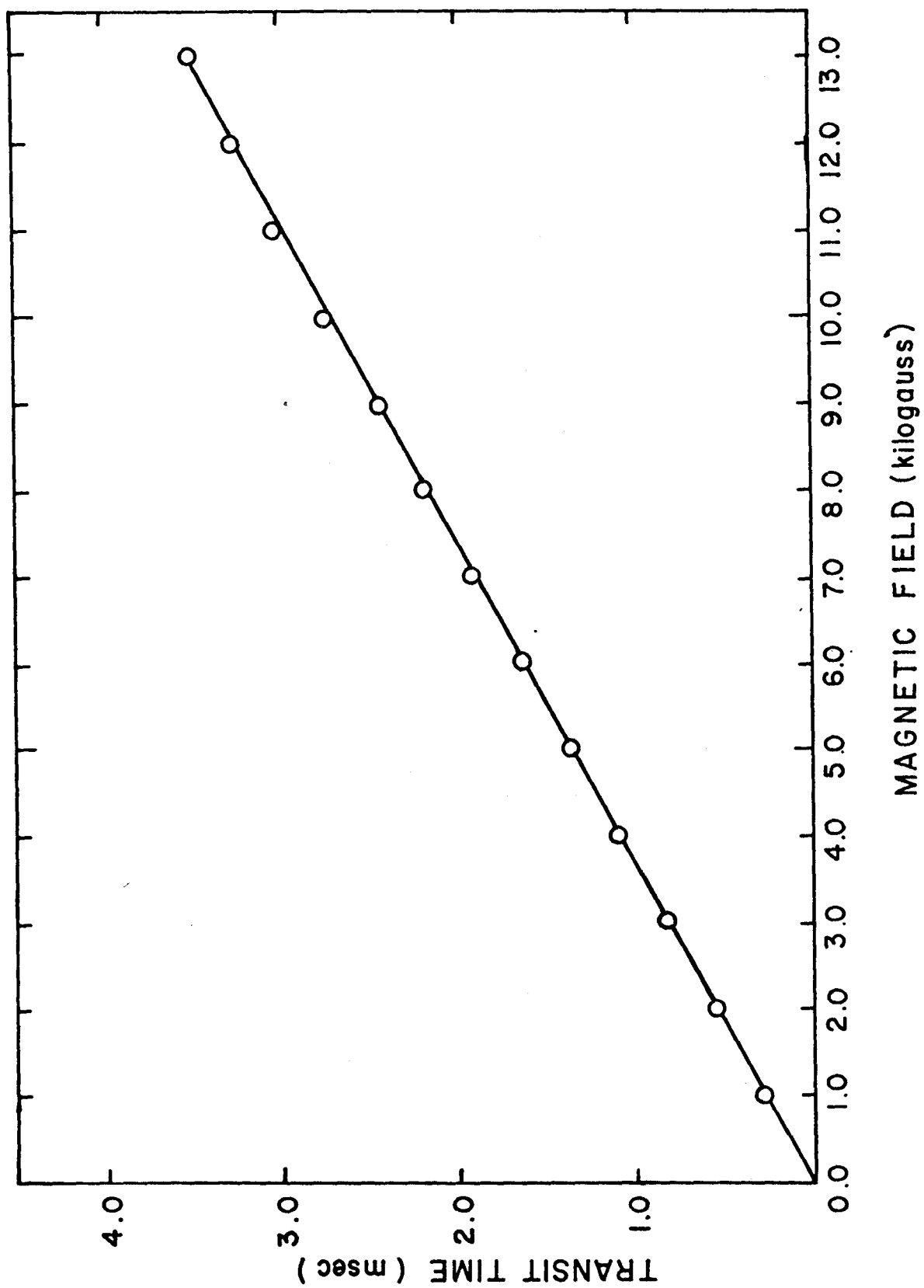
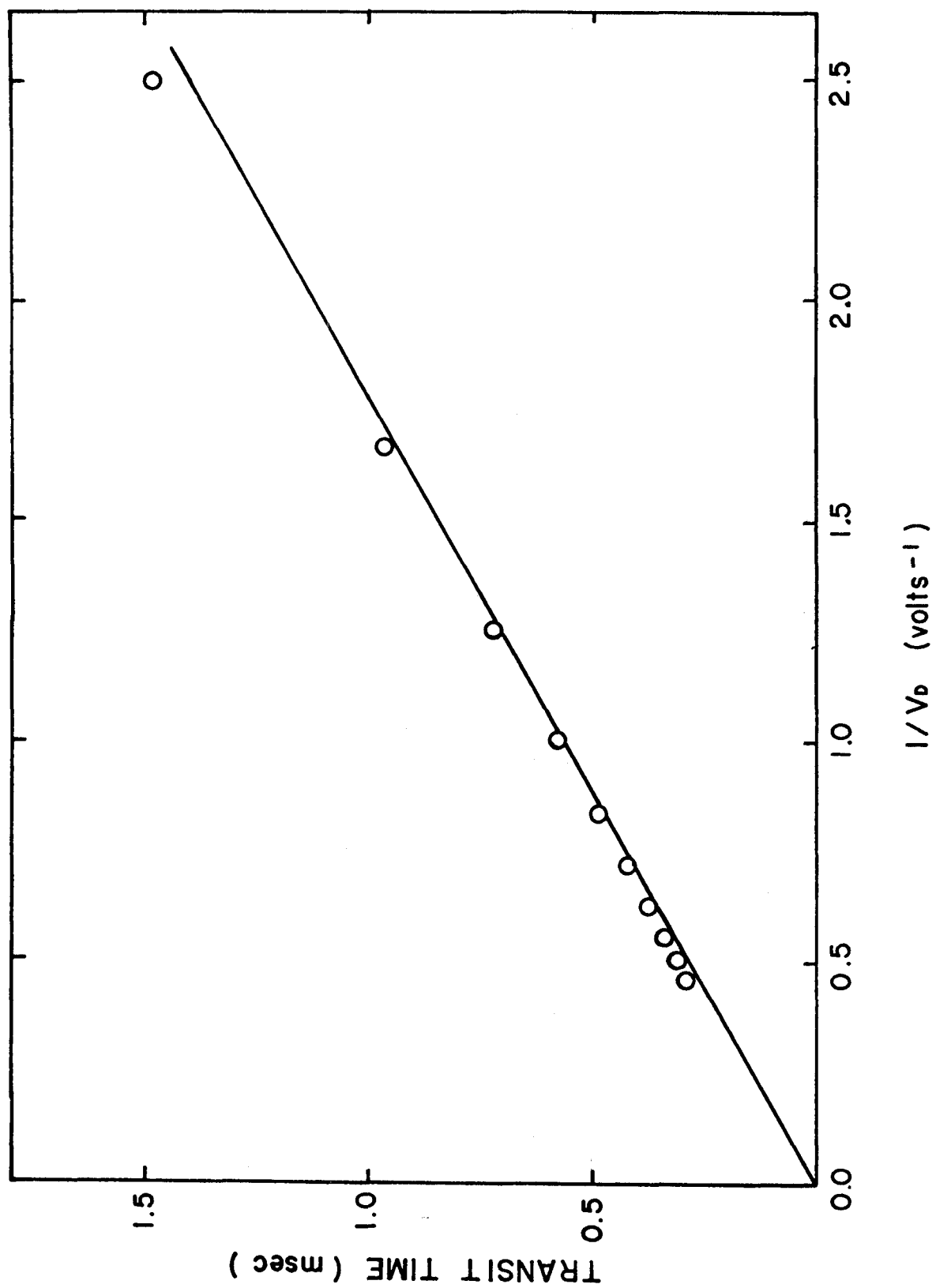


Figure 8

Variation of ion transit time with drift voltage. The points represent experimentally determined mean ion transit times. The line indicates the calculated times using Equation 11 in the text. Other conditions were $V_{DR} = V_{DS} = V_D$ (varied), $V_T = 0.4$ volts, $H = 5.0$ kilogauss.



$$\tau' = \tau + \frac{(\ell_2 - \ell_1)Hd}{2c V_{DR}} . \quad (12)$$

Thus by measuring the ion transit time at fixed magnetic field strength for various values of the drift voltage in the resonance region, V_{DR} , and making a plot of τ' vs V_{DR}^{-1} , the source residence time, τ , is obtained as the intercept of the τ' axis. Typical experimental results are shown in Fig. 9. The experimental value of τ is 0.39 msec, to be compared with a calculated source transit time of 0.41 msec. Relatively more weight is given to those points at higher values of V_{DR}^{-1} . Fringing of the electric fields in the source regions is likely to occur at high electric field strength in the resonance region and may cause the observed deviation from linearity at low values of V_{DR}^{-1} in Fig. 9.

5. Variation of Transit Time with Trapping Voltage

The effects of trapping voltage, V_T , and position of an ion in the cell, x/d , on the transit time of an ion are illustrated in Fig. 10. The results indicate a good qualitative agreement between experimental transit times and those calculated using ion velocities given by Eqs. (8) and (9). A lack of better quantitative agreement can be attributed to the approximation inherent in the parameterization of the electrostatic field in Eq. (11), which does not satisfy Laplace's equation ($\nabla^2 V = 0$) unless $A = B$. If the drift voltages are balanced in the source and resonance

Figure 9

Variation of transit time with drift voltage applied to the resonance region. Relatively more weight is given to the points at higher values of V_{DR}^{-1} to compensate for the effect of fringing fields. The transit time axis intercept is the source residence time. Other conditions were $V_{DS} = V_T = 0.4$ volts and $H = 5.0$ kilograms.

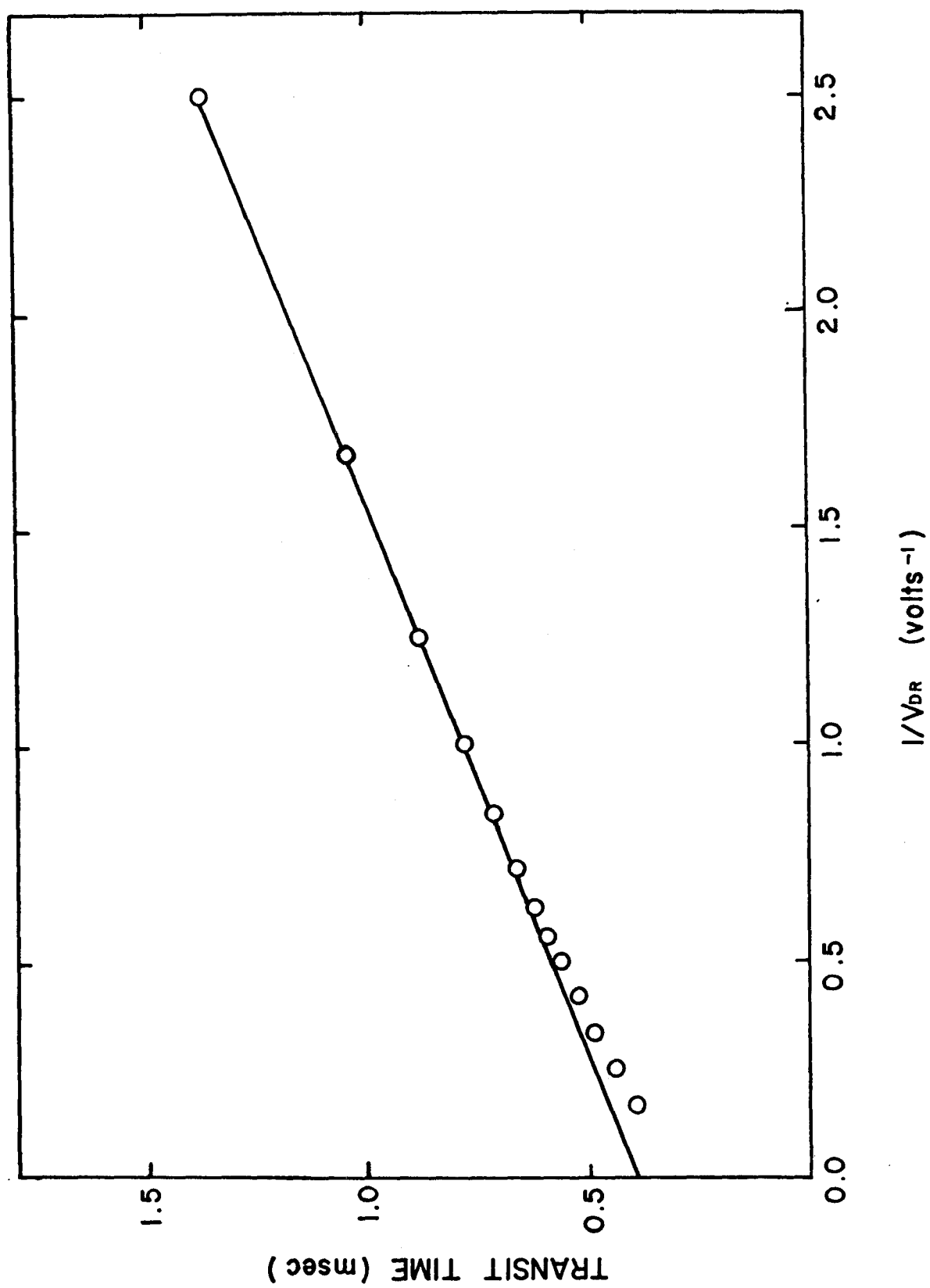


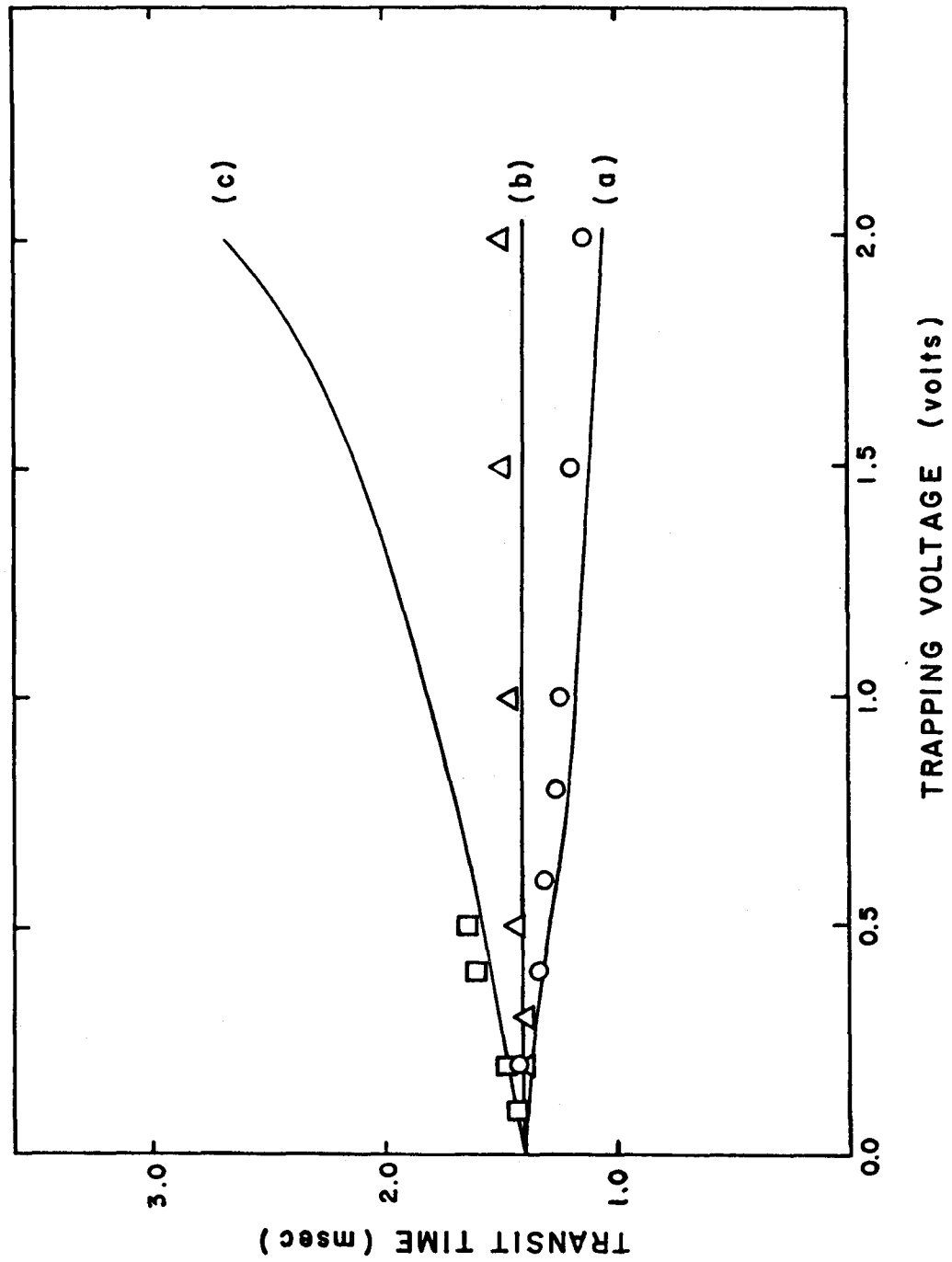
Figure 10

Effect of trapping voltage on ion transit time for three different field situations:

- (a) $V_{DR} = 0.4$ volts (+0.3 volts on top plate and -0.1 volts on bottom plate).
- (b) $V_{DR} = 0.4$ volts (+0.2 volts on top plate and -0.2 volts on bottom plate).
- (c) $V_{DR} = 0.4$ volts (+0.1 volts on top plate and -0.3 volts on bottom plate).

In each case, $V_T = V_{DS} = 0.4$ volts with the drift voltage divided evenly between the top and bottom plates in the source region. Other conditions were $H = 5.0$ kilogauss.

In the three cases shown, the ions are in the plane defined by (a) $x = +d/4$, (b) $x = 0$, and (c) $x = -d/4$ as they pass through the resonance region.



regions it is found, as predicted, that transit lines are relatively insensitive to a wide range of trapping voltage.

6. Effects of Ion Energy on Transit Time

It is assumed in a double resonance experiment that at low irradiating power the change in product ion intensity observed upon irradiation of a reactant ion reflects the change in reaction rate with ion kinetic energy (6). If the higher ion kinetic energy resulting from irradiation leads to a modification of the ion transit time, then the extent of conversion from reactant to product will be similarly altered, independent of any variation in the reaction rate constant with ion kinetic energy. To test this possibility the mean arrival times of ions were measured as a function of the field strength of the double resonance oscillator used to irradiate the only species present, N_2^+ , in the source region. Ion transit times were found to be independent of irradiating field strength up to the point where ions were ejected from the cell by striking the drift plates. This corresponds to an ion energy of ~ 100 eV.

7. Variation of Ion Transit Time with Pressure

At pressures high enough such that a significant number of collisions occur in the ICR cell, it is necessary to consider possible effects this might have on the ion transit times. A damping term representing the effects of momentum transfer is added to Eq. (4) to give

$$m \frac{dv}{dt} = q \left(E + \frac{v \times H}{c} \right) - \xi v, \quad (13)$$

where ξ is the collision frequency for momentum transfer.

The time averaged solution to this equation yields (7)

$$\langle v_x \rangle = \frac{\xi q E}{m(\omega_c^2 + \xi^2)} \cong \frac{\xi c E}{\omega_c H} \quad (14)$$

$$\langle v_y \rangle = \frac{-\omega_c q E}{m(\omega_c^2 + \xi^2)} \cong \frac{c E}{H} \left[1 - \left(\frac{\xi}{\omega_c} \right)^2 \right] \quad (15)$$

In the limit of no collisions $\langle v_x \rangle$ is zero and $\langle v_y \rangle$ gives the drift velocity. Based on the long range attraction between the ion neutral pair being dominated by the ion-induced dipole interaction, the approximate collision frequency is given by (8,9,10)

$$\xi = 2.21 n \pi q \mu \alpha^{\frac{1}{2}} \mu^{\frac{1}{2}} / m \quad (16)$$

where n is the number density of neutrals, α is the angle-averaged polarizability, and μ is the reduced mass of the collision pair.

Ion transit times were measured for N_2^+ at pressures up to 6×10^{-3} torr with a magnetic field strength of 5.0 kilogauss. At 6×10^{-3} torr a collision frequency of $9.7 \times 10^4 \text{ sec}^{-1}$ is calculated from Eq. (16), while ω_c is $1.7 \times 10^6 \text{ sec}^{-1}$. From Eq. (15) less than 1% decrease in transit time is predicted. This was experimentally verified within our limit of accuracy. No change in ion

transit time was observed with increasing pressure, up to the highest pressure obtainable, 6×10^{-3} torr. At higher pressures, where the effect would measurably influence drift times, the loss of ions to the negative drift plate becomes appreciable in accordance with the pressure dependent transverse drift velocity given by Eq. (14). A measurable ion current is, however, not registered under such conditions, and transit times cannot be determined.

It is evident that measured transit times are adequately reproduced by the straightforward analysis leading to Eqs. (10) and (11) when the drift voltages applied to the source and resonance regions are appropriately balanced so as to match at the center of the cell, the equipotential along which the ions move in each region. The trapping voltage is found to influence transit times only when the drift equipotentials are mismatched at the center of the cell.

C. Ion Motion in Trapped-Ion Mode

1. General Description of the Method

The cell used to conduct trapped-ion experiments is basically the conventional Varian flat cell described in the previous section of this chapter. In a typical experiment, ions are formed by an electron beam pulse of variable energy and duration. Trapping is effected with the aid of a new cell plate added to the rear of the source region of the cell. With the source drift plates and the new

rear plate at ground, the analyzer drift plates at some negative potential and the trapping plates at a positive potential, a potential configuration is created in the source region very much like that in the trapped ion analyzer cell described by McIver (3) for trapping positive ions. The space potential everywhere within the source is positive with respect to the surrounding cell plates and adjacent resonance region. This constrains the ions to move on equipotentials of the drift field which close on themselves within the source region of the cell. To trap negative ions the polarity of the voltage applied to the trapping and analyzer drift plates is reversed.

Ion detection is effected by switching all voltages to appropriate values for normal drift mode of operation. The ions are consequently drifted through the analyzer region of the cell where they are observed with the usual marginal oscillator detector. The ion motion for this sequence of pulses is shown schematically in Fig. 11. A more detailed analysis of ion motion in the trapping configuration is presented in the following section.

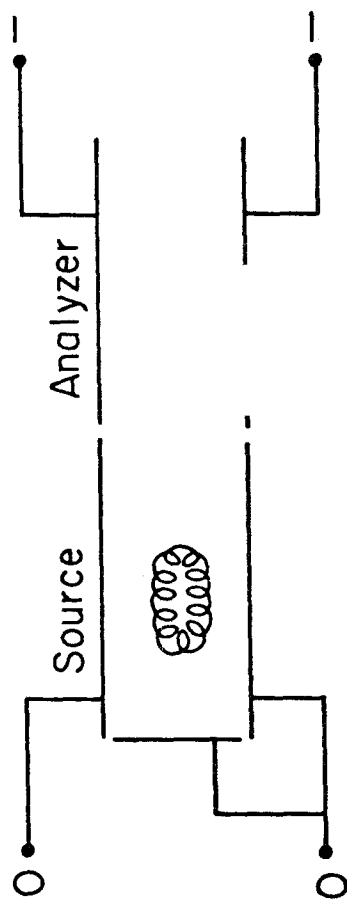
2. Description of Fields and Ion Motion

Sharp, Eylar and Li (11) have presented an analysis to explain the trapping action of combined electric and magnetic fields in the trapped-ion analyzer cell developed by McIver (3). In that case the geometry is that of a parallelepiped enclosed on all six sides by plates to

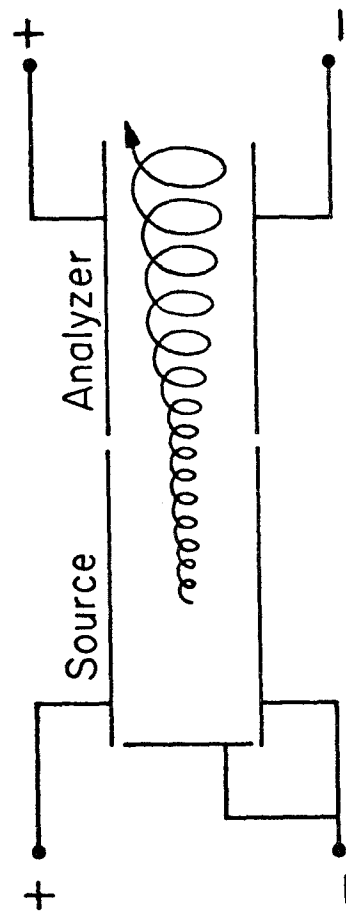
Figure 11

Schematic depiction of ion motion in the ICR cell in trapped-ion and drift modes.

Potentials Applied in Trapping Mode (Side View of ICR Cell)



Potentials Applied in Detect Mode



which individually variable potentials may be applied. For such a geometry an exact solution to Laplace's equation is possible. However, in the trapped-ion cell described in this thesis (4) one of the ends of the trapping region is open to allow ions to drift through to be analyzed. This geometry is shown in Fig. 11. A straightforward exact solution to Laplace's equation is not possible in this case. However, a reasonably accurate approximation may be obtained by assuming that the open end is a plate at ground potential. The solution to Laplace's equation for such an approximation is

$$\phi(x,y,z) = \quad (17)$$

$$\frac{16V_T}{\pi^2} \sum_{n=1}^{\infty} \sum_{m=1}^{\infty} \frac{\sin \frac{(2n-1)\pi x}{a} \sin \frac{(2m-1)\pi y}{5a} \cosh \frac{\sqrt{25(2n-1)^2 + (2m-1)^2} z}{5a}}{(2n-1)(2m-1)}$$

where V_T is the trapping voltage and the origin of coordinates is in one corner of the cell. Sharp et al. (11) have shown for such an analytical solution for the McIver geometry that the potential at the midplane ($y = \ell/2$ where ℓ is the length of the cell) is almost exactly that obtained for the two-dimensional solution. They have also shown that near the midplane the potentials inside the cell can be accurately approximated by a three-dimensional quadrupolar potential. Since the two-dimensional quadrupolar approximation carried out in the first part of this chapter (2)

very accurately predicted ion motion in drift mode, the approximation was extended to three dimensions for the trapped ion cell described here. Fitting this potential to the boundary conditions the result obtained is

$$V_Q = \alpha V_T + V_T \left(\beta \left(\frac{x}{a} \right)^2 + \gamma \left(\frac{y}{a} \right)^2 + \lambda \left(\frac{z}{a} \right)^2 \right) \quad (18)$$

where $\alpha = 0.1132$, $\beta = -0.4528$, $\gamma = -1.8112 \times 10^{-2}$, $\lambda = 0.8868$ and the origin of coordinates is now taken at the center of the trapping (source) region of the ICR cell. Like the two-dimensional quadrupolar case, this approximation does not satisfy Laplace's equation ($\nabla^2 V = 0$) and hence a completely quantitative description of ion motion may not be possible although the qualitative features should certainly be adequate.

The motion of an ion under the combined effects of the potential of eqn. (18) and a homogeneous magnetic field in the z direction can be regarded as a superposition of oscillation in the z direction due to trapping voltage and cycloidal drift due to the $E \times B$ constraint. The components of drift velocity are obtained from the equations

$$v_{dx} = cEy/B \quad (19a)$$

$$v_{dy} = -cEx/B \quad (19b)$$

$$v_{dz} = 0 \quad (19c)$$

The components of E for our quadrupolar potential are obtained from $E_Q = -\nabla V_Q$ and the components of drift are given by

$$v_{dx} = \frac{2 \gamma_y V_T C}{B a^2} \quad (20a)$$

$$v_{dy} = \frac{-2 \beta_x V_T C}{B a^2} \quad (20b)$$

$$v_{dz} = 0 \quad (20c)$$

Differentiating eqn. (20b) and substituting

$$\frac{dv_{dy}}{dt} = v_{dy} \frac{dv_{dy}}{dy} \quad (21)$$

we can integrate and obtain

$$\frac{v_{dy}^2}{2} = \frac{-2 \beta \gamma V_T^2 C^2 y^2}{B^2 a^4} + \text{const.} \quad (22)$$

Substituting for v_{dy} we obtain

$$\beta x^2 + \gamma y^2 = \text{const.} \quad (23)$$

Assuming as our initial condition that ions are formed at the origin at time $t = 0$ with initial velocity (v_{xo} , v_{yo} , v_{zo}) then the constant of equation 23 may be evaluated. At time zero the generating circle for the cycloidal motion has a center initially at (13)

$$x_c = v_{yo} / \omega \quad (24a)$$

$$y_c = -v_{xo} / \omega \quad (24b)$$

and substituting into eqn. (23) we obtain

$$\beta x^2 + \gamma y^2 = \beta x_c^2 + \gamma y_c^2 \quad (25)$$

Using this condition and the coupled equations (20) the cycloidal motion in the xy plane is defined as

$$x = x_c \cos \Omega t + \left(-\frac{\delta}{\beta}\right)^{\frac{1}{2}} y_c \sin \Omega t \quad (26a)$$

$$y = y_c \cos \Omega t - \left(-\frac{\beta}{\delta}\right)^{\frac{1}{2}} x_c \sin \Omega t \quad (26b)$$

$$\text{where } \Omega = \frac{2V_T}{Ba^2} (\beta\delta)^{\frac{1}{2}} \quad (27)$$

From these equations the individual ion motion can be seen to be that of a corkscrew motion, circling around magnetic field lines at the cyclotron frequency while executing simple harmonic motion in the z direction due to the trapping potential, V_T . This motion takes place on a microsecond time scale with a frequency (12)

$$\omega_T = 163 \left(\frac{V_T}{m}\right)^{\frac{1}{2}} \quad (28)$$

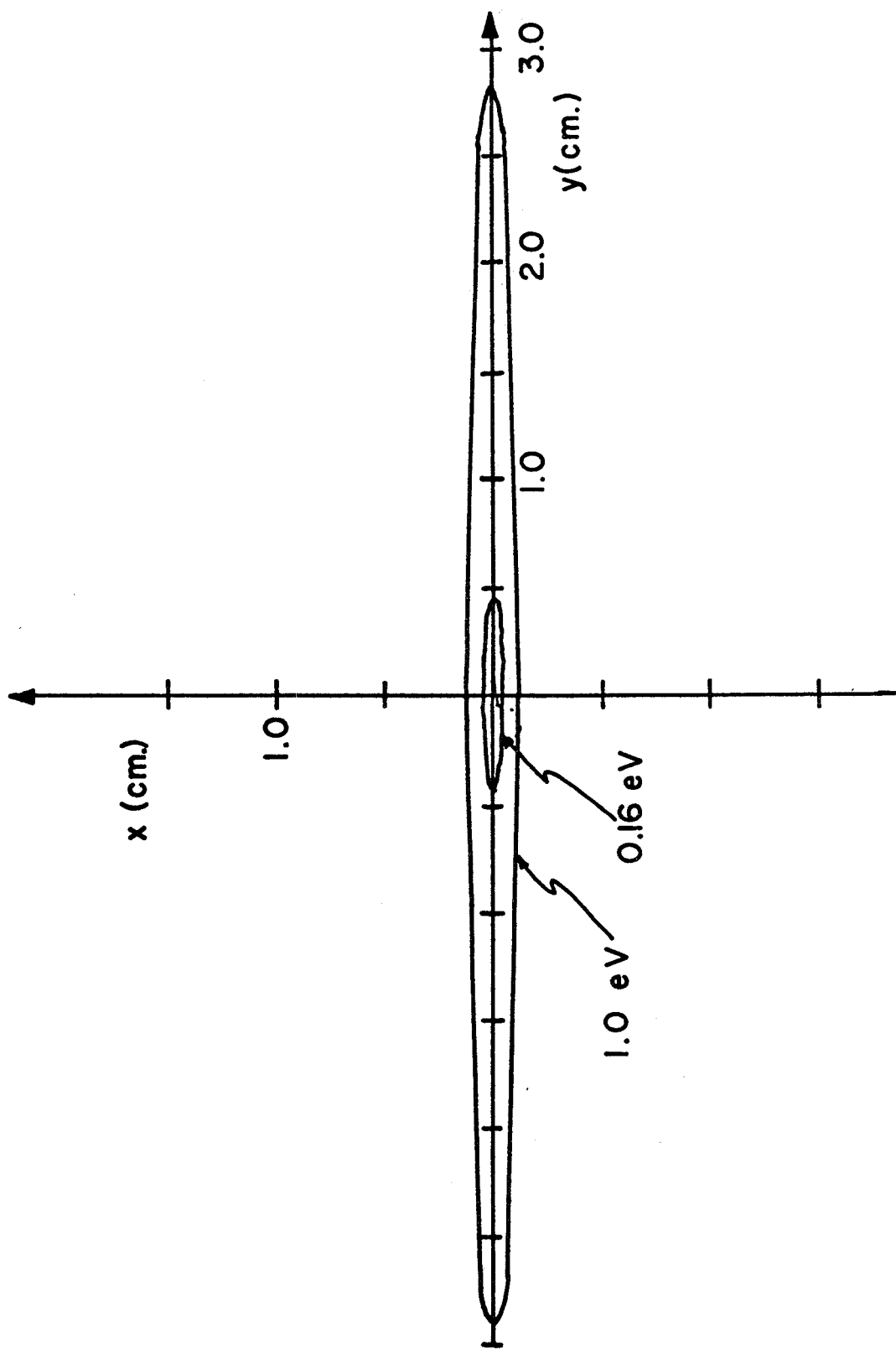
and each ion traces out the surface of a cylinder. On a millisecond time scale, the cylinder moves on the ellipses described by equation (26) with the axis of the cylinder along the magnetic field lines and at a frequency Ω .

Figure 12 shows the maximum loci of generating centers for Ar^+ ions formed with the initial kinetic energy indicated, all directed in the y direction. As can be seen, for thermal energy ions the maximum excursion is less than 0.5 cm. This means that thermal energy ions will all stay very close to the center of the cell in a region where the quadrupolar approximation is most accurate (11).

For a thermal population of ions, Sharp et al. (11)

Figure 12

Maximum loci of generating centers for Ar^+ ions formed at the origin with the initial kinetic energy shown, calculated from equations (24) and (26) based on β and γ obtained from the approximate potential of equation (18). The maximum locus is generated by an ion with all of its initial velocity in the y direction.



shown that the distribution of initial centers of generating circles of the cycloids is given by

$$dN(x_c, y_c) = \frac{N_0}{(2\pi kT)^{1/2}} \omega^2 \exp \left[-\frac{1}{2} m \omega^2 \left(\frac{x_c^2 + y_c^2}{kT} \right) \right] dx_c dy_c \quad (29)$$

Initially for a thermal situation the population contours will be concentric circles about (x_c, y_c) . However, it can be readily seen from equation (26) that after one-quarter period of the elliptical motion at time $t = \frac{\pi}{2\Omega}$ the generating center of the cycloid has moved to

$$x = \left(-\frac{\delta}{\beta} \right)^{1/2} y_c \quad (30a)$$

$$y = -\left(-\frac{\beta}{\delta} \right)^{1/2} x_c \quad (30b)$$

Since $\beta \gg \delta$ the ions have all moved to positions very near the $x = 0$ plane. After another quarter period, the population contours will again return to concentric circles.

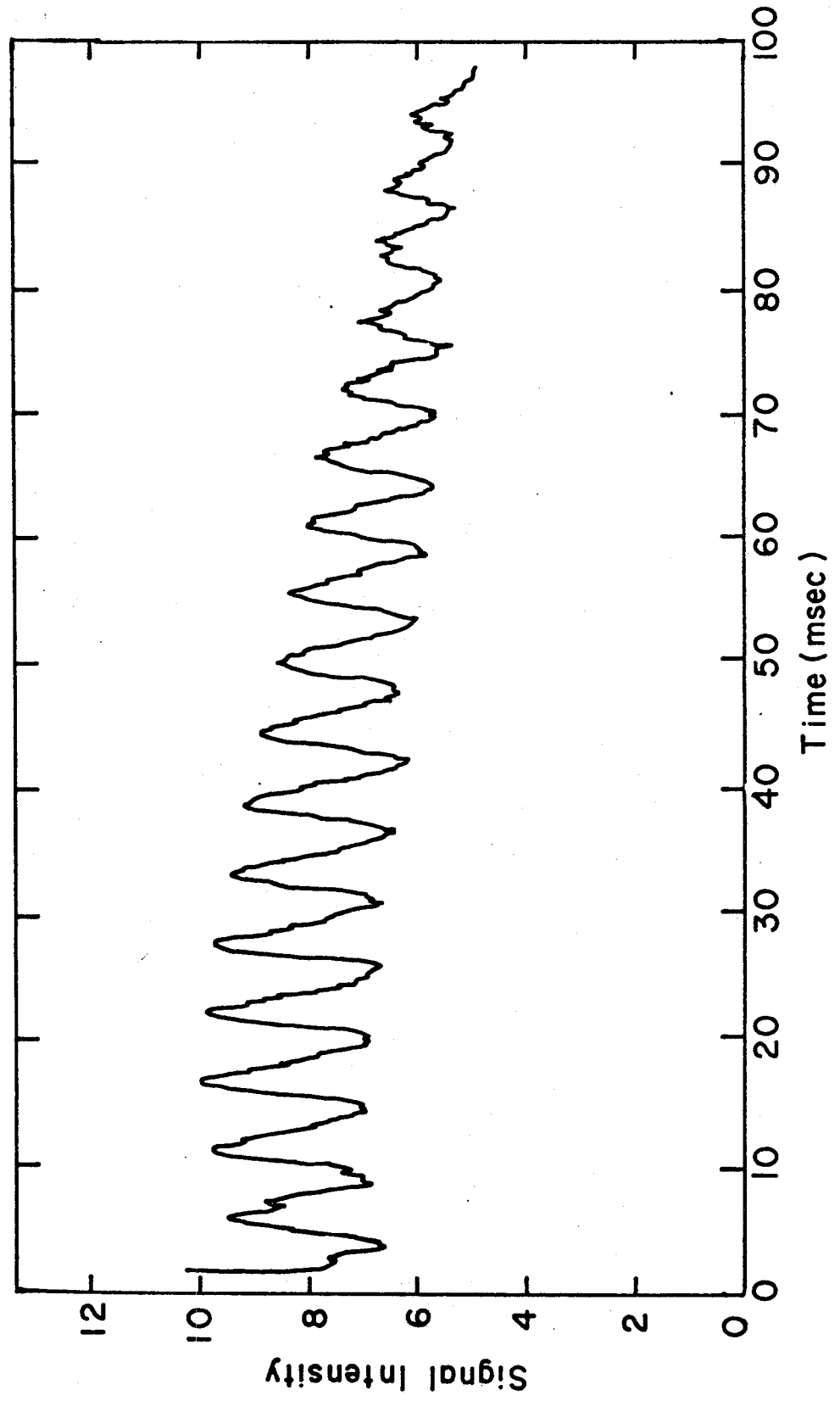
This periodic behavior serves to explain a seemingly anomalous behavior occasionally observed in trapped-ion spectra. Large oscillations in intensity as a function of trapping time with periods on the order of milliseconds such as those shown in Fig. 13 are often seen. Space charge effects, which have been ignored in the above analysis would prevent the concentration of ions near the $x = 0$ plane. Hence, each time the circular population contains collapsed to thin ellipses a space charge force would accelerate the ions to the cell plates and the ions would

Figure 13

A typical spectrum exhibiting oscillations in intensity as a function of time. This trace shows CF_3^+ generated from CF_3CHF_2 at 70 eV and a pressure of 2×10^{-6} torr. The fluoride transfer reaction



occurs causing the decrease in CF_3^+ intensity. Trapping voltage was 0.5 volts, magnetic field 13.8 kilogauss and the observed oscillation frequency 185.8 Hz.



be lost. It is experimentally observed that these oscillations generally become damped at longer trapping times or higher pressures. This can be explained on the basis of ion-neutral collisions. Collisions, also ignored in this analysis, will randomize the positions of the generating circles for the cycloids and the population contours will no longer oscillate.

The experimentally observed variation of the oscillation frequency with trapping voltage, V_T , predicted from equation (27) is shown in Fig. 14. It can be seen that the variation is very nearly linear and the slope yields a value of β of 0.0845, very close to the theoretically predicted value of 0.082.

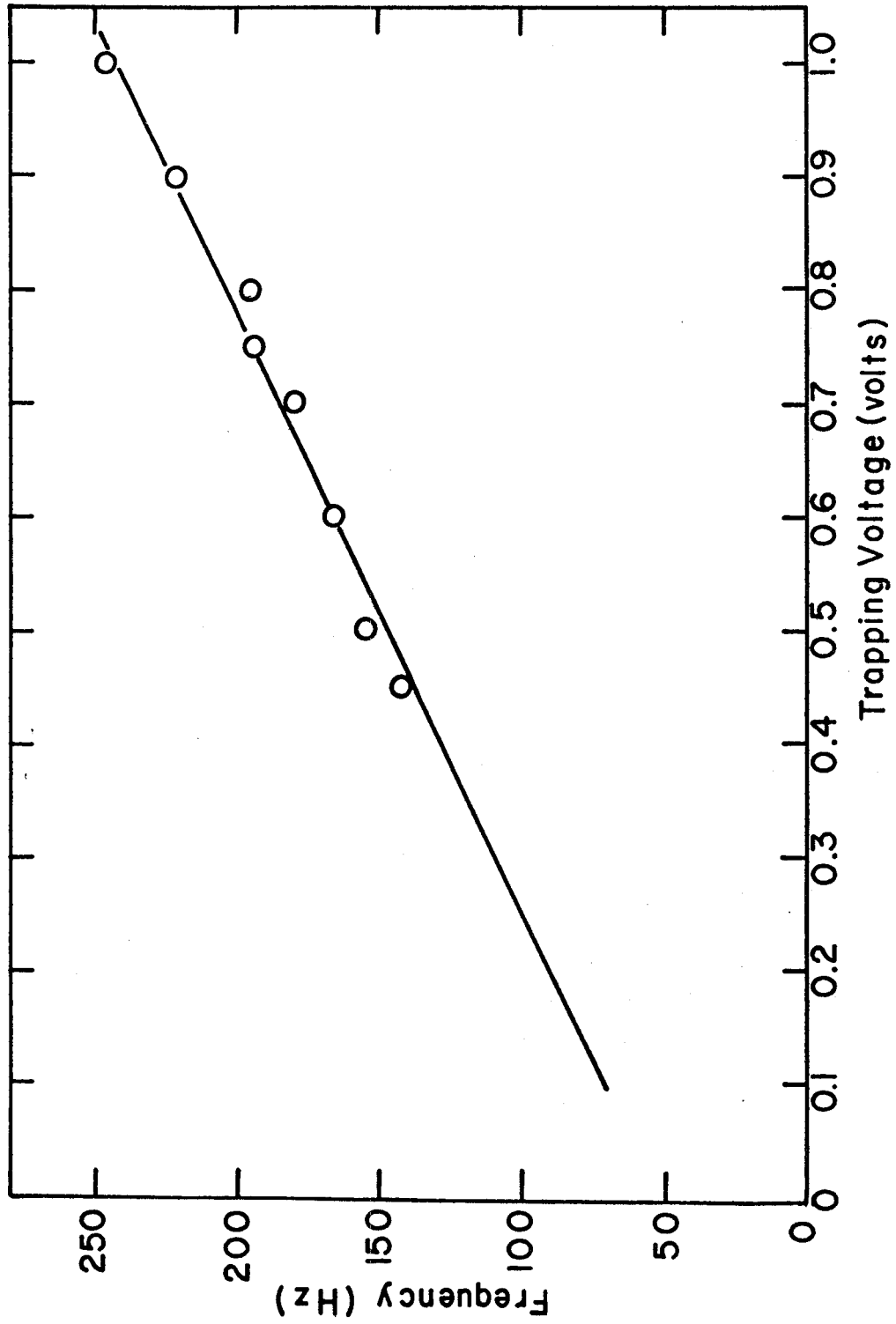
The above analysis for trapped-ion motion suggests several considerations for trapped-ion cell design and for alignment of a light beam in experiments involving photo-ionization (13), photo-detachment (14) or photo-induced reaction (15). The principle mechanism for ion loss other than the space charge effects discussed above is due to random walk of the ions to the cell walls as a result of collisions. Sharp et al. (11) have shown that the average retention time of ions in the cell is given by

$$\tau = \frac{D^2 q^2 B^2 \pi^{\frac{1}{2}}}{4.8 P \sigma (mkT)^{\frac{1}{2}}} \quad (31)$$

where D is the distance from the origin to the cell wall in the x direction, P is the pressure in dynes/cm² and σ

Figure 14

Experimental variation of the oscillation frequency with trapping voltage for CF_3^+ ions generated under the conditions described in Figure 13.



is the average collision cross section. This suggests that enlarging the space between the drift plates should lead to a dramatic increase in trapping efficiency, a consideration worthy of note for future cell construction.

In addition to randomizing the distribution of generating centers, ion-neutral collisions should thermalize the ion motion in the z -direction. Hence after relatively few collisions most of the ions will be distributed near the $z=0$ plane. Hence, any attempt to irradiate ions with an external light source should have a thin light beam aligned in this plane to minimize the interaction volume of photons and ions.

REFERENCES

1. J. D. Jackson, Classical Electrodynamics (Wiley, New York, N.Y., 1962).
2. T. B. McMahon and J. L. Beauchamp, Rev. Sci. Instrum. 42, 1632 (1971).
3. R. T. McIver, Jr., Rev. Sci. Instrum. 41, 555 (1970).
4. T. B. McMahon and J. L. Beauchamp, Rev. Sci. Instrum. 43, 509 (1972).
5. J. L. Beauchamp and J. T. Armstrong, Rev. Sci. Instrum. 40, 123 (1969).
6. J. L. Beauchamp and S. E. Buttrill, Jr., J. Chem. Phys. 48, 1783 (1968).
7. J. L. Beauchamp, Ph.D. Thesis, Harvard University (1967).
8. J. L. Beauchamp, J. Chem. Phys. 46, 1231 (1967).
9. E. W. McDaniel, Collision Phenomena in Ionized Gas, Wiley, New York, (1964).
10. It should be noted that collision frequencies calculated for N_2^+ in N_2 with equation (16) will be somewhat low due to the occurrence of charge exchange outside the orbiting impact parameter.
11. T. E. Sharp, J. R. Eylar and E. Li, Int. J. Mass Spectrom. Ion Phys. 9, 421 (1972).
12. B. S. Freiser, T. B. McMahon and J. L. Beauchamp, Int. J. Mass Spectrom. Ion Phys., in press.

13. J. M. Weigel, Masters' Thesis, California Institute of Technology (1972).
14. K. C. Smythe and J. I. Brauman, J. Chem. Phys. 56, 4620 (1972) and references contained therein.
15. R. C. Dunbar, J. Amer. Chem. Soc. 93, 4354 (1971).

CHAPTER III

Design, Construction and Operation of a Trapped-Ion
Cyclotron Resonance Spectrometer

A. Introduction

The principle consideration in the design of the trapped-ion ICR cell was the need for versatility. It was essential that the frequent change from the trapped-ion mode of operation to either trapping voltage or electron energy modulation in drift mode be routinely possible with a minimum of alteration to the instrument. In particular, it was mandatory that there be no need to change cells, necessitating breaking of the vacuum seal and a tedious and time-consuming bake-out procedure. The minimum of mechanical modifications and the aid of several integrated circuits, FET switches and switching transistors made the change from one mode of operation to another possible with a single multi-deck wafer switch.

B. Mechanical Modifications to the ICR Cell

The only physical alterations to the conventional ICR cell necessary to effect ion trapping are the addition of a plate to the rear of the source region (connected to either of the source drift plates) and the mounting of 90% open mesh gold grids between the filament and trapping plate on one side of the cell and between the electron collector

and the trapping plate on the other. These grids, operated at the potential of the adjacent trapping plate, shield the trapping region from the bias voltages applied to the filament and electron collector and were found to greatly reduce ion losses during the trapping period.

C. Electronic Design.

1. Ion Trapping Circuitry

A block diagram, illustrating the control and sequence of pulses during the trapped-ion mode of operation is shown in Fig. 1. The actual circuitry for control of drift plate potentials in the trapped ion mode is shown in Fig. 2. The time base for each trapping cycle is supplied by a Tektronix Type 454 Oscilloscope which generates a 0 to 10 volt ramp exactly the length of the oscilloscope trace. The common experimental range of trapping times from 10 milliseconds up to several seconds are routinely available by changing the time base setting of the oscilloscope.

A slow scanning ramp is obtained from the output of the sweep potentiometer of the Fieldial (1) control for the magnet. The Fieldial may be decoupled from the magnet to generate a 0 to 10 volt ramp in times ranging from 30 seconds to 50 minutes while the magnetic field remains constant.

Each of the ramps are input to high impedance operational amplifiers, IC's 1 and 2 (Fairchild- μ A 741) (2) wired as voltage followers. These devices prevent the pulsing

Figure 1

Block diagram illustrating the control of pulsing sequences for the trapped ion cell. Ramp 1 is generated by a Tectronix Type 454 Oscilloscope, Ramp 2 by the Fieldial of a Varian electromagnet. The boxcar integrator is a PAR Model CW-100 Boxcar Integrator. All other components are home-built.

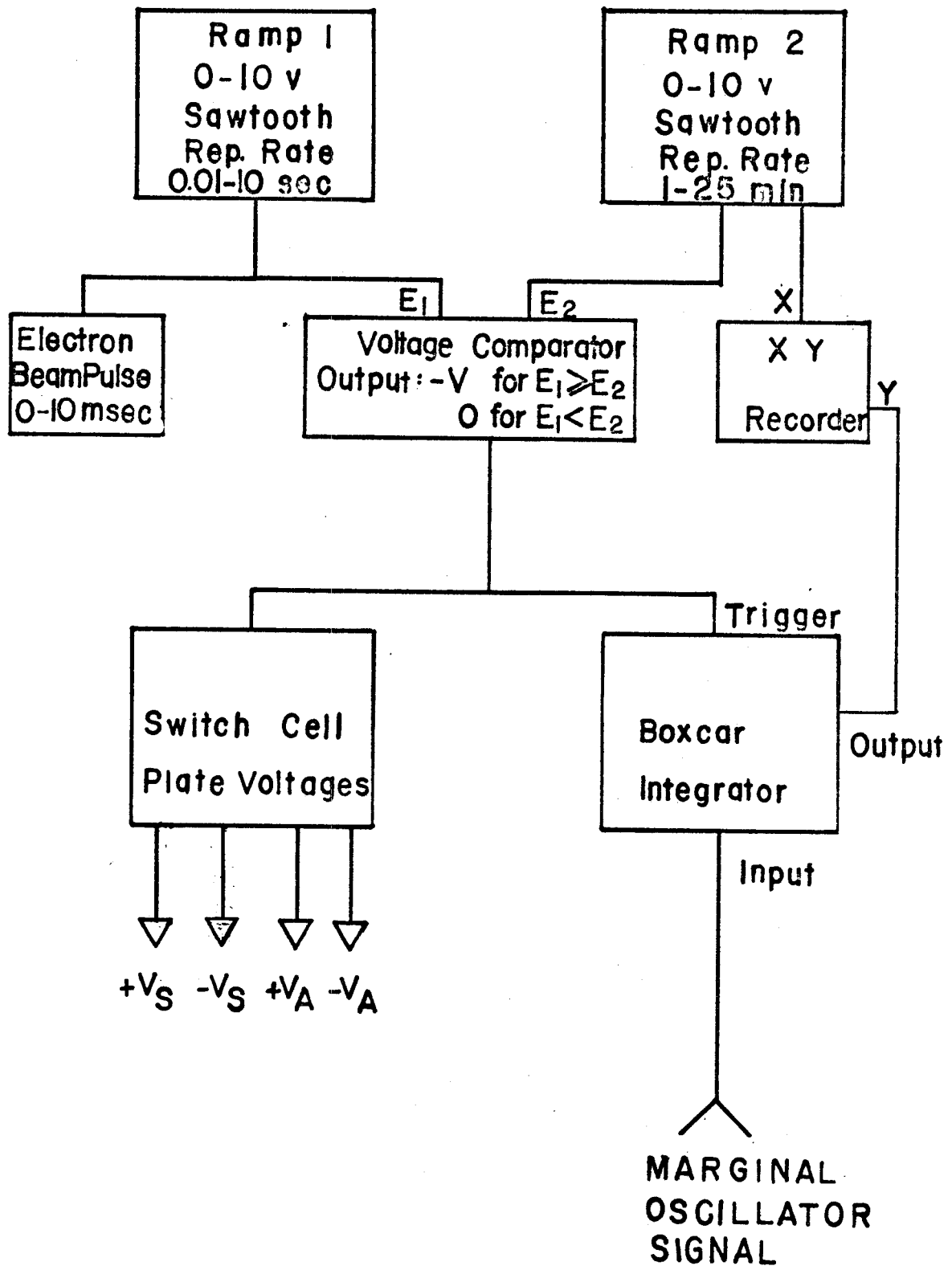
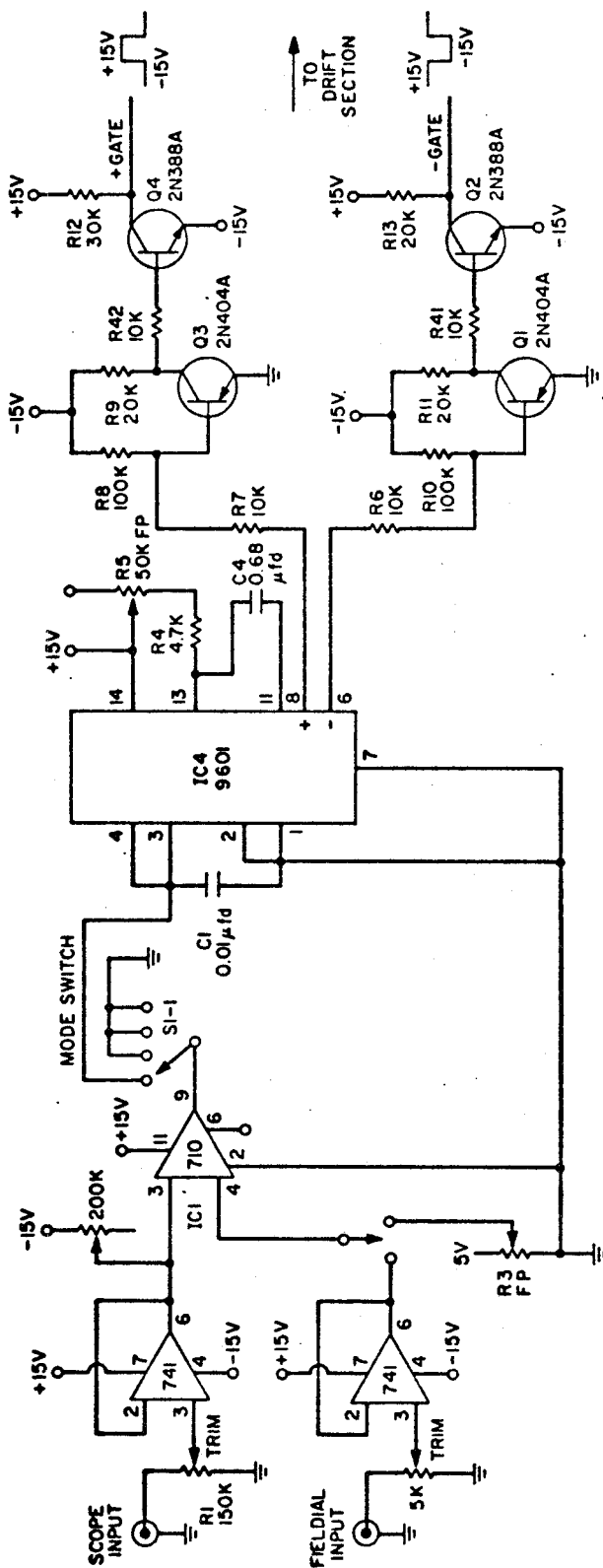


Figure 2

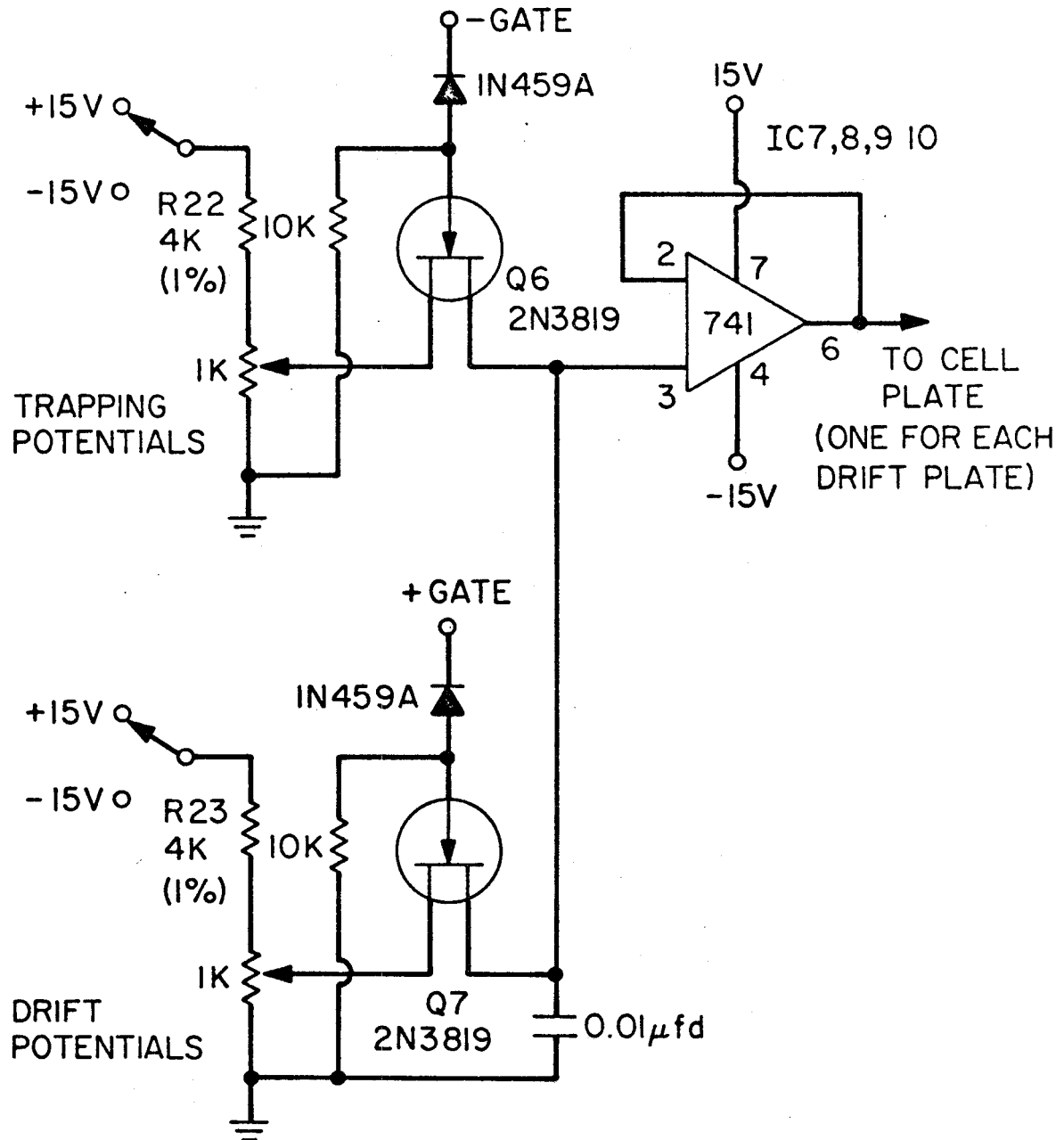
(a) Circuitry to generate the pulsing of the ICR cell drift plates by comparing the outputs of the fast and slow ramps. Pulses from the monostable multivibrator (μ A-9601) also trigger the boxcar integrator.

(b) Outputs of the FET gate drivers in the last stage of Figure 2(a) are each input to the gates of four separate FET switches (2N 3819), one for each of the ICR cell drift plates. Each plate may be pulsed between any two given voltages. In practice, the lower resonance drift plate is not usually pulsed since this seriously perturbs the marginal oscillator.

TRAPPED ION CELL CIRCUITRY - PULSING SECTION



-TRAPPED ION CELL CIRCUITRY- DRIFT SECTION



circuitry from loading either of the ramps.

The outputs of the two voltage followers are used as reference voltages for a voltage comparator, IC 3 (Fairchild- μ A 710) (3). When the output voltage from the oscilloscope ramp exceeds that from the Fieldial the output of the comparator switches from 0 to 3 volts. It is this transient that is used to trigger the detect pulse. An optional constant reference voltage is also supplied to allow the Fieldial to be coupled to the magnet and permit mass spectra to be taken at any desired reaction time.

The output of the comparator is used to trigger a monostable multivibrator, IC 5 (Fairchild- μ A 9601) (4). When the input to the monostable multivibrator is 0 volts the logic 0 and logic 1 outputs are 0 and 3 volts respectively. However, when the input voltage switches to 3 volts and logic 0 and logic 1 outputs generate a pulse of 3 volts and 0 volts respectively of controlled width. This width is given by

$$\tau = 0.32 R_1 C_2 (1 + 0.7/R_1) \quad (1)$$

where R_1 , R_2 , and C_1 are resistors and capacitor wired externally to the monostable multivibrator. This pulse width is the width of the detect pulse during which ions are drifted from the trapping region into the resonance region where they are detected. It is desirable that the pulse width be variable since the ion drift velocity is dependent on the magnetic field strength according to the relation (5)

$$v_D = \frac{cE}{H} \quad (2)$$

At higher magnetic field strengths the ions will drift slower and hence in order that the detect pulse be on for a time approximately equal to the ion transit time through the resonance region of the apparatus the value of R_1 was made easily controllable by a potentiometer on the control panel of the instrument. This was done to ensure that only marginal oscillator signal would be integrated by the box-car integrator and thus optimize the signal to noise ratio.

Since it was decided to use inexpensive FET switches for pulsing the cell plate voltages from a trapping to drift configuration, it was necessary to convert the output pulses of the monostable multivibrator to voltage pulses of sufficient magnitude to gate the FET's. This is done by means of FET gate drivers (6). The FET gate drivers shown here employ small signal germanium switching transistors with breakdown voltages above 30 volts and high current gain. The 2N 404A transistor is a PNP type while the 2N 388A is an NPN although any switching transistors with comparable characteristics could be used. These drivers convert the logic 0 pulse (0 to +3 volts) of the μA 9601 to a -15 to +15 volt pulse, while the logic 1 pulse (+3 to 0 volts) is transformed to a +15 to -15 volt pulse. When the potential applied to the gate of a 2N 3819 FET is -15 volts the effective drain source resistance approaches infinity. Therefore, the logic 1 driver output (+15 to -15 volts) can be used to supply the gate for the FET switch which will

be on for the trapping period while the logic 0 driver pulse (-15 to +15 volts) can be used to turn on the detect pulse by supplying the appropriate potentials for drift motion.

The drains of both FET's supply the inputs for high input impedance operational amplifiers (Fairchild μ A 741) wired as voltage followers. The output of these amplifiers go directly to the cell plates. Since their output impedance is very low the pick-up of stray noise is minimized and thus improves signal to noise characteristics of the instrument. While one FET is in the off position the other is on and in this way voltages can be switched very rapidly (rise time ~ 10 ns.) from trapping to drift configuration.

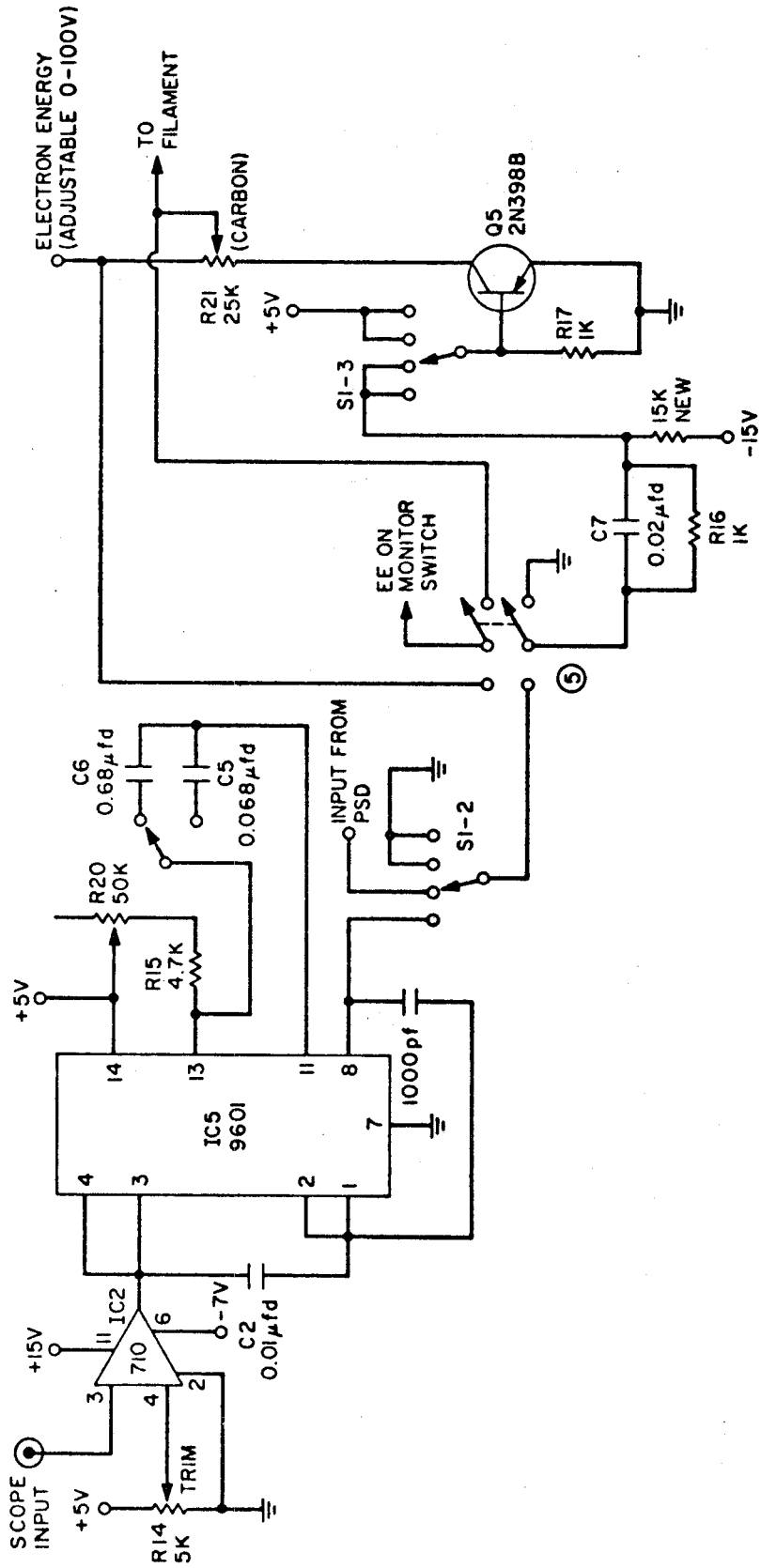
2. Electron Energy Pulsing Circuitry

In the trapped-ion experiment ions are formed for a period of time short compared to the reaction time. This is done by pulsing the electron energy from below the ionization potential of the molecule being investigated to some voltage above the ionization potential. In addition, in drift mode, where detection is accomplished by a phase-sensitive detector electron energy modulation at the reference frequency of the phase sensitive detector is a very useful technique. The circuitry for accomplishing both these functions is shown in Fig. 3.

The electron energy pulse for the trapped-ion experiment is supplied in a manner analogous to the detect pulse.

Figure 3

Circuitry for control of the electron energy in ICR experiments. In both trapped ion and electron energy modulation modes, the circuit provides pulsing from below to above the ionization potential of the molecule studied. In the trapping voltage modulation mode the electron energy is held constant.



The oscilloscope ramp is again used as one input to a voltage comparator (Fairchild- μ A 710) (3). The reference input is supplied by an external constant voltage set at some low value so that the electron energy pulse will be initiated very near the beginning of the duty cycle determined by the width of the oscilloscope ramp. The width of the pulse is again determined by a monostable multivibrator. A two position switch allows variation of the pulse width from 0 to 1 millisecond and from 0 to 10 milliseconds. The logic 0 output (0 to 3 volts) is used to gate a high voltage switching transistor (2N 398B). When the voltage applied to the base of Q5 is negative, the transistor is conducting and the voltage applied to the filament is determined by the setting of potentiometer R21. However, when the monostable multivibrator changes levels to +3 volts the base of Q5 is positive and the transistor will not conduct. The voltage applied to the filament is then determined by the setting of a remote programmable power supply.

In order to use electron energy modulation the output of the monostable is replaced by a 0 to 3 volt square wave from the phase sensitive detector. The transistor Q5 operates in a fashion similar to that described above except that the voltage applied to the filament is now a square wave.

In cases where constant electron energy is desired, the voltage applied to the base of Q5 is switched to +5 volts.

The transistor is then held continuously non-conducting and the filament voltage is constant.

3. Trapping Voltage Circuitry

Another possible modulation scheme in drift-mode ICR experiments is trapping voltage modulation. A single resonance spectrum in absorption mode may be obtained if one trapping plate is modulated between some positive and some negative potential with a period longer than the transit time of the ions through the cell. This technique is especially useful for studying negative ions where ion formation can often take place over a wide range of electron energies and in photoionization ICR experiments. A typical spectrum taken with trapping voltage modulation (25 Hz) is shown in Fig. 4 for a mixture of ethyl nitrite and ethanol. A reversal of the sign of the potential applied to the trapping plate held at constant voltage serves to detect negative rather than positive ions. Since mass discrimination effects are not important in ICR experiments and the applied fields are symmetric for both positive and negative ions, it is possible to quantitatively assess the relative abundance of positive and negative ions.

The circuitry to apply trapping plate potentials in all modes of operation is shown in Fig. 5. For trapping voltage modulation, reversal of the sign of the potential applied to the modulated plate is again accomplished with the use of FET switches. The 0 to 3 volt square wave

Figure 4

Positive and negative ion cyclotron resonance spectra of a mixture of ethylnitrite and ethanol recorded using trapping voltage modulation. Both spectra were recorded using the same gain and an observing oscillator frequency of 153.7 kHz.

$\text{CH}_3\text{CH}_2\text{ONO}$ and $\text{CH}_3\text{CH}_2\text{OH}$

25 eV

10^{-5} torr

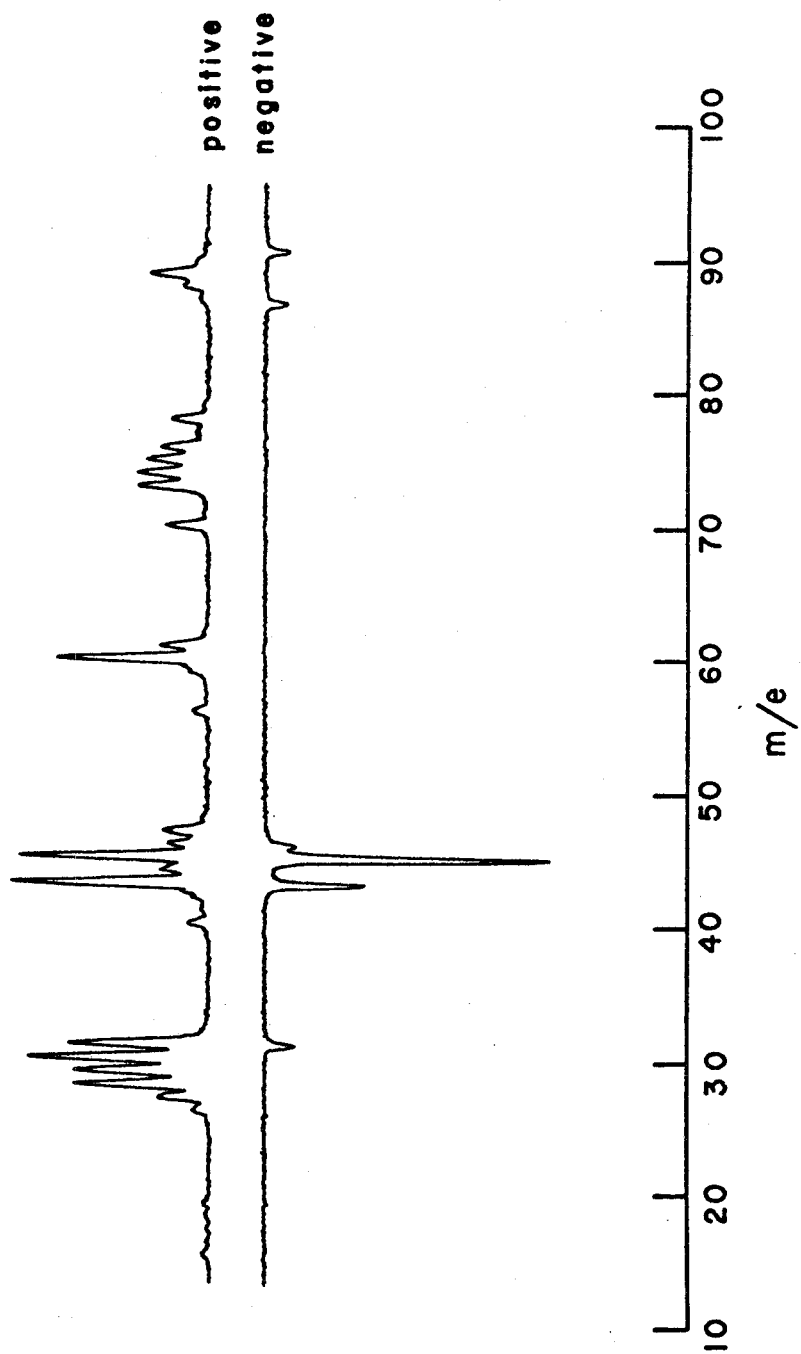
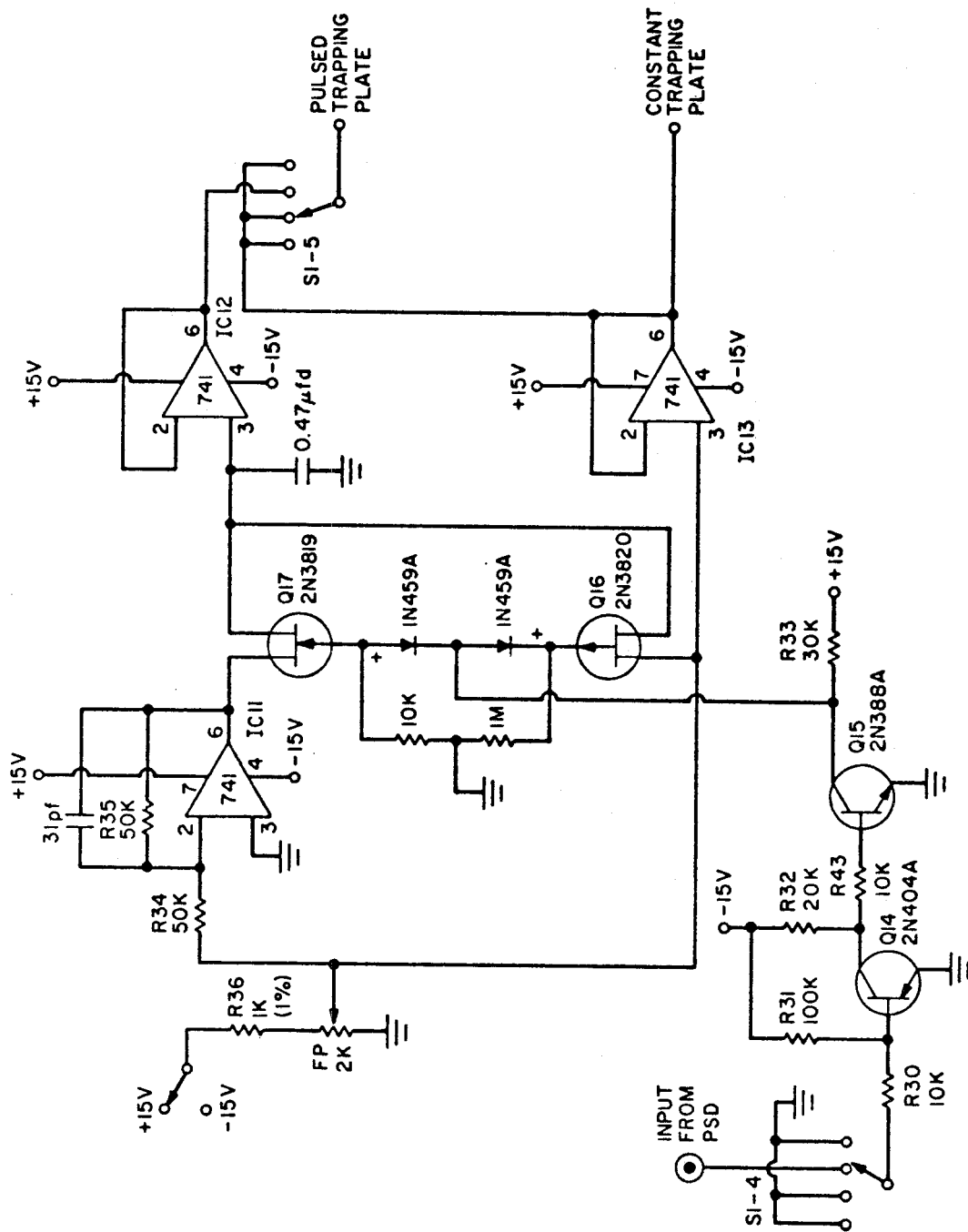


Figure 5

Circuitry for control of trapping plate voltages in ICR experiments. In trapping voltage modulation mode the modulation frequency is supplied by the phase sensitive detector. In all other modes both trapping plates are held at constant voltage.

TRAPPED ION CELL CIRCUITRY — TRAPPING SECTION



supplied by the phase sensitive detector is converted to a suitable magnitude (-15 to +15 volts) to act as a gate driver by the switching transistors Q14 and Q15. Using two FET's of opposite polarity a single gate driver can act to switch one FET off while switching the other on. As can be seen from Fig. 5, the desired trapping voltage is input to two separate operational amplifiers, one wired as a voltage follower (IC 13), and the other as a unity gain inverting amplifier (IC 11). The output of the voltage follower is applied to the trapping plate held at constant voltage. The output of the inverting amplifier is the source voltage for one FET while the potential applied to the constant trapping plate is the source voltage for the FET of opposite polarity. The drains of both FET's are input to another voltage follower (IC 12). Thus, the potential applied to the modulated trapping plate is switched between plus and minus the potential on the constant trapping plate at the reference frequency of the phase sensitive detector.

In trapped ion and electron energy modulation operations the potential on both trapping plates is held constant by grounding the input to the gate driver circuit. This holds the gates of the FET switches at -15 volts and keeps the switch supplying the inverted potential continuously off.

4. Radio Frequency Pulse Circuitry

One of the unique features of ICR is the ability to

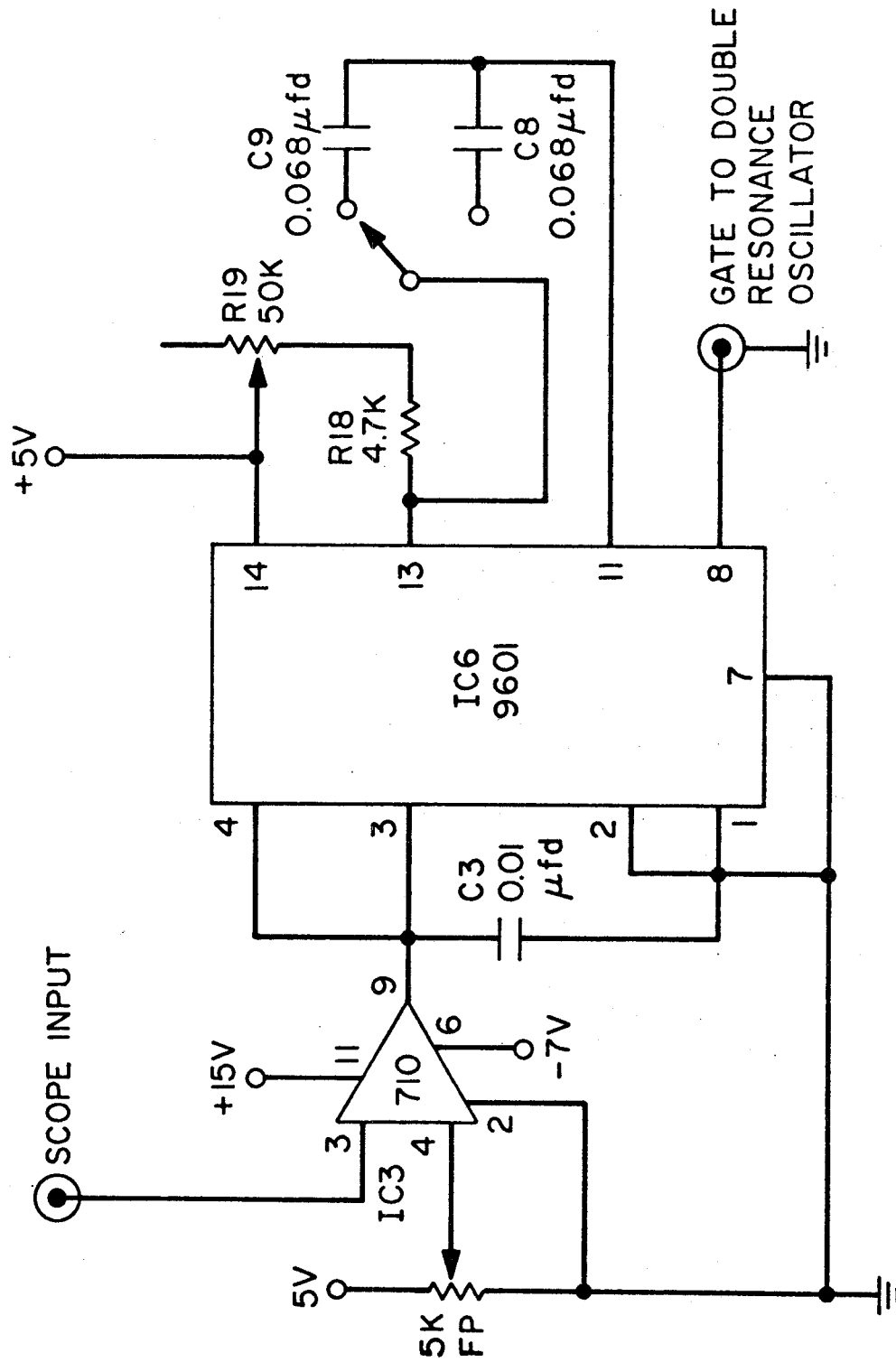
alter ion populations and ion kinetic energies by applying a secondary radio frequency field at the cyclotron frequency of a particular ion. It was desired to extend this feature to the trapped-ion mode of operation and to allow for the capability to initiate the RF pulse at any time during the trapping cycle for a controlled duration. This was accomplished by means of the simple circuit shown in Fig.6 .

The oscilloscope ramp again supplies one input to a voltage comparator. A variable front panel adjustment supplies the reference input to the comparator. The output pulse from the comparator triggers another monostable multivibrator. A front panel switch and potentiometer control the width of the output pulse from several microseconds to the remaining length of the duty cycle.

Several investigators (7-9) have used microsecond radiofrequency pulses in drift mode ICR experiments to accelerate ions to a known kinetic energy and examine reactions and rate constants for ions as a function of kinetic energy. The increased ease of kinetic measurements in trapped-ion mode make the ion kinetic energy experiments much simpler. In a typical experiment an electron energy pulse of several milliseconds forms ions of thermal energy. These ions are subsequently accelerated to a known kinetic energy by a radiofrequency pulse on the order of microseconds. These translationally excited ions are then allowed to react and reactant and product ion intensities

Figure 6

Circuitry for initiating r.f. pulses from the double resonance oscillator. The circuit allows the double resonance oscillator to be turned on in trapped ion mode after a suitable delay time for any desired length of time.



are recorded as a function of time as in the normal trapped ion experiments.

In addition to examining reactions of translationally excited ions, the time delayed irradiation technique has several other useful purposes (10). One of these is the ability to selectively remove a particular ion from the trapping region at a given time during the trapping cycle. The utility and results derived from this type of experiment will be discussed later in this thesis in the treatments of fast charge and particle transfer and in the equilibria of organic ions.

As well as these experiments, it is also possible to do the usual double resonance experiment in trapped-ion mode by allowing the radiofrequency irradiation to be continuous.

D. Pressure Measurement

The accuracy of rate constants determined by ICR techniques depends on the ability to accurately measure the pressure of gas in the ICR cell. In drift-mode ICR where reaction times are about one millisecond, most reaction occurs above 10^{-5} torr. In this pressure range accurate pressure measurement is possible with a capacitance manometer (11). However, in trapped-ion experiments reaction times can be on the order of several seconds and operating pressures in the range 5×10^{-8} torr to 5×10^{-6} torr are desirable. In this region, no absolute method to

measure pressure exists and pressure measurement must be carried out by indirect methods. The most convenient method for our purposes is an ionization gauge. Because of space limitations and the need to measure pressure in a strong magnetic field, an ionization gauge of Shulz-Phelps geometry was chosen (12,13). Such a gauge is shown schematically in Fig. 7. Accelerating fields draw positive ions to a collector plate while electrons (and possibly negative ions) are drawn to another collector. The current at the electron collector is a measure of the emission current while the positive ion current registered at the collector opposite is a measure of the neutral gas density. Since every molecule has a unique ionization cross section, the gauge is calibrated against a capacitance manometer above 10^{-5} torr for each gas studied. It is assumed that the calibration curve is linear from the measured range down to zero pressure. The pressures of interest for trapped-ion experiments are thus obtained from extrapolation of the calibration curve.

Since the emission properties of the filament surface can vary with pressure of the added gas or with temperature it was found necessary to regulate the emission from the ionization gauge filament. This was done with the emission regulation circuit shown in Fig. 8 (14). Satisfactory emission regulation was obtained from $0.1 \mu\text{A}$ to $200 \mu\text{A}$.

Ion currents are in the range of 10^{-12} A to 10^{-7} A and

Figure 7

Schematic of the Schulz-Phelps ionization gauge adopted for pressure measurement in trapped-ion ICR experiments.

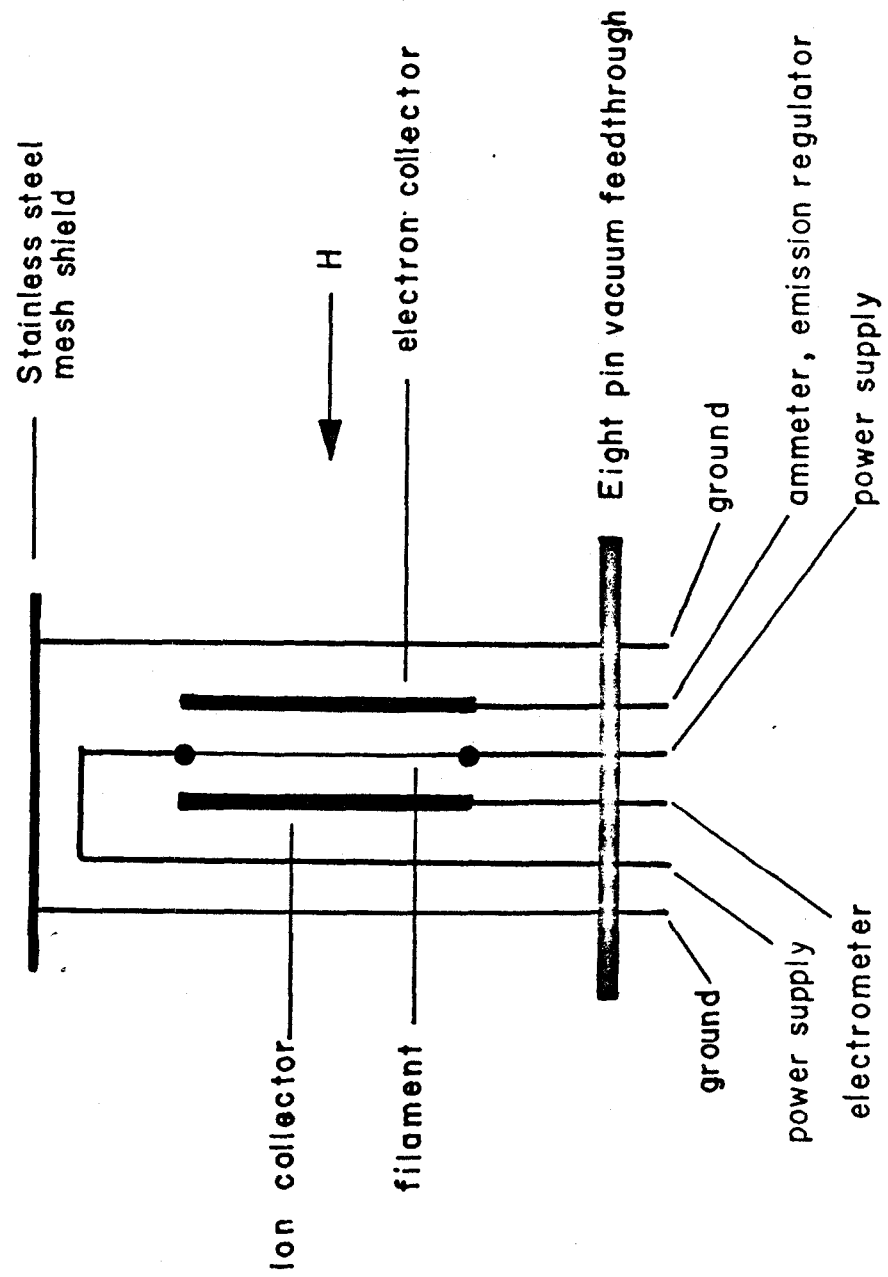
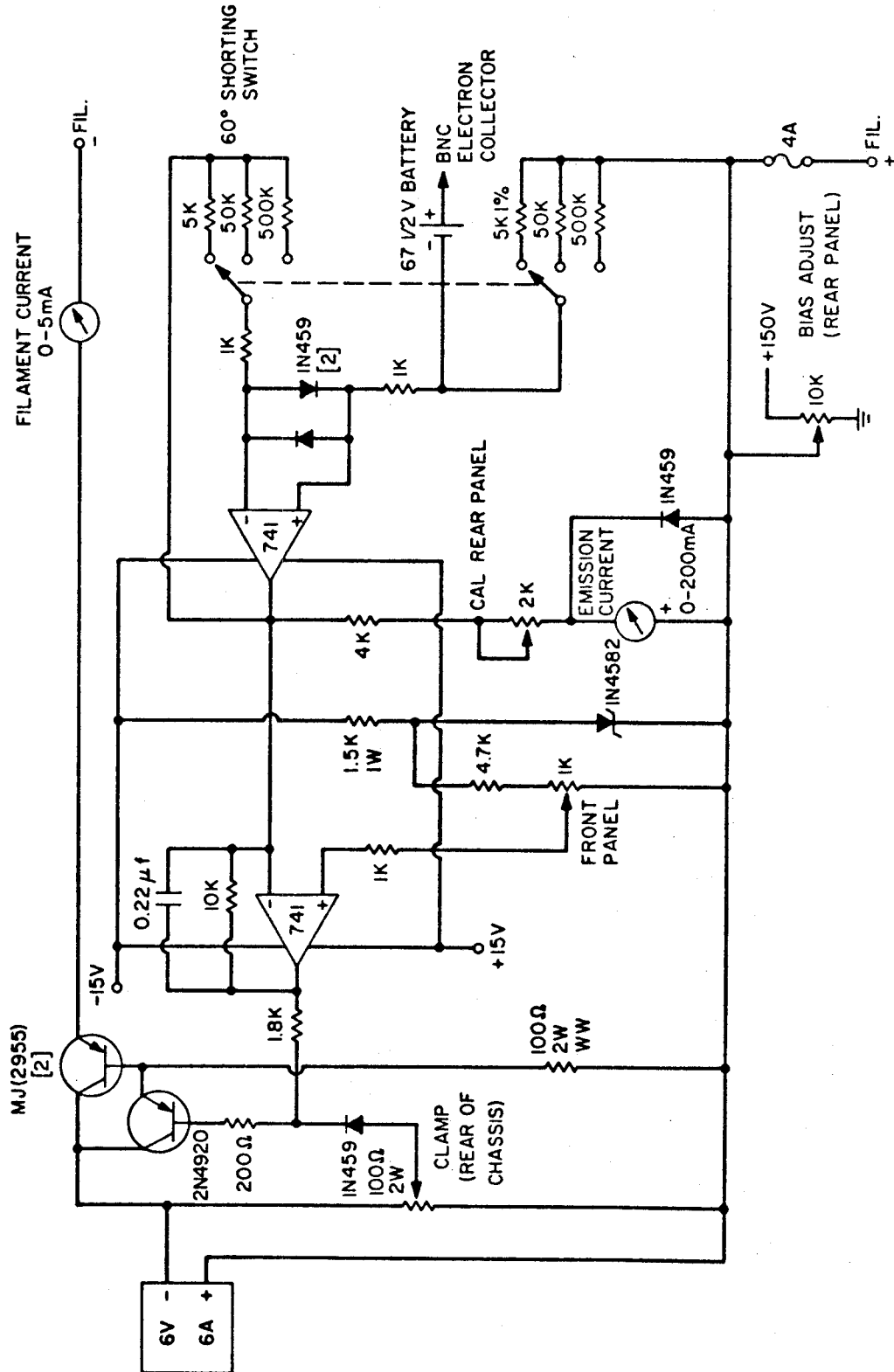


Figure 8

Circuit to provide emission regulation for the filament of the Schulz-Phelps gauge.

EMISSION REGULATOR



are measured using a Keithley Model 610 Electrometer.

Emission currents are monitored on a Simpson MicroAmmeter.

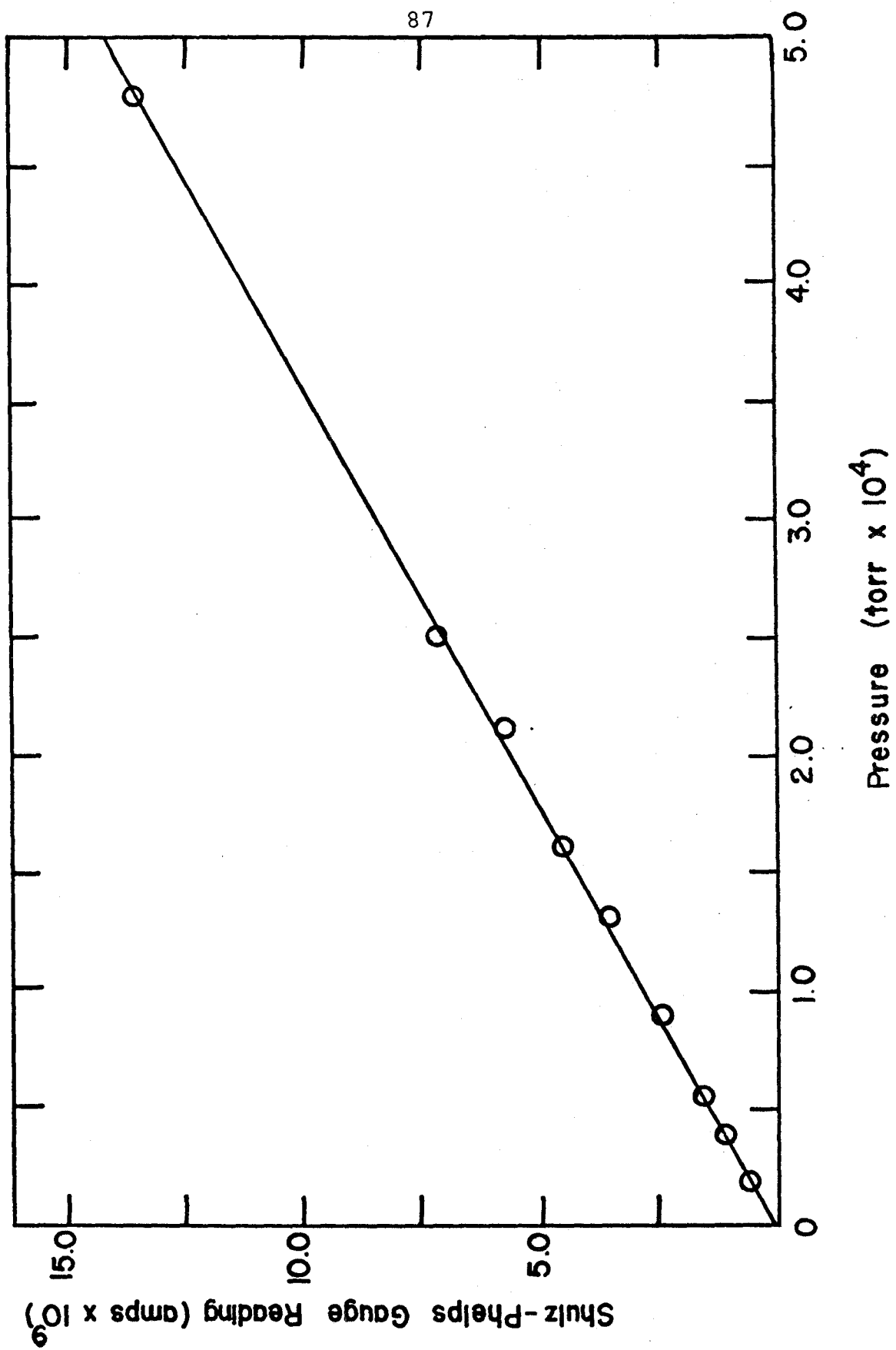
A typical calibration curve of ion current as a function of pressure of methane measured by the capacitance manometer is shown in Fig. 9. For most gases studied these calibration curves are linear over the measured range and give rate constants in good agreement with literature data. Occasionally highly polar species will give non-linear calibration curves, presumably due to absorption on metal surfaces. Due to the change of cyclotron radius with magnetic field the gauge sensitivity also varies with magnetic field. For this reason all calibration curves for gases were conducted at 6 kilogauss and 10 μ A emission current to insure consistency of observations.

E. Data Collection and Analysis

As ions drift through the analyzer region of the cell, the power absorption at their cyclotron frequency is monitored with the usual ICR marginal oscillator detector. The transient output of the marginal oscillator is integrated by a Princeton Applied Research model CW-1 Boxcar Integrator. The boxcar integrator is gated externally using the detect pulse output of the monostable multivibrator (IC 4) in the ion trapping circuit (Fig. 3). The integrated output of the boxcar integrator is displayed on a Hewlett Packard xy recorder.

Figure 9

Typical calibration curve for the Schulz-Phelps gauge for CH_4 at 6 kilogauss and 10 A emission current.



The instantaneous power absorption of ions at resonance is given by (15,16)

$$A(t) = \frac{N(0)q^2 E_{rf}^2 t}{4m} \quad (3)$$

where $N(0)$ is the number of ions with mass to charge ratio m/q , E_{rf} the radiofrequency electric field strength and t is the time the ions have been in the analyzer region. The drift velocity of ions in the resonance region is determined by the static electric field strength E and the magnetic field strength H , according to the relation (5)

$$v_D = \frac{cE \times H}{|H|^2} \quad (4)$$

Thus knowing the drift velocity and the length of the resonance region, ℓ , the drift time through the resonance region is given by

$$\tau = \frac{\ell H}{cE} \quad (5)$$

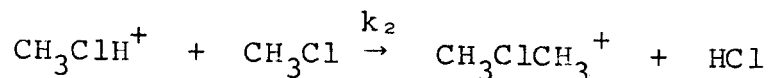
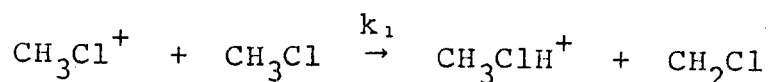
when E and H are perpendicular. Hence the power absorption increases linearly with time, reaching a maximum at $t = \tau$ beyond which it falls to zero as ions leave the resonance region. The boxcar detector integrates the transient power absorption giving the measured signal intensity

$$I = N(0) \frac{q^2 E_{rf}^2 \tau^2}{8m} \quad (6)$$

At a fixed observing frequency, higher mass ions come into resonance at proportionately higher magnetic field strength.

Thus it follows from equations (5) and (6) that the integrated power absorption will be directly proportional to ion mass.

In order to illustrate the ion trapping technique and to demonstrate its usefulness for kinetic measurements the positive ion molecule reactions of the parent ion of methyl chloride are shown in Fig. 10. The reaction sequence occurring in this system is



A solution to the kinetic equations for a simple primary (P), secondary (S), tertiary (T) ion system such as this yields the abundances of the various ions as

$$P = P(0) e^{-nk_1 t} \quad (7)$$

$$S = \frac{k_1 P(0)}{k_2 - k_1} (e^{-nk_1 t} - e^{-nk_2 t}) \quad (8)$$

$$T = \frac{k_1 k_2 P(0)}{k_2 - k_1} \left(\frac{1 - e^{-nk_1 t}}{k_1} + \frac{e^{-nk_2 t} - 1}{k_2} \right) \quad (9)$$

where $P(0)$ represents the initial concentration of primary ions. A plot of \log_{10} (relative ion abundance) vs time for each of the ions in methyl chloride is shown in Fig. 11. The negative slope for the disappearance of CH_3Cl^+ gives $k_1 = 1.2 \times 10^{-9} \text{ cm}^3 \text{ molecule}^{-1} \text{ sec}^{-1}$. This compares favorably with values of $1.5 \times 10^{-9} \text{ cm}^3 \text{ molecule}^{-1}$

Figure 10

Typical trace of variation of ion intensity with time for ions observed in methyl chloride at 13.0 eV and 2.1×10^{-6} torr. Each trace represents a 5 minute scan. The observing oscillator was operated at 307 kHz and the magnetic field was varied to observe each resonance.

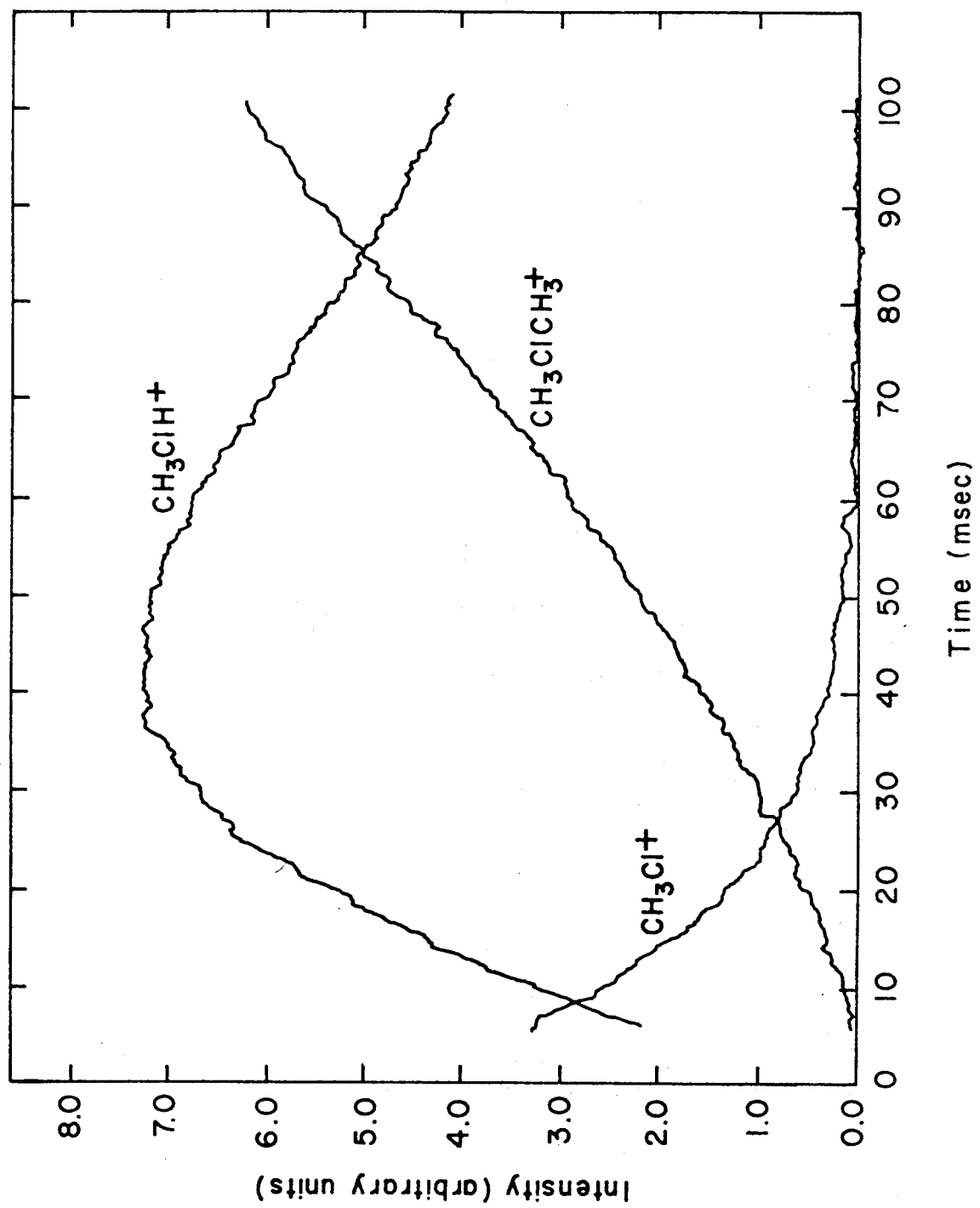
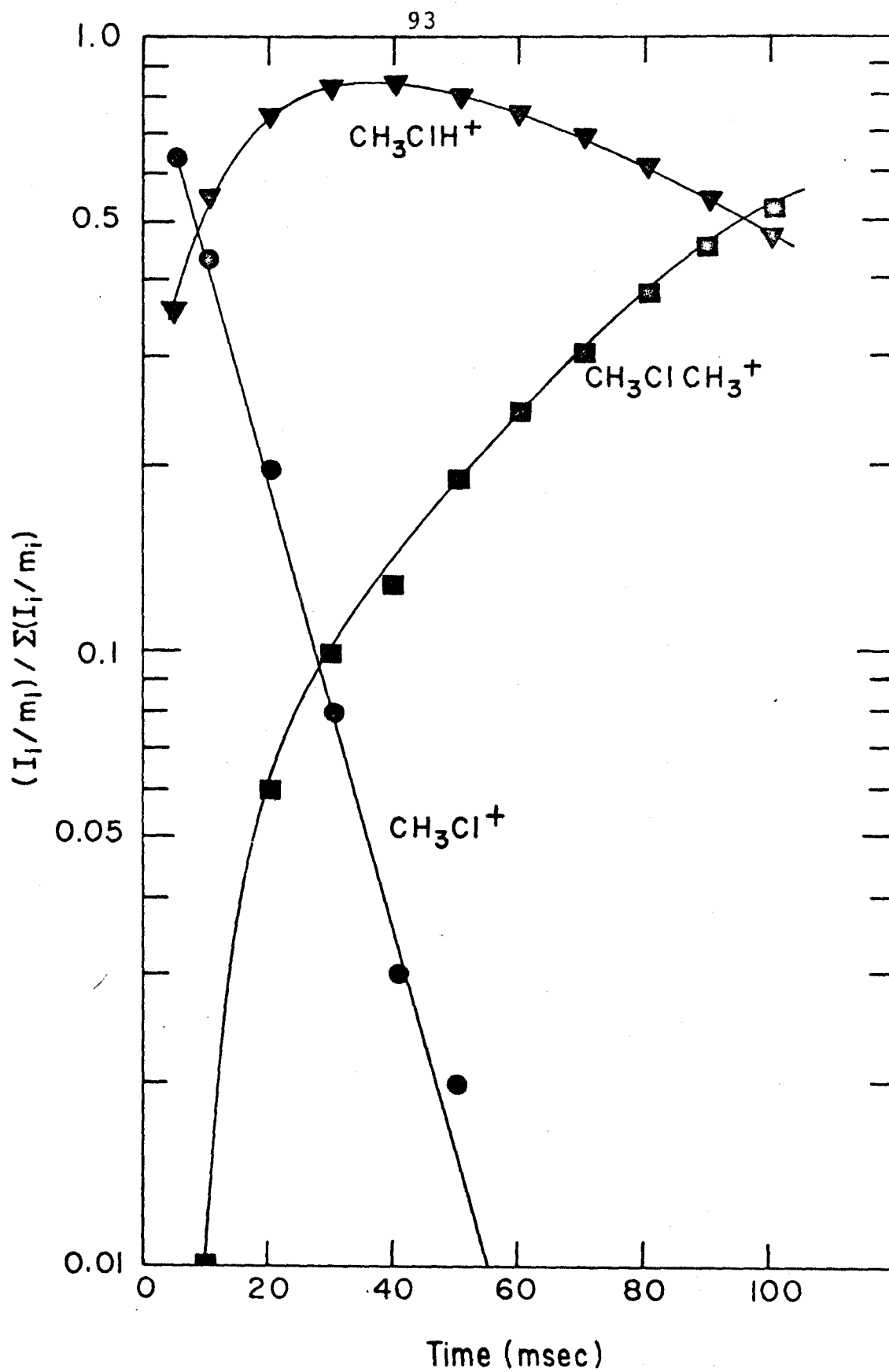


Figure 11

Plot of \log_{10} (relative ion abundance) vs. time for the three ions of the methyl chloride system.

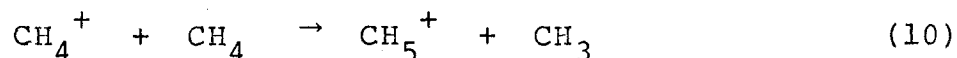


sec^{-1} obtained by Herod et al. (17), $1.94 \times 10^{-9} \text{ cm}^3$ molecule $^{-1} \text{ sec}^{-1}$ obtained by McAskill (18) and $1.25 \times 10^{-9} \text{ cm}^3$ molecule $^{-1} \text{ sec}^{-1}$ obtained by conventional ICR techniques (19). The rate constant for formation of the dimethyl chloronium ion was obtained from the limiting negative slope for the disappearance of CH_3ClH^+ . The value of $k_2 = 1.8 \times 10^{-10} \text{ cm}^3 \text{ molecule}^{-1} \text{ sec}^{-1}$ agrees well with the reported values of $1.0 \times 10^{-10} \text{ cm}^3 \text{ molecule}^{-1} \text{ sec}^{-1}$ of Herod et al. (17) and $1.4 \times 10^{-10} \text{ cm}^3 \text{ molecule}^{-1} \text{ sec}^{-1}$ of Beauchamp et al. (19).

F. Effect of Trapping Voltage on Rate Constants

To optimize ion trapping, it is often necessary to operate at relatively high trapping voltages, V_T . Ions moving in the trapping well produced by the trapping voltage will have varying degrees of kinetic energy depending on their point of formation along the electron beam axis. This varies from ion kinetic energies equal to $0.8868 V_T$ for ions formed near the trapping plates to $0.1132 V_T$ for ions formed at the center of the cell. As seen from the discussion of ion motion in the previous chapter, however, the effect of ion-neutral collisions is to translationally relax the ions so they reside very near the center of the cell. Since ion-molecule reactions have been shown theoretically and experimentally to depend on ion energy, it was deemed necessary to ascertain the effect of high trapping voltages on ion-molecule reaction rate constants.

In order to examine this effect, the well-documented rate constant for the reaction



was examined as the trapping voltage was varied (20-22).

The results of this study are illustrated graphically in Fig. 12. Determinations at both 16 eV and 70 eV yield a rate constant of $1.04 \times 10^{-9} \text{ cm}^3 \text{ molecule}^{-1} \text{ sec}^{-1}$.

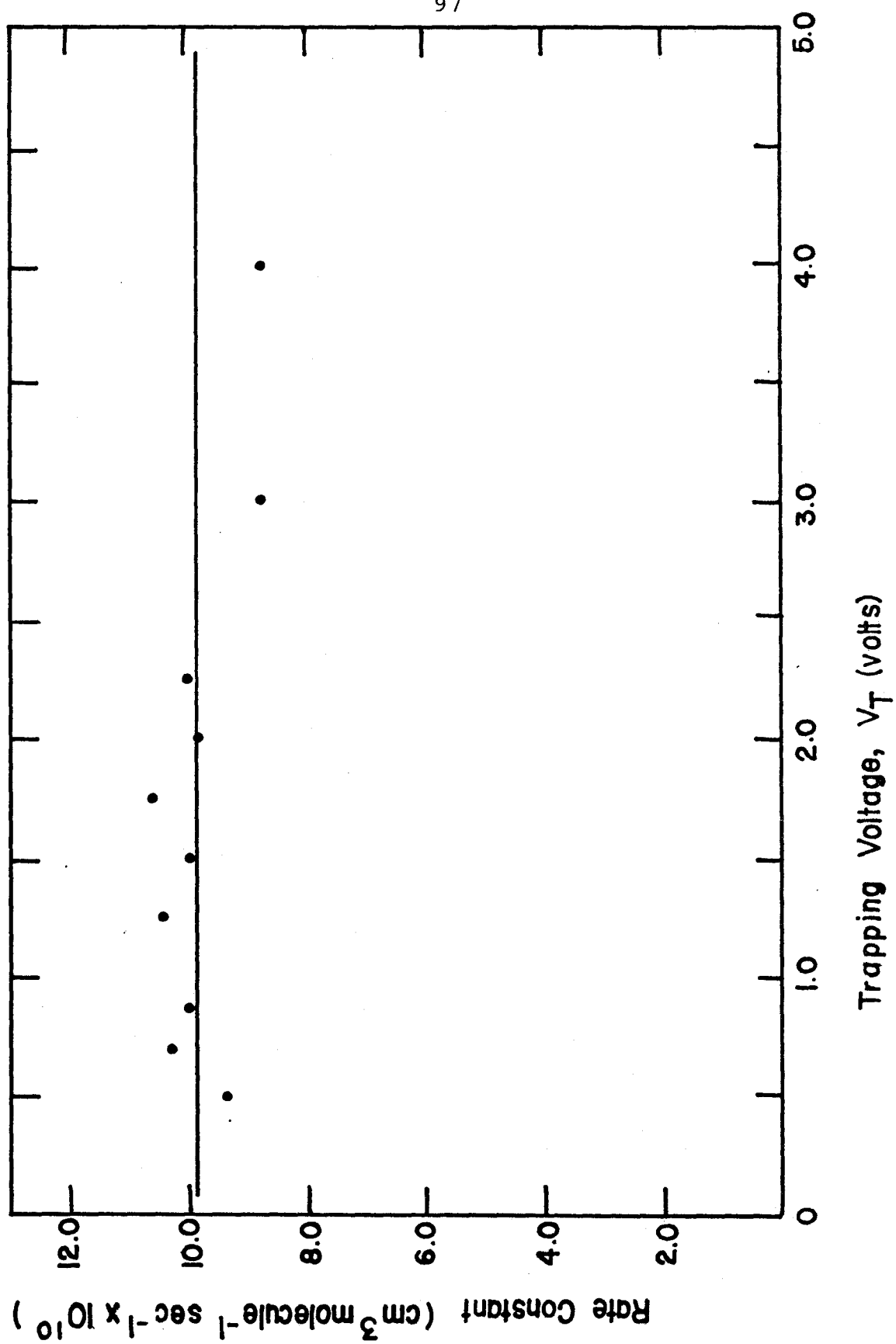
However, at higher trapping voltages the rate constant appears to fall off. It was characteristic of spectra taken at trapping voltages above 3.0 volts that primary ion intensities were abnormally low relative to secondary ion intensities. This can be explained in terms of ion losses for higher kinetic energy ions. It appears that primary ions formed with higher kinetic energies are trapped less efficiently and may be lost from the source region by striking the trapping plates before an ion-neutral collision occurs. However, upon collision with a neutral the ion kinetic energy may be partitioned between the ionic and neutral products. Thus, secondary ions formed have a lower kinetic energy and are trapped more efficiently, accounting for the anomalously high secondary to primary ion intensity ratio at short times. Hence the lower rate constants at higher trapping voltages may be attributed to a differential ion loss factor rather than a rate variation with ion kinetic energy. Since most trapped ion experiments are carried out with trapping voltages between

Figure 12

Variation of rate constant with trapping voltage for the ion-molecule reaction



determined by the ICR trapped ion technique described in this thesis.



0.5 and 2.5 volts, rate constants determined in this manner should be fairly accurate. This is verified by the excellent agreement between the rate constant for reaction (10) determined by trapped-ion ICR at lower trapping voltages and literature data.

G. Error Limits on Rate Constants

Uncertainties in rate constant measurements by the trapped ion cyclotron resonance technique are largely due to uncertainties in pressure measurements. Unless otherwise indicated, all rate constants quoted in this thesis may be assumed to be accurate to $\pm 10\%$.

REFERENCES

1. V-5900 ICR mass spectrometer, Varian Associates.
2. Fairchild Linear Integrated Circuits, A-741 Operational Amplifier.
3. Fairchild Linear Integrated Circuits, A-710 Voltage Comparator.
4. Fairchild Linear Integrated Circuits, A-9601 Mono-stable Multivibrator.
5. J. D. Jackson, Classical Electrodynamics (Wiley, New York, 1962).
6. T. C. O'Haver, Chem. Instrumentation 3, 1 (1971).
7. L. R. Anders, J. Phys. Chem. 73, 469 (1969).
8. R. P. Clow and J. H. Futrell, Int. J. Mass. Spectrom. Ion Phys. 4, 165 (1970).
9. W. T. Huntress, Jr., M. M. Mosesman, and D. D. Elleman, J. Chem. Phys. 54, 843 (1971).
10. This thesis, chapters 4, 5, 6.
11. M. K. S. Instruments, Baratron Capacitance Manometer, Lexington, Massachusetts.
12. F. Rosebury, Handbook of Electron Tube and Vacuum Techniques, Addison Wesley, Reading, Mass. (1965).
13. G. J. Schulz and A. V. Phelps, Rev. Sci. Instrum. 28, 1051 (1957).
14. R. Chapman, Rev. Sci. Instrum. 43, 1536 (1972).
15. S. E. Buttrill, Jr., J. Chem. Phys. 50, 4125 (1969).

16. J. L. Beauchamp, Ph.D. Thesis, Harvard University, 1968.
17. A. A. Herod, A. G. Harrison and N. A. McAskill, Can. J. Chem. 49, 2217 (1971).
18. N. A. McAskill, Aust. J. Chem. 22, 2275 (1969).
19. J. L. Beauchamp, D. Holtz, S. D. Woodgate and S. L. Patt, J. Amer. Chem. Soc. 94, 2798 (1972).
20. N. A. McAskill, Aust. J. Chem. 22, 2267 (1969).
21. A. A. Herod and A. G. Harrison, Int. J. Mass Spectrom. Ion Phys. 4, 415 (1970).
22. F. H. Field, J. L. Franklin and M. S. B. Munson, J. Amer. Chem. Soc. 85, 3575 (1963).

CHAPTER IV

Trapped Ion Cyclotron Resonance Studies of Symmetric Charge and Proton Transfer Processes

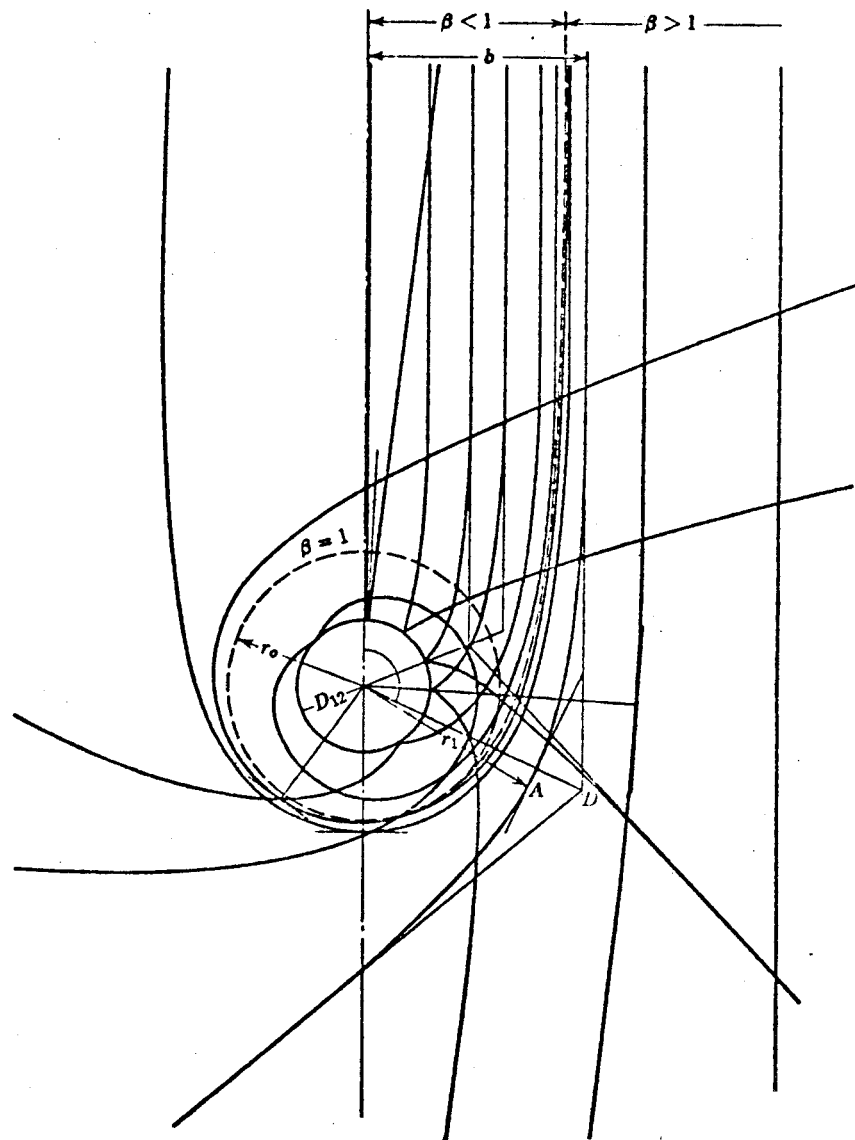
A. Molecular Resonant Charge Transfer

Symmetric charge exchange reactions involving atomic ions and atoms have been the subject of much theoretical interest since it is possible to treat them quantum mechanically with some degree of rigor (1-3). Similar theoretical calculations on molecular charge transfer have been few due to difficulties in accurately describing complex systems using existing quantum mechanical techniques.

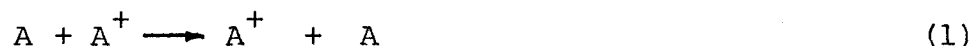
Rapp and Francis (1) have separated charge exchange between gaseous ions and neutrals into three categories of ion velocity according to the theoretical model most suitable for its characterization. At very high ion velocities ($v > 10^8$ cm/sec) the Born-Oppenheimer approximation breaks down since nuclear motion is no longer slow compared to electronic motion. This region has been the subject of very little theoretical treatment. Considerably more attention has been directed to the intermediate velocity range where the semi-classical impact parameter method may be applied. This method assumes a rectilinear trajectory, such as that shown in Fig. 1, in which charge transfer occurs at large impact parameter with little or no transfer of momentum (3).

Figure 1

Diagram of rectilinear trajectory for charge transfer. The neutral molecule is located at a fixed distance R_0 from the x axis. The ion moves along the x axis from $x = -\infty$ to $x = +\infty$.



The resonant charge transfer process may be represented by the equation



where the initial state of the system having a wavefunction ψ_i , and the final state of the system, ψ_f , correspond to the left and right sides of equation (1) with the ion and neutral at infinite separation. The total wavefunction for the system is then given by

$$\Psi = (c_i \psi_i + c_f \psi_f) \exp \left[\frac{-Et}{\hbar} \right] \quad (2)$$

where c_i and c_f are constants which are functions of time, t , and E is the total energy of the system exclusive of the relative motion of the ion and molecule.

The probability of charge exchange taking place during a collision may be derived from the method of perturbed stationary states which is based on consideration of an A_2^+ system as a one electron problem (2,3). The A_2^+ system is assumed to have two degenerate states of energy, E , which are split into symmetric and antisymmetric stationary states of energy ϵ_s and ϵ_a , respectively, by the relative motion of the ion and molecule. Charge transfer is then interpreted to arise from a phase interference between the symmetric and antisymmetric stationary states and the probability of charge transfer in a given collision with relative velocity, v , and impact parameter b is given by (1)

$$P(b,v) = \sin^2 \left[\int_{-\infty}^{\infty} \frac{(\epsilon_a - \epsilon_s) dx}{2\hbar v} \right] \quad (3)$$

The corresponding cross section may then be calculated from

$$\sigma(v) = 2\pi \int_0^{\infty} P(b,v) b db \quad (4)$$

An exact calculation of σ depends only upon $(\epsilon_a - \epsilon_s)$ along the trajectory, which must be calculated from a quantum mechanical description of the system. The \sin^2 dependence causes the probability function to oscillate rapidly between 0 and 1 with disappearance of the oscillations occurring as the impact parameter is increased. This oscillatory behavior corresponds to a rapid electron transfer between the nuclei. In the region of oscillation the probability function is taken to be 0.5 (3).

Accurate quantum mechanical calculations have been carried out only for the $H^+ + H$ system(4), although fairly detailed calculations have been carried out for $He^+ + He$ (5) and for resonant and non-resonant charge transfer between alkali ions and atoms (6). For more complex systems, calculations are very difficult and approximate methods using Slater orbitals (3), hydrogenic orbitals (7) and semi-empirical orbitals (8) have been used.

Gurnee and Magee (3) have treated diatomic species in resonance using Heitler London electronic wavefunctions constructed from normalized one electron wavefunctions having the Slater nodeless form

$$\psi = N r^{n-1} e^{-\alpha r} \quad (5)$$

This function satisfies the wave equation for large values of r if α is taken to be $(2I)^{1/2}$ where I is the ionization

potential in atomic units. At sufficiently large r , the shielding by other electrons is complete enough that the hydrogenic description is accurate. At smaller distances the shielding is not complete and larger effective values of α are necessary.

Based on the use of a screening constant for atomic nitrogen, Leventhal, Moran and Friedman (9) used $\alpha = 1.95$ in a calculation of charge exchange in N_2 rather than the value of 1.2 obtained from $\alpha = (2I)^{1/2}$. Using this larger value of α they carried out a calculation similar to that of Gurnee and Magee (3) and obtained a velocity dependent charge transfer cross section in good agreement with experimental data.

The above methods apply only to ion velocities for which the impact parameter approximation holds. At low ion velocities the ion trajectories can no longer be assumed to be rectilinear with constant velocity since ion induced dipole and ion dipole attractive forces result in curved trajectories. In order to continue to use a semi-classical approach these curved trajectories must be included in calculations of charge transfer probabilities. At very large impact parameters the trajectories will continue to be approximately rectilinear. However, as the initial impact parameter is reduced the trajectories will become noticeably curved, until inside some critical impact parameter, b_0 , reflection at the repulsive wall of the ion-molecule potential

will occur. Such a family of trajectories is shown in Fig. 2. In the Langevin model for ion-molecule reaction (10,11) it is assumed that all trajectories with impact parameter less than b_0 lead to ion-molecule reaction. In this case the cross section for ion-molecule reaction is given by

$$\sigma(v) = \frac{2\pi e}{v} \left(\frac{\alpha}{\mu}\right)^{\frac{1}{2}} \quad (6)$$

where e is the charge of the ion, α is the polarizability of the neutral molecule and μ is the reduced mass of the ion-molecule pair. In cases where the molecule has a permanent dipole moment, μ_D , the cross section has been represented by a number of investigators (12,13) as

$$\sigma(v) = \frac{2\pi e}{v} \left(\frac{\alpha}{\mu}\right)^{\frac{1}{2}} + \frac{2\pi e \mu_D \cos \theta}{v^2} \quad (7)$$

where θ is the angle between the dipole moment vector and the velocity vector of the projectile ion.

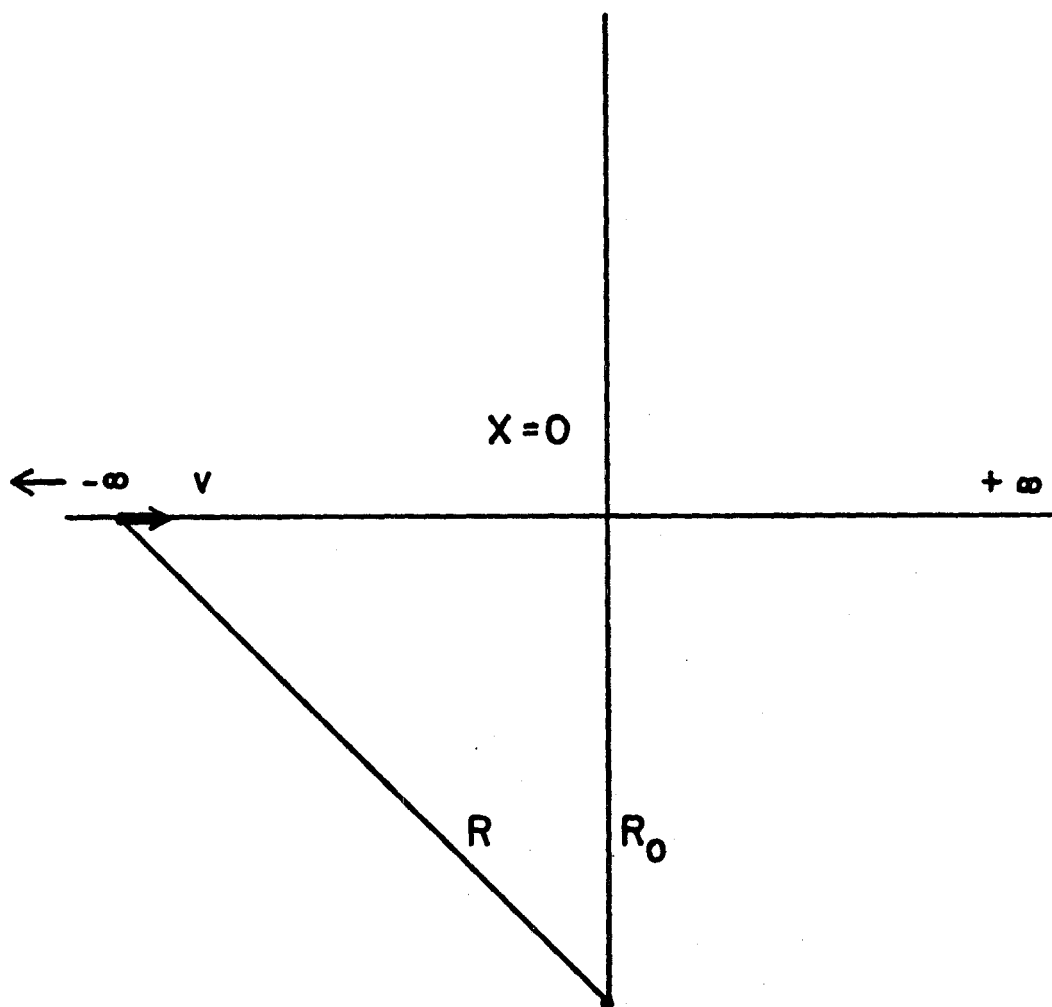
Rapp and Francis (1) have designated the region of thermal ion velocities as a transition zone where both rectilinear and Langevin trajectories must be considered. In this case the mean ion velocity is given by (14)

$$v = \left(\frac{8kT}{\pi m}\right)^{\frac{1}{2}} \quad (8)$$

It has been well established that ions in ICR experiments have near thermal velocities (15) and hence charge exchange must be considered to take place both within and outside the orbiting impact parameter, b_0 . If a Langevin collision complex is indeed formed in a symmetric charge exchange

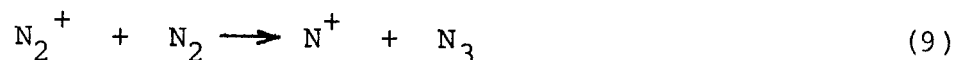
Figure 2

Family of trajectories as a function of impact parameter b ,
for the Langevin ion-induced dipole, $1/r^4$ potential.



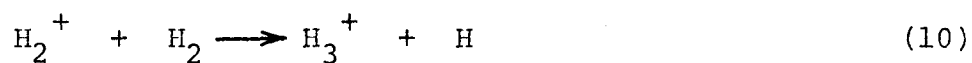
reaction there will be two thermodynamically equivalent channels available for dissociation. Thus in each collision there will be a probability of one-half that an electron transfer will occur. As was pointed out previously, for rectilinear encounters the probability of charge exchange oscillates as a function of impact parameter and the average charge transfer probability is one-half. Hence, for either mechanism the symmetric charge exchange rate will be one-half the collision rate in the absence of other reaction channels.

Leventhal, Moran and Friedman (9) have obtained interesting results in the case where ion-molecule reaction and symmetric charge exchange can both occur. In a study of symmetric charge exchange in N_2 a sharp rise in charge transfer cross section was observed at ion energies below 10 eV. The behavior was attributed to the fact that at higher ion energies the ion-molecule reaction



may occur (16). This reaction is endothermic for ground state N_2^+ and requires that ion kinetic energy take part in the reaction. Thus at low ion energies the only reaction channel is symmetric charge exchange.

Quite a different situation was observed in H_2 (9). At low ion energies the charge transfer cross section is observed to fall off as a result of the increase in cross section for the exothermic ion-molecule reaction



These results imply that at low ion energies resonant charge exchange does not compete favorably with exothermic ion-molecule reaction inside the critical impact parameter. However, long range charge transfer does continue to occur.

Hence, in ICR experiments contributions to the symmetric charge exchange cross section from large impact parameters must be considered when other ion-molecule processes occur as well as when resonant charge exchange is the only reaction channel. Both cases are treated in this chapter.

B. Symmetric Charge Exchange Reactions

1. Nitrogen, Carbon Monoxide and Carbon Dioxide

At thermal ion energies the parent molecular ions of N_2 , CO and CO_2 exhibit no ion-molecule reactions other than symmetric charge exchange. Using isotopically labelled molecules and ion ejection techniques in the trapped ion mode of operation the kinetics of symmetric charge exchange reactions of the form



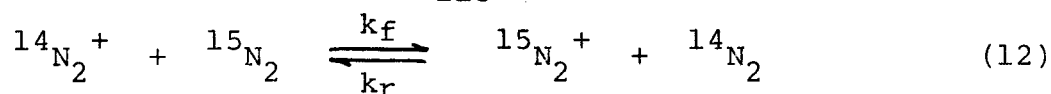
where A and A^1 differ only by isotopic substitution, may be readily examined.

A typical experiment is that carried out for a mixture of $^{14}\text{N}_2$ and $^{15}\text{N}_2$. The forward (k_f) and reverse (k_r) rate constants of reaction 12 may be measured using an ion ejection technique.

TABLE 1

Typical Ejection Times for Some Combinations
of Magnetic Field and Double Resonance Oscillator Level

H (kGauss)	E_{rf} (mV)	τ_{ej} (msec)
10	2	64
10	20	6.4
10	200	0.64
5	2	32
5	20	3.2
5	200	0.32



For the duration of the trapped ion timing sequence an irradiating radiofrequency field is applied to the trapping region of the ICR cell at the cyclotron frequency of one of the isotopic nitrogen ions. As a result, these ions are continuously removed in a time short compared to the time between collisions. The time necessary for ejection of ions is given by

$$\tau = \frac{2rH}{E_{rf}} \quad (13)$$

where H is the magnetic field strength, E_{rf} is the applied irradiating voltage and r is the cyclotron radius at which ejection occurs, in this case 0.635 cm. The ejection times τ are shown in Table 1 for a number of values of H and E_{rf} . Usually an ejection field of 200 mV was used to insure ejection in less than 1 msec.

Ejection of one of the ions forces reaction 12 to proceed in only one direction and an exponential decay of the unejected ion is observed as it reacts to form the isotopic counterpart which is ejected. The abundance of $^{15}\text{N}_2^+$ with and without ejection of $^{14}\text{N}_2^+$ is shown in Fig. 3 for a mixture of $^{14}\text{N}_2$ and $^{15}\text{N}_2$. A simple kinetic analysis yields the expressions

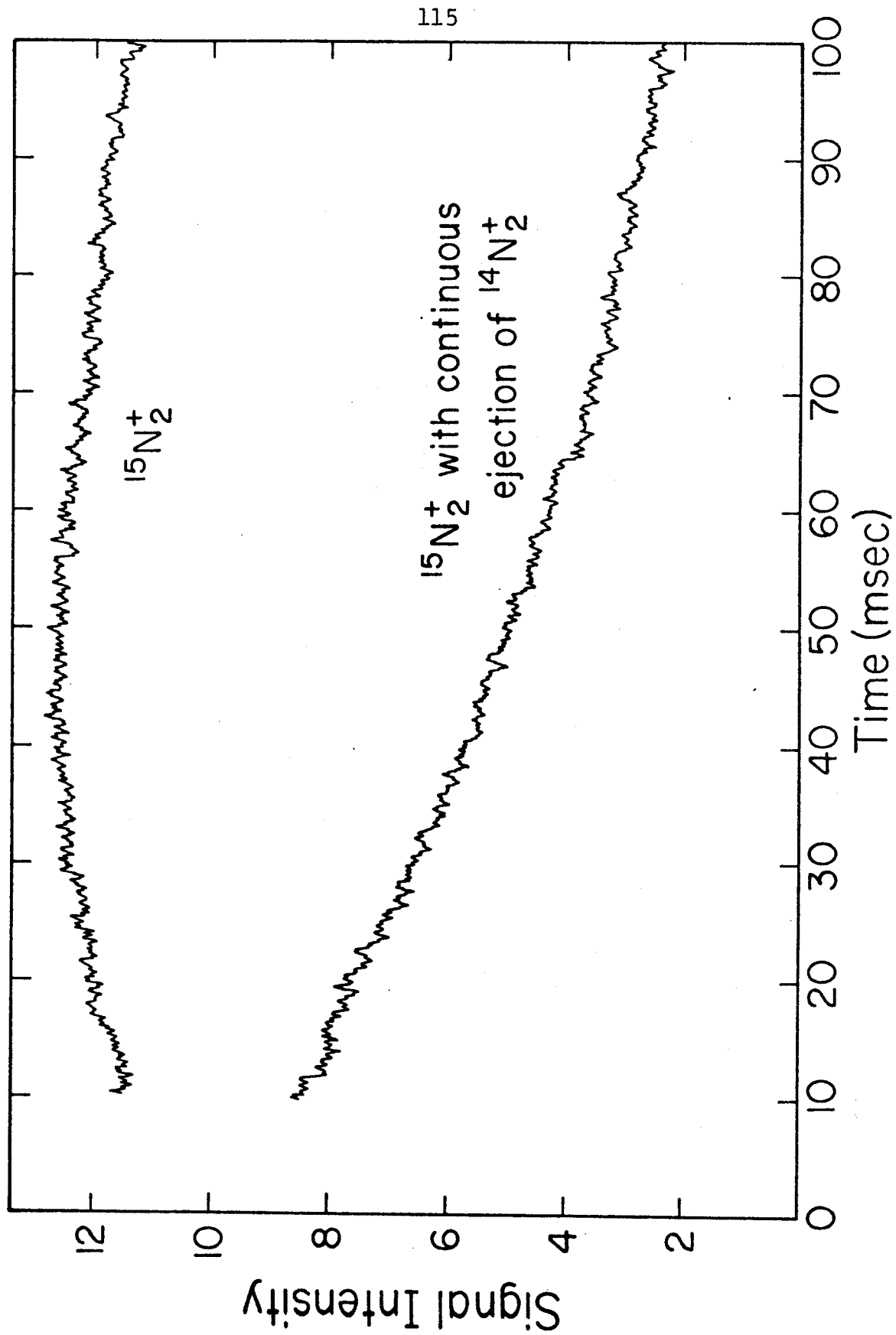
$$[^{14}\text{N}_2^+]_{ej} = [^{14}\text{N}_2^+]_0 e^{-^{15}\text{N}_2 k_f t} \quad (14a)$$

$$[^{15}\text{N}_2^+]_{ej} = [^{15}\text{N}_2^+]_0 e^{-^{14}\text{N}_2 k_f t} \quad (14b)$$

where the subscripts ej and 0 indicate the ion intensity

Figure 3

Typical trace of variation of ion intensity with time for the $^{15}\text{N}_2^+$ ion with and without continuous ejection of $^{14}\text{N}_2^+$. Ions were formed in 5 msec, 70 eV electron beam pulse, in a 1.4:1 mixture of $^{15}\text{N}_2$ and $^{14}\text{N}_2$ and a total pressure of 1.25×10^{-6} torr.



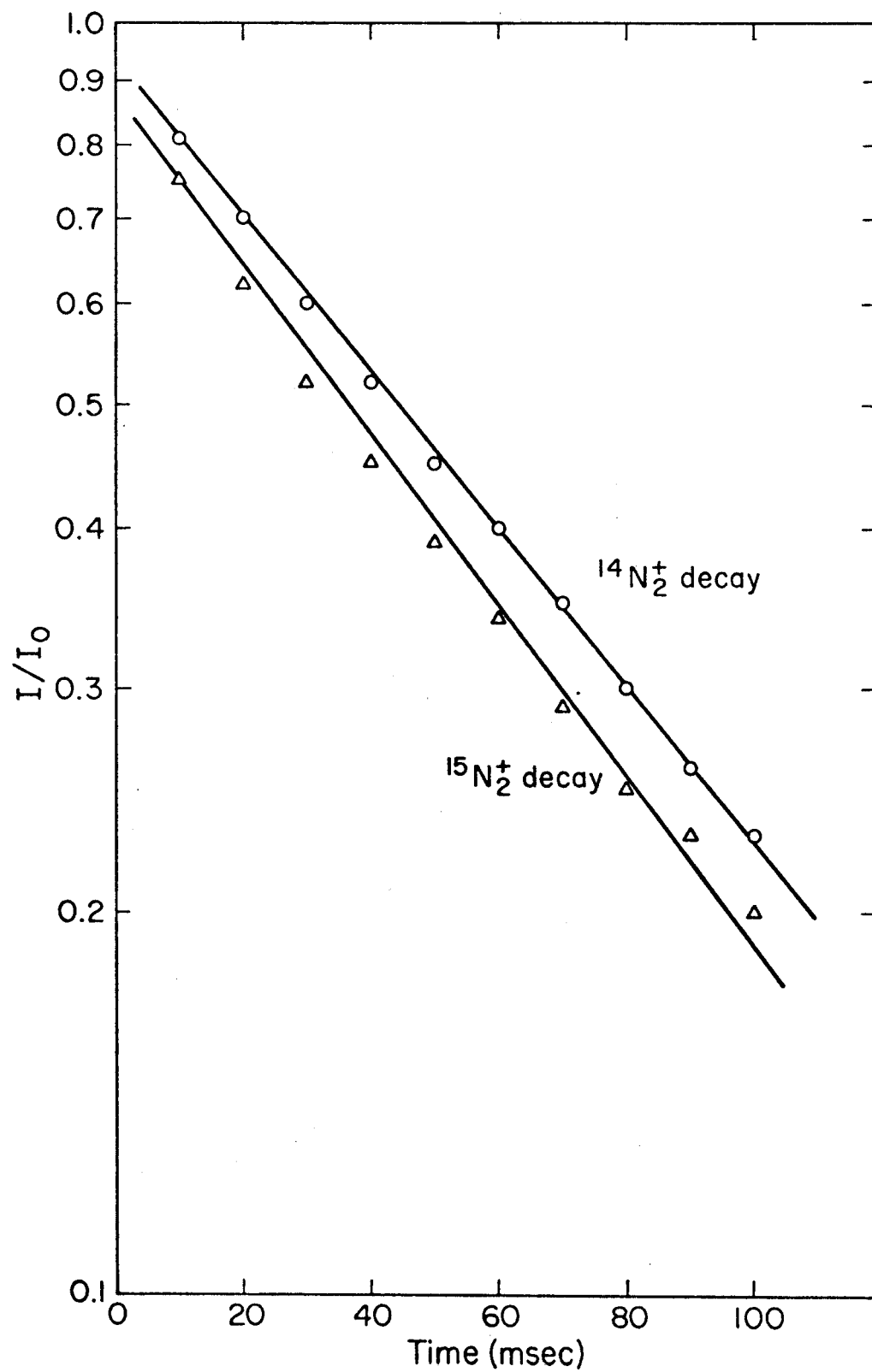
with and without the ejection field. Plots of $\log(I_{ej}^+/I_0^+)$ vs time are shown in Fig. 4 and exhibit the linear behavior expected from equation 14. The slopes of these plots are readily related to the rate constants and a number of replicate determinations give rate constants of $k_f = 6.2 \times 10^{-10} \text{ cm}^3 \text{ molecule}^{-1} \text{ sec}^{-1}$ and $k_r = 7.1 \times 10^{-10} \text{ cm}^3 \text{ molecule}^{-1} \text{ sec}^{-1}$. Intuitively it would be expected that $k_f = k_r$. While the difference in rate constants is well within experimental error it was reproducible with the reverse reaction exhibiting a larger rate constant in every determination. An analysis showed that the difference is not due to differences in nuclear spin degeneracies or differences in zero point energies for the isotopic ions and neutrals.

Taking an average rate constant for charge exchange of $6.65 \times 10^{-10} \text{ cm}^3 \text{ molecule}^{-1} \text{ sec}^{-1}$ an encounter rate of $1.3 \times 10^{-9} \text{ cm}^3 \text{ molecule}^{-1} \text{ sec}^{-1}$ is obtained. This is considerably in excess of the Langevin encounter rate of $8.2 \times 10^{-10} \text{ cm}^3 \text{ molecule}^{-1} \text{ sec}^{-1}$ and strongly suggests that electron transfer is occurring well outside the orbiting impact parameter.

Using a tandem isotope separator mass spectrometer Leventhal, Moran and Friedman (9) obtained a cross section of 39 \AA^2 for charge exchange between 1 eV $^{14}\text{N}_2^+$ ions and $^{15}\text{N}_2$. This value yields a rate constant for charge exchange of $7.0 \times 10^{-10} \text{ cm}^3 \text{ molecule}^{-1} \text{ sec}^{-1}$, in excellent agreement with the value obtained in this work.

Figure 4

Plot of $\log_{10} (I/I_0)$ vs. time for each of the isotopic nitrogen ions. Conditions are the same as those in Figure 3.



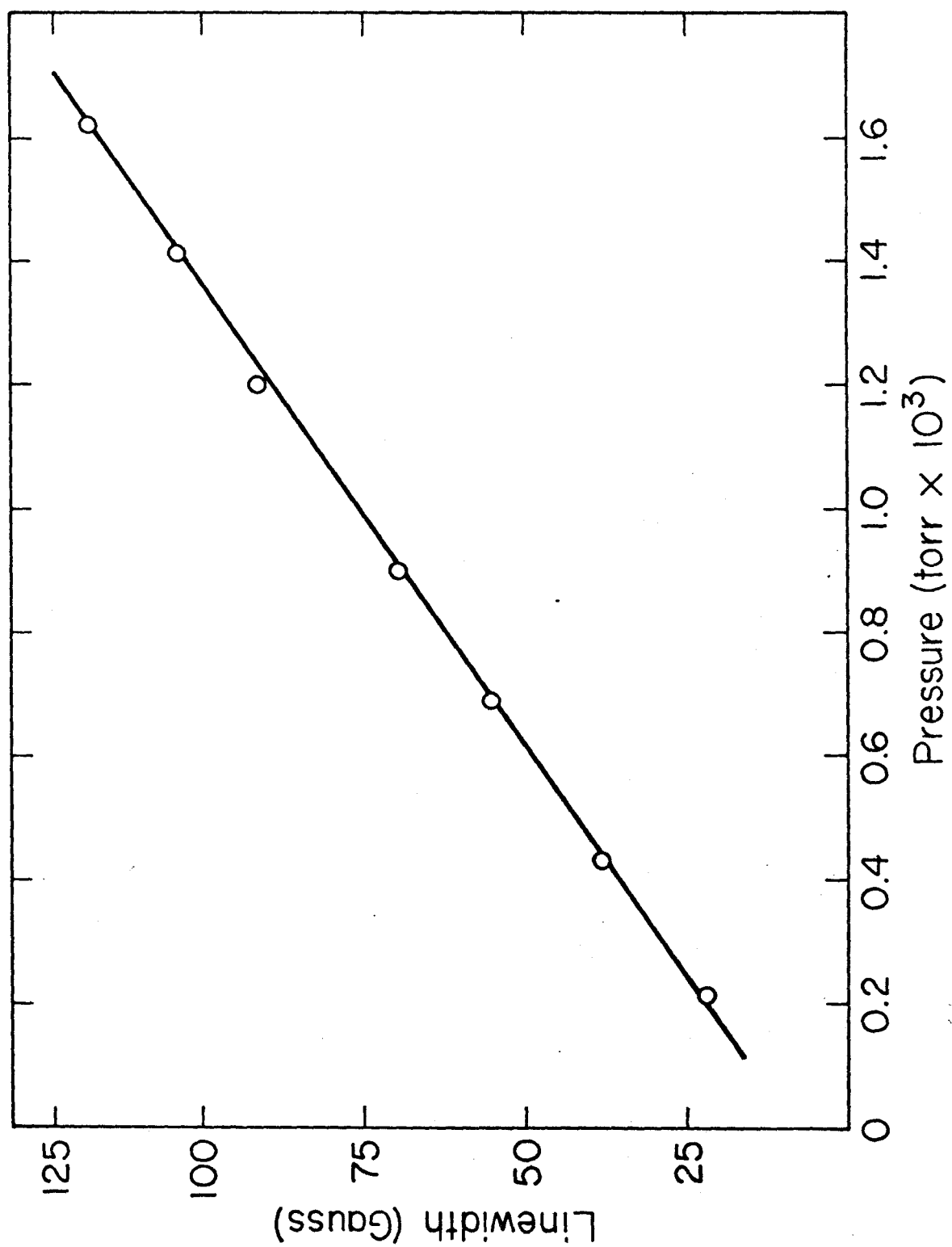
Other experimental evidence indicating that long range electron transfer is occurring in nitrogen has been obtained from an ICR study of momentum transfer. At pressures above approximately 5×10^{-5} torr the ICR linewidth varies linearly with pressure (17,18). The momentum transfer collision frequency for elastic collisions is given by (19)

$$\gamma = \frac{nm}{(m + M)} \langle v \sigma_d(v) \rangle \quad (15)$$

where n and M are the number density and mass of the neutral, m is the mass of the ion, and $\sigma_d(v)$ and v are the diffusion cross section and relative velocity of the ion-neutral pair. The brackets indicate an average over the distribution of relative velocities. It can be shown that the halfwidth at half height of the ICR peak is equal to γ (17). A plot of linewidth vs pressure for N_2^+ in N_2 is shown in Fig. 5 from which a momentum transfer collision frequency of $7.2 \times 10^{-10} \text{ cm}^3 \text{ molecule}^{-1} \text{ sec}^{-1}$ is obtained (Buttrill (20) has also carried out this experiment and obtained a value of $7.4 \times 10^{-10} \text{ cm}^3 \text{ molecule}^{-1} \text{ sec}^{-1}$). In the case that the ion and neutral masses are equal the encounter rate is twice the momentum transfer collision frequency. An electron transfer event in which no kinetic energy is transferred represents a very efficient means of momentum transfer. Hence the momentum transfer collision frequency also reflects the symmetric charge exchange rate. Huntress has also measured the momentum transfer collision frequency by a

Figure 5

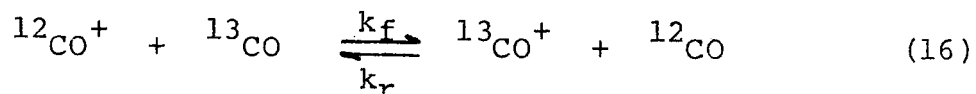
Plot of fullwidth at half maximum for $^{14}\text{N}_2^+$ peaks as a function of pressure.



method in which the instantaneous power absorption is monitored at resonance as ions enter the resonance region of the ICR cell (21). He obtained a value of $6.7 \times 10^{-10} \text{ cm}^3 \text{ molecule}^{-1} \text{ sec}^{-1}$ in good agreement with the linewidth determination and the measurement of the charge exchange rate.

These results all verify the occurrence of a long range charge exchange mechanism for nitrogen. This fact has important thermochemical consequences since no kinetic energy is transferred in this reaction and as such provides an efficient means for de-exciting translationally hot nitrogen ions. In order to test the generality of this mechanism similar experiments were carried out in carbon monoxide and carbon dioxide. At thermal ion energies the molecular ions of these molecules show no reaction with the parent neutral other than symmetric charge exchange.

The symmetric charge exchange process in carbon monoxide was examined in the reaction



The ion ejection technique was used to observe the rate of decay of one of the isotopic ions as the other was continuously ejected. This is illustrated in Fig. 6 for $^{12}\text{CO}^+$ with and without ejection of $^{13}\text{CO}^+$. Plots of $(I_{\text{ej}}^+/I_{\text{o}}^+)$ vs time for the two ions in this system are shown in Fig. 7. These data yield a rate constant of $4.1 \times 10^{-10} \text{ cm}^3$

Figure 6

Trace of variation of ion intensity with time for $^{12}\text{CO}^+$ with and without continuous ejection of $^{13}\text{CO}^+$. Ions were formed by a 5 msec, 70 eV electron beam pulse in a 3.5:1 mixture of ^{12}CO and ^{13}CO and a total pressure of 2.5×10^{-6} torr.

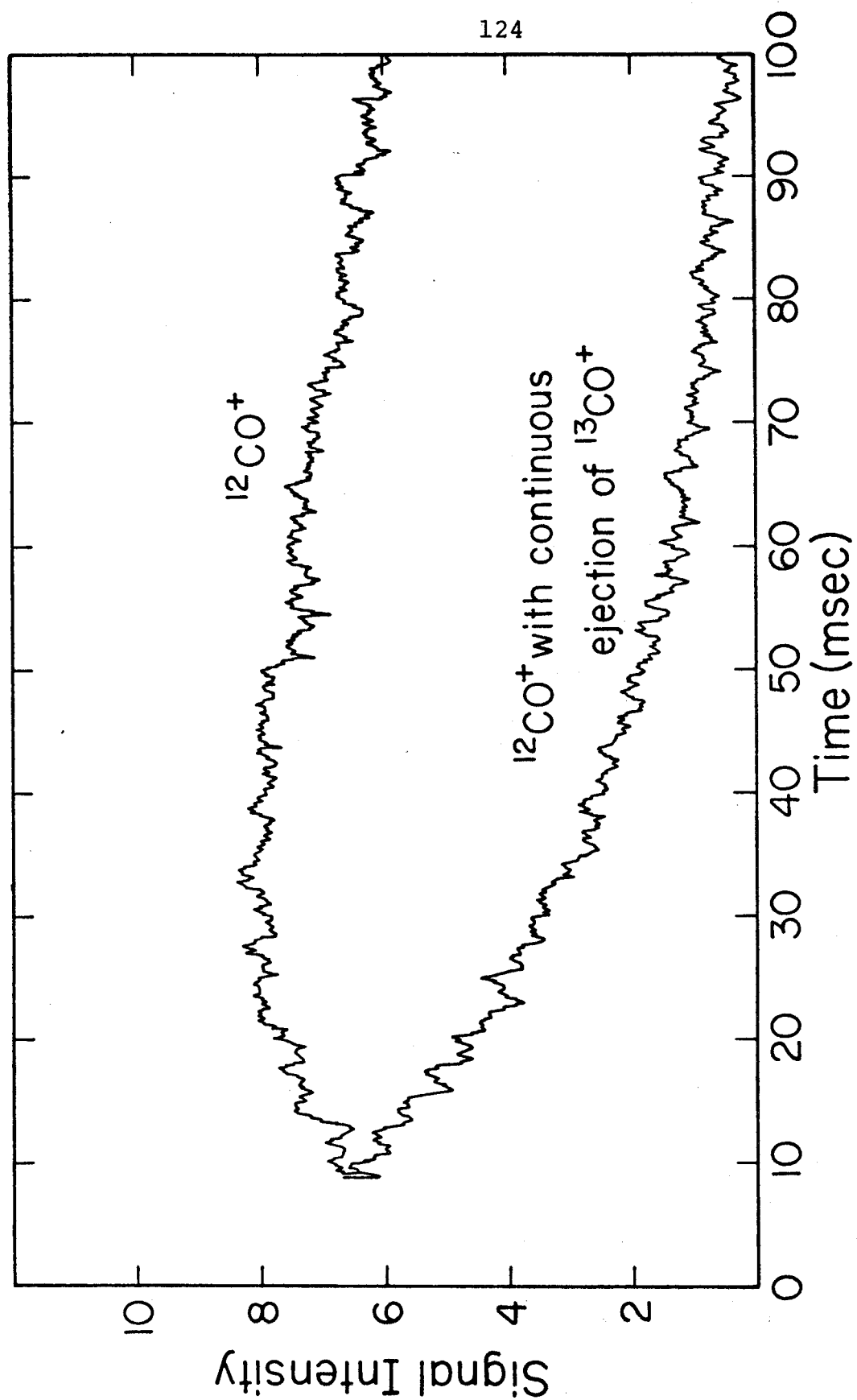
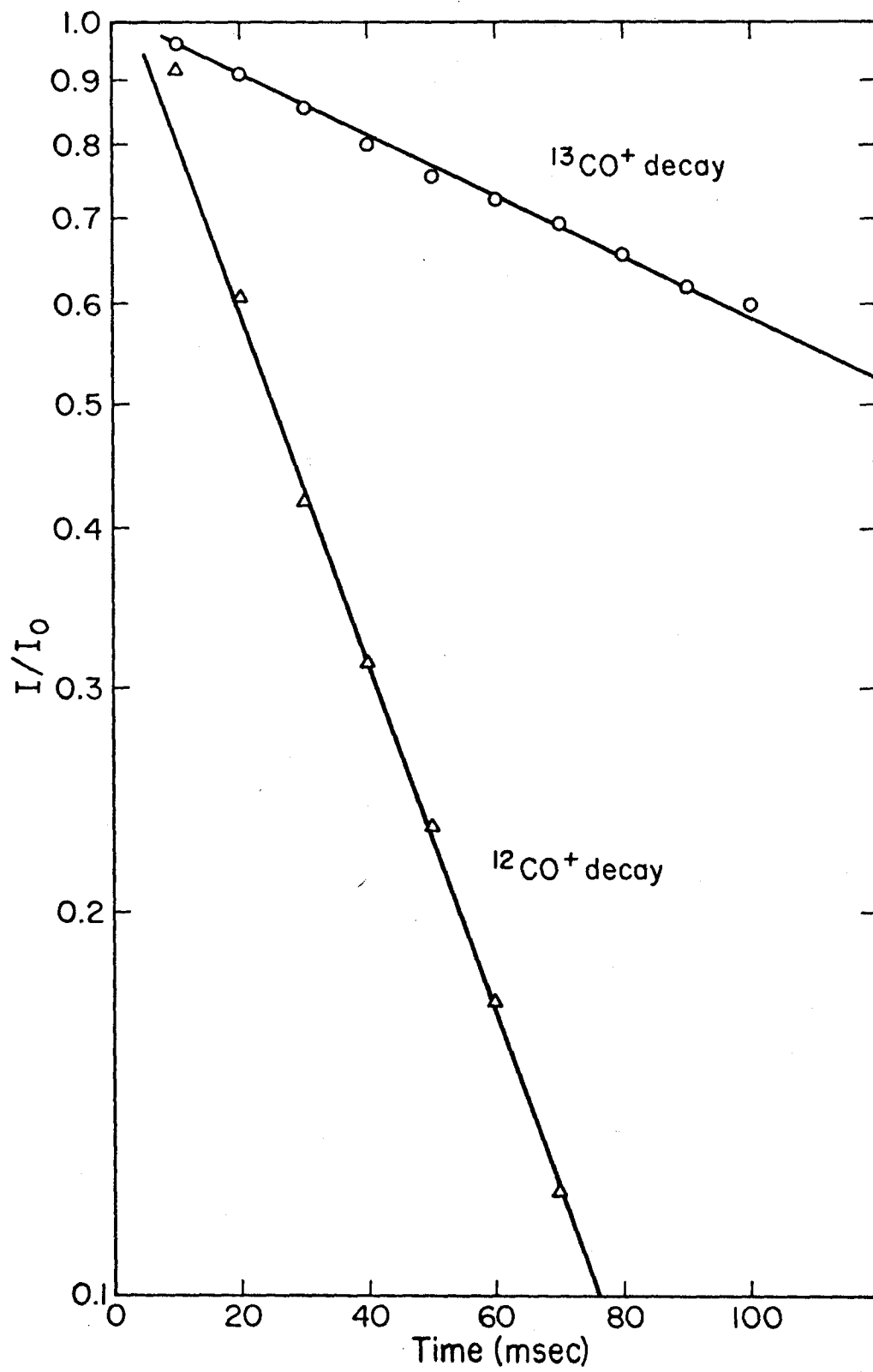


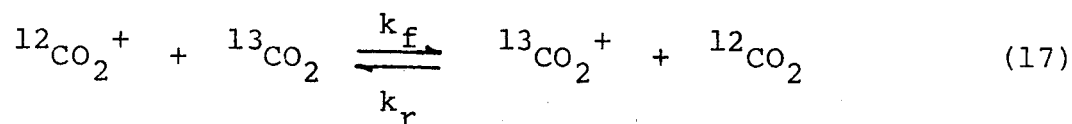
Figure 7

Plot of $\log_{10} (I/I_0)$ vs. time for each of the isotopic carbon monoxide ions. Conditions are the same as those in Figure 6.



molecule⁻¹ sec⁻¹ for symmetric charge exchange in CO with the forward and reverse reactions being equal in this case.

In similar fashion the charge exchange rate in CO₂ was determined from the reaction



As shown in Fig. 8 continuous ejection of ¹²CO₂⁺ results in exponential decay of ¹³CO₂⁺ with time. The appropriate plots of log(I_{ej}⁺/I₀⁺) vs time for ¹²CO₂⁺ and ¹³CO₂⁺ are shown in Fig. 9. From these plots a rate constant of 3.7 x 10⁻¹⁰ cm³ molecule⁻¹ sec⁻¹ is obtained for both forward and reverse reactions.

It can be seen that symmetric charge exchange in CO and CO₂ is slower than that in N₂. In Table 2 the experimental encounter rates for these molecules are compared to those calculated from the Langevin model based on the angle averaged, parallel and perpendicular polarizabilities (22). It can be seen that the experimental nitrogen value is well in excess of the maximum value predicted from the parallel polarizability of nitrogen, indicating that long range electron transfer must be taking place. However, the carbon monoxide and carbon dioxide results correlate fairly well with the values predicted from the angle averaged polarizabilities. This indicates that symmetric charge exchange in CO and CO₂ may not be occurring via a long range

Figure 8

Trace of variation of ion intensity with time for $^{13}\text{CO}_2^+$ with and without continuous ejection of $^{12}\text{CO}_2^+$. Ions were formed by a 5 msec, 70 eV electron beam pulse in a 1.5:1 mixture of $^{13}\text{CO}_2$ and $^{12}\text{CO}_2$ and a total pressure of 8×10^{-7} torr.

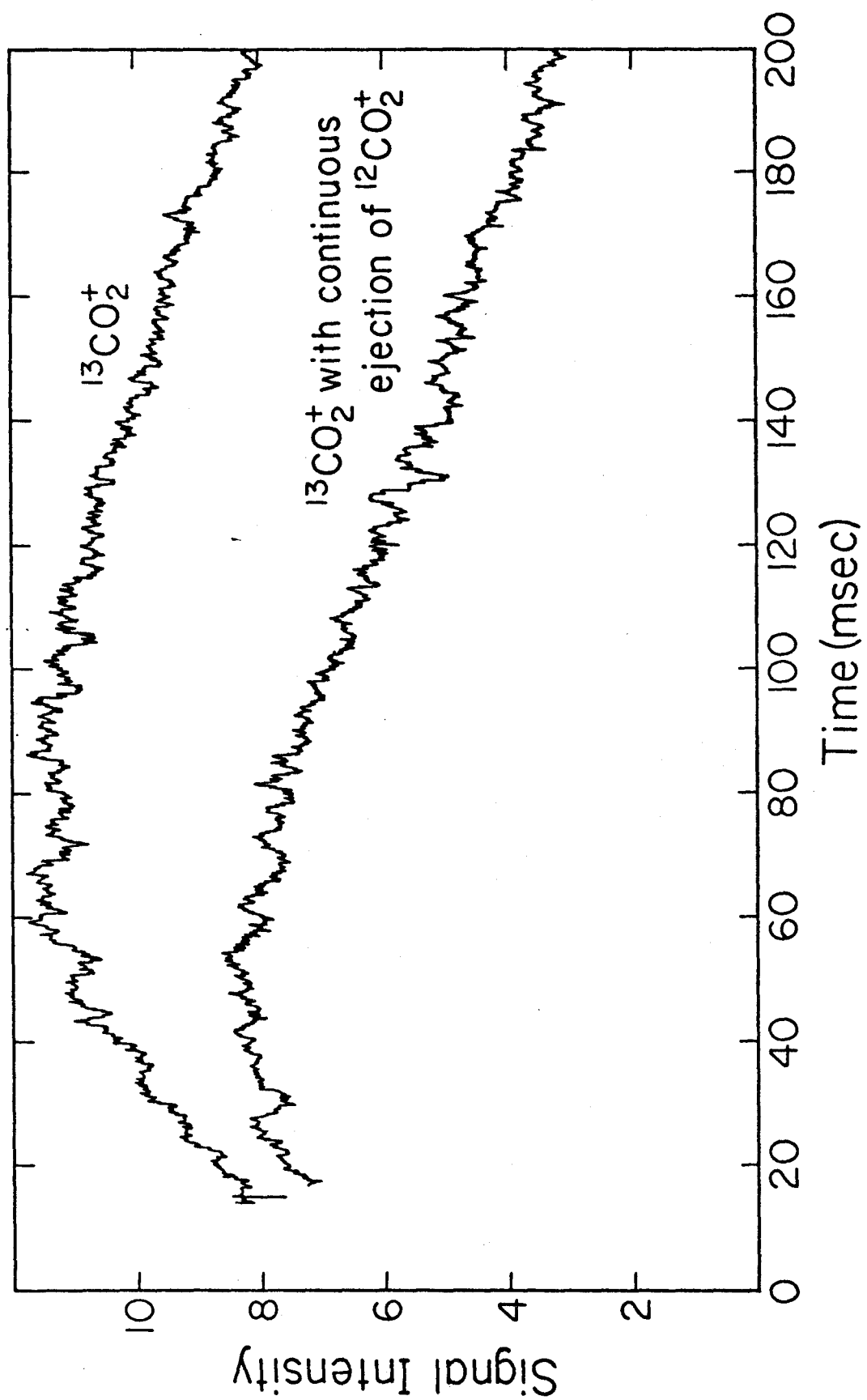


Figure 9

Plot of $\log_{10} (I/I_0)$ vs. time for each of the isotopic carbon dioxide ions. Conditions are the same as those in Figure 8.

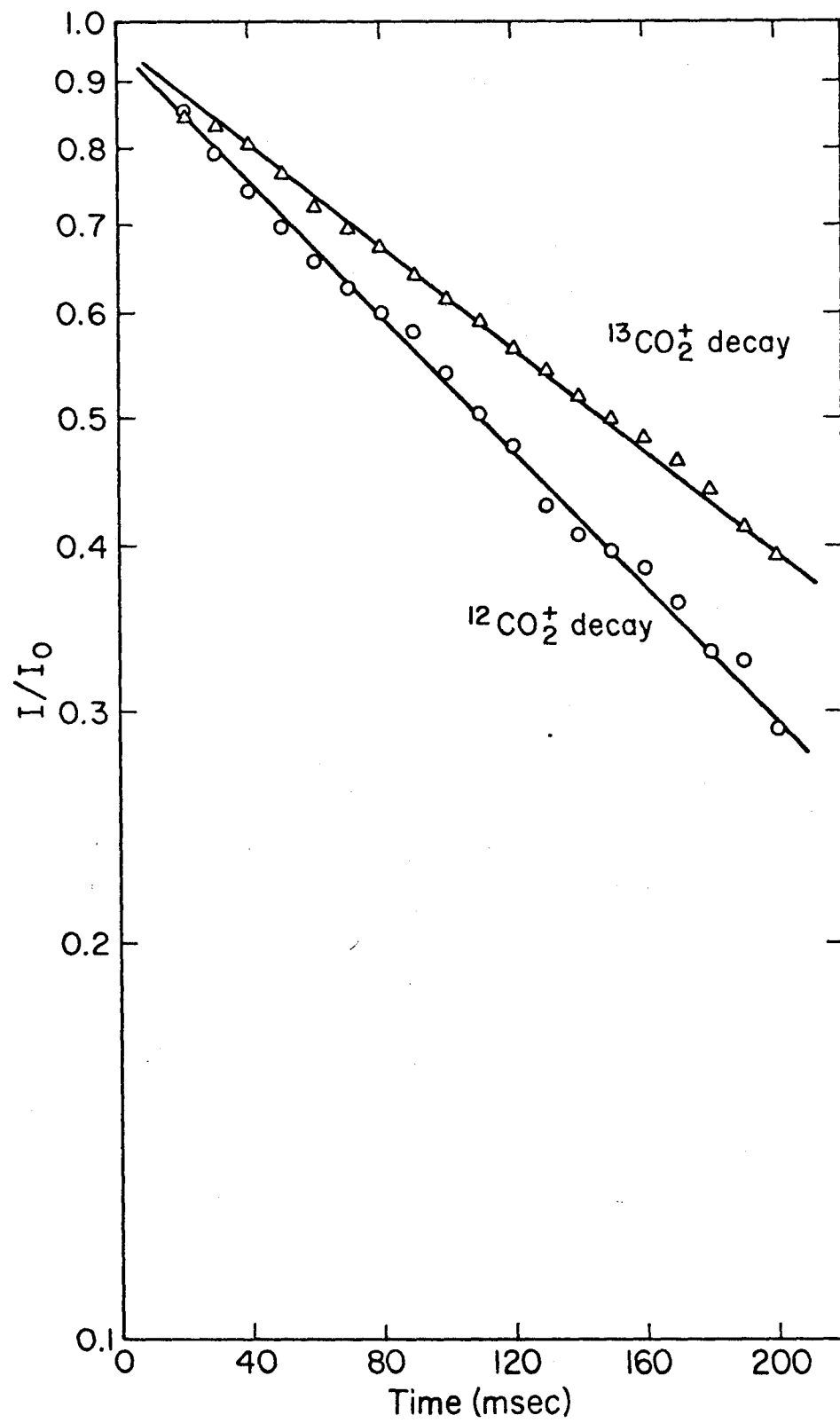


TABLE 2

Experimental and Calculated Charge Exchange Rates

Molecule	α_{av} ($\times 10^{-24}$ cm ³)	α_{II} cm ³)	α_I	Expt'l charge exchange rate 10 ⁻¹⁰ cm ³ molecule ⁻¹ sec ⁻¹	Encounter rate x10 ⁻¹⁰ cm ³ molecule ⁻¹ sec ⁻¹	Langevin encounter rate x10 ⁻¹⁰ cm ³ molecule ⁻¹ sec ⁻¹		
						α_{av}	α_{II}	α_I
N ₂	1.76	2.38	1.45	6.65	13.0	8.2	9.6	7.5
CO	1.95	2.60	1.625	4.1	8.2	8.6	9.6	7.9
CO ₂	2.65	4.01	1.97	3.7	7.4	8.0	9.9	6.9

132

$$\alpha_{av} = \frac{1}{3} (\alpha_{II} + 2\alpha_I)$$

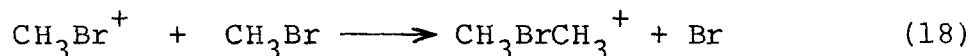
electron transfer.

Recently, Futrell (23) has examined the velocity dependence of a number of charge exchange reactions. At near thermal ion energy he obtained a rate constant for symmetric charge exchange in CO at 0.1 eV ion energy of $8.5 \times 10^{-10} \text{ cm}^3 \text{ molecule}^{-1} \text{ sec}^{-1}$ in poor agreement with the result obtained in this work. At higher ion energies an encounter cross-section well in excess of the calculated Langevin value was observed and on the basis of these results Futrell concludes that electron transfer is occurring well outside the critical impact parameter. The reason for the serious disagreement ~~between his results and~~ those reported here is not known. Several other results reported by Futrell in the same study appear to be extraordinarily large and in at least one case disagrees considerably with other literature data (24,25).

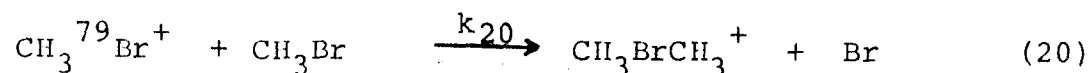
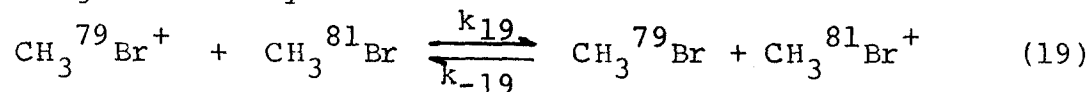
Bates and Lynn (26) have conjectured that only reactions in which the interaction potential between the ion and neutral is spherically symmetric will be resonant at long range. If this is indeed the case, then the small dipole moment of CO (0.112 Debye) and the bond dipoles and largely anisotropic polarizability of CO₂ may preclude the occurrence of resonant charge exchange at large impact parameters. Obviously several further experiments involving homonuclear and heteronuclear diatomics must be done before any conclusion may be drawn.

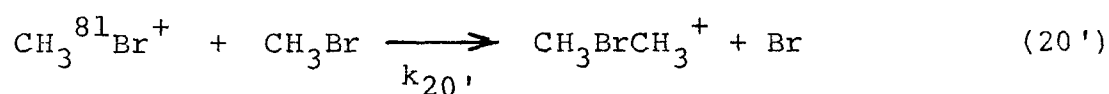
2. Methyl Bromide

Symmetric charge exchange was examined in methyl bromide as an illustration of charge transfer as a competitive reaction channel. The only normally observed reaction of the parent ion of CH_3Br is dimethyl bromonium ion formation (reaction 18).



This reaction is very slow, proceeding with a rate constant of $5.5 \times 10^{-11} \text{ cm}^3 \text{ molecule}^{-1} \text{ sec}^{-1}$ (27). Since the encounter rate predicted from an ion-induced dipole potential is $8.2 \times 10^{-10} \text{ cm}^3 \text{ molecule}^{-1} \text{ sec}^{-1}$ it was considered likely that symmetric charge exchange might be taking place. Bromine has two naturally occurring isotopes, ^{79}Br (50.57%) and ^{81}Br (49.43%) and as a result the ion ejection technique can be used for methyl bromide to determine charge exchange rates in the same manner as described in the previous section for N_2 , CO , and CO_2 . However, in order to determine whether the competing reaction of dimethyl bromonium ion formation would cause difficulties in interpretation of the results, a detailed kinetic analysis was carried out. The reactions occurring in this system are





Assuming that $k_{19} = k_{-19}$ the solutions to the coupled kinetic equations are

$$[\text{CH}_3^{79}\text{Br}^+] = [\text{CH}_3^{79}\text{Br}^+]_0 e^{-nk_{20}t} \quad (21)$$

$$[\text{CH}_3^{81}\text{Br}^+] = [\text{CH}_3^{81}\text{Br}^+]_0 e^{-nk_{20}'t} \quad (21')$$

where the subscript indicates ion intensity at $t = 0$, and n is the total pressure of methyl bromide. However, in the ion ejection experiment one of the isotopic bromides is continuously removed. Under these conditions the intensity equations become

$$[\text{CH}_3^{79}\text{Br}^+]_{\text{ej}} = [\text{CH}_3^{79}\text{Br}^+]_0 e^{-(nk_{20} + \text{CH}_3^{81}\text{Br} k_{19})t} \quad (22)$$

$$[\text{CH}_3^{81}\text{Br}^+]_{\text{ej}} = [\text{CH}_3^{81}\text{Br}^+]_0 e^{-(nk_{20}' + \text{CH}_3^{79}\text{Br} k_{19})t} \quad (22')$$

where $[\text{CH}_3^{79}\text{Br}^+]_{\text{ej}}$ indicates the intensity of that isotopic ion when $[\text{CH}_3^{81}\text{Br}^+]$ is ejected continuously. Thus the ratio of ionic intensities with and without ejection is given by

$$\frac{[\text{CH}_3^{79}\text{Br}^+]_{\text{ej}}}{[\text{CH}_3^{79}\text{Br}^+]} = e^{-k_{19}[\text{CH}_3^{81}\text{Br}]t} \quad (23)$$

A similar relation holds for $\text{CH}_3^{81}\text{Br}^+$ and hence a logarithmic plot of this ratio as a function of time will yield the rate constant for symmetric charge exchange. This experiment is illustrated in Fig. 10 while semi-logarithmic plots of the appropriate ratios are shown in Fig. 11. From these plots a charge transfer rate constant of $9.7 \times 10^{-10} \text{ cm}^3 \text{ molecule}^{-1}$

Figure 10

Trace of variation of ion intensity with time for $\text{CH}_3^{79}\text{Br}^+$ with and without continuous ejection of $\text{CH}_3^{81}\text{Br}^+$. Ions were formed by a 5 msec, 15 eV electron beam pulse in CH_3Br at a pressure of 1.45×10^{-6} torr.

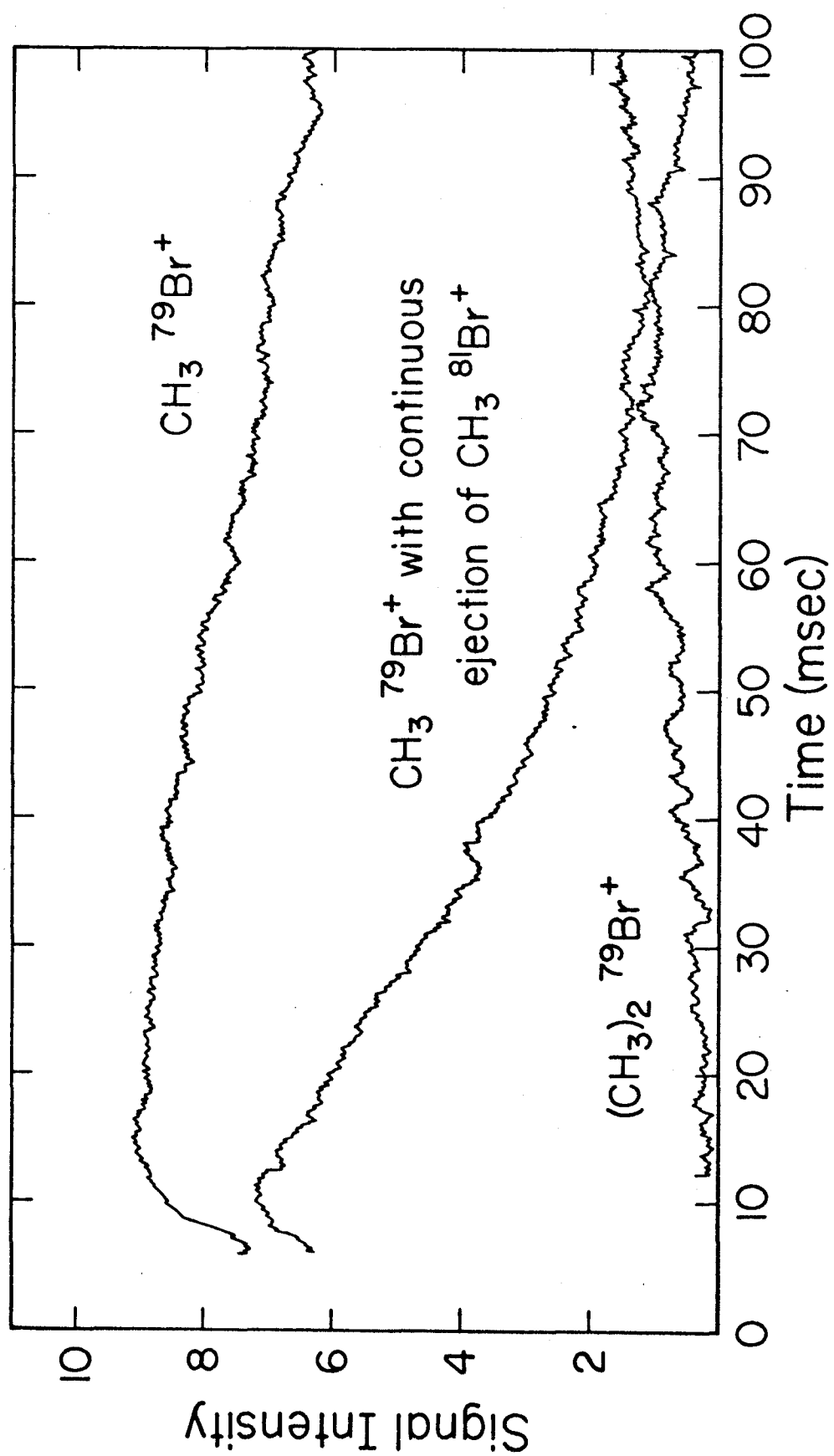
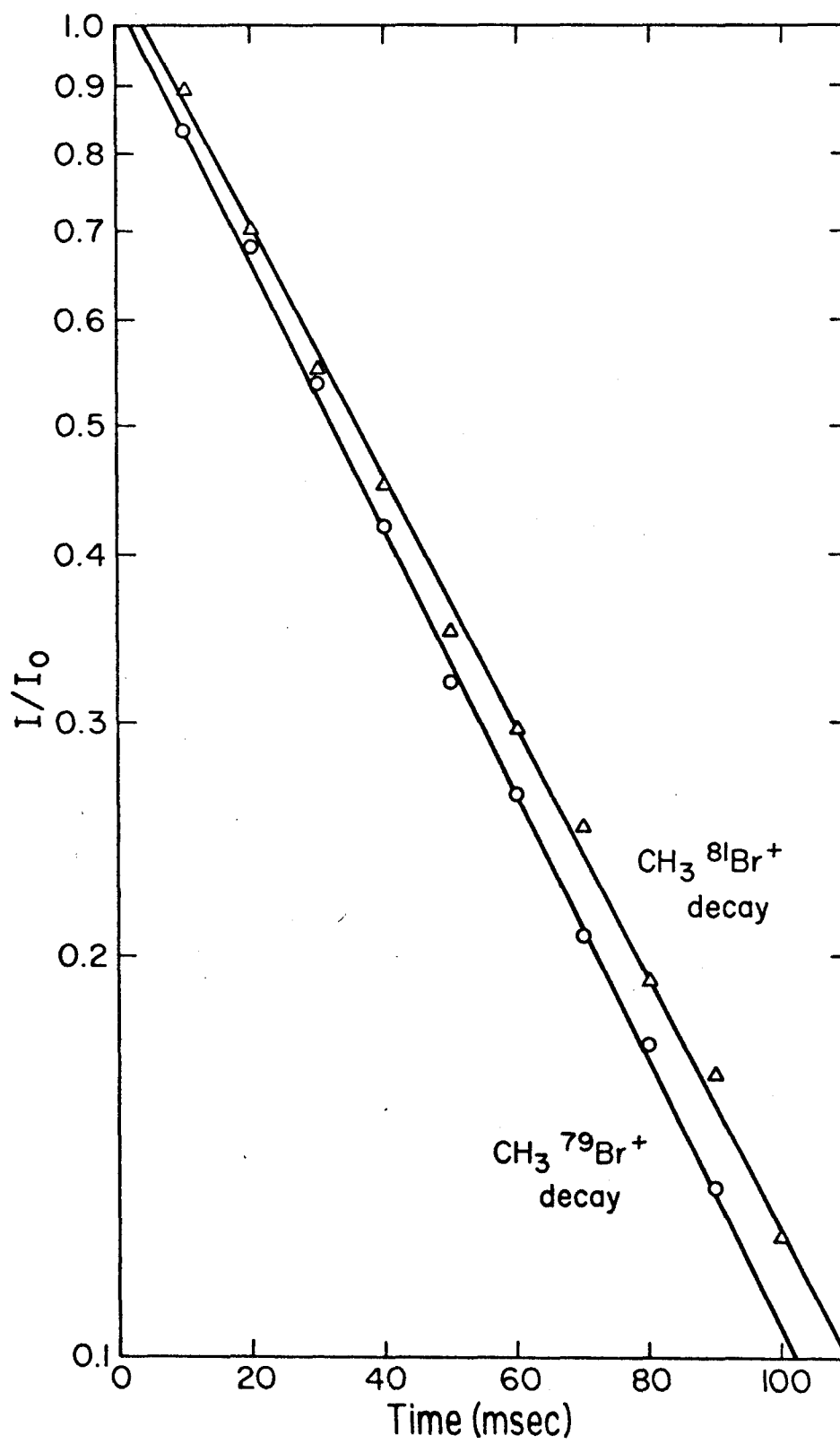


Figure 11

Plot of $\log_{10} (I/I_0)$ vs. time for each of the isotopic methyl bromide ions. Conditions are the same as those in Figure 10.



sec^{-1} was obtained. Since it can be assumed, as before, that the ionic species will change its isotopic identity on only one-half of the collisions, an encounter rate of $1.94 \times 10^{-9} \text{ cm}^3 \text{ molecule}^{-1} \text{ sec}^{-1}$ for charge exchange events may be inferred. Adding to this the rate constant for dimethyl bromonium ion formation, a total encounter rate of $2.0 \times 10^{-9} \text{ cm}^3 \text{ molecule}^{-1} \text{ sec}^{-1}$ is obtained for CH_3Br^+ interacting with CH_3Br . This value is sufficiently in excess of the predicted Langevin rate that the possibility of long range symmetric charge transfer must be considered. To a crude approximation the $\text{CH}_3\text{Br}^+ + \text{CH}_3\text{Br}$ situation resembles $\text{Kr}^+ + \text{Kr}$. A number of investigators have found that symmetric charge exchange in Kr occurs well outside the critical impact parameter (23-25). Alternatively, it may be that the CH_3Br dipole moment of 1.81 debye (28), plays a significant part in the ion-molecule potential. There is no convenient way to experimentally distinguish these two models until considerably more data on ion-molecule reaction rates is available.

In a previous ICR investigation of alkyl halides (27) it had been determined from isotopic double resonance experiments that the bromine atom in the dimethyl bromonium ion came with equal probability from the ionic and neutral CH_3Br . This conclusion is confirmed by the occurrence of fast symmetric charge exchange in which the initial isotopic identities of ion and molecule are rapidly lost after a few collisions. Such experiments may require re-evaluation to

determine what takes place in a single collision since the identity of reactants is obscured by multiple charge transfer events.

C. Symmetric Proton Transfer Reactions

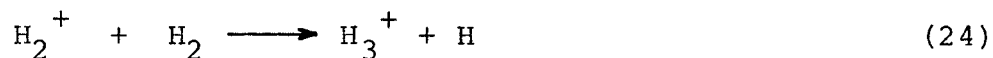
The most commonly observed gas phase ion-molecule reactions are protonation and proton transfer reactions. Proton transfer reactions may be used to establish the intrinsic basicity or proton affinity of gas phase bases. The recent ordering of gas phase basicities of organic molecules (15, 29, 30) has answered questions concerning substituent effects that have been confounding physical organic chemists for years. This type of study will be discussed later in this thesis.

In addition to the thermochemical information obtained from proton transfer reactions, insights into the mechanisms of ion-molecule reactions and the structures of gas phase ions may be obtained from the kinetics of proton transfer reactions. Comparison to theoretical models can answer many questions regarding dynamics of proton transfer. For instance, can symmetric proton transfer reactions take place via a long range resonant process as was observed for charge exchange? In order to elucidate the mechanism proton transfer was studied for a number of simple systems.

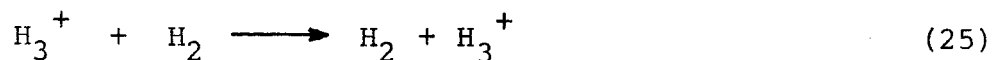
1. Hydrogen

The first ion-molecule reaction to be identified was H_3^+ production by reactions of ions generated in hydrogen.

The reaction involved was early determined to be (31,32)



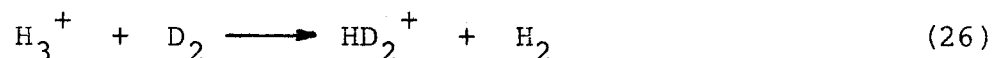
Since that time, theoretical investigations have shown H_2^+ to be a stable species with two possible geometrics (33,34). Of these, the triangular has been shown to be more stable than the linear form. In the early 1930's Eyring demonstrated that the rate of H_3^+ production could be predicted using the newly developed absolute rate theory (35). The theoretical description of ion-molecule reactions developed for this reaction gave an expression identical to that developed by Gioumousis and Stevenson almost twenty-five years later (11). Since then, numerous investigators have examined the ion-molecule reactions in isotopic hydrogen systems and the rates of production of the various protonated and deuterated species are well documented (36-40) and have been found to be in excellent agreement with the predicted values. However, the symmetric proton and deuteron transfer reactions of the species thus formed have not been well characterized, largely due to the fact that reactions of the form



are undetectable by most means of investigation. Reactions of this type have been invoked as the chain propagation steps in radiation induced isotopic exchange in mixtures of hydrogen isotopes (41,42). In order to quantitatively assess the dynamics of this process a number of attempts have been made

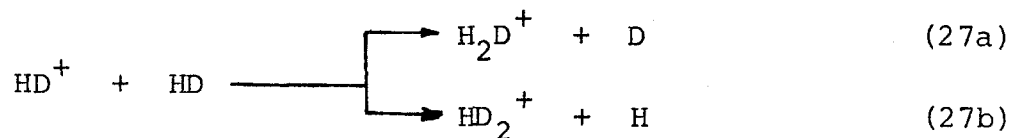
to measure the rate constant for reaction (25).

Dawson and Tickner (41) have estimated a rate constant of $3 \times 10^{-10} \text{ cm}^3 \text{ molecule}^{-1} \text{ sec}^{-1}$ for the reaction

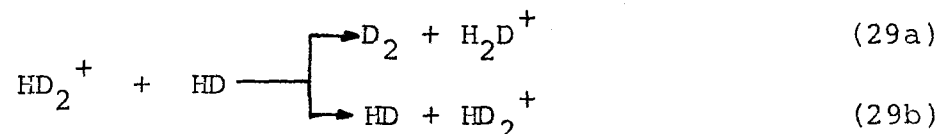
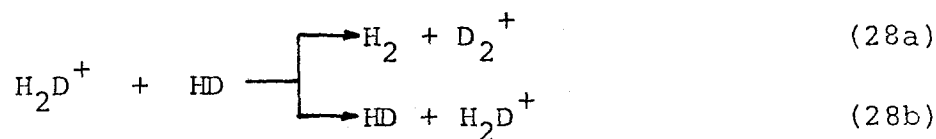


to account for the amount of isotopic exchange observed in a mixture of H_2 and D_2 subjected to a glow discharge. This agrees well with a value of $3.3 \times 10^{-10} \text{ cm}^3 \text{ molecule}^{-1} \text{ sec}^{-1}$ obtained by Terao and Back (42) for the same reaction in a study of radiation induced isotope exchange in a mixture of H_2 and D_2 . In addition, a high pressure mass spectrometric investigation of arrival time distributions of ions in H_2 , D_2 mixtures by Chang, Sroka and Meisels (43) established a lower limit of $9 \times 10^{-11} \text{ cm}^3 \text{ molecule}^{-1} \text{ sec}^{-1}$ for reaction (24).

Using ion ejection techniques, it is possible to observe normally undetectable reactions of isotopic $(\text{H,D})_3^+$ species at equilibrium. In pure HD, the observable sequence of ion-molecule reactions is



However, symmetric proton and deuteron reactions also occur under conditions where the protonated and deuterated HD species can undergo successive collisions with the neutral HD (reactions 28 and 29)



Rate constants for reactions (28a) and 29a) may be obtained by a technique similar to that described for the charge exchange reactions. However, in this case a time delayed ion ejection technique is used. After approximately 100 collisions have occurred, steady state concentrations of H_2D^+ and HD_2^+ will be established and a secondary radio frequency oscillator tuned to the cyclotron frequency of one of these ions is switched on in the trapping region of the ICR cell. Ions are thus selectively ejected in a time short compared to the time between ion-molecule collisions. This pulsing sequence is illustrated in Fig. 12. The perturbation causes the system to respond at the rate of reaction to achieve a new equilibrium. By monitoring the decay in abundance of one ion while the other is continuously removed from the cell, the rate constants for reactions (28a) and (29a) may be easily determined. The variation of ion abundance with time for the three ions observed in HD is illustrated in Fig. 13. From the decay of HD^+ with time, rate constants of $6.0 \times 10^{-10} \text{ cm}^3 \text{ molecule}^{-1} \text{ sec}^{-1}$ and $1.0 \times 10^{-9} \text{ cm}^3 \text{ molecule}^{-1} \text{ sec}^{-1}$ were

Figure 12

Pulsing sequence for initiating ion ejection partway through a trapped ion sequence.

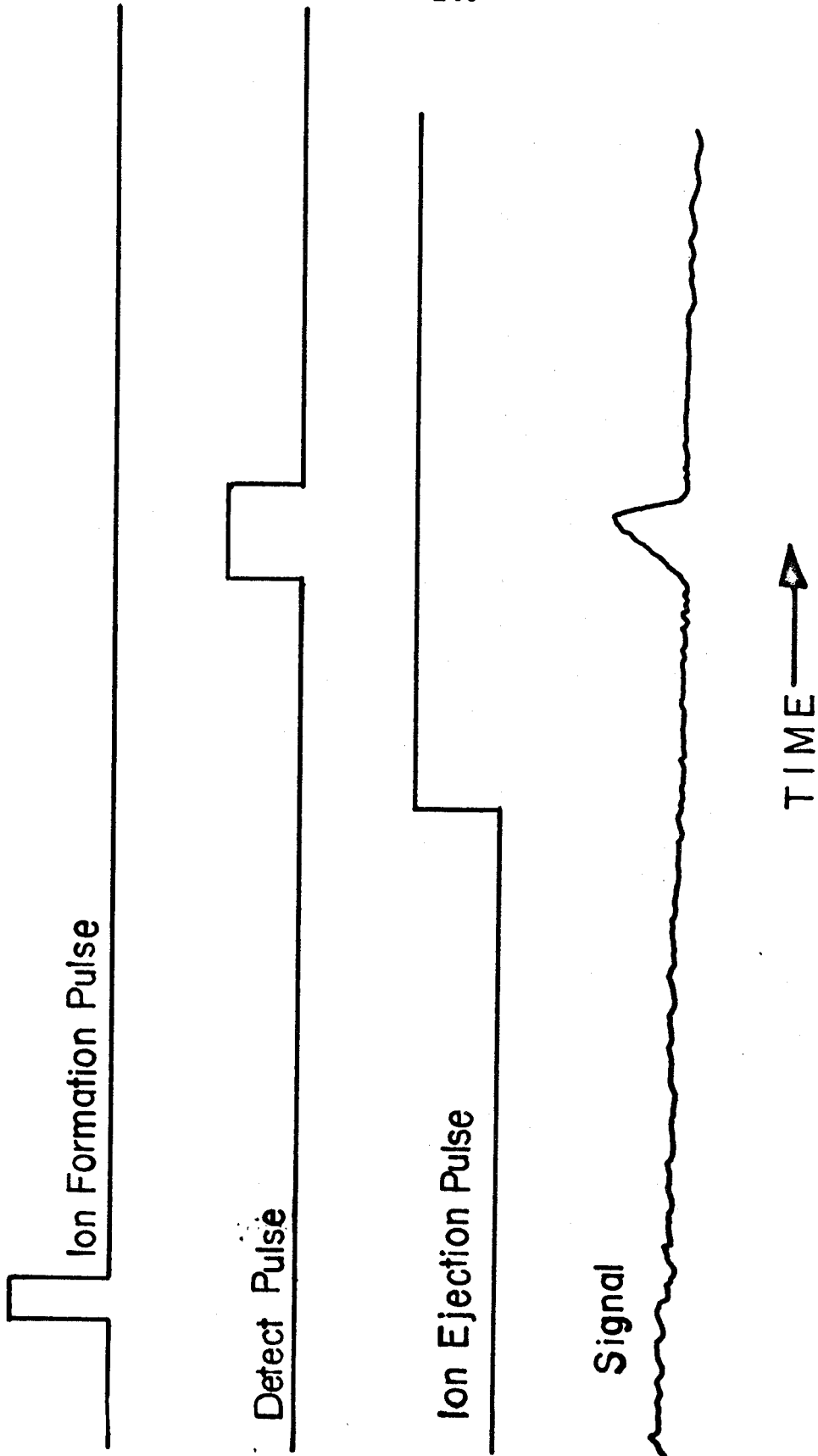
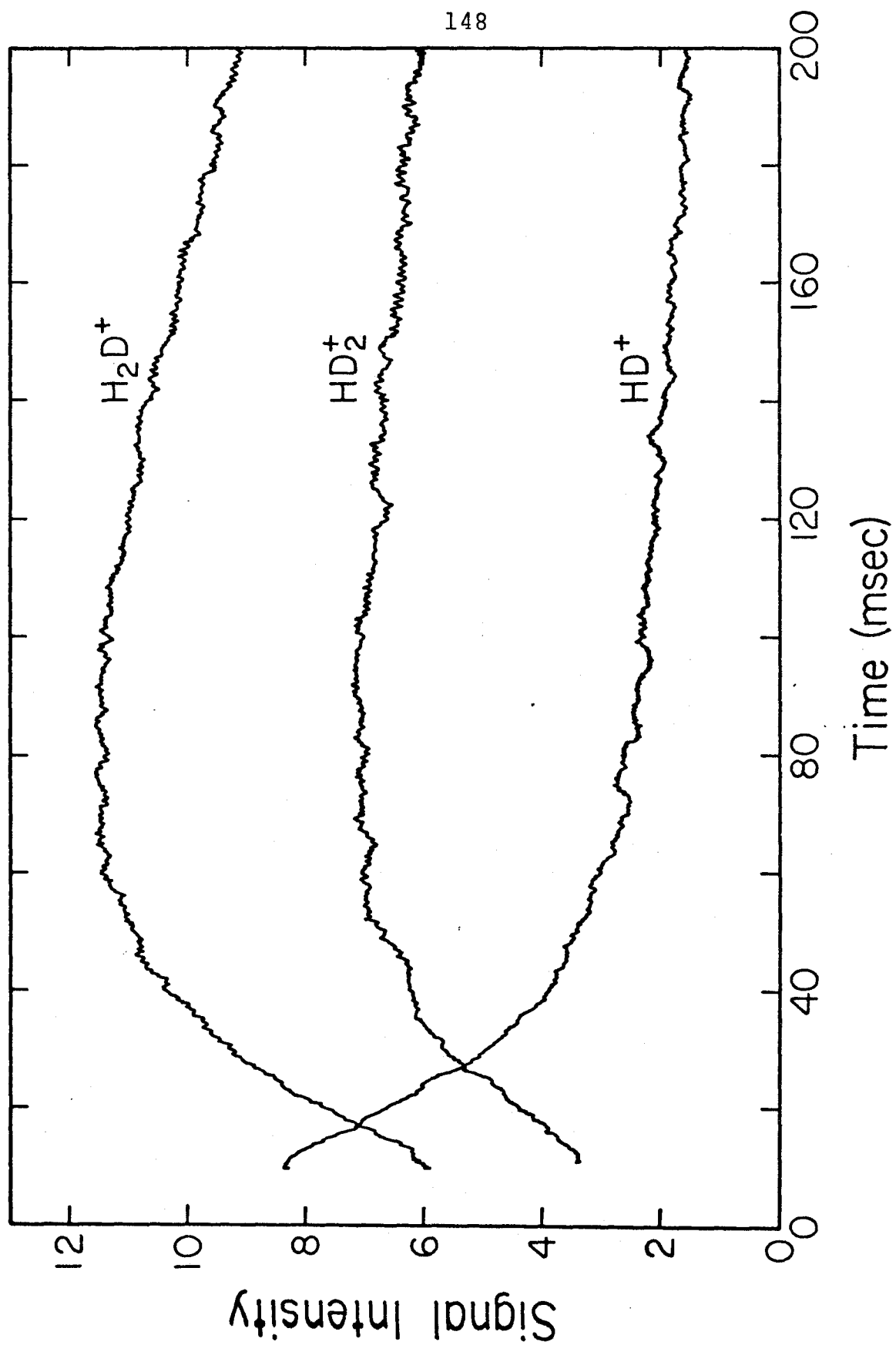


Figure 13

Variation of ion intensity with time for ions in HD. Ions are formed by a 5 msec 70 eV electron beam pulse in HD at a pressure of 9×10^{-7} torr.



obtained for production of H_2D^+ and HD_2^+ , respectively, in good agreement with other workers. A time delayed ion ejection experiment is shown in Fig. 14. After 100 msec, the ions H_2D^+ and HD_2^+ have reached equilibrium and at this time the irradiating oscillator is turned on for the duration of the trapping cycle to eject HD_2^+ . The subsequent decay of H_2D^+ is monitored and the ratio $\log (I/I_0)$ is plotted vs time after ejection. These plots are shown in Fig. 15 for both H_2D^+ and HD_2^+ . The rate constants obtained from this method are summarized in Table 3. Included for comparison are the theoretical Langevin encounter rates.

In order to relate the observed reaction rate to an actual encounter rate, the mechanism of the proton transfer reaction in hydrogen systems must be understood. If an H_5^+ complex is formed in which all of the hydrogen atoms are equivalent, statistically 10% H_3^+ and D_3^+ would be expected to be formed as a result of reactions of H_2D^+ and HD_2^+ . Less than 5% H_3^+ or D_3^+ is observed which arises from H_2 and D_2 impurities, ruling out a complex in which statistical scrambling of the hydrogen atoms occur. Recent theoretical SCF MO calculations have shown that H_5^+ should be a stable species with a binding energy of approximately 4.25 kcal/mole (44). These calculations predict a spirane-like geometry of the form

TABLE 3

Rate Constants for Reactions in HD

<u>Reaction</u>	Rate Constant (cm ³ molecule ⁻¹ sec ⁻¹)	
	<u>Expt.</u>	<u>Langevin</u>
$\text{HD}^+ + \text{HD} \begin{cases} \rightarrow \text{H}_2\text{D}^+ + \text{D} \\ \rightarrow \text{HD}_2^+ + \text{H} \end{cases}$	6.0×10^{-10} 1.0×10^{-9}	1.66×10^{-9}
$\text{H}_2\text{D}^+ + \text{HD} \longrightarrow \text{HD}_2^+ + \text{H}_2$	2.6×10^{-10}	1.59×10^{-9}
$\text{HD}_2^+ + \text{HD} \longrightarrow \text{H}_2\text{D}^+ + \text{D}_2$	3.5×10^{-10}	1.52×10^{-9}

Figure 14

Variation of intensity of HD_2^+ with and without continuous ejection of H_2D^+ after 100 msec. Conditions are the same as those for Figure 13.

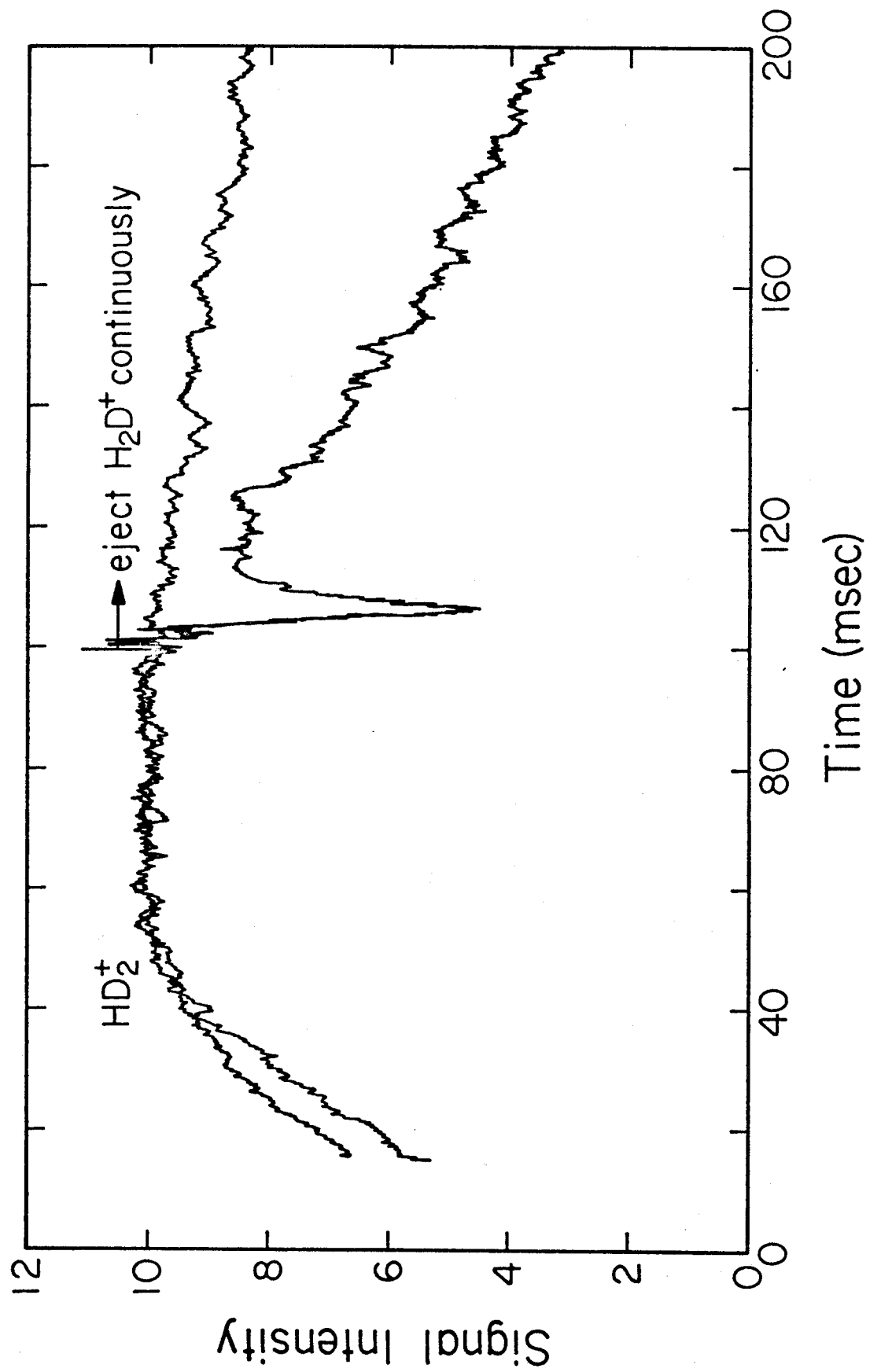
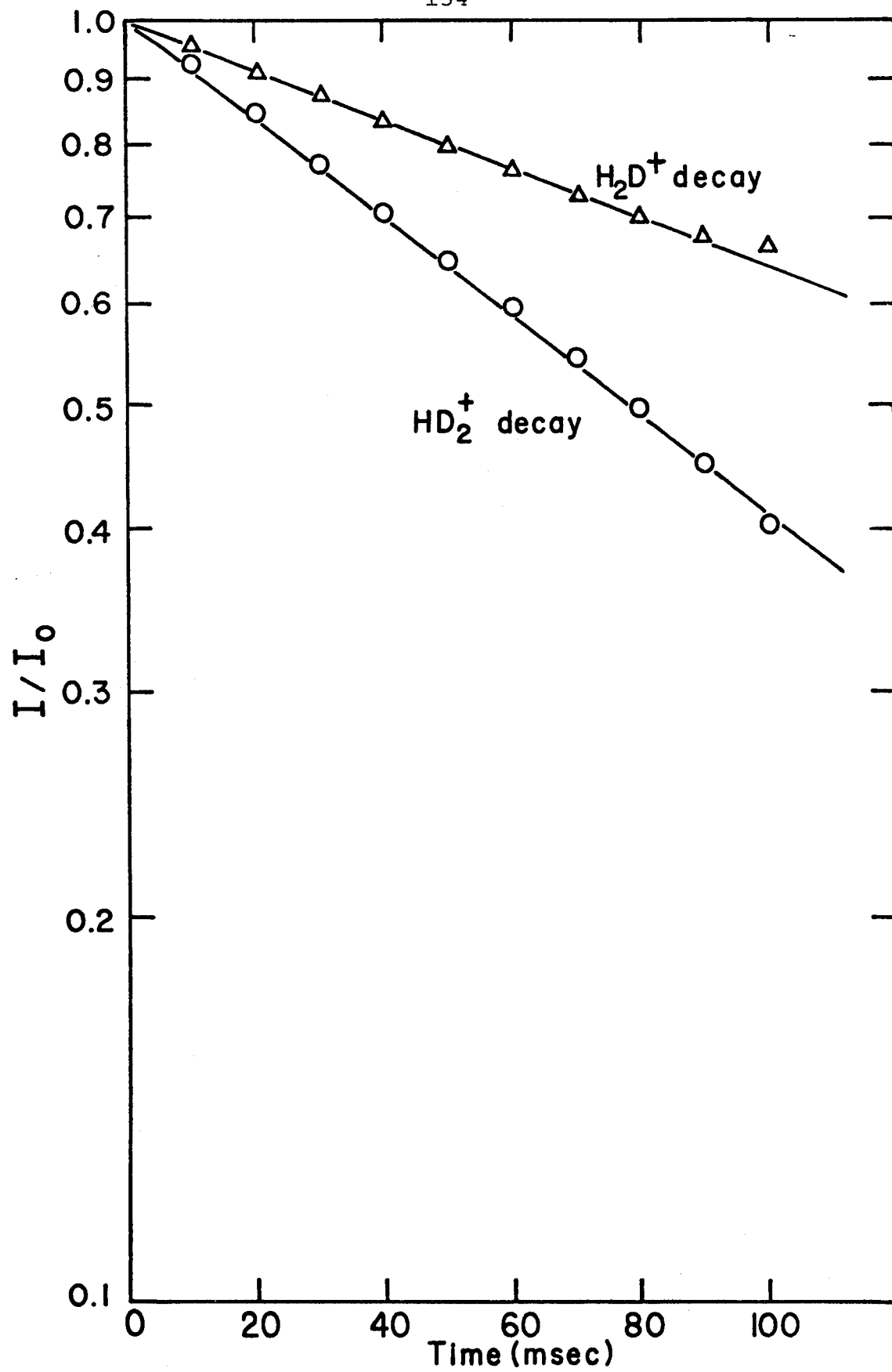
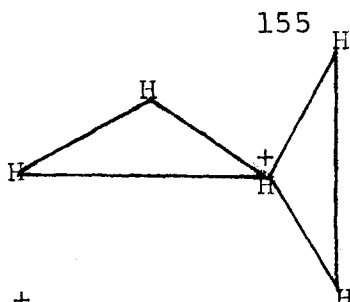


Figure 15

Plot of $\log_{10} (I/I_0)$ for H_2D^+ and HD_2^+ . Conditions are the same as those for Figure 13.





In addition, H_5^+ and other higher order hydrogen aggregates have been observed mass spectrometrically (45,46), and the binding energy of H_5^+ determined to be 9.7 kcal/mole (46). If we assume that the nature of the intermediate involved in proton transfer reactions is that of the H_5^+ species shown above, it would presumably be the "bridging" proton which is transferred. Ignoring any isotope effects, in the reaction



the bridgehead position would be occupied by a proton twice as often as by a deuteron. The proton transfer leads to products identical to the reactants and as a result is not detectable. Therefore, the total rate of proton and deuteron transfer may be approximated by three times the measured deuteron transfer rate. However, we must consider the fact that in every encounter there is an equal probability that the bridgehead proton will leave the H_5^+ complex with the hydrogen molecule with which it entered; that is to say, 50% of the encounters are non-reactive. Hence to obtain the actual encounter rate the measured rate must be multiplied by a factor of 6. It is very satisfying to note that the encounter rate thus determined is nearly identical to that predicted by the Langevin model. Discrepancies may

be attributed to deuterium isotope effects and possibly to the different centers of mass of the triangular H_2D^+ and HD_2^+ ions which would result in different moments of inertia and rotational frequencies of these ions.

These fast rates of proton transfer have important implications for the de-excitation of excited H_3^+ species. Upon formation via reaction (20) H_3^+ contains up to 2 eV of internal excitation which may participate in subsequent ion-molecule reactions (47). Leventhal and Friedman (48) have suggested that de-excitation of H_3^+ may occur after only one collision in which the transferred proton carries no excess energy. If this is the case, de-excitation of H_3^+ may occur as rapidly as $1 \times 10^{-9} \text{ cm}^3 \text{ molecule}^{-1} \text{ sec}^{-1}$. The ion-molecule reactions of H_3^+ with neutrals other than H_2 have been shown to have a strong dependence on the internal energy of H_3^+ . The fast proton transfer rate obtained here indicates that under usual ICR conditions, H_3^+ will be completely relaxed and implies that past thermochemical inferences made assuming ground state H_3^+ may be presumed valid.

As a final comment it is interesting to note that if reactions (28a) and (29a) are summed the overall sequence is a chain reaction

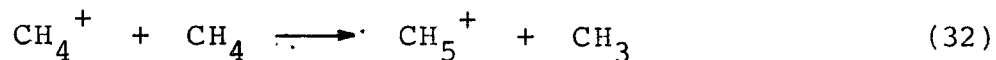


This is in agreement with observations of radiation induced conversion of H_2 to D_2 to mixtures containing HD (41,42).

It has been observed that samples of initially pure HD kept for long periods of time show a buildup of H_2 and D_2 , presumably due to cosmic radiation.

2. Methane

With the rekindling of interest in mass spectrometry in the 1950's, the ion-molecule reaction product CH_5^+ was observed in mass spectrometric investigations of methane (49). Since that time, the ion-molecule reactions of methane have been extensively studied and CH_5^+ has been shown to arise from the reaction



The rate constant for this reaction, $1.1 \times 10^{-9} \text{ cm}^3 \text{ molecule}^{-1} \text{ sec}^{-1}$, has become the standard on which accuracy of kinetic measurements are based (50). While the dynamics of CH_5^+ formation have been studied exhaustively, its structure is still a matter of controversy. The most commonly accepted structures for CH_5^+ are shown in Fig. 16. Recently, two independent theoretical studies using STO-SCF (51) and LCAO-HF (52) calculations have been carried out on these structures. The results of these calculations are summarized in Table III. It is readily seen that the three structures are found to be of roughly comparable energy.

Recently, Harrison has shown in the isotopic scrambling reaction (53)

Figure 16

The three suggested structures for the CH_5^+ ion.

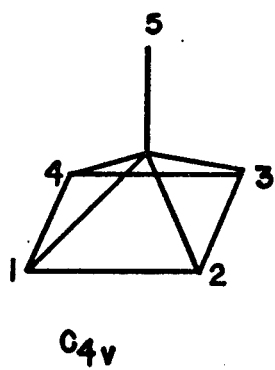
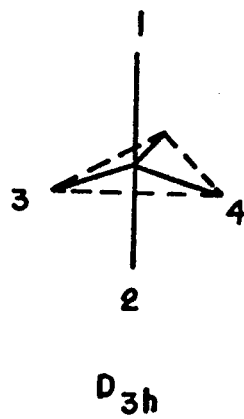
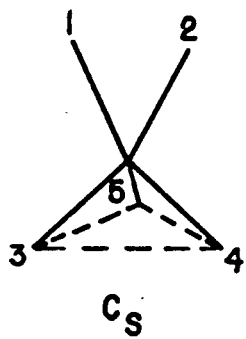
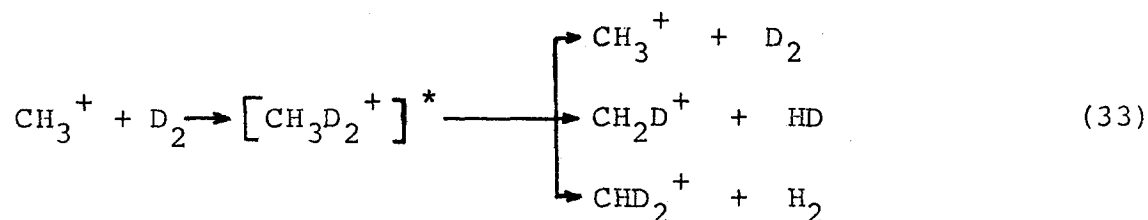


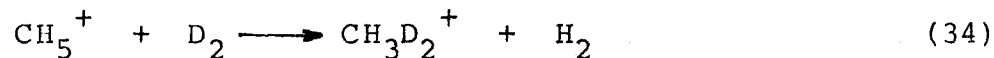
TABLE 4

Geometries, Relative Energies and Charge Distributions for CH_5^+

	<u>Mulder and Wright</u>			<u>Van der Lugt and Ros</u>		
	<u>Cs</u>	<u>D_{3h}</u>	<u>C_{4v}</u>	<u>C_s</u>	<u>D_{3h}</u>	<u>C_{4v}</u>
C-H ₁ distance (au)	2.294	2.104	2.127	2.21	2.13	2.14
C-H ₅ distance (au)	2.066	2.084	2.019	2.08	2.11	2.03
H ₁ CH ₂ angle (degrees)	60°		80°	58°		82°
H ₄ CH ₅ angle (degrees)	109.5°			108°		
qC				-1.113	-1.367	-1.239
qH ₁				0.436	0.561	0.462
qH ₅				0.413	0.415	0.390
E _{rel} (kcal/mole)	2.5	3.1	0.0	9.0	3.5	0.3

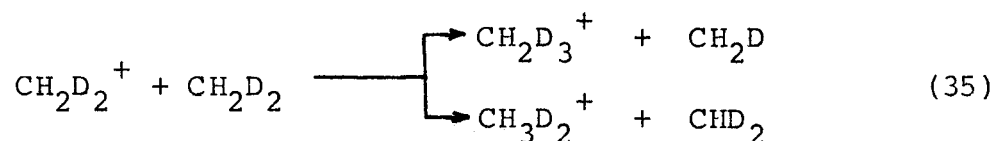


that the hydrogen and deuterium atoms become scrambled and that the product distribution is statistical. However, the total rate of reaction is observed to be less than half of that predicted by the Langevin model. This suggests a strong preference for the complex to return to the $\text{CH}_3^+ + \text{D}_2$ reactants. The C_s structure in Fig. 16 would exhibit such a preference if H_1 and H_2 were deuterium atoms. This structure has been calculated to have a bonding interaction between these two atoms. Therefore, since the deuteriums are bonded when they enter the complex it might be expected that this bond would be partially maintained in a complex of C_s geometry and exhibit a preference for return to $\text{CH}_3^+ + \text{D}_2$. However, attempts to displace a molecule of hydrogen from CH_5^+ by the reaction

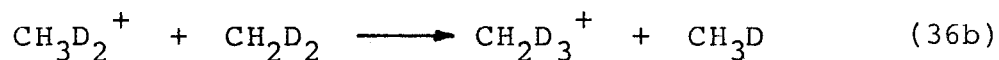
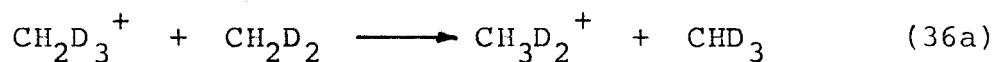


have failed (54). In order to further examine the feasibility of the C_s geometry the measurement of the symmetric proton transfer in CH_5^+ like species suggested itself. This experiment was carried out straightforwardly by analyzing the ion-molecule reactions of CH_2D_2 using the time delayed ion ejection technique. Upon ionization the parent ion of

CH_2D_2 reacts rapidly to form the protonated and deuterated parent ions as shown in Fig. 17.



These ions may subsequently interconvert by the symmetric proton and deuteron transfer reactions



Ejection of one of these ions will cause the decay of the other if they are chemically coupled by proton-deuteron transfer reactions. That this is the case is illustrated in Fig. 18. The rate constants obtained for reaction 36a and 37b were both $3 \pm 1 \times 10^{-11} \text{ cm}^3 \text{ molecule}^{-1} \text{ sec}^{-1}$. These rate constants have large error limits due to the fact that proton transfer reactions to impurities, especially water, are very rapid. Within the limits of accuracy of these measurements the rate constants are identical. Statistically the measured rate constant represents only two-fifths of the possible reactive events. The actual proton-deuteron transfer rate is about $7.5 \times 10^{-11} \text{ cm}^3 \text{ molecule}^{-1} \text{ sec}^{-1}$, ignoring any isotope effects. The fact that this rate constant is so slow is likely a consequence of the instability of any possible C_2H_9^+ intermediate (55). If such an intermediate can be formed, it would

Figure 17

Variation of ion intensity with time for ions in CH_2D_2 generated by a 5 msec, 70 eV electron beam pulse at a pressure of CH_2D_2 of 2.3×10^{-6} torr.

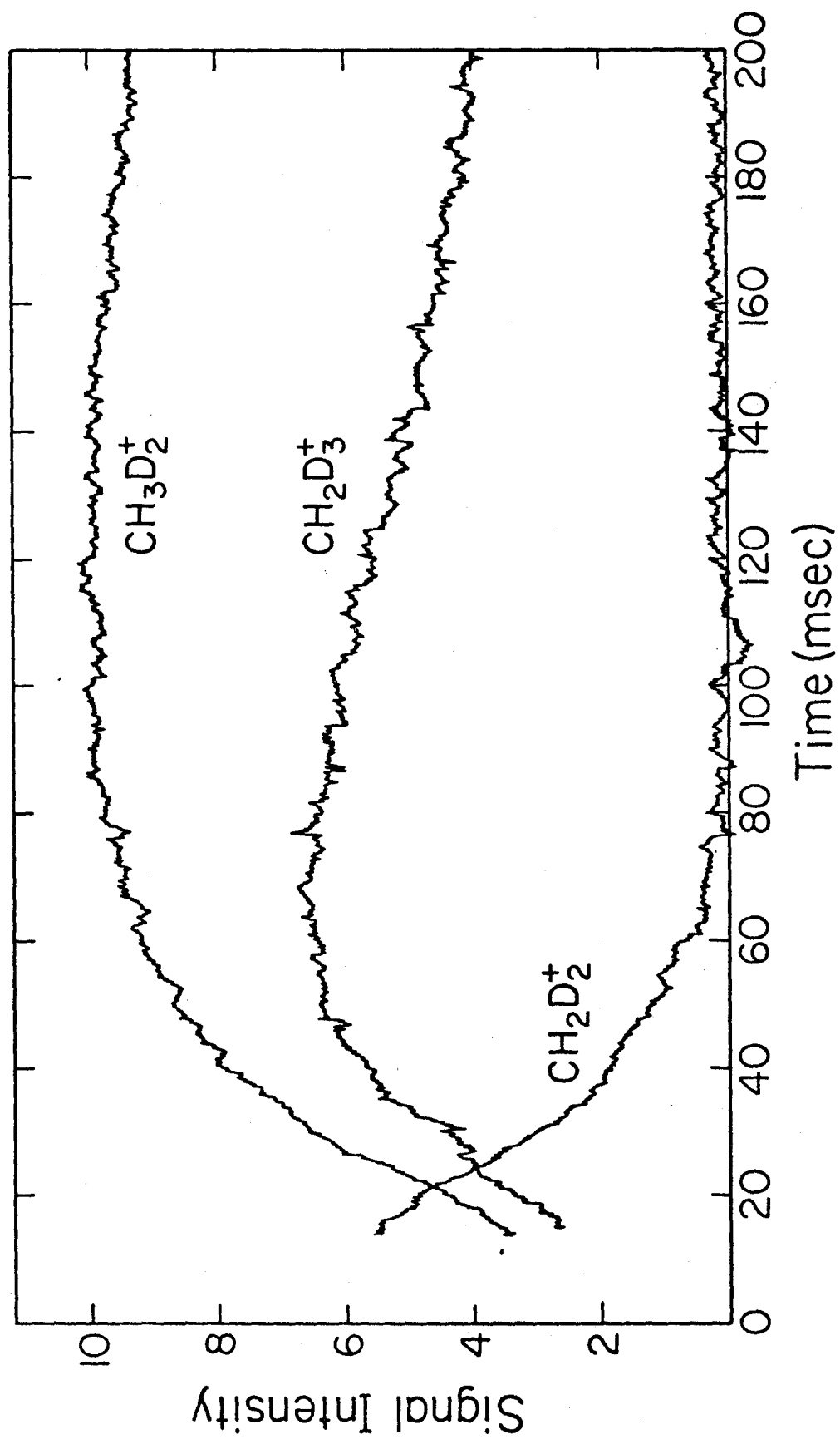
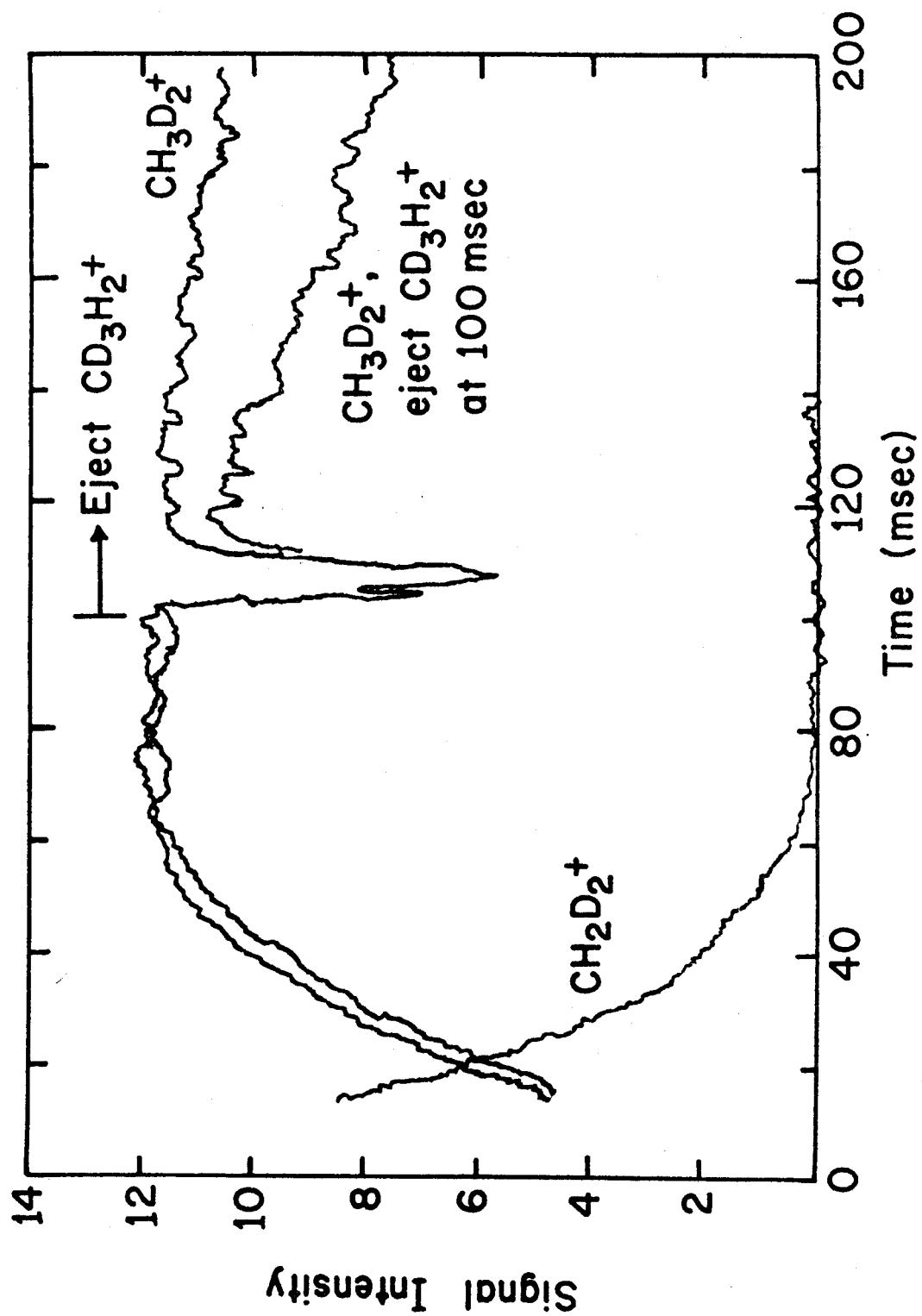


Figure 18

Variation of CH_3D_2^+ with and without continuous ejection CH_2D_3^+ after 100 msec. Conditions are the same as those for Figure 17.



likely dissociate before the reorganization necessary for proton transfer can take place. An alternative mechanism for this reaction would be transfer of a labile proton from CH_5^+ at long range; that is, in the absence of complex formation. The probability of this occurring would be rather low, however, since the transfer of a proton to neutral CH_4 involves extensive reorganization of the molecular geometry. However, in cases of exothermic proton transfer from CH_5^+ to polar neutrals where a stable proton bound intermediate may be envisioned, the proton transfer rate has been found to be very large (18).

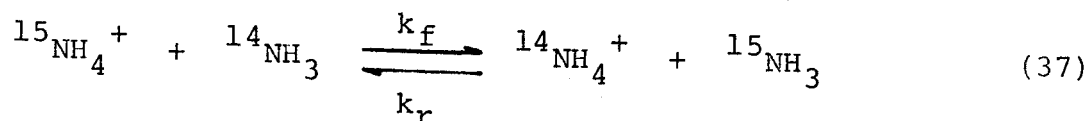
The slowness of proton transfer reactions of CH_5^+ in CH_4 has important consequences for momentum transfer experiments. On the basis of ICR linewidth studies of CH_5^+ in CH_4 it had been suggested that the anomalously high momentum transfer rate might be due to rapid symmetric proton transfer (20). As seen from the experiments presented here this cannot be the case since proton transfer is twenty times slower than the collision rate.

It is also apparent from the slowness of the proton transfer rate that this reaction will not be an efficient mechanism for de-excitation of excited CH_5^+ ions. Therefore excited CH_5^+ ions, such as those formed in the reaction of CH_3^+ with H_2 , will not be efficiently relaxed by proton exchange with CH_4 . Such ions will likely be stabilized only through collision.

Based on theoretical calculations and the experiments presented above, it is still not possible to absolutely determine the structure of CH_5^+ . However, the experiments of Harrison (53) implicate a C_s structure which is consistent with the observation of proton transfer presented here.

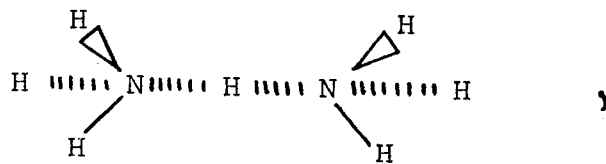
3. Ammonia

A time delayed ion ejection experiment, shown in Fig. 19, was carried out to determine the symmetric proton transfer rate in ammonia. The rate constant for both the forward and reverse reactions of the equilibrium



were obtained from the plots of $\log(I_{ej}^+/I_0^+)$ vs time shown in Fig. 20. The forward, k_f , and reverse, k_r , rate constants were found to be $6.0 \times 10^{-10} \text{ cm}^3 \text{ molecule}^{-1} \text{ sec}^{-1}$.

A symmetric intermediate for this reaction may be imagined to be of the form ,



a proton bound structure. Theoretical calculations have shown that the most stable form of N_2H_7^+ has a double potential minimum for binding of the proton with an equilibrium N-N distance 2.713 \AA and a binding energy of 36.0

Figure 19

Variation of ion intensity of $^{15}\text{NH}_4^+$ with and without continuous ejection of $^{14}\text{NH}_4^+$ after 100 msec. Ions were formed by a 5 msec, 13 eV electron beam pulse in a 1.5:1 mixture of $^{14}\text{NH}_3$ and $^{15}\text{NH}_3$ at a total pressure of 1.1×10^{-6} torr.

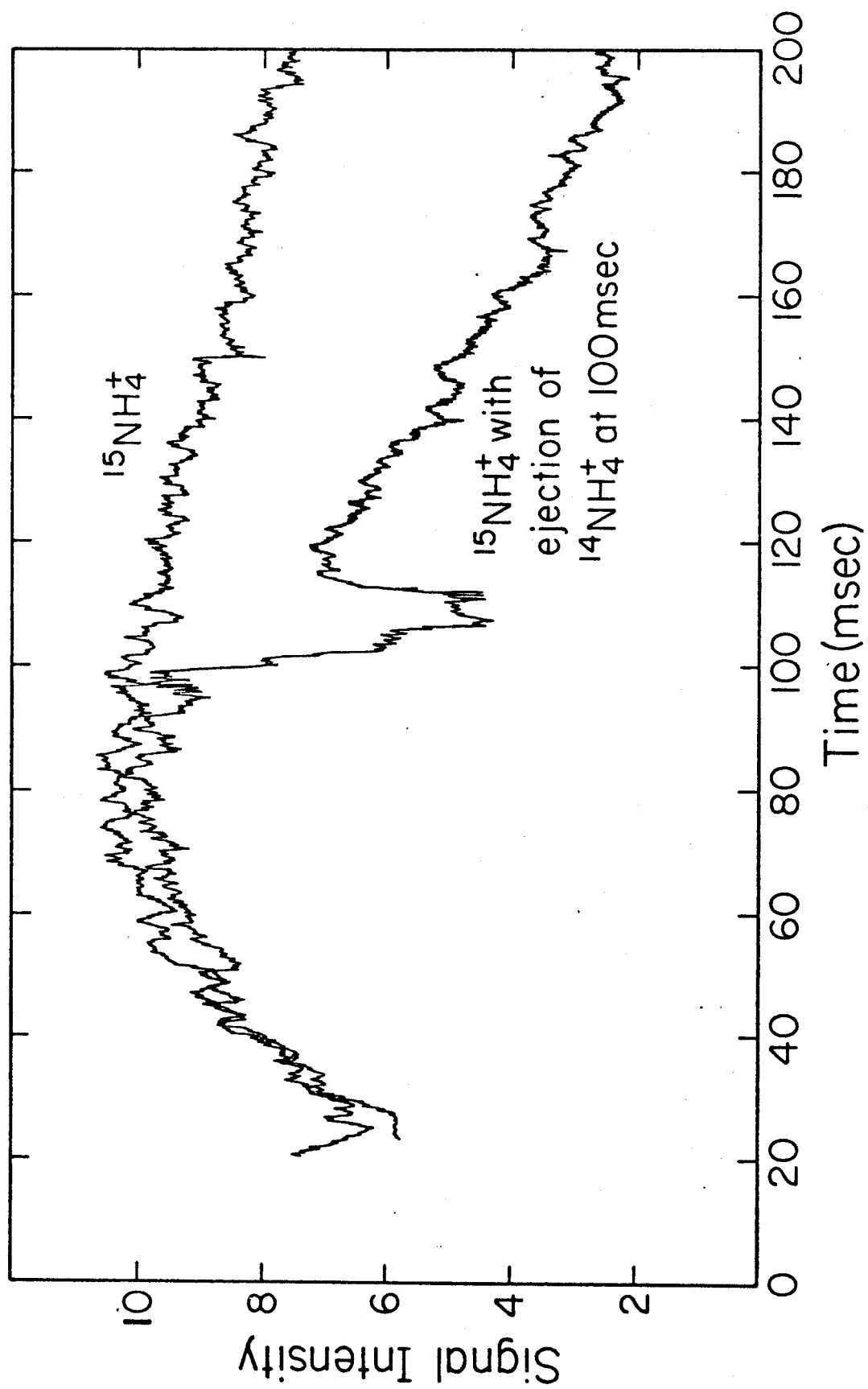
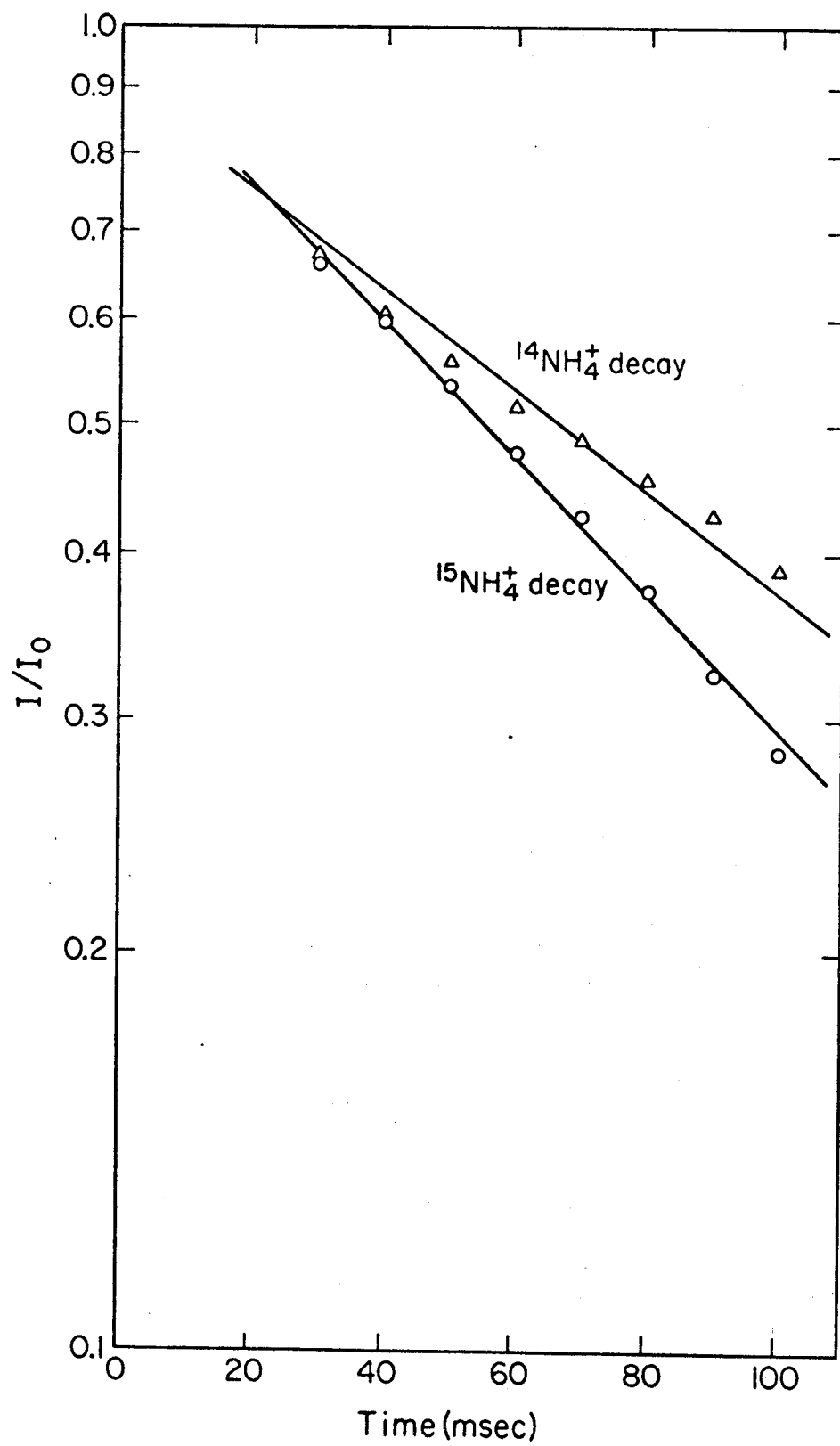


Figure 20

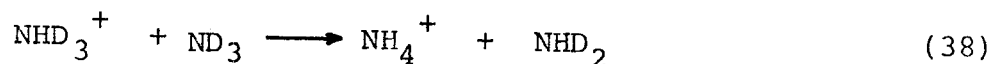
Plot of $\log_{10} (I/I_0)$ for each of the isotopic NH_4^+ ions.
Conditions are the same as those for Figure 19.



kcal/mole (56). Kebarle has also obtained an experimental binding energy of 27 kcal/mole for the proton bound dimer of ammonia (57).

Since such an intermediate may dissociate with equal probability to give reactants as products an encounter rate of $1.2 \times 10^{-9} \text{ cm}^3 \text{ molecule}^{-1} \text{ sec}^{-1}$ is obtained by doubling the measured proton transfer rate. This value is in good agreement with the predicted Langevin encounter rate of $1.16 \times 10^{-9} \text{ cm}^3 \text{ molecule}^{-1} \text{ sec}^{-1}$, indicating that the molecular dipole of ammonia plays no important role in the ion-molecule potential.

Munson and Field (58) have also found an approximate rate constant of $1 \times 10^{-9} \text{ cm}^3 \text{ molecule}^{-1} \text{ sec}^{-1}$ for the reaction

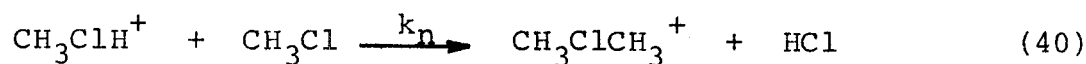
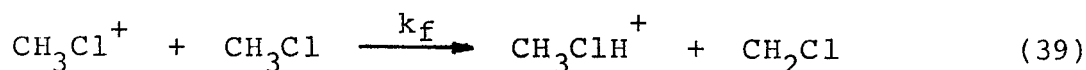


in good agreement with the result reported here.

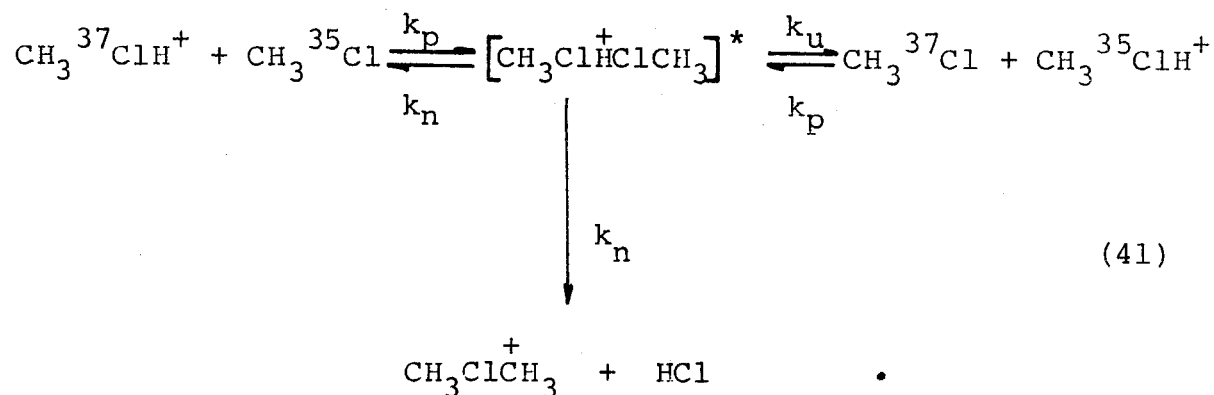
From these results it may be concluded that symmetric proton transfer will be an efficient means of relaxing excited NH_4^+ ions.

4. Methyl Chloride

As with charge exchange in methyl bromide, symmetric proton transfer in methyl chloride presents an example of proton transfer as a competitive channel to further reaction. The reaction sequence in methyl chloride has been shown to be (27)



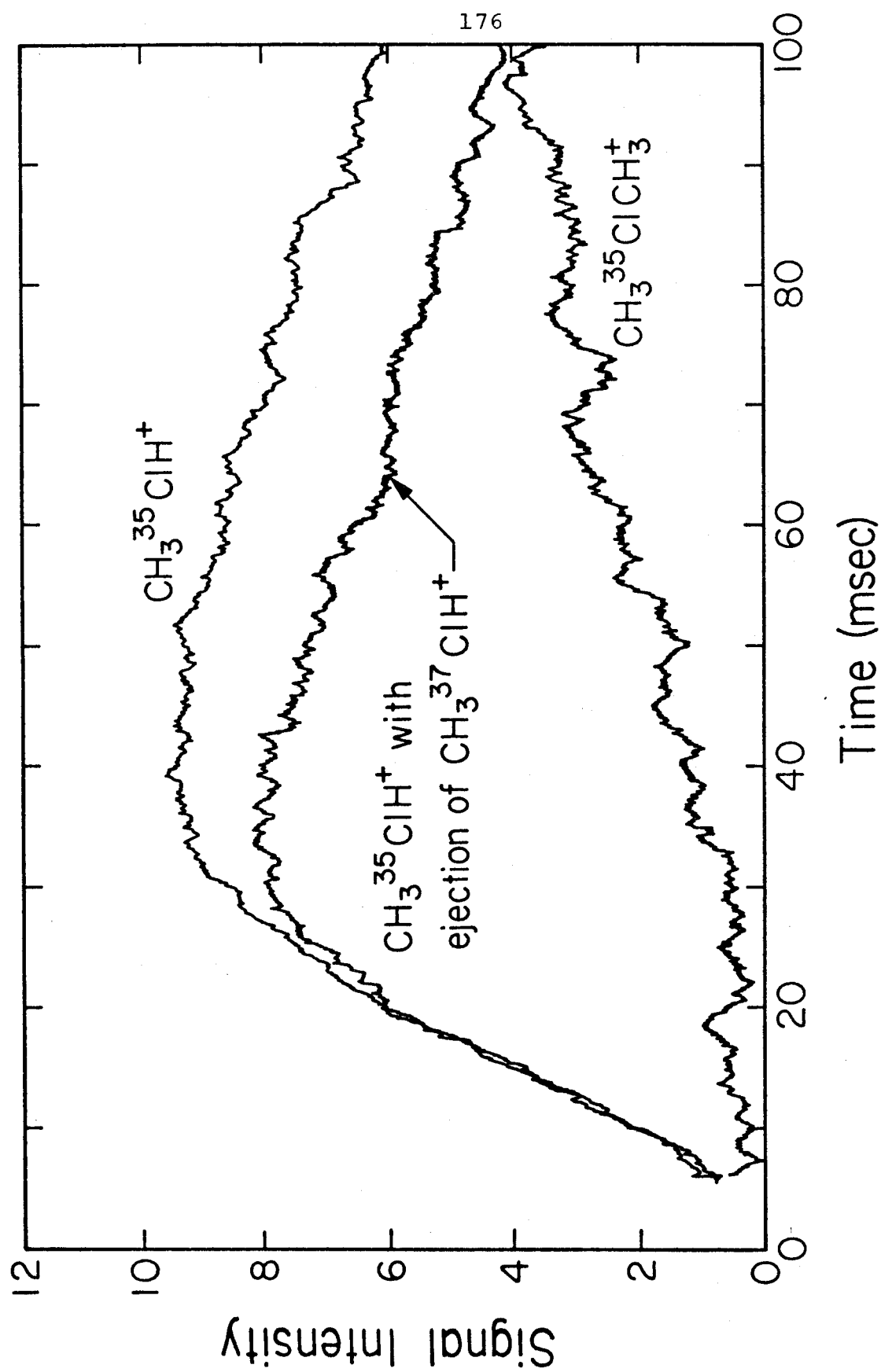
As was shown in the third chapter of this thesis, the rate constant for reaction (39) is almost seven times slower than that for reaction (40), even though the encounter rates for both pairs of reactants should be almost identical. This observation led to the suspicion that symmetric proton transfer might be a competing reaction channel. As with ammonia, a chlorine lone pair supplies a convenient means for formation of a proton bound dimer intermediate. The sequence of events involving the protonated parent ion of methyl chloride might be viewed as follows:



An ion ejection experiment was carried out involving continuous ejection of one of the isotopic protonated parent ions while monitoring the time variation of the other ions. This experiment is shown in Fig. 21. The kinetic analysis for this system is more complex than any of the others previously discussed. An exact solution to

Figure 21

Variation of intensity of $\text{CH}_3^{35}\text{ClH}^+$ with and without continuous ejection of $\text{CH}_3^{37}\text{ClH}^+$. The $\text{CH}_3^{35}\text{ClCH}_3^+$ ion is included to obtain relative ion abundances. Ions were formed by a 5 msec 13 eV electron beam pulse in CH_3Cl at a pressure of 1.5×10^{-6} torr.



the rate equations yields a ratio of protonated parent ion $\text{CH}_3^{35}\text{ClH}^+$, with and without ejection of the isotopic protonated parent, $\text{CH}_3^{37}\text{ClH}^+$, as

$$\frac{[\text{CH}_3^{35}\text{ClH}^+]}{[\text{CH}_3^{37}\text{ClH}^+]}_{\text{ej}} = \frac{n(k_n - k_f)}{n(k_n - k_f) + n_{37}k_p} \cdot \left[\frac{e^{-nk_ft} - e^{-(nk_n + n_{37}k_p)t}}{e^{-nk_ft} - e^{-nk_nt}} \right] \quad (42)$$

where n represents the total pressure of methyl chloride and n_{37} represents the partial pressure of $\text{CH}_3^{37}\text{Cl}$. This expression does not have the convenient form necessary to extract the rate constant k_p , for symmetric proton transfer. We know that k_n is much smaller than k_f and thus if $nk_f \gg nk_n + n_{37}k_p$. The ratio can be approximated by

$$\frac{[\text{CH}_3^{35}\text{ClH}^+]}{[\text{CH}_3^{37}\text{ClH}^+]}_{\text{ej}} \approx \frac{n(k_n - k_f)}{n(k_n - k_f) + n_{37}k_p} e^{-n_{37}k_pt} \quad (43)$$

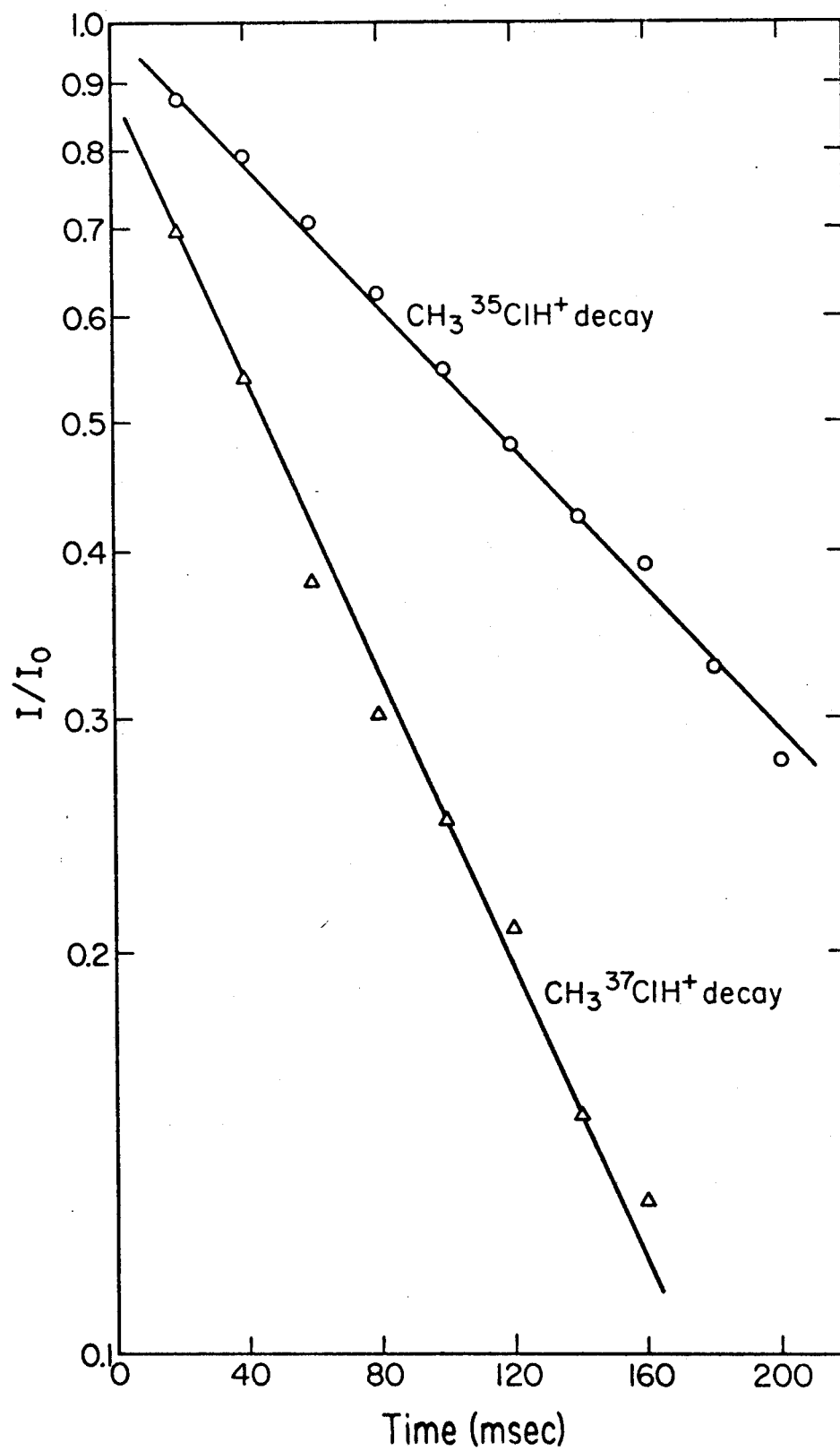
A plot of the log of this ratio vs time gives a straight line of slope $n_{37}k_p t$. From this and a similar plot of

$$\log \frac{[\text{CH}_3^{37}\text{ClH}^+]}{[\text{CH}_3^{37}\text{ClH}^+]}_{\text{ej}}$$

such as those shown in Fig. 22, a rate constant for symmetric proton transfer of $4.5 \times 10^{-10} \text{ cm}^3 \text{ molecule}^{-1} \text{ sec}^{-1}$ is obtained. If we assume that the proton bound dimer intermediate formed decomposes to produce products isotopically distinct from the reactants in one-half of the

Figure 22

Plot of $\log_{10} (I/I_0)$ for each of the isotopic CH_3ClH^+ ions.
Conditions are the same as those for Figure 21.



encounters a rate constant of $9.0 \times 10^{-10} \text{ cm}^3 \text{ molecule}^{-1} \text{ sec}^{-1}$ is obtained. Adding to this the rate of dimethyl chloronium ion formation a total encounter rate of $1.1 \times 10^{-10} \text{ cm}^3 \text{ molecule}^{-1} \text{ sec}^{-1}$ results. This is well within experimental error for agreement with the rate of reaction of the methyl chloride parent ion.

In order to establish whether protonation occurred for every collision of methyl chloride parent ion an ion ejection experiment was done on this ion to determine whether symmetric charge exchange was taking place. It was found not to, implying that all encounters of ion and molecule lead to protonation. The predicted Langevin rate for this reaction is $9.8 \times 10^{-10} \text{ cm}^3 \text{ molecule}^{-1} \text{ sec}^{-1}$ while the predicted locked dipole rate is $4.5 \times 10^{-9} \text{ cm}^3 \text{ molecule}^{-1} \text{ sec}^{-1}$. The experimental rate can thus be taken to be a measure of the importance of the molecular dipole in the ion-molecule potential. Assuming the potentials for CH_3Cl^+ and CH_3ClH^+ interacting with CH_3Cl are the same, an encounter rate of $1.2 \times 10^{-9} \text{ cm}^3 \text{ molecule}^{-1} \text{ sec}^{-1}$ is predicted for the protonated parent ion. This model for the reaction is consistent with an intermediate in which the proton is bound equally strong by either of the two chlorine atoms.

REFERENCES

1. D. Rapp and W. E. Francis, J. Chem. Phys. 37, 2631 (1962).
2. D. R. Bates, H. S. W. Massey, and A. L. Stewart, Proc. Roy. Soc. (London) A216, 437 (1953).
3. E. F. Gurnee and J. L. Magee, J. Chem. Phys. 26, 1237 (1957).
4. D. R. Bates, K. Ledsham, and A. L. Stewart, Phil. Trans. Roy. Soc. A246, 215 (1953).
5. B. L. Moisevitch, Proc. Phys. Soc. (London) A69, 653 (1956).
6. C. F. Melius, Ph.D. Thesis, California Institute of Technology, 1973.
7. D. Rapp and I. B. Ortenburger, J. Chem. Phys. 33, 1230 (1960).
8. A. Dalgarno, Phil. Trans. Roy. Soc. A250, 426 (1958).
9. J. J. Leventhal, T. F. Moran and L. Friedman, J. Chem. Phys. 46, 4666 (1967).
10. P. Langevin, Ann. Chim. Phys. 5, 245 (1905).
11. G. Gioumousis and D. P. Stevenson, J. Chem. Phys. 29, 294 (1958).
12. T. F. Moran and W. H. Hamill, J. Chem. Phys. 39, 1413 (1963).
13. S. K. Gupta, E. G. Jones, A. G. Harrison, and J. J. Myher, Can. J. Chem. 45, 3107 (1967).

14. F. Daniels and R. A. Alberty, Physical Chemistry, J. Wiley, New York, N.Y. (1965), p. 720.
15. J. L. Beauchamp, Ann. Rev. Phys. Chem. 22, 527 (1971).
16. J. J. Leventhal and L. Friedman, J. Chem. Phys. 46, 997 (1967).
17. S. E. Buttrill, Jr., J. Chem. Phys. 50, 4125 (1969).
18. D. P. Ridge, Ph.D. Thesis, California Institute of Technology (1973).
19. J. L. Beauchamp, J. Chem. Phys. 46, 1231 (1967).
20. S. E. Buttrill, Jr., J. Chem. Phys. 58, 656 (1973).
21. W. T. Huntress, Jr., J. Chem. Phys. 55, 2146 (1971).
22. J. D. Hirschfelder, C. F. Curtiss and R. B. Bird, Molecular Theory of Gases and Liquids, J. Wiley, New York, N.Y. (1951), p. 951.
23. D. L. Smith and J. H. Futrell, J. Chem. Phys. 59, 463 (1973).
24. E. G. Jones and A. G. Harrison, Int. J. Mass Spectrom. Ion Phys. 5, 178 (1970).
25. B. Ziegler, Z. Physik, 136, 108 (1953).
26. D. R. Bates and N. Lynn, Proc. R. Soc. A253, 141 (1959).
27. J. L. Beauchamp, D. Holtz, S. D. Woodgate, and S. L. Patt, J. Amer. Chem. Soc. 94, 2798 (1972).
28. R. D. Nelson, Jr., D. R. Lide, Jr., and A. A. Maryott, "Selected Values of Electric Dipole Moments for Molecules in the Gas Phase," NSRDS-NBS 10, U.S. Gov't. Printing Office, Washington, D.C. (1967).

29. M. Taagepera, W. G. Henderson, T. R. C. Brownlee, D. Holtz, J. L. Beauchamp, and R. W. Taft, J. Amer. Chem. Soc. 94, 4728 (1972).
30. R. Yamdagni and P. Kebarle, J. Amer. Chem. Soc. 95, 3504 (1973).
31. A. J. Dempster, Phil. Mag. 31, 438 (1916).
32. H. D. Smythe, Phys. Rev. 25, 452 (1925).
33. I. G. Csizmadia, R. E. Kari, J. C. Polanyi, A. G. Roach and M. A. Robb, J. Chem. Phys. 52, 6205 (1970).
34. H. Conroy, J. Chem. Phys. 51, 3979 (1969).
35. H. Eyring, J. O. Hirschfelder and H. S. Taylor, J. Chem. Phys. 4, 479 (1936).
36. B. G. Reuben and L. Friedman, J. Chem. Phys. 37, 1636 (1963).
37. J. H. Futrell and F. P. Abramson, Adv. Chem. Ser. 58, 107 (1966).
38. M. T. Bowers, D. D. Elleman and J. King, Jr., J. Chem. Phys. 50, 4787 (1969).
39. W. T. Huntress, Jr., D. D. Elleman and M. T. Bowers, J. Chem. Phys. 55, 5413 (1971).
40. R. P. Clow and J. H. Futrell, Int. J. Mass Spectrom. Ion Phys. 8, 119 (1972).
41. P. H. Dawson and A. W. Tickner, J. Chem. Phys. 37, 672 (1962).
42. T. Terao and R. A. Back, J. Phys. Chem. 73, 3884 (1969).

43. C. Chang, G. J. Sroka and G. G. Meisels, J. Chem. Phys. 55, 5154 (1971).
44. J. J. Huang and M. E. Schwartz, J. Chem. Phys. 56, 755 (1972).
45. R. Clappitt and L. Gowland, Nature 223, 815 (1969).
46. S. L. Bennett and F. H. Field, J. Amer. Chem. Soc. 94, 8669 (1972).
47. J. J. Leventhal and L. Friedman, J. Chem. Phys. 49, 1974 (1968).
48. J. J. Leventhal and L. Friedman, J. Chem. Phys. 50, 2928 (1969).
49. V. L. Tal'roze and A. K. Lyubimova, Dokl. Akad. Nauk. SSSR, 86, 909 (1952).
50. M. Henschman, in Ion Molecule Reactions, v. I, (J. L. Franklin, ed.), pp. 101-259, Plenum Press, New York, N.Y. (1972).
51. J. J. C. Mulder and J. S. Wright, Chem. Phys. Lett. 5, 445 (1970).
52. W. Th. A. M. Van der Lugt and P. Ros, Chem. Phys. Lett. 4, 389 (1969).
53. A. G. Harrison and D. G. Keyes, Can. J. Chem. 51, 1265 (1973).
54. Unpublished results, this laboratory.
55. Field and Beggs (J. Amer. Chem. Soc. 93, 1585 (1971) have observed $C_2H_9^+$ mass spectrometrically at high pressures of CH_4 and have determined its binding energy

to be 4.14 kcal/mole

56. P. Lerlet, S. D. Peyerimhoff, and R. J. Buenker, J. Amer. Chem. Soc. 94, 8301 (1972).
57. P. Kebarle, in Ion Molecule Reactions, V. I, (J. L. Franklin, ed.), Plenum Press, New York, N.Y. (1972).
58. M. S. B. Munson and F. H. Field, J. Amer. Chem. Soc. 87, 4242 (1965).

CHAPTER V

Kinetics of Symmetric Proton Transfer Reactions in Alcohols and Amines. De-excitation Mechanisms in Equilibrium Studies of Gas Phase Basicities and Structures of Proton Bound Dimer Intermediates

A. Introduction

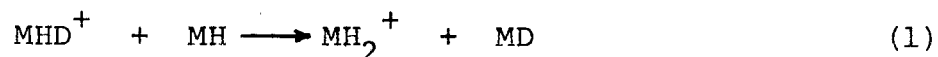
Product ions in ion-molecule reactions are frequently formed with varying amounts of internal energy. Haney and Franklin (1) have shown that a large fraction of the exothermicity of a gas phase ion-molecule reaction may appear as vibrational excitation of the products. If the reaction is sufficiently exothermic the ionic product may be short-lived compared to the time scale for its detection unless all or at least some part of this excitation energy is efficiently removed. If excited ions thus formed do not dissociate they may be sufficiently long lived to be detected in the excited state or they may undergo subsequent reaction in the excited state. If this is the case, any thermochemical inferences made from reactions in which the internal energy content of the reactant ions is in doubt will necessarily be uncertain also. An accurate assessment of relative proton affinities and a choice of efficient chemical ionization reagents depends strongly on a precise knowledge of the internal excitation of reactant ions.

Since the most useful and extensively tabulated data are for ground state ions, it is important to determine under what conditions gas phase ions may be determined to have relaxed to the ground state.

The previous chapter of this thesis examined the rates of electron and proton transfer in simple molecules. In these simple cases, where the ion-molecule potentials are least complex, it is more easy to evaluate the mechanisms for these reactions. In favorable circumstances, it may be assumed that the mechanism is general and applied to situations where more complex ion-molecule potentials are involved. In the case of proton transfer, it is apparent that the mechanism for that reaction most commonly involved formation of an intermediate. To characterize the efficiency of proton transfer as an ionic stabilization mechanism the rate of symmetric proton transfer between protonated parent ion and neutral molecule is used.

Of more general interest than the simple systems of the previous chapter are the analogous rates of symmetric proton transfer in more complex organic species to be used to determine the validity of thermochemical data obtained for gas phase organic ions. Of particular interest are the proton affinities or gas phase basicities of organic ions. Among the most commonly used reagents to determine the proton affinity of a particular organic molecule are the protonated parent ions of simple alcohols and alkyl amines.

In order to ascertain that these reagents are in their ground states, the rate of symmetric proton and deuterium transfer reactions of the form

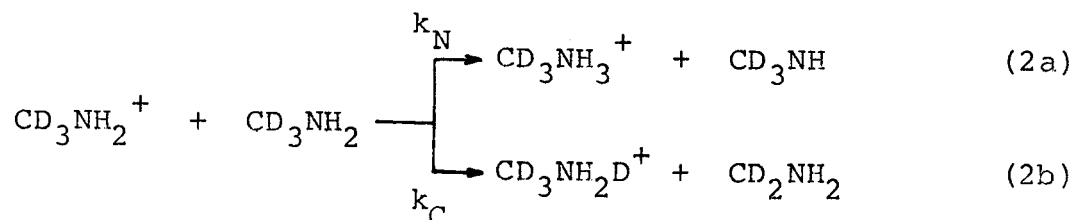


were examined. Although only applied to alcohols and amines in this chapter the techniques used are general and may be applied to a wide range of systems where MH may be alkyl halides, carboxylic acids, thiols, and alkyl phosphines. By measuring the rates of reaction for these molecules, it is possible to infer the rate of de-excitation of protonated molecular ions, should they be formed in excited states.

B. Methylamine

The gas phase ion chemistry of alkyl amines has been studied extensively in connection with attempts to characterize substituent effects on amine basicities (2-4). However, few attempts have been made to analyze the kinetics of reactions of amines. While the rate of formation of the protonated parent ion from the parent ion of methylamine has been documented (5) no attempt has been made to examine the relative rates of proton transfer from carbon and from nitrogen. In connection with the study of symmetric proton transfer these rates were measured for CD_3NH_2 . In both conventional drift and trapped ion experiments the relative rate constants for proton transfer

(eqn. 2a) and deuteron transfer (eqn. 2b) were obtained from the ratio of protonated and deuterated ion intensities at low conversion. It can be readily seen from the variation



of ion intensities with both pressure (Fig. 1) and with time (Fig. 2) this ratio is not constant as the reaction sequence progresses. The results indicate that $\text{CD}_3\text{NH}_2\text{D}^+$ is converted to CD_3NH_3^+ by a symmetric proton transfer reaction which can be envisioned as proceeding through an excited proton bound dimer intermediate. This reaction sequence resulting from the parent ion of methyl amine is shown in Fig. 3.

If it is assumed that every ion-molecule encounter of the parent ion leads to reaction, then the encounter rate for CD_3NH_2^+ may be taken to be $k_C + k_N$. Since the encounter rate of the protonated and deuterated parent ions is predicted by theory to be nearly identical to that of the parent ion the rate of formation of excited proton bound dimers, k_d , is predicted to be $k_C + k_N$. In the absence of termolecular stabilization these excited ions undergo unimolecular decomposition. Ignoring any deuterium isotope effects the dimers formed by reaction of $\text{CD}_3\text{NH}_2\text{D}^+$ will favor proton rather than deuteron bound dimers by a statistical

Figure 1

Variation of ion abundance with pressure for CD_3NH_2 at 11.0 eV. The solid line indicates the variation of ion intensity with pressure calculated from the average rate constant obtained from several determinations. The points indicate experimentally determined intensities.

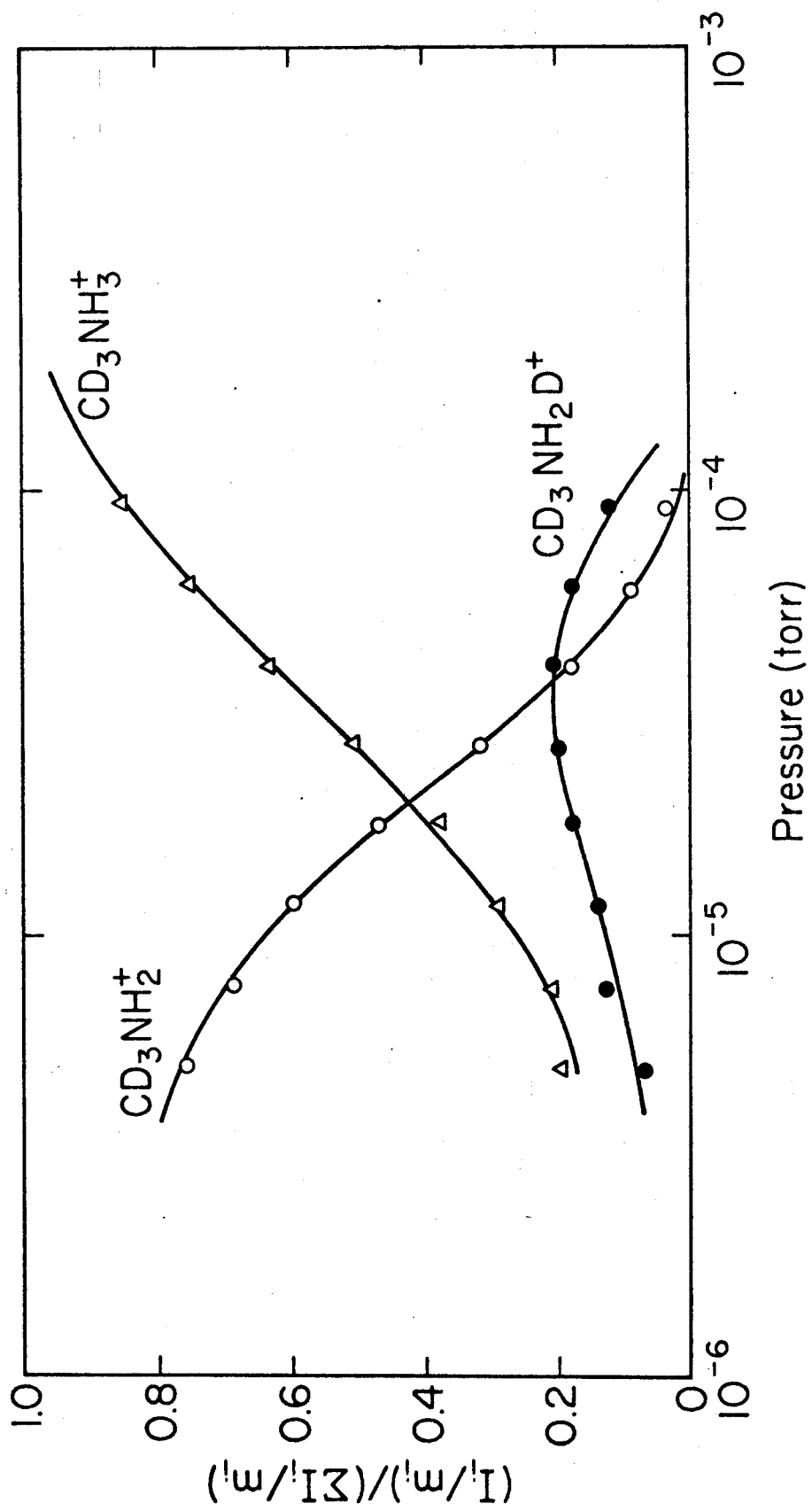


Figure 2

Variation of ion abundance with time for CD_3NH_2 at 12.0 eV and 6.5×10^{-7} torr with a 6 msec electron beam pulse.

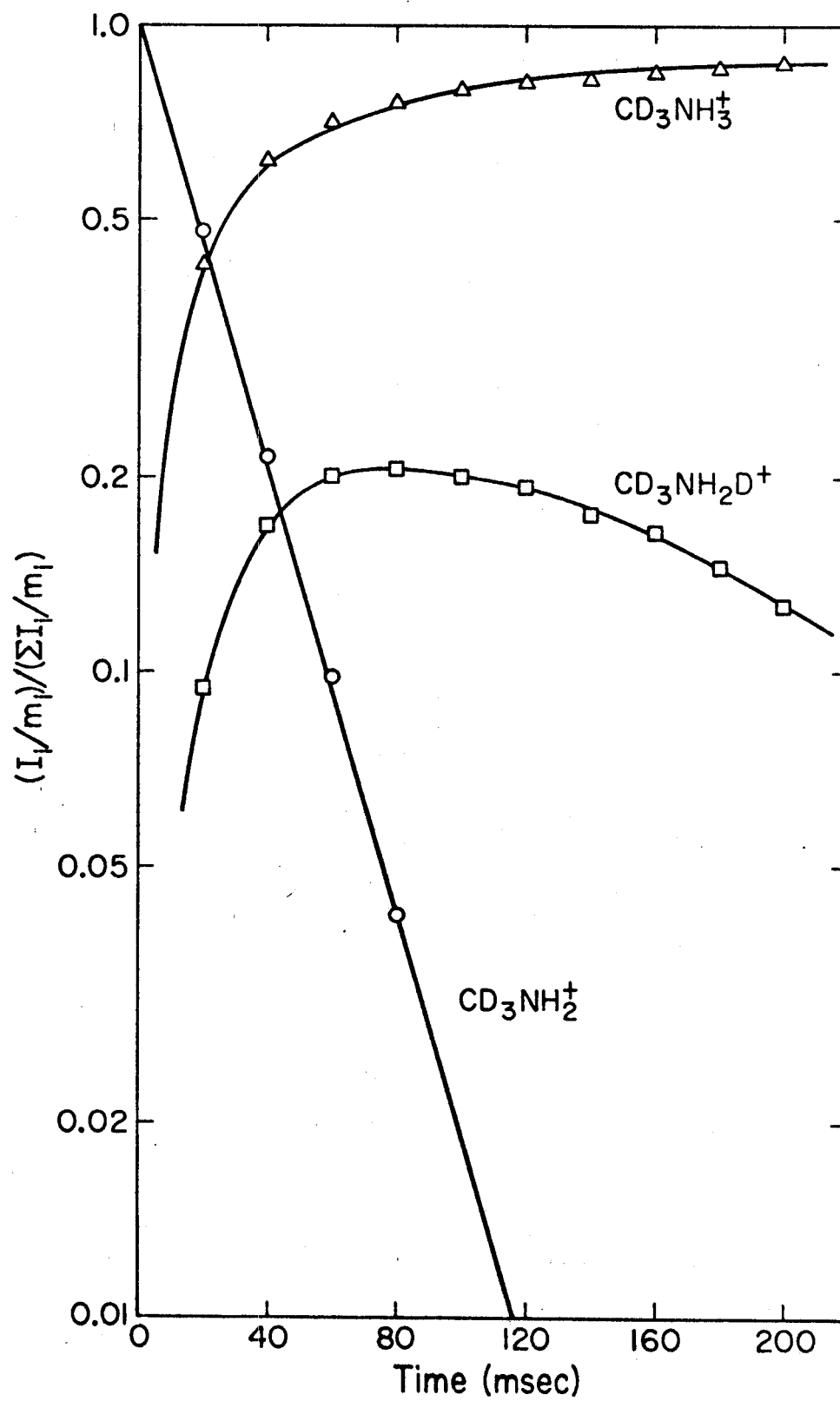
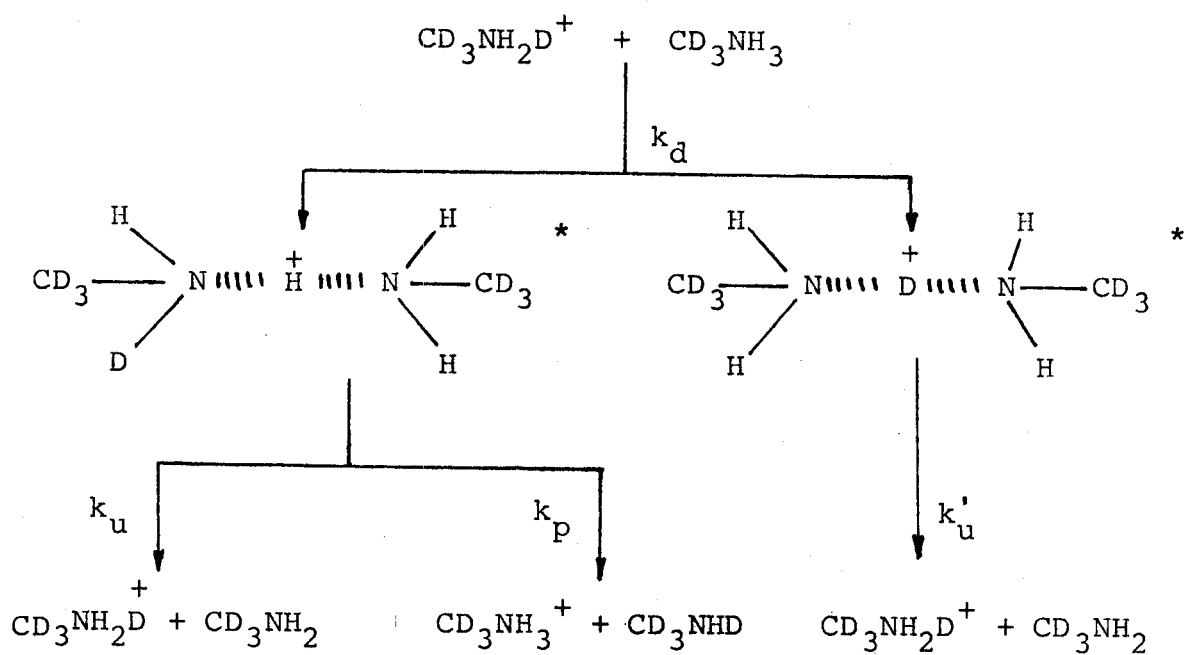
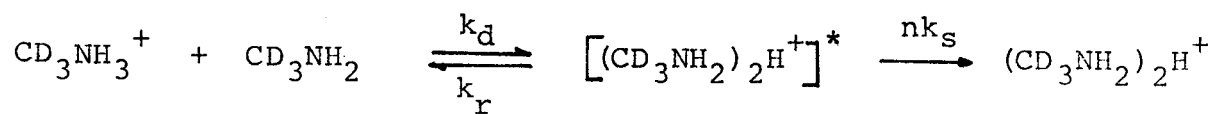
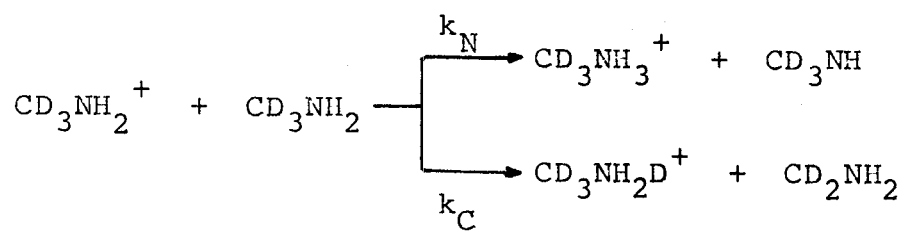


Figure 3

General ion-molecule reaction sequence for reactions of the parent ion of primary alkyl amines, represented by CH_3NH_2 .



probability of 2:1. The deuteron bound dimer will always dissociate to $\text{CD}_3\text{NH}_2\text{D}^+$ but the proton bound dimer will dissociate with equal probability to $\text{CD}_3\text{NH}_2\text{D}^+$ and CD_3NH_3^+ . Therefore in one-third of its encounters $\text{CD}_3\text{NH}_2\text{D}^+$ will produce CD_3NH_3^+ , accounting for the changing ratio of protonated and deuterated molecules.

ICR experiments provide a means for measuring the apparent bimolecular rate constant for conversion of $\text{CD}_3\text{NH}_2\text{D}^+$ to CD_3NH_3^+ . At sufficiently low pressures, collisional stabilization of the excited intermediate is not an important reaction channel and the steady state assumption may be applied to this species. The limiting slope for the disappearance of $\text{CD}_3\text{NH}_2\text{D}^+$ may then be represented by

$$\frac{d[\text{CD}_3\text{NH}_2\text{D}^+]}{dt} = -nk_d [\text{CD}_3\text{NH}_2\text{D}^+] \left(\frac{2k_p}{2k_u + 2k_p + k_u} \right) \quad (3)$$

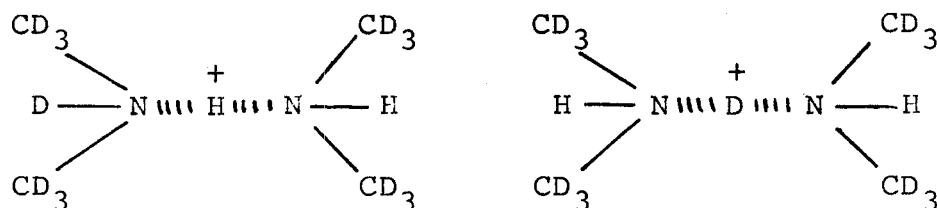
where n is the number density of methyl amine neutrals and the rate constants are defined in Fig. 3. The apparent bimolecular rate constants, $k_d \left(\frac{2k_p}{2k_u + 2k_p + k_u} \right)$, is found to be $4.2 \times 10^{-10} \text{ cm}^3 \text{ molecule}^{-1} \text{ sec}^{-1}$. If this rate does represent one-third of the ion-molecule encounters as predicted, an overall encounter rate of $1.3 \times 10^{-9} \text{ cm}^3 \text{ molecule}^{-1} \text{ sec}^{-1}$ is obtained, which is in fair agreement with the rate constant for reactions of the parent ion. If this assumption is true, the small discrepancy may be assigned

to experimental uncertainties or a possible small deuterium isotope effect.

The rate constants obtained using ICR techniques are summarized in Table 1 for both CH_3NH_2 and CD_3NH_2 . Included for comparison are available literature data for these reactions.

C. Dimethylamine

Analogous to deuterated methylamine an investigation of the ion-molecule reactions of dimethylamine- d_6 , $(\text{CD}_3)_2\text{NH}$, revealed a changing ratio of protonated and deuterated amine as the reaction sequence progressed. This is shown in the plots of variation of ion abundances with pressure, Fig. 4, and with time, Fig. 5. As in methylamine, an excited proton bound dimer intermediate is implicated. However, in the case of dimethylamine the dimer formed from the deuterated parent ion has a statistically equal probability of being bound by a proton and a deuteron. These two species, of the form,



have a one-fourth probability of undergoing unimolecular dissociation to $(\text{CD}_3)_2\text{NH}_2^+$.

The experimentally obtained rate constants are

TABLE 1
Rate Constants for Ion-Molecule Reactions of Methylamine

Reaction	Rate Constant ($\times 10^{-10}$ cm ³ molecule ⁻¹ sec ⁻¹)	
	<u>This work</u>	<u>Other</u>
$\text{CH}_3\text{NH}_2^+ + \text{CH}_3\text{NH}_2 \longrightarrow \text{CH}_3\text{NH}_3^+ + \text{CH}_4\text{N}$	19.8	21.0 (a)
$\text{CD}_3\text{NH}_2^+ + \text{CD}_3\text{NH}_2 \longrightarrow \text{CD}_3\text{NH}_3^+ + \text{CD}_3\text{NH}$	12.8	
$\text{CD}_3\text{NH}_2^+ + \text{CD}_3\text{NH}_2 \longrightarrow \text{CD}_3\text{NH}_2\text{D}^+ + \text{CD}_2\text{NH}_2$	6.2	
$\text{CD}_3\text{NH}_2\text{D}^+ + \text{CD}_3\text{NH}_2 \longrightarrow \text{CD}_3\text{NH}_3^+ + \text{CD}_3\text{NHD}$	4.2	

(a) Ref. 5

Figure 4

Variation of ion abundance with pressure for $(\text{CD}_3)_2\text{NH}$ at 11.0 eV. The solid line indicates the variation of ion intensity with pressure calculated from the average rate constant obtained from several determinations. The points indicate experimentally determined intensities.

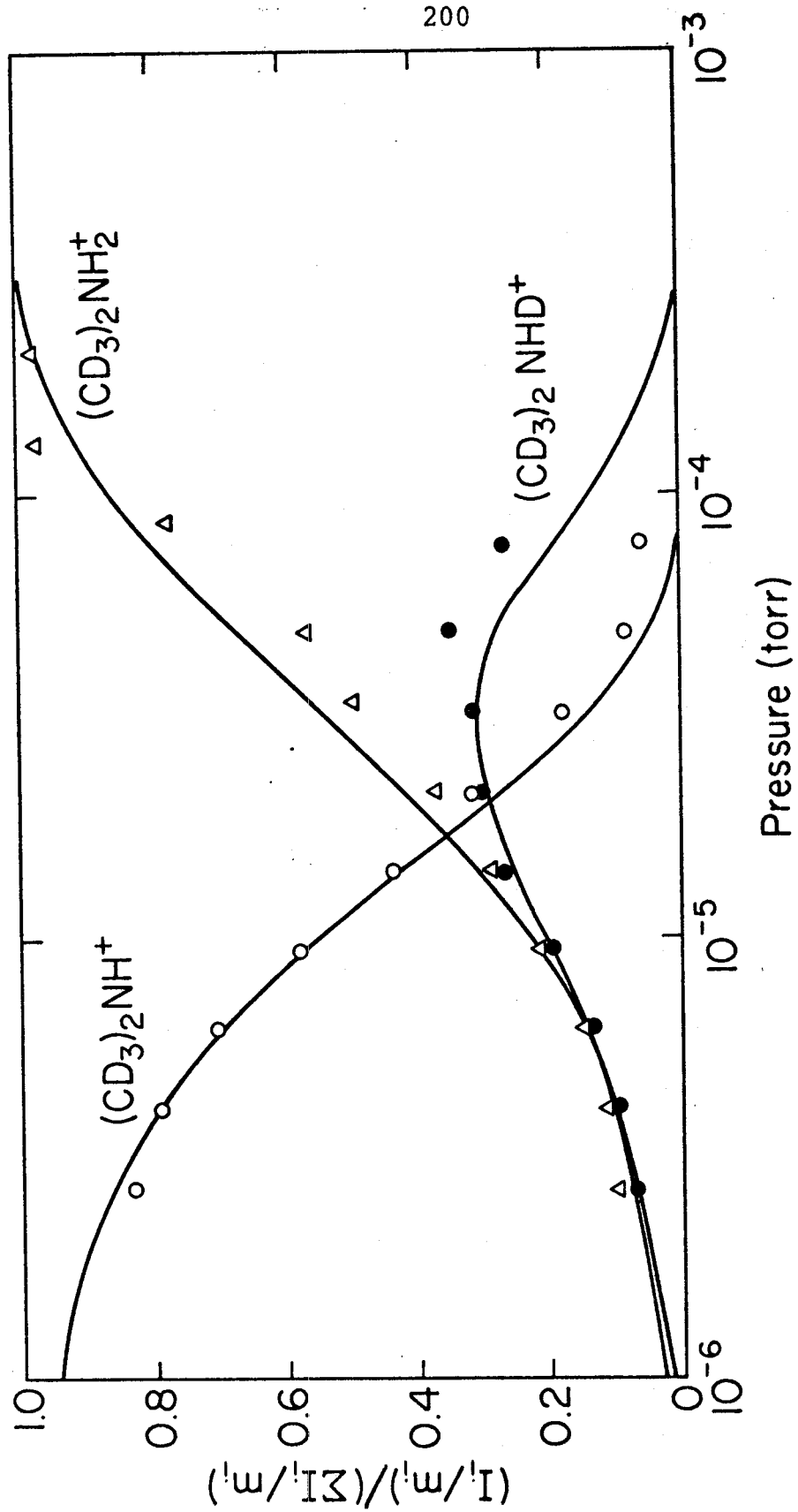
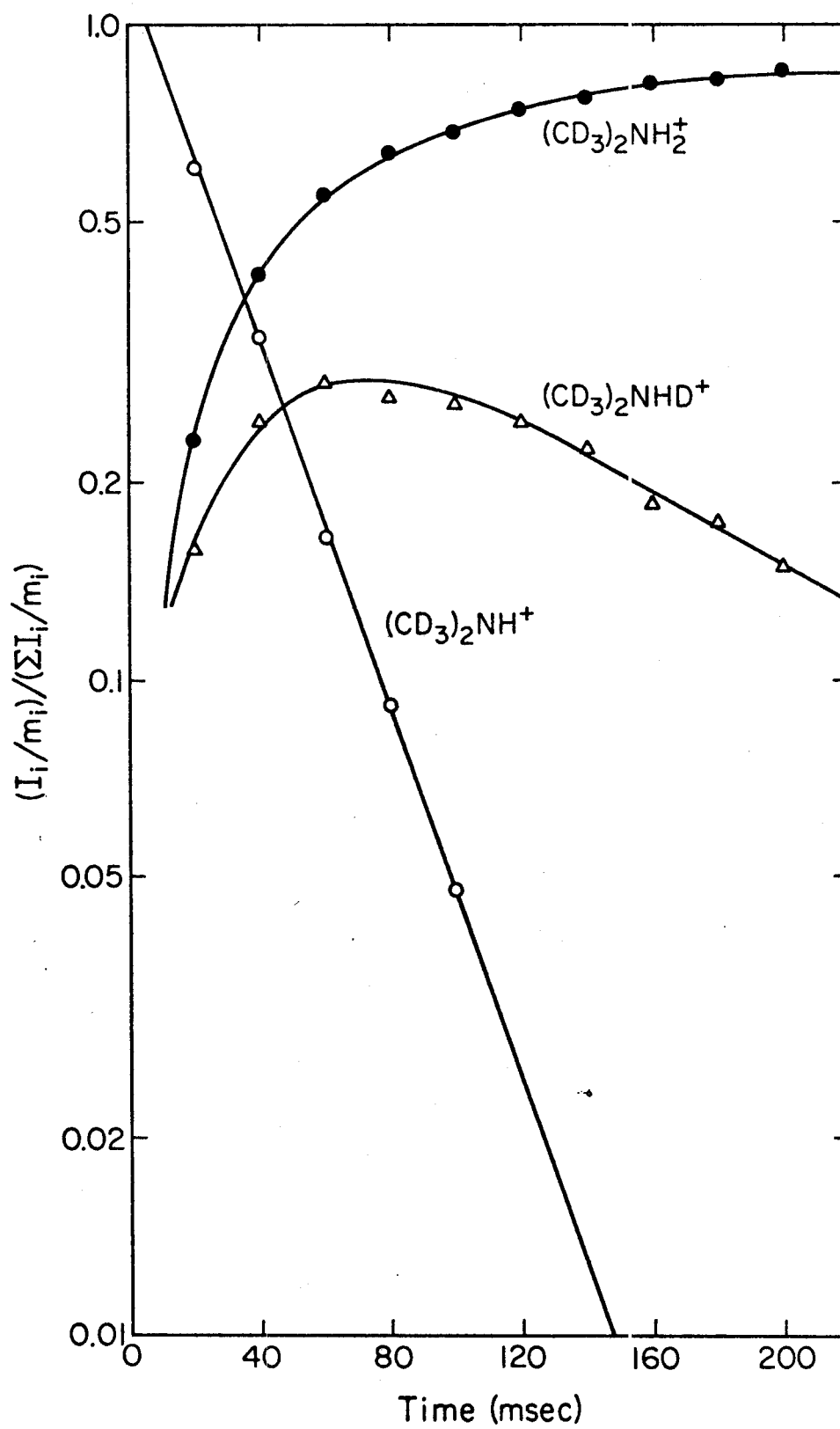


Figure 5

Variation of ion abundance with time for $(\text{CD}_3)_2\text{NH}$ at 10.5 eV and 7.5×10^{-7} torr with a 6 msec electron beam pulse.



summarized in Table 2 for both $(\text{CH}_3)_2\text{NH}$ and $(\text{CD}_3)_2\text{NH}$. The symmetric proton transfer rate obtained from the limiting slope for the disappearance of $(\text{CD}_3)_2\text{NHD}^+$ is $1.24 \times 10^{-9} \text{ cm}^3 \text{ molecule}^{-1} \text{ sec}^{-1}$ and is in good agreement with the predicted rate of dimer formation of $1.42 \times 10^{-9} \text{ cm}^3 \text{ molecule}^{-1} \text{ sec}^{-1}$.

D. Methanol

The ion-molecule reactions of simple alcohols are slightly more complex than alkyl amines due to the formation of protonated dialkyl ethers via a nucleophilic displacement reaction analogous to that producing dialkylhalonium ions in alkyl halides (6-10). The parent ion of methanol- d_3 , CD_3OH^+ exhibits the same behavior as CD_3NH_2^+ in transferring both protons and deuterons to the neutral molecule.

The sequence of reactions arising from the parent ion, CD_3OH^+ , in methanol- d_3 is shown in Fig. 6. The conversion of deuterated parent to protonated parent through the excited dimer complex is illustrated in the variation of ion intensities with pressure (Fig. 7) and with time (Fig. 8). Analysis of the kinetics of disappearance of the deuterated and protonated parent molecules gives the apparent bimolecular rate constants for symmetric proton transfer and protonated ether formation, respectively. These rate constants are summarized in Table 3 together with the analogous rate constants in undeuterated methanol. The fact that symmetric proton transfer occurs much faster than

TABLE 2

Rate Constants for Ion-Molecule Reactions of Dimethylamine

<u>Reaction</u>	Rate Constant ($\times 10^{-10} \text{ cm}^3 \text{ molecule}^{-1} \text{ sec}^{-1}$)	
	<u>This work</u>	<u>Other</u>
$(\text{CH}_3)_2\text{NH}^+ + (\text{CH}_3)_2\text{NH} \longrightarrow (\text{CH}_3)_2\text{NH}_2^+ + \text{C}_2\text{H}_6\text{N}$	13.1	
$(\text{CD}_3)_2\text{NH}^+ + (\text{CD}_3)_2\text{NH} \longrightarrow (\text{CD}_3)_2\text{NH}_2^+ + (\text{CD}_3)_2\text{N}$	7.4	
$(\text{CD}_3)_2\text{NH}^+ + (\text{CD}_3)_2\text{NH} \longrightarrow (\text{CD}_3)_2\text{NHD}^+ + (\text{CD}_3)\text{NH}(\text{CD}_2)$	6.8	
$(\text{CD}_3)_2\text{NHD}^+ + (\text{CD}_3)_2\text{NH} \longrightarrow (\text{CD}_3)_2\text{NH}_2^+ + (\text{CD}_3)_2\text{ND}$	3.1	

Figure 6

General ion-molecule reaction sequence for reactions of the parent ion of aliphatic alcohols represented by CD_3OH .

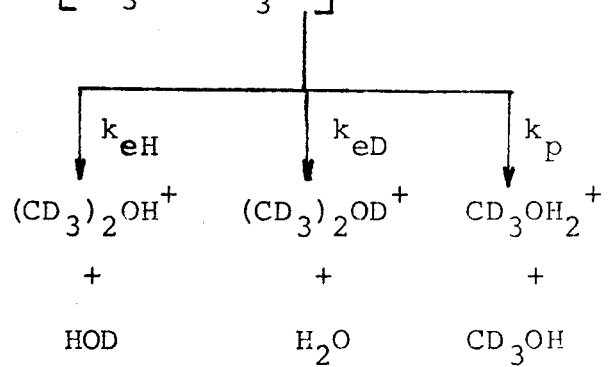
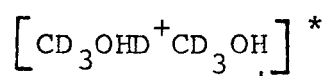
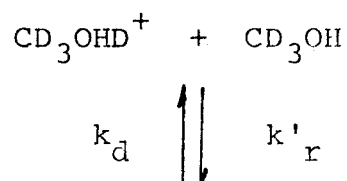
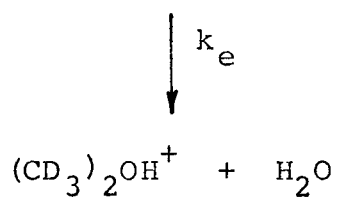
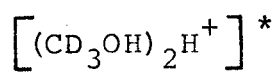
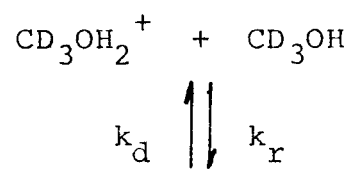
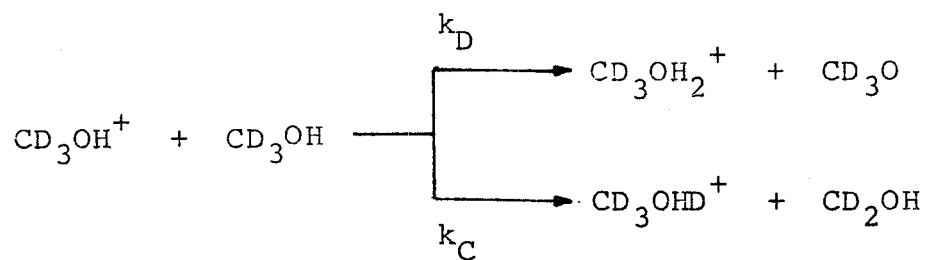


Figure 7

Variation of ion abundance with pressure for CD_3OH at 11.0 eV. The solid line indicates the variation of ion intensity with pressure calculated from the average rate constant obtained from several determinations. The points indicate experimentally determined intensities.

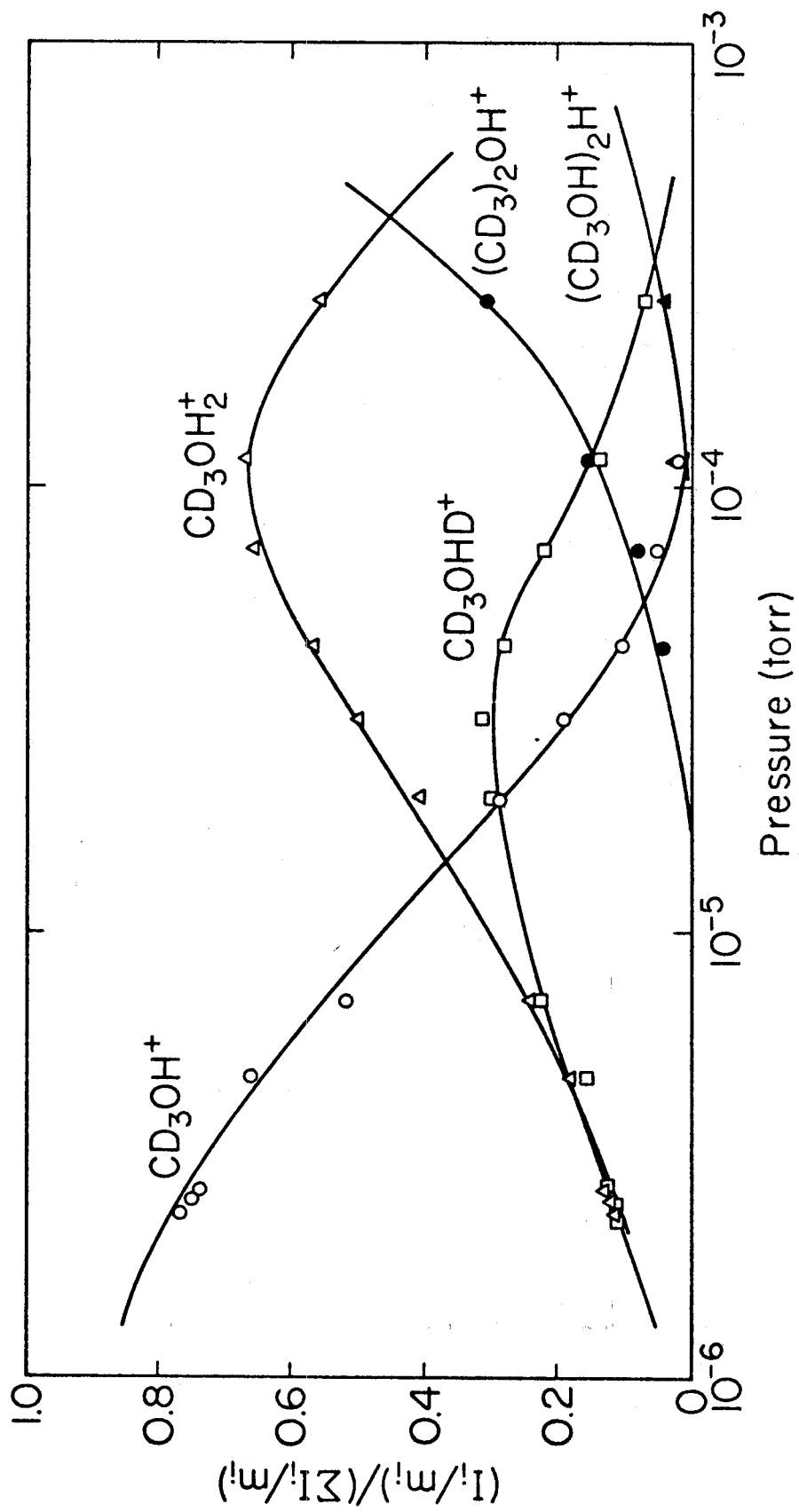


Figure 8

Variation of ion abundance with time for CD_3OH at 14.0 eV and 3.5×10^{-7} torr with a 6 msec electron beam pulse.

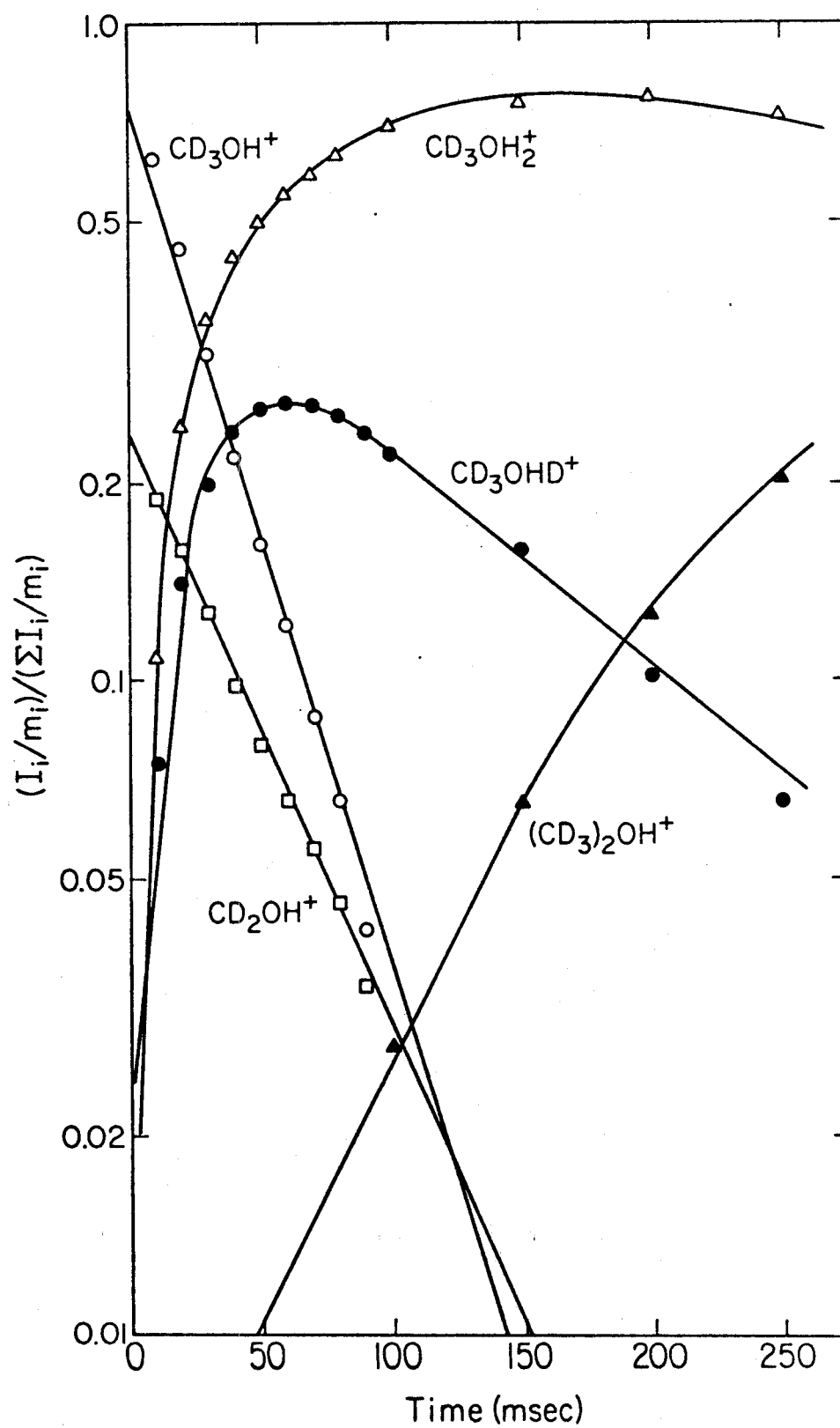


TABLE 3

Rate Constants for Ion-Molecule Reactions of Methanol

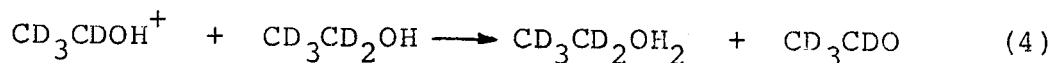
<u>Reaction</u>	Rate Constant ($\times 10^{-10}$ cm ³ molecule ⁻¹ sec ⁻¹)	
	<u>This work</u>	<u>Other</u>
$\text{CH}_3\text{OH}^+ + \text{CD}_3\text{OH} \longrightarrow \text{CD}_3\text{OH}_2^+ + \text{CH}_3\text{O}$	21.3	2.5 (a)
$\text{CH}_3\text{OH}_2^+ + \text{CH}_3\text{OH} \longrightarrow (\text{CH}_3)_2\text{OH}^+ + \text{H}_2\text{O}$	1.0	
$\text{CD}_3\text{OH}^+ + \text{CD}_3\text{OH} \longrightarrow \text{CD}_3\text{OH}_2^+ + \text{CD}_3\text{O}$	11.7	0.9 (a)
$\text{CD}_3\text{OH}^+ + \text{CD}_3\text{OH} \longrightarrow \text{CD}_3\text{OHD}^+ + \text{CD}_2\text{OH}$	13.5	1.2 (a)
$\text{CD}_3\text{OHD}^+ + \text{CD}_3\text{OH} \longrightarrow \text{CD}_3\text{OH}_2^+ + \text{CD}_3\text{OD}$	4.6	
$\text{CD}_3\text{OH}_2^+ + \text{CD}_3\text{OH} \longrightarrow (\text{CD}_3)_2\text{OH}^+ + \text{H}_2\text{O}$	1.5	

(a) Ref. 9

ether formation is convincingly shown by the lack of any deuterated dimethyl ether formation. At higher pressures the proton bound dimer of methanol may be collisionally stabilized before dissociation takes place and the apparent bimolecular rate constants for symmetric proton transfer and protonated ether formation will fall off (11). It is important therefore to work at pressures where termolecular reaction is inoperable to gain an insight into the actual mechanisms of reactions involved.

E. Ethanol

In addition to the molecular ion of ethanol, it was found necessary to work under conditions where the parent minus H ion was also present. The reactions observed in ethanol-d₅ are basically the same as those observed for methanol-d₃ with the addition of the new reaction



The reactions observed for ethanol-d₅ are illustrated graphically by the variation of ion abundances with both pressure and time in Figures 9 and 10, respectively. The rate constants obtained for these reactions and those observed in undeuterated ethanol are shown in Table 4.

F. Discussion

The occurrence of symmetric proton transfer reactions and the formation of proton bound dimers at high pressure are strong evidence for an excited proton bound dimer

Figure 9

Variation of ion abundance with pressure for $\text{CD}_3\text{CD}_2\text{OH}$
at 12.0 eV.

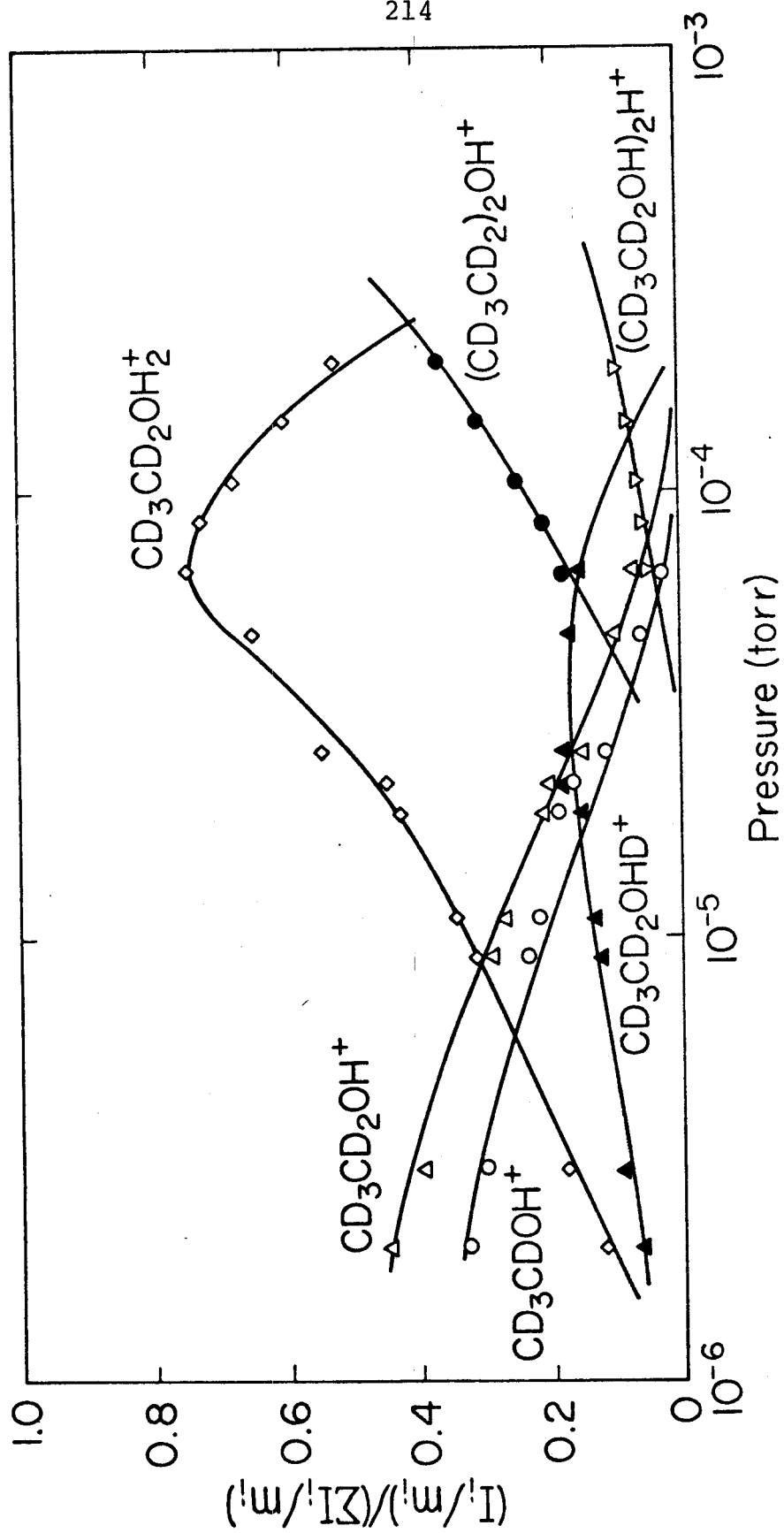


Figure 10

Variation of ion abundance with time for $\text{CD}_3\text{CD}_2\text{OH}$ at 16.0 eV and 8.0×10^{-7} torr with a 6 msec electron beam pulse.

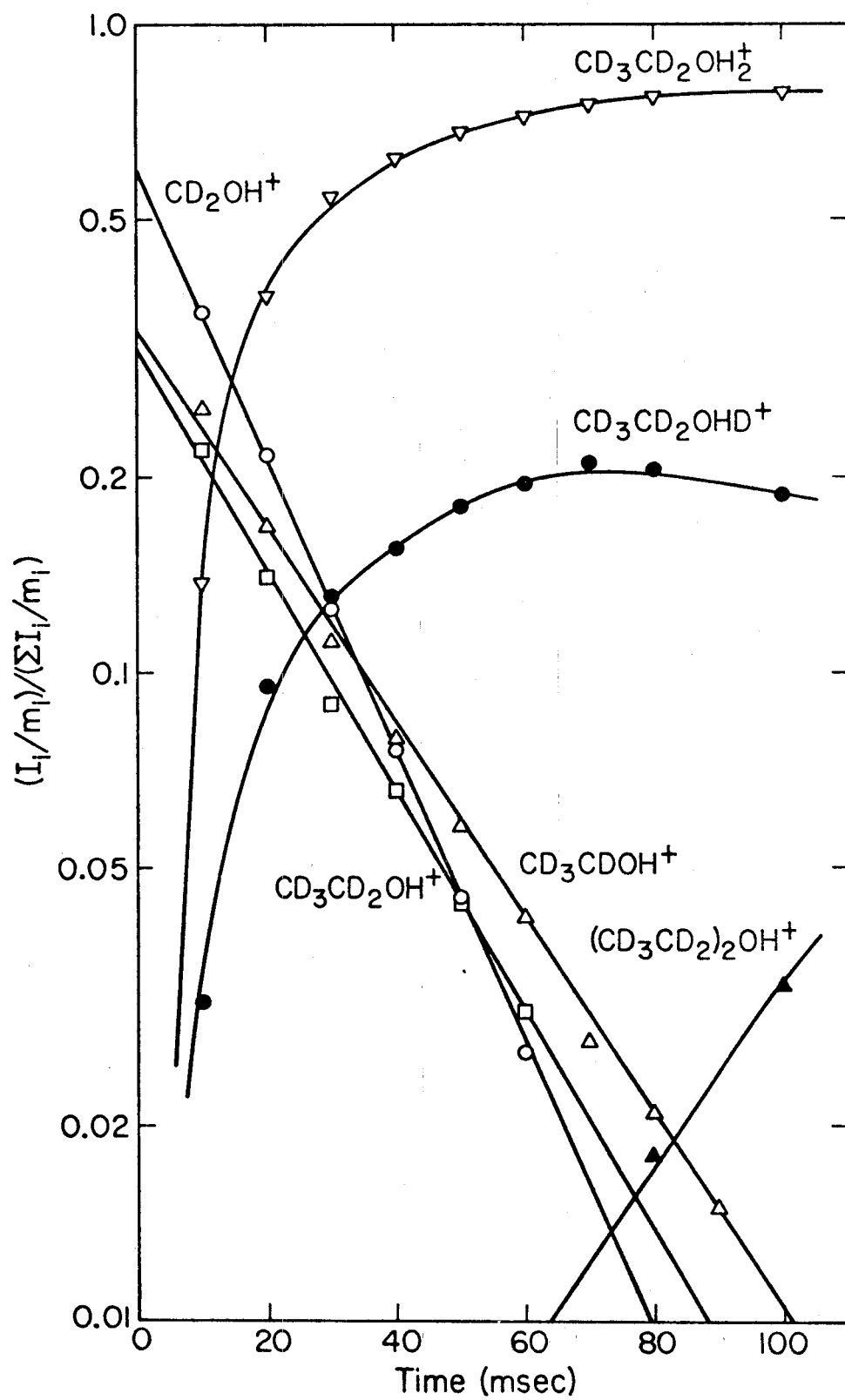


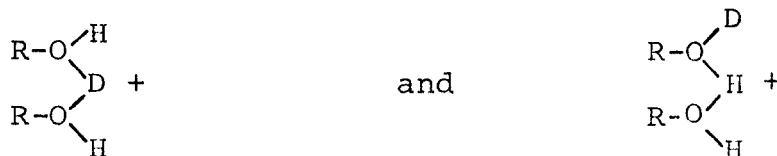
TABLE 4

Rate Constants for Ion-Molecule Reactions of Ethanol

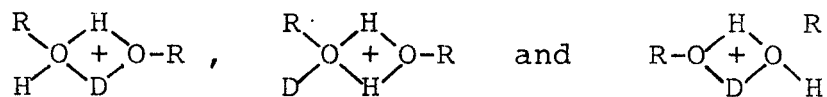
Reaction	Rate Constant ($\times 10^{-10}$ cm ³ molecule ⁻¹ sec ⁻¹)	
	<u>This work</u>	<u>Other</u>
$\text{CH}_3\text{CH}_2\text{OH}^+ + \text{CH}_3\text{CH}_2\text{OH} \longrightarrow \text{CH}_3\text{CH}_2\text{OH}_2^+ + \text{C}_2\text{H}_5\text{O}$	18.0	
$\text{CH}_3\text{CHOH}^+ + \text{CH}_3\text{CH}_2\text{OH} \longrightarrow \text{CH}_3\text{CH}_3\text{CH}_2\text{OH}_2^+ + \text{CH}_3\text{CHO}$	9.0	
$\text{CH}_3\text{CH}_2\text{OH}_2^+ + \text{CH}_3\text{CH}_2\text{OH} \longrightarrow (\text{CH}_3\text{CH}_2)_2\text{OH}^+ + \text{H}_2\text{O}$	2.2	
$\text{CD}_3\text{CD}_2\text{OH}^+ + \text{CD}_3\text{CD}_2\text{OH} \longrightarrow \text{CD}_3\text{CD}_2\text{OH}_2^+ + \text{CD}_3\text{CD}_2\text{O}$	5.2	
$\text{CD}_3\text{CD}_2\text{OH}^+ + \text{CD}_3\text{CD}_2\text{OH} \longrightarrow \text{CD}_3\text{CD}_2\text{OHD}^+ + \text{CD}_3\text{CDOH}$	6.7	
$\text{CD}_3\text{CDOH}^+ + \text{CD}_3\text{CD}_2\text{OH} \longrightarrow \text{CD}_3\text{CD}_2\text{OH}_2^+ + \text{CD}_3\text{CDO}$	14.0	12.0 (a)
$\text{CD}_3\text{CD}_2\text{OHD}^+ + \text{CD}_3\text{CD}_2\text{OH} \longrightarrow \text{CD}_3\text{CD}_2\text{OH}_2^+ + \text{CD}_3\text{CD}_2\text{OD}$	3.3	
$\text{CD}_3\text{CD}_2\text{OH}_2^+ + \text{CD}_3\text{CD}_2\text{OH} \longrightarrow (\text{CD}_3\text{CD}_2)_2\text{OH}^+ + \text{H}_2\text{O}$	1.7	

(a) Ref. 8

complex as a reaction intermediate for the ion-molecule reactions of protonated alcohols and amines. In the case of alcohols there are two plausible complexes which could be postulated to permit facile proton or deuteron transfer. The first of these complexes has two equivalent forms for reaction of the deuterated molecule,



Dissociation of these complexes would yield ROH_2^+ in one out of every four formed. However, an alternative, cyclic intermediate may be postulated with the three equivalent forms

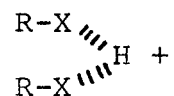


where R is the alkyl group originally part of the ion and R is the alkyl group associated with the neutral molecule. Dissociation of these complexes would produce ROH_2^+ from one-third of those formed.

The nature of the proton bound complexes in the case of alkyl amines is less ambiguous. Since the nitrogen atom of an amine has one less non-bonded electron pair than the oxygen atom of an alcohol, a cyclic complex is not possible. The complexes formed from protonated amines must then take

the linear form discussed previously. In Table 5 the total rate constant for symmetric proton transfer inferred from the intermediates discussed above are compared with the total rate constant for protonation of the parent molecule. The theoretical Langevin and locked-dipole rate constants are also included for comparison.

It is instructive to compare the rate of protonated dialkyl ether formation in alcohols to the analogous reaction in alkyl halides, dialkyl halonium ion production (12). The intermediate for the latter process can also be thought of as a proton bound dimer of the form



Generally, the rate constant for the condensation reaction of alkyl halides proceeds at a rate very close to that for alcohols but in amines no such reaction is observed. The allyl halide complex can rearrange to eliminate HX by a concerted process of bond breakage and formation in which a non-bonding chlorine lone-pair participates. A linear alcohol dimer would be able to eliminate H₂) by an entirely analogous process. In a cyclic alcohol dimer, however, the concerted process is hindered since the oxygen lone-pair is tied up in a second proton bond. The fact that the observed rate constants for the analogous reactions of alcohols and alkyl halides are nearly identical is an indication that the linear proton bound dimer is more likely.

TABLE 5

Comparison of Protonation and Proton Transfer Rate Constants

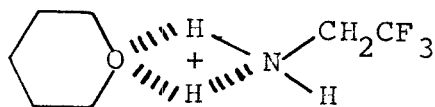
<u>Species</u>	<u>Rate Constant ($\times 10^{-10}$ cm³ molecule⁻¹ sec⁻¹)</u>			
	<u>Protonation</u>	<u>Proton transfer</u>	<u>Locked dipole</u>	<u>Langevin</u>
CH ₃ NH ₂	19.0	12.6	40	11.7
(CH ₃) ₂ NH	14.2	12.4	35	11.9
CH ₃ OH	25.2	17.4, (a) 13.8 (b)	45	10.5
CH ₃ CH ₂ OH	11.9	13.2, (a) 9.9 (b)	40	11.7

(a) Linear proton bound dimer

(b) Cyclic proton bound dimer

A proton bound amine dimer must also have a linear form. However, the nitrogen atoms in such a complex have no lone pair of electrons to allow a concerted condensation reaction to occur by elimination of NH_3 .

Although the above arguments favor a linear proton bound dimer for alcohols, an interesting example adding credence to cyclic proton bound dimers does exist. In an investigation of the relative basicities of tetrahydropyran and trifluoroethylamine ($\text{CF}_3\text{CH}_2\text{NH}_2$) it was found that although the proton affinities were nearly identical, the crossed proton bound dimer was favored strongly at higher pressures (13). While neither of the protonated species is able to form a cyclic proton bound dimer with its parent molecule, it is possible for the crossed dimer to take the cyclic form



The formation of two proton bonds thermodynamically favors the cyclic crossed dimer causing this species to be preferentially formed after many encounters.

It is of interest to note the wide variation in rates of formation of proton bound dimers of the species studied here. Both ethanol and dimethylamine dimers appear at much lower pressures than methanol and methylamine.

Simple RRKM theory relating the rate of chemical reaction to the amount of excess energy in the transition state and

the number of vibrational degrees of freedom it has offers an explanation for this. Assuming that each of the proton bound dimers initially contain comparable amounts of excess energy equal to the proton bond strength than the ethanol and dimethylamine dimers will have longer lifetimes due to the greater number of vibrational modes available for distribution of this energy (14). This longer lifetime results in an increased probability of stabilizing collisions occurring to remove excess energy before it can participate in unimolecular decomposition. This argument is consistent with the recent empirical expression derived by Good (15) for termolecular reactions

$$k = C \left[\frac{D + rRT}{rRT} \right]^{s-2} \quad (5)$$

where C is an empirical constant, D is the bond dissociation energy of the intermediate, R is the gas constant, T is the Kelvin temperature, r is the number of square term contributing to the internal energy of the molecule and s is the number of vibrational degrees of freedom of the intermediate.

G. Conclusions

Proton transfer reactions in which the proton carries no excess energy and the neutral rather than ionic product is left in an excited state are plausible de-excitation mechanisms. As indicated by this study, these reactions are relatively fast and de-excitation should then be rapid.

A summary of some of the thermochemical properties for

the molecules studied here along with the maximum amount of internal excitation in protonated molecules is shown in Table 6. Polyatomic species of this sort are capable of accomodating excess energy in their vibrational modes quite well. The probability of proton transfer occurring after complex formation has taken place and the relative amounts of energy in the ionic and neutral products will depend on the potential in which the proton finds itself. Recently, calculations of potential surfaces for proton bound dimers of water have indicated a symmetric potential well with a broad minimum (16,17). The nature of the potential well for proton bound dimers would determine its structure and the strength of the proton bond and thus the probability for its dissociation.

The polyatomic species studied here would likely have potentials similar to that for water. Thus, protonated ions formed with excess energy may facilely relax by a proton transfer mechanism involving a proton bonded intermediate. These reactions occur rapidly and hence the protonated species formed with varying amounts of excess energy may be de-excited rapidly. Hence when further reaction takes place the protonated ion can be assumed to be in its ground state, implying that thermochemical inferences derived from proton transfer reactions to other neutrals are likely valid since the reagent ions contain no excess energy.

TABLE 6

Summary of Thermochemical Data (a)

Species (MH)	ΔH_f° (MH) (b)	IP (MH) (b)	ΔH_f° (MH ₂ ⁺) (b)	PA (MH) (c)	E_{\max}^* (MH ₂ ⁺) (d)
Methanol	-48.1	10.85	138	180	24
Ethanol	-56.2	10.48	124	186	23
Methylamine	- 5.49	8.97	144.2	216.3	17
Dimethylamine	- 4.41	8.24	139.2	222.4	8.5

- (a) All thermochemical data are given in kcal/mole at 298°K except ionization potentials which are in eV.
- (b) J.L. Franklin, J.G. Dillard, H.M. Rosenstock, J.T. Herron, K. Draxl, and F.H. Field, "Ionization Potentials, Appearance Potentials, and Heats of Formation of Gaseous Positive Ions," N5RDS-NBS.26, U.S. Government Printing Office, Washington, D.C., 1969.
- (c) PA(M) = proton affinity of M, defined as the negative of the enthalpy change for the process $M + H^+ \rightarrow MH^+$.
- (d) Calculated from the exothermicity for the reaction

$$MH^+ + MH \rightarrow MH_2^+ + M.$$
 In cases where radical heats of formation ($\Delta H_f^\circ(M)$) are not known they have been estimated by the group equivalent methods outlined in reference (b).

H. Experimental Details

The experiments described in this chapter were carried out on the modified ICR spectrometer described in Chapter 3 of this thesis. Rate constants from intensity vs. pressure spectra were calculated by an iterative computer solution to the ICR lineshape equations formulated by Marshall and Buttrill (18). The computer program together with sample data cards is listed in Appendix I. Rate constants from trapped-ion spectra were obtained from semi-logarithmic plots (19).

Methylamine- d_3 and dimethylamine- d_6 were obtained from Merck, Sharpe, and Dohme of Canada. Methanol- d_3 and ethanol- d_5 were prepared by refluxing methanol- d_4 and ethanol- d_6 with magnesium turnings to produce the dialkoxide magnesium salts. These salts were then treated with water and distilled to obtain the exchanged alcohol. All samples were further purified by bulb to bulb distillation and were found to be greater than 99% isotopically pure by mass spectrometric analysis.

REFERENCES

1. M. A. Haney and J. L. Franklin, J. Chem. Phys. 48, 4093 (1968).
2. D. Holtz, J. L. Beauchamp, W. G. Henderson and R. W. Taft, Inorg. Chem. 10, 201 (1971).
3. M. Taagepera, W. G. Henderson, R. T. C. Brownlee, D. Holtz, J. L. Beauchamp, and R. W. Taft, J. Amer. Chem. Soc. 94, 4728 (1972).
4. E. M. Arnett, F. M. Jones III, M. Taagepera, W. G. Henderson, J. L. Beauchamp, D. Holtz and R. W. Taft, J. Amer. Chem. Soc. 94, 4727 (1972).
5. E. G. Jones and A. G. Harrison, Can. J. Chem. 45, 3119 (1967).
6. K. R. Ryan, L. W. Sieck and J. H. Futtrell, J. Chem. Phys. 41, 111 (1968).
7. J. C. J. Thynne, F. K. Amenu-Kpodo and A. G. Harrison, Can. J. Chem. 44, 1655 (1966).
8. L. W. Sieck, F. P. Abramson and J. H. Futtrell, J. Chem. Phys. 45, 1655 (1966).
9. S. K. Gupta, E. G. Jones, A. G. Harrison and J. J. Myher, Can. J. Chem. 45, 3107 (1967).
10. J. M. S. Henis, J. Amer. Chem. Soc. 90, 844 (1968).
11. P. G. Miasek, Ph.D. Thesis, California Institute of Technology, 1973.
12. J. L. Beauchamp, D. Holtz, S. D. Woodgate, and S. L. Patt, J. Amer. Chem. Soc. 94, 2798 (1972).

13. W. G. Henderson and J. L. Beauchamp, unpublished results.
14. The proton bond strengths of the proton bound dimers of water and ammonia have been measured recently (P. Kebarle in "Ion Molecule Reactions," Vol. 1, ed. J. L. Franklin, Plenum, New York, 1972) to be 31.6 kcal/mole and 27 kcal/mole, respectively, indicating that the proton bond strengths of methanol, ethanol, methylamine, and dimethylamine might be roughly comparable.
15. A. Good, Trans. Far. Soc. 67, 3495 (1971).
16. W. P. Kraemer and G. H. F. Dierckson, Chem. Phys. Lett. 5, 463 (1970).
17. P. A. Kollman and L. C. Allen, J. Amer. Chem. Soc. 92, 6101 (1970).
18. A. G. Marshall and S. E. Buttrill, Jr., J. Chem. Phys. 52, 2752 (1970).
19. T. B. McMahon and J. L. Beauchamp, Rev. Sci. Instrum. 43, 509 (1972).

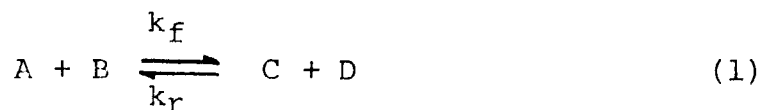
CHAPTER VI

Trapped Ion Cyclotron Resonance Investigations of Equilibria of Organic Ions

A. Gas Phase Ion Molecule Equilibria

Within recent years several research groups using a variety of techniques have begun investigations of bimolecular gas phase equilibria involving a wide range of ion-molecule reactions (1-5). Of the large number of experimental techniques available for determination of thermochemical quantities such as heats of formation, bond strengths, proton affinities, electron affinities and carbonium ion stabilities, equilibrium techniques provide the most accurate methods, allowing relative thermochemical properties to be determined within 0.1 kcal/mole. From the equilibrium conditions established in reversible gas phase ion-molecule reactions, thermochemical data may be derived based on thermodynamic and statistical mechanical principles correlating free energies of reaction with equilibrium constants and forward and reverse rate constant ratios (6). These principles have been successfully applied to equilibria involving free radical reactions (7) and to reactions in solution (8).

For the hypothetical reversible ion-molecule reaction



the equilibrium constant may be obtained from the principle of detailed balancing and expressed by

$$K_{eq} = \frac{[C]_{eq} [D]_{eq}}{[A]_{eq} [B]_{eq}} = \frac{k_f}{k_r} \quad (2)$$

where $[]_{eq}$ denotes the steady state concentration of each of the species. In order to relate kinetic and equilibrium observations to thermodynamic quantities the thermodynamic equation for the free energy,

$$\Delta G = -RT \ln K_{eq} \quad (3)$$

is applied. The free energy is related to the enthalpy and entropy change for the reaction by

$$\Delta G = \Delta H - T \Delta S \quad (4)$$

Thus, by an examination of the equilibrium constant, and hence the ΔG , as a function of temperature for a given reaction, both the ΔH and ΔS of reaction may also be determined. In the absence of temperature dependent studies, it is usually assumed that in gas phase ion molecule equilibria, particularly those involving proton transfer between homologous pairs of molecules or anions, that the entropy change involved is usually zero or at least does not contribute significantly to ΔG (3). This assumption is based on the reasoning that once a proton bound dimer intermediate is formed from a homologous pair of bases, it is equally favorable entropically for the proton to be bound to either

base when the intermediate dissociates.

Studies of equilibria involving bimolecular reactions of neutrals in solution and the gas phase have resulted in empirical correlations between thermodynamic quantities and the parameters of the Arrhenius expressions for reversible reactions (9). According to the Arrhenius equation for bimolecular reaction the reaction rate constant is given by

$$k = A e^{-E_a/RT} \quad (5)$$

where A is called the Arrhenius "A" factor and E_a is the experimental activation energy necessary for reaction to occur. In the simple collision theory (9) (SCT) for bimolecular reaction the rate constant is given by

$$k = pze^{-E_a/RT} \quad (6)$$

where z is the collision frequency and p is the probability that any given collision of sufficient energy will result in products. These models of reaction have been successfully applied to reactions where the intermolecular forces are weak and collisions are diffusion controlled. However, for gas phase ion-molecule reaction the interactions are dominated by relatively strong ion-induced dipole and ion-dipole attractions. This increased understanding of the factors governing ion-molecule equilibria allows greater insight into and greater confidence in the thermochemical data derived from these experiments.

Although there is little experimental justification, it

is interesting to attempt empirical correlations of Arrhenius forms for ion-molecule reactions with thermochemical quantities. It is generally accepted that sufficiently exothermic ($\Delta H \leq -1$ kcal/mole) ion-molecule reactions proceed with zero activation energy. If reaction (1) is considered to be an ion-molecule reaction exothermic in the forward direction then the forward and reverse rate constants might conform to the relations

$$k_f = p_f z_f \quad (7)$$

$$k_r = p_r z_r e^{-E_a/RT} \quad (8)$$

in which case the equilibrium constant would have the form

$$K_{eq} = \frac{p_f z_f}{p_r z_r e^{-E_a/RT}} \quad (9)$$

Using equation (3) to relate this quantity to ΔG the empirical correlations to ΔH and ΔS are given by

$$\Delta H = -E_a \quad (10)$$

$$\Delta S = -R \ln \left(\frac{p_f z_f}{p_r z_r} \right) \quad (11)$$

In cases where the ion-molecule reaction proceeds through a near symmetric intermediate, such as the proton bound dimer of a homologous pair of bases, it will probably be true that $p_f \approx p_r$. In this case, an approximate expression for the entropy change may be taken as

$$\Delta S \approx -R \ln \left(\frac{z_f}{z_r} \right) \quad (12)$$

For non-polar neutrals the ion-molecule collision frequency is given by the Langevin relation (10-12)

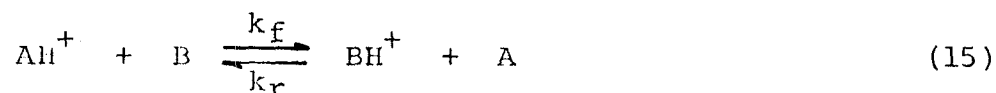
$$z = 2\pi e \left(\frac{\alpha}{\mu}\right)^{\frac{1}{2}} \quad (13)$$

where e is the charge of the ion, α is the neutral polarizability and μ is the reduced mass of the ion molecule pair. In cases where the neutral molecule has a permanent dipole moment, μ_D , several investigators have suggested that the collision frequency may be represented by (13)

$$z = 2\pi e \left(\frac{\alpha}{\mu}\right)^{\frac{1}{2}} + 2\pi e \mu_D \cos \theta \left(\frac{2}{\pi \mu kT}\right) \quad (14)$$

where k is the Boltzmann constant, T the Kelvin temperature and θ the average angle between the molecular dipole and the trajectory of the approaching ion. While these equations do not always provide exact collision frequencies they can provide qualitative relative collision frequencies. If the ion-molecule reactions of the equilibrium do conform to an Arrhenius form it should then be possible to predict the sign of the ΔS term involved from equation (13).

Consider for example the hypothetical case in which a proton is transferred between a homologous pair of bases of comparable polarizability but with one of them having an appreciable dipole moment. The equilibrium may be represented by



where B is the base having a dipole. It would then be

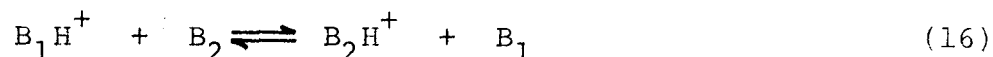
expected that the collision frequency for the forward reaction will be larger than that for the reverse reaction and as a result of a collision frequency ratio, z_f/z_r , greater than unity the apparent entropy change for the forward reaction will be predicted by equation (12) to be negative.

Recently developed trapped ion cyclotron resonance experiments (14,15) provide an excellent means for examination of equilibria involving organic and inorganic gas phase ions at thermal energies. Examination of ion abundances as a function of time can be undertaken at sufficiently low pressures that no complicating termolecular stabilization reactions occur. Thus after a sufficient number of collisions have taken place an equilibrium may be established and the steady state relative ion abundances measured routinely. If the ratio of neutral molecules participating is accurately known equilibrium constants may be routinely obtained. In addition, ion ejection experiments which permit removal of one of the ionic reactants after equilibrium is established allow the forward and reverse rate constants of the equilibrium to be measured, providing an independent determination of the equilibrium constant.

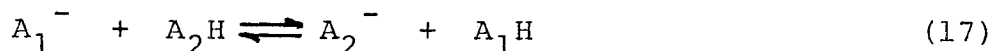
These techniques have been applied to a variety of reactions to provide information pertaining to a wide range of chemical phenomena. The results of these studies are the subject of this chapter.

B. Proton Transfer Equilibria. Gas Phase Basicities and Acidities

By far the most commonly studied gas phase ion-molecule equilibria have been those of the proton transfer variety. These reactions are of two types. The first of these,



involves transfer of a proton between two gas phase bases and is used to establish relative gas phase basicities or proton affinities (PA) of molecules. The second reaction is of the form



and involves proton transfer between anions. The relative binding strengths of a proton to the two anions A_1^- and A_2^- may be used to establish the relative acidities of the neutrals A_1H and A_2H and in favorable cases where the radical heats of formation for A_1 and A_2 are known their relative electron affinities may be determined (2).

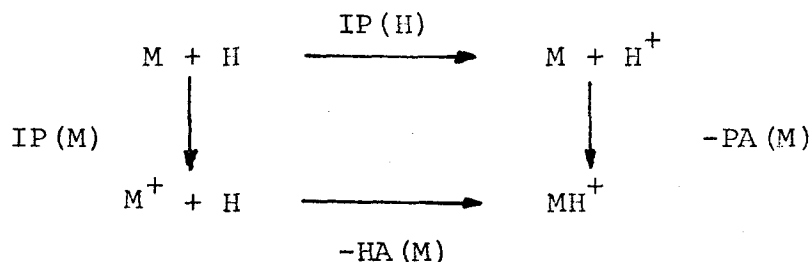
1. Proton Affinities

The proton affinity of a molecule, M, may be defined by the negative enthalpy change for the reaction (16)



A convenient method for relating proton affinities to other thermochemical quantities is to construct a thermochemical cycle as shown in Scheme I.

Scheme I.

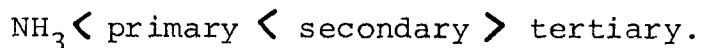


Here, IP denotes the ionization potential and HA the hydrogen affinity as defined by the appropriate reaction. The proton affinity may thus be expressed as

$$\text{PA}(\text{M}) = \text{IP}(\text{H}) - \text{IP}(\text{M}) + \text{HA}(\text{M}) \quad (19)$$

Within any given homologous series of molecules it has generally been observed that the hydrogen affinity is constant (17). Since the ionization potential of hydrogen atom is a constant in equation (19), it can be readily seen that within a given homologous series the proton affinity a particular molecule will increase relative to some reference base by an amount equal to the decrease in ionization potential relative to the same reference base. This relationship is illustrated in Table I for the proton affinities of a series of primary alkyl amines determined by ICR techniques (18-20).

Simple alkyl amines present a particularly interesting group of molecules for study of gas phase basicities. In aqueous solution the order of amine basicities has been convincingly shown to be (8)



This ordering bears no obvious relation to simple molecular

TABLE I

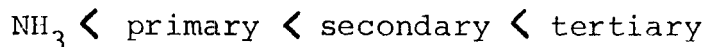
Thermochemical Properties of Alkyl Amines^(a,b)

<u>Base (M)</u>	<u>IP (M)</u>	<u>PA (M)</u>	<u>HA (M)</u>
CH ₃ NH ₂	206.8	216.3	109.5
EtNH ₂	204.3	218.8	109.5
i-PrNH ₂	201.1	221.2	108.7
t-BuNH ₂	199.2	223.3	108.9

(a) All values given in kcal/mole at 298° K.

(b) Data taken from Reference 18.

properties nor any correlation with consecutive substituent effects. The anomolous ordering was consequently attributed to a solvent effect whereby tertiary amines were poorer bases due to difficulties in solvation. However, recent gas phase mass spectrometric observations have shown that the intrinsic order of amine basicities is (18-20)



and can be much more readily explained as arising from cumulative alkyl substituent effects.

The most satisfactory method for determining gas phase amine basicities is the high pressure mass spectrometric technique described by Kebarle (3). His apparatus has the capability of variation of temperature and by means of Vant Hoff plots both the enthalpy and entropy change involved in proton transfer between amine pairs may be determined. However, the strong tendency of amines to cluster to form proton bound dimers and higher aggregates restricts the operating temperature range to between 500°K and 800°K (3,21). In some cases the ΔS change observed for proton transfer reactions of amines is significant but the usual assumption that $\Delta S \approx 0$ has still been employed.

The trapped ion ICR techniques described in Chapters 2 and 3 of this thesis provide an excelled method for examination of competitive protonation of gas phase amines at ambient temperatures. At pressure low enough that no collisionally stabilized proton-bound dimers appear the

ion-molecule reactions of amines lead solely to production of the protonated molecule. As further collisions occur in binary amine mixtures a proton transfer equilibrium is reached and from the equilibrium abundances of ions and neutrals the relative free energies of protonation of the amines may be derived.

A typical experiment involves ionization by a brief ionizing pulse (usually 6 msec or less) in which the electron energy is switched above the ionization potential of the species present. Ions are then trapped for a variable reaction time at which point they are drifted into the analyzer region of the ICR cell to be detected. A representative trace for the ion-molecule reactions occurring in dimethylamine is shown in Fig. 1. The protonation reaction can be seen to be rapid ($k > 10^{-9} \text{ cm}^3 \text{ molecule}^{-1} \text{ sec}^{-1}$) and at moderate pressures and short times it can be readily seen that the protonated molecule is the predominant ion. If a second amine is added both protonated molecules are formed rapidly and further collisions between ion and molecule lead to proton transfer. Within 50 proton transfers it may be assumed that proton transfer equilibrium has been reached. Such a situation is shown in Fig. 2 for a mixture of dimethylamine and isopropylamine. The ΔG determined for this reaction is 1.4 kcal/mole with dimethylamine being determined to be the stronger base. No temperature dependent examination for this pair of amines has been reported

Figure 1

Trace of ion intensities vs. time for parent and protonated parent ions of $(\text{CH}_3)_2\text{NH}$. Ion formation was by a 5 msec, 10.5 eV electron beam pulse at 1.1×10^{-6} torr.

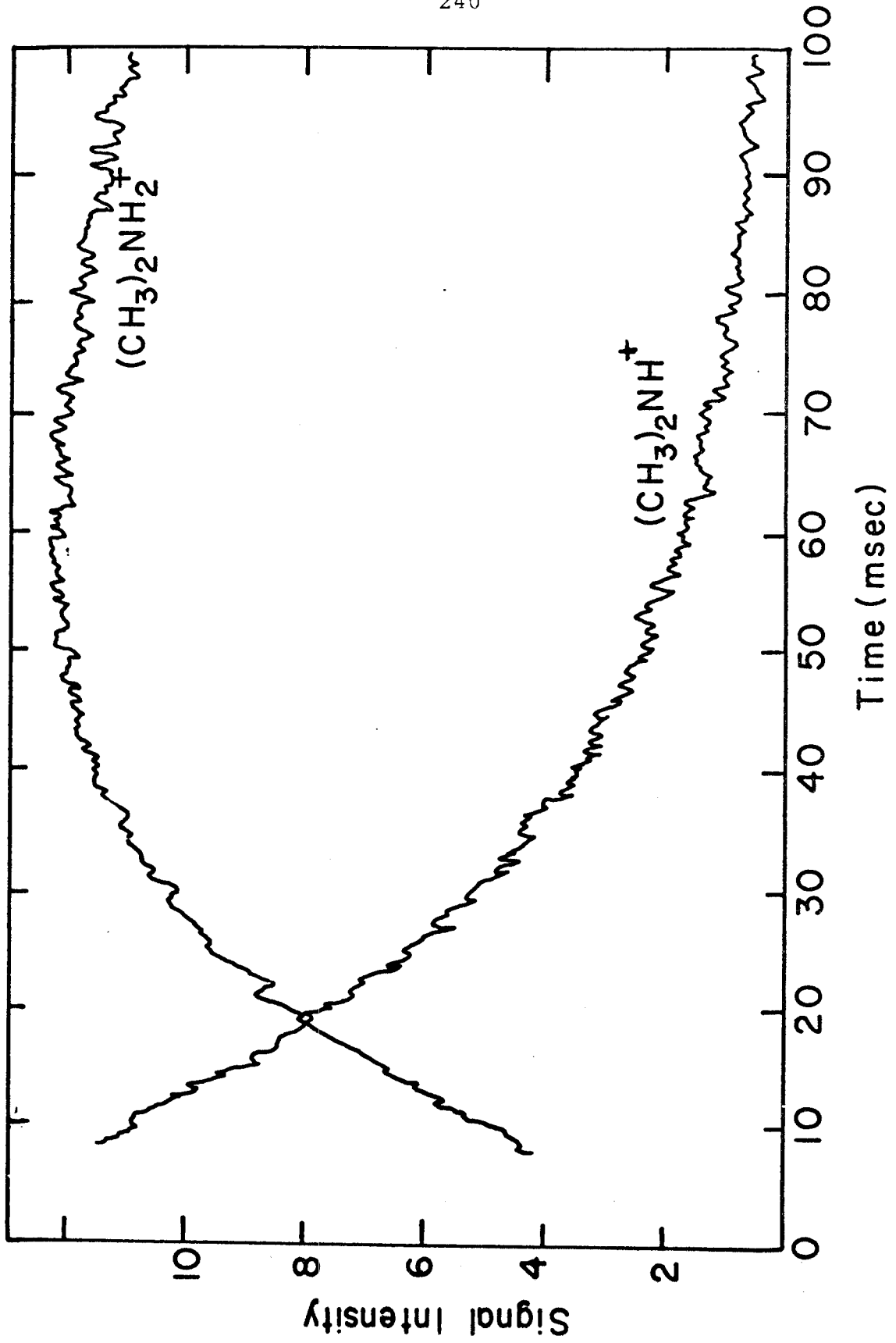
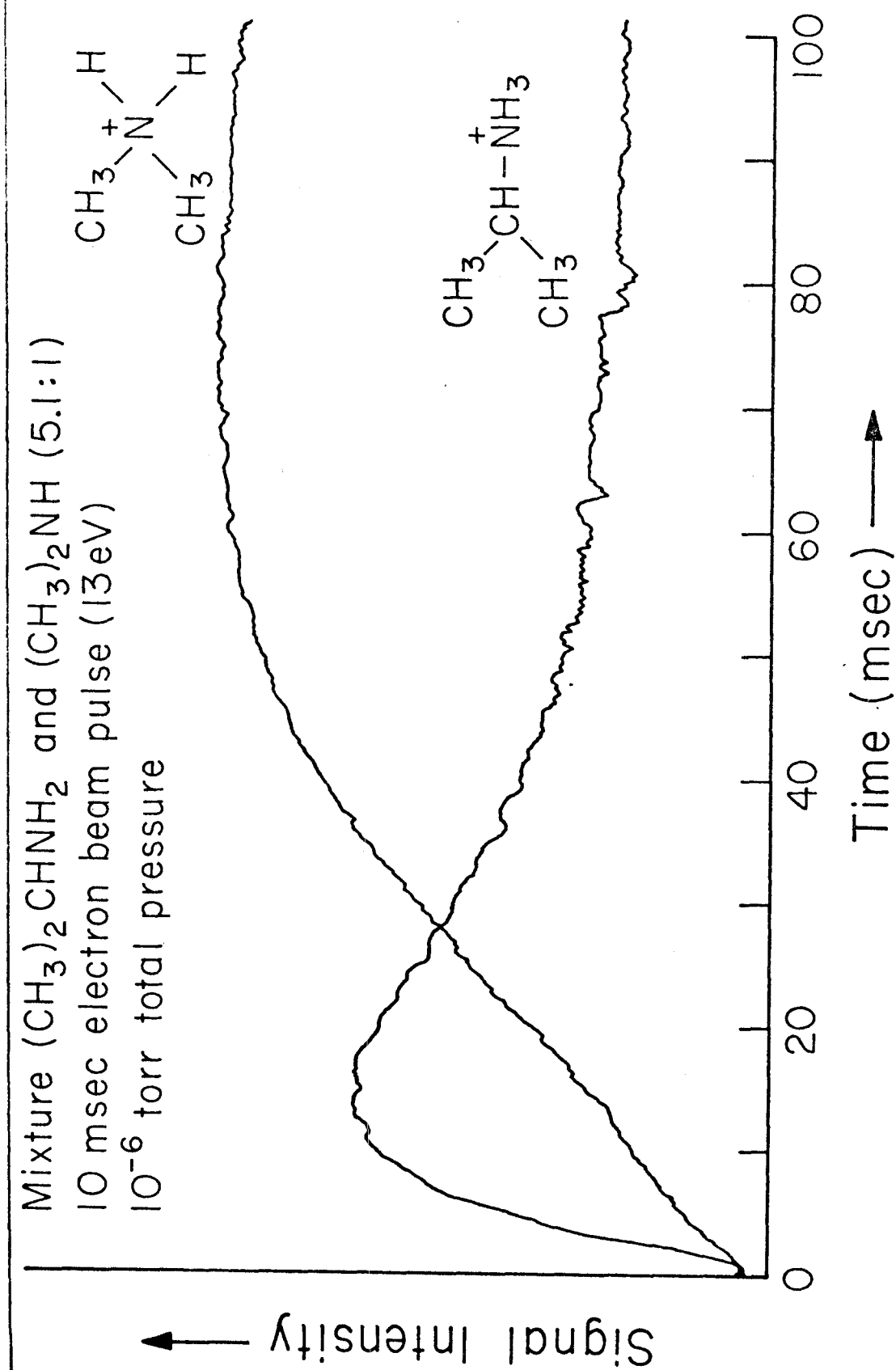


Figure 2

Trace of the ion intensities of protonated dimethylamine and isopropylamine vs. time. Steady state concentrations indicate that equilibrium is established. Ion formation was by a 5 msec, 13 eV electron beam pulse in a 5.1:1 mixture of $(\text{CH}_3)_2\text{CHNH}_2$ and $(\text{CH}_3)_2\text{NH}$ at a total pressure of 1×10^{-6} torr.



and as such it was previously assumed that the only factor contributing to an entropy change is that due to rotational symmetry number differences. Kebarle has conducted a study of temperature dependences of ΔG for a number of amine pairs (3). The results of this study are shown in Fig. 3 together with data from room temperature studies using ICR techniques. The ΔS values derived from these plots are -5.3 eu, -4.3 eu, and -4.0 eu for the A₁B and C plots, respectively. These are all much larger than the ΔS values inferred by rotational symmetry differences of -2.0 eu, -0.67 eu and -0.67 eu, respectively.

It is of some consequence to note that in all three cases the ΔS difference has the correct sign that would be predicted by the arguments inferred from differences in collision frequencies presented in the introduction to this chapter and based on an assumption that the molecular dipole plays a small role in determining collision frequency. This assumption gains some credence from the symmetric proton transfer data for ammonia presented in Chapter 4 of this thesis in which it is shown that the NH_4^+ , NH_3 collision frequency is very close to that predicted from the Langevin theory and as such the molecular dipole plays a small part in the ion-molecule potential.

2. Gas Phase Acidities

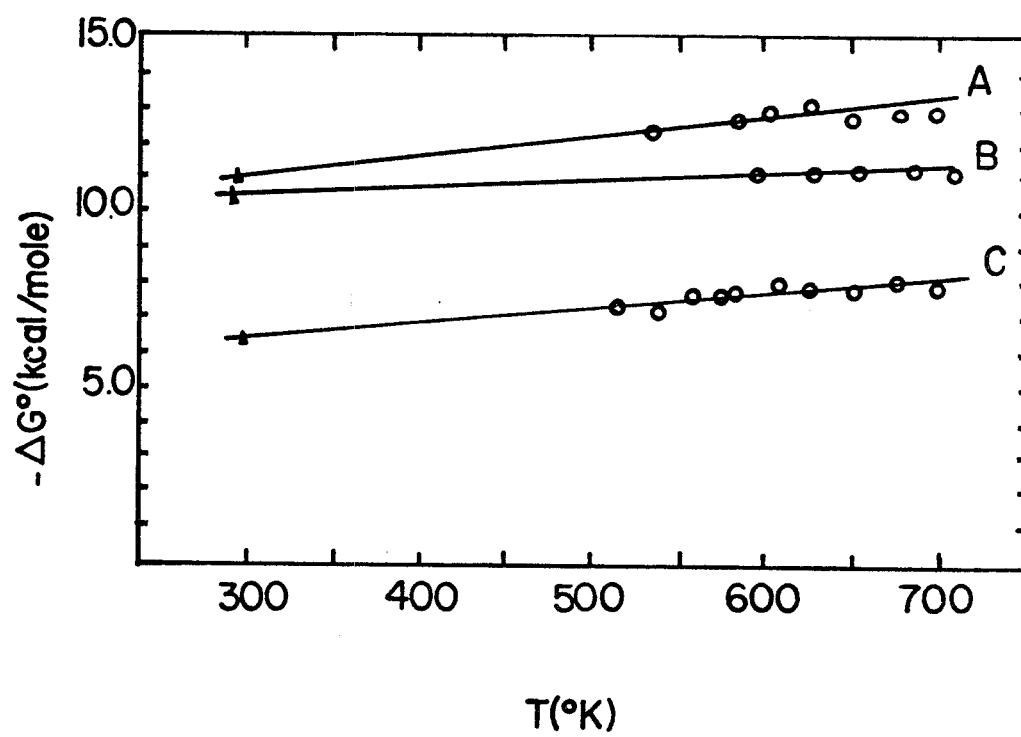
The most comprehensive equilibrium studies of gas phase acidities have been those of Kebarle (22), using high

Figure 3

Temperature dependence of $\Delta G = -2.3 RT \ln K_{eq}$ for proton transfer equilibria:



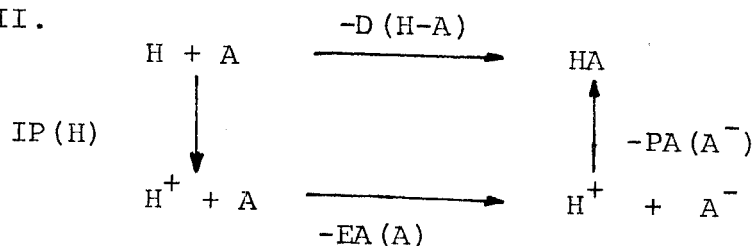
- M_1, M_2 are:
- (A) $CH_3NH_2, (CH_3)_3N$
 - (B) NH_3, CH_3NH_2
 - (C) NH_3, CH_3NH_2



pressure mass spectrometric techniques, Bohme (23) using flowing afterglow apparatus and McIver, et al. (24) using ICR techniques. These studies are fairly recent but to date include fairly comprehensive studies of substituted and unsubstituted carboxylic acids, amines and substituted phenoles in addition to studies involving simple hydrides and other inorganic anions.

It is again useful to construct a thermochemical cycle such as Scheme II to relate the measured anion proton affinity to other thermochemical quantities

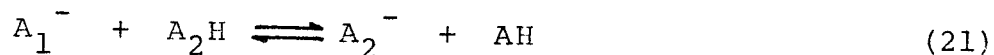
Scheme II.



The quantity measured in mass spectrometric studies is the proton affinity of the anion A^- which may be expressed as

$$\text{PA}(\text{A}^-) = D(\text{HA}) + \text{IP}(\text{H}) - \text{EA}(\text{A}) \quad (20)$$

In determinations of relative acidities an equilibrium of the form



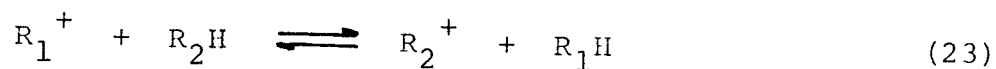
is established. Within a given homologous series of acids, for instance carboxylic acids, the bond dissociation energy $D(\text{HA})$ is usually constant. As a result the difference in proton affinities of the anions may be written

$$PA(A_2^-) - PA(A_1^-) = EA(A_1) - EA(A_2) \quad (22)$$

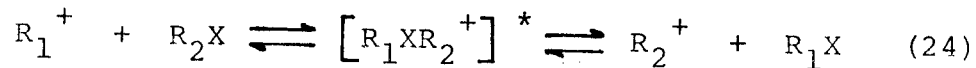
Hence a measurement of the relative proton affinities of the anions also yields the relative electron affinities of the radicals.

C. Fluoride Transfer Equilibria. Carbonium Ion Stabilities

The utility of trapped ion cyclotron resonance studies in the determination of gas phase acidities and basicities has been demonstrated. In similar fashion, it should in principle be possible to determine relative carbonium ion stabilities from studies of hydride transfer equilibria in the gas phase of the form (5,25)



It has generally been observed that the forward and reverse rate constants for hydride transfer reactions involving interesting pairs of carbonium ions (e.g. tert-butyl and isopentyl) are very slow with rate constants between 10^{-11} and $10^{-10} \text{ cm}^3 \text{ molecule}^{-1} \text{ sec}^{-1}$ (25) and equilibrium being established only after several hundred collisions. An alternate and more successful approach for determination of carbonium ion stabilities has been developed involving the study of halide transfer equilibria (equation 24) (4)



Among the most interesting of the substituted carbonium ions for study are the fluoromethyl cations (CH_nF_{3-n} ,

n = 0-3). The effects of fluorine substituents on carbonium ion stabilities are of particular interest since they exhibit ambiguous behavior. While dative π bonding from the fluorine p- π orbitals to the empty carbon p orbital has a stabilizing effect, the large electronegativity of fluorine relative to hydrogen serves to destabilize positive charge on carbon.

Both the occurrence of halide transfer reactions and the concept of dialkyl halonium ions as reaction intermediates in the ion-molecule reactions of alkyl halides have been previously documented (26). The major fragment ions derived from electron impact of methylene fluoride are CH_2F^+ and CHF_2^+ . Reaction (25) accounts for the disappearance of CHF_2^+ at high pressures or long reaction times (27).

$$\text{CHF}_2^+ + \text{CH}_2\text{F}_2 \longrightarrow \text{CH}_2\text{F}^+ + \text{CHF}_3 \quad (25)$$

Similarly in fluoroform the fragment ion CF_3^+ reacts to generate CHF_2^+ which is unreactive with CHF_3 (27). Thus, in a mixture of CH_2F_2 and CHF_3 , reaction (25) may proceed reversibly. This conjecture is confirmed by the data shown in Fig. 4 where the relative abundances of CH_2F^+ and CHF_2^+ are observed not to vary significantly with time beyond 100 msec and in Fig. 5 where these same ion abundances achieve a constant ratio above 5×10^{-4} torr in a conventional ICR experiment. The former experiment yields an equilibrium constant of 0.65 for reaction (25) while the latter gives a value of 0.74 for that quantity.

Figure 4

Variation with time of CH_2F^+ and CHF_2^+ ion abundances in a 4.5:1 mixture of CH_2F_2 and CHF_3 . Other conditions are 5 msec 70 eV electron beam pulse, total pressure 3.15×10^{-6} torr. Initial buildup of CH_2F^+ and CHF_2^+ is due to reaction of CF_3^+ (decay not shown).

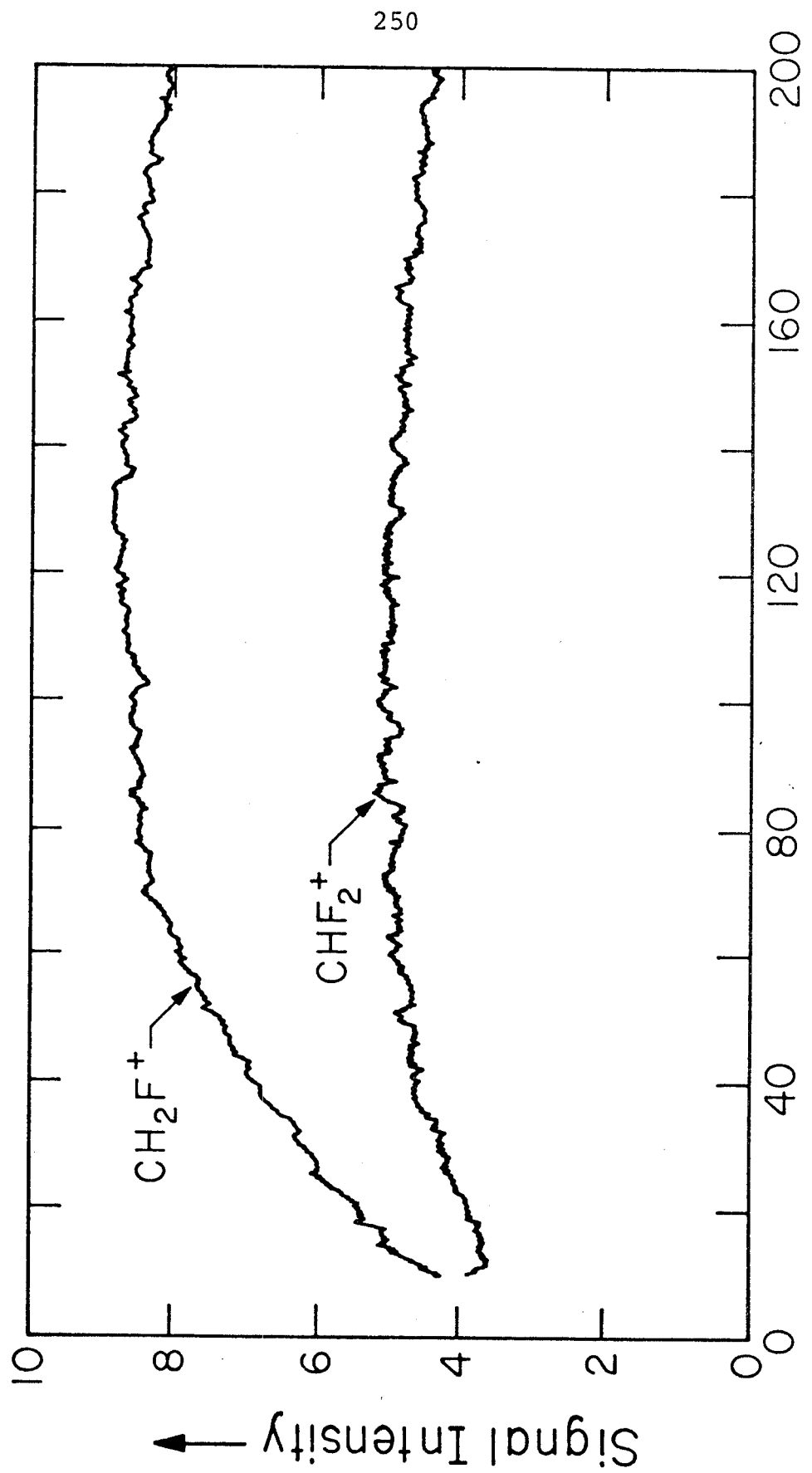
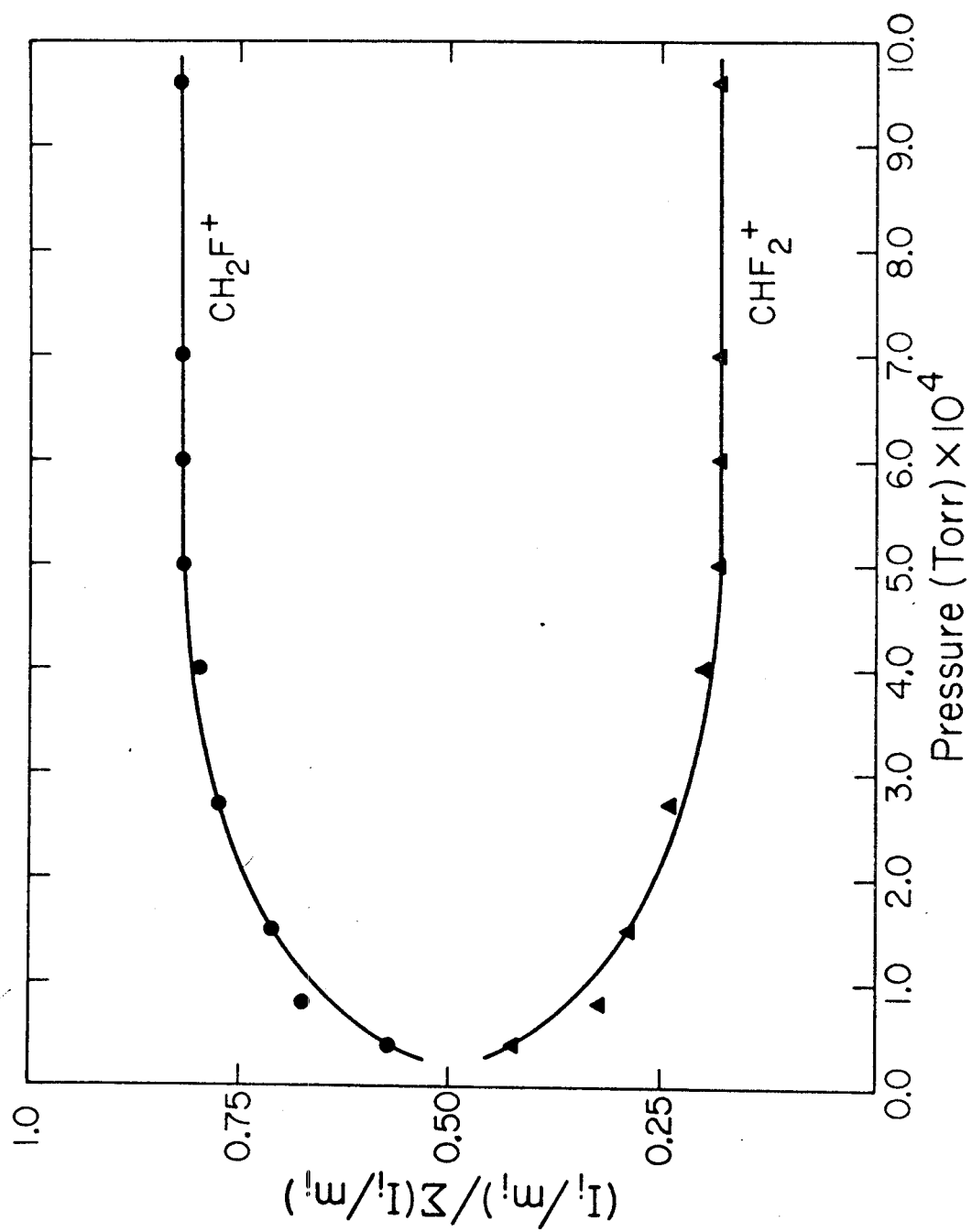


Figure 5

Variation of ion abundance with pressure for a 6.2:1 mixture of CH_2F_2 with CHF_3 at 70 eV. For the range of pressures indicated the species shown are the only ionic species present in abundance greater than 5% of the total ionization. Above 5.0×10^{-4} torr the ratio $\text{CH}_2\text{F}^+/\text{CHF}_2^+$ is found to be independent of electron energy.



To check that an equilibrium actually has been established, the time delay ion ejection technique is used. In the trapped-ion timing sequence an irradiating radio-frequency field is switched on at 100 msec to continuously remove CH_2F^+ by cyclotron ion ejection in a time short compared to the time between collisions. This constrains reaction (25) to proceed exclusively to the right, causing the subsequent decay of CHF_2^+ . This experiment is illustrated by the data of Fig. 6. The ratio I/I_0 where I and I_0 are the intensities with and without the ejection field, respectively, exhibits the exponential decay shown in Fig. 7. From an analysis of the resulting kinetic data the forward ($k_f = 1.4 \times 10^{-10} \text{ cm}^3 \text{ molecule}^{-1} \text{ sec}^{-1}$) and reverse ($k_r = 2.2 \times 10^{-10} \text{ cm}^3 \text{ molecule}^{-1} \text{ sec}^{-1}$) rate constants have been independently obtained for reaction (25). The calculated equilibrium constant $K = k_f/k_r = 0.64$ is in excellent agreement with those obtained by ion and neutral abundance ratios. This equilibrium constant was examined as a function of electron energy from 13 eV to 70 eV and was found to be invariant even though the fragmentation patterns of both neutrals change markedly and the internal energies of the fragments are likely to vary considerably.

From these data the free energy change $\Delta G_{298}^{\circ} = 0.25$ kcal/mole may be calculated for reaction (25). The entropy change $\Delta S_{298}^{\circ} = -1.86$ eu was estimated using the standard

Figure 6

Repeat of CHF_2^+ of Figure 4 scan with and without continuous ejection of CHF_2^+ after 100 msec. The anomalous feature in the CHF_2^+ decay curve results from transients generated by turning on the irradiating oscillator in the timing sequence.

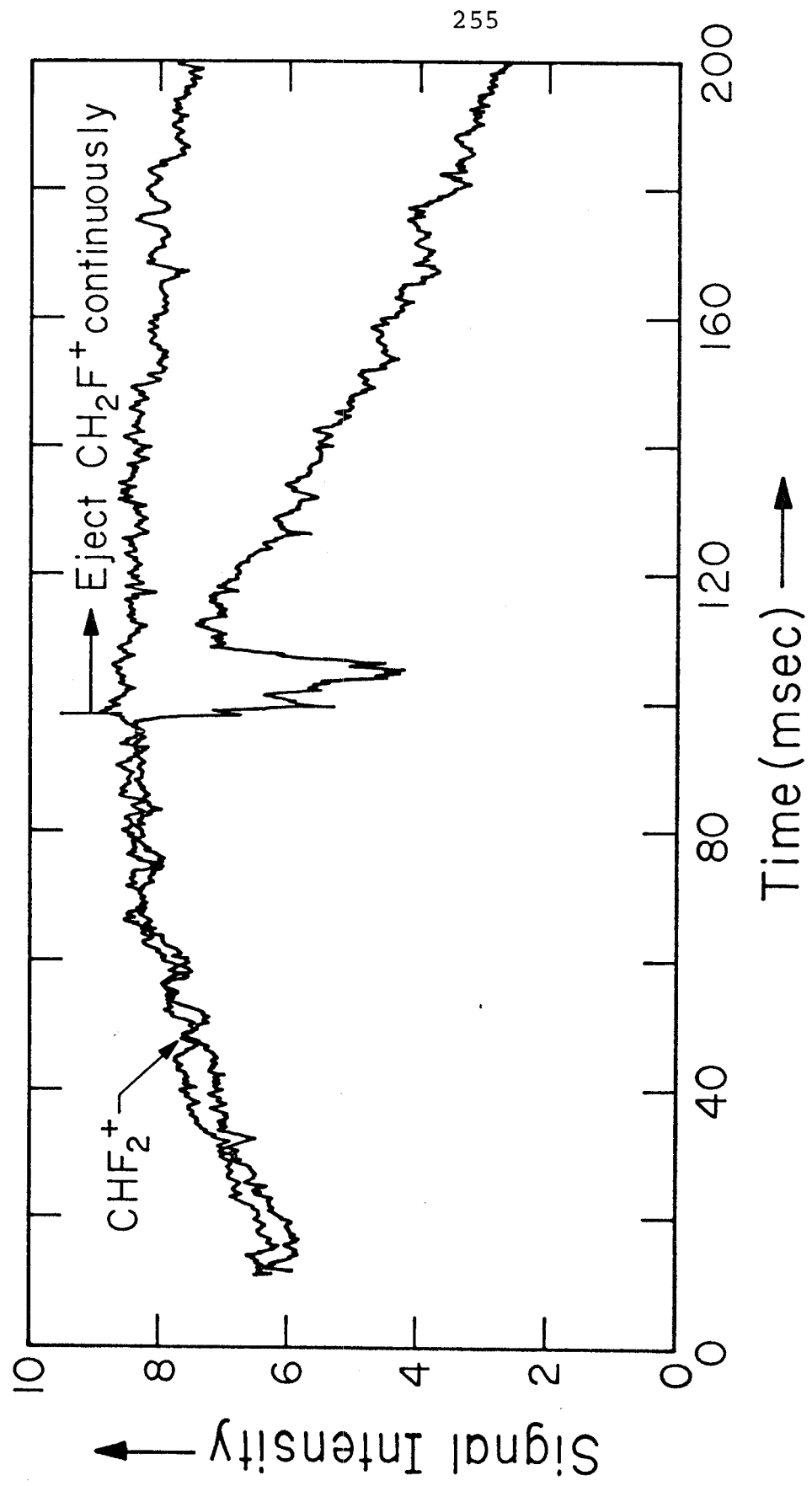
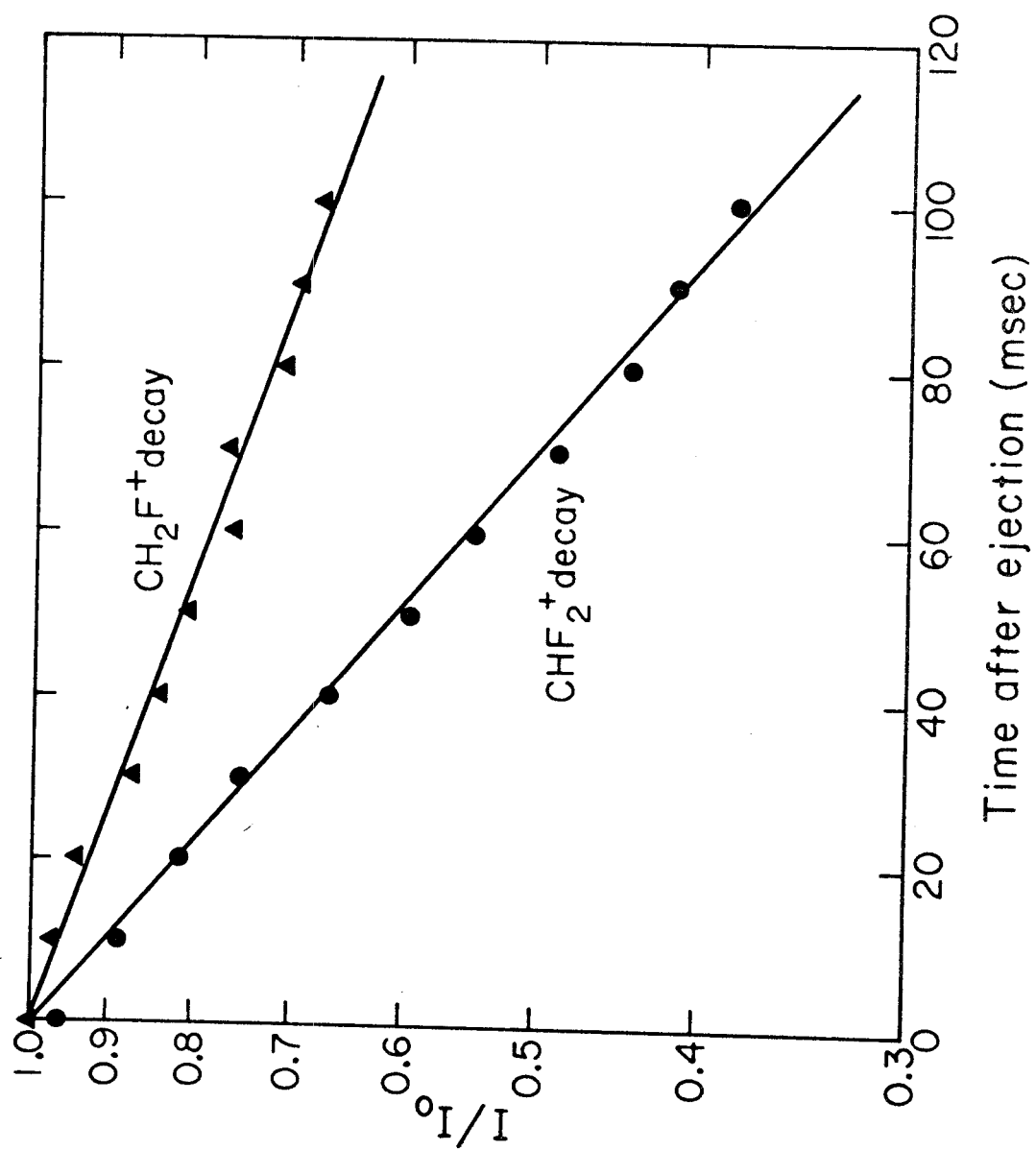


Figure 7

Illustration of exponential decay of CH_2F^+ and CHF_2^+ following ejection of the reaction partner after equilibrium is established for the process $\text{CH}_2\text{F}^+ + \text{CHF}_3 \rightleftharpoons \text{CHF}_2^+ + \text{CH}_2\text{F}_2$. The slopes for CH_2F^+ and CHF_2^+ give, respectively, the forward and reverse reaction rate constants. Other conditions are indicated in Figure 6.



entropy data of Benson (28) for the neutral molecules and calculating the entropies of the ions assuming the geometries obtained for these ions by Baird and Datta (29), giving $\Delta H_{298}^{\circ} = -0.3$ kcal/mole. The standard entropies are summarized in Table 2. In addition, a preliminary temperature dependent high pressure mass spectrometric study has indicated that the value for ΔS° to be 1.78 eu (30).

Only in the mixture of CH_2F_2 and CHF_3 was equilibrium observed for fluoride or hydride transfer reactions between fluoromethyl cations. The dynamic range of ICR experiments permits observation of equilibria at ambient temperature only when $\Delta G \leq 3$ kcal/mole. However, double resonance experiments allow for the relative ordering of fluoride and hydride affinities to be determined by examination of the variation of rate constants, k , with ion energy, E . Empirically, it has been observed that dk/dE is negative for exothermic reactions and must be positive for strongly endothermic reactions. For near thermoneutral reactions, the expectations are less clear although it is generally observed that dk/dE is negative for both forward and reverse reactions. This is the case for reaction (25).

The observed fluoride and hydride transfer reactions involving substituted methyl cations are summarized in Table 3. Together with the rate constants determined by trapped-ion techniques and the sign of dk/dE as determined by double resonance. In mixtures it is observed that

TABLE 2

Standard Entropies of Fluoromethyl Species

<u>Species</u>	<u>Entropy S^0 (eu)</u>
CH_2F^+	
CHF_2^+	$S_{\text{CH}_2\text{F}^+} - S_{\text{CHF}_2^+} = -4.86 \text{ eu}^{(a)}$
CH_2F_2	59.0
CHF_3	62.0

(a) Calculated from the difference in standard entropy expressions for the two ionic species

$$\Delta S = R \ln \left(\frac{m_{\text{CH}_2\text{F}^+}}{m_{\text{CHF}_2^+}} \right) + R \ln \left(\frac{(I_A I_B I_C)^{\frac{1}{2}}_{\text{CH}_2\text{F}^+}}{(I_A I_B I_C)^{\frac{1}{2}}_{\text{CHF}_2^+}} \right)$$

where the first term represents the translational entropy difference and the second term the rotational entropy difference. Vibrational entropies were determined to be negligible. m represents the ion mass and $I_A I_B I_C$ are the three principle moments of inertia.

TABLE 3

Summary of Fluoride and Hydride Transfer ReactionsInvolving Fluoromethyl Cations

Species or Mixture	Reaction ^a	k (10 ⁻¹⁰ cm ³ molecule ⁻¹ sec ⁻¹) ^b	$\frac{dk}{dE}$	ΔH^c
CH ₃ F	CH ₃ ⁺ + CH ₃ F → CH ₂ F ⁺ + CH ₄	10.2	-	-22.6
	CH ₂ F ⁺ + CH ₃ F → CH ₃ ⁺ + CH ₂ F ₂		NR ^d	+ 8.4
CH ₂ F ₂	CHF ₂ ⁺ + CH ₂ F ₂ → CH ₂ F ⁺ + CHF ₃	1.9	-	- 0.3
	CH ₂ F ⁺ + CH ₂ F ₂ → CHF ₂ ⁺ + CH ₃ F	0.10	-	- 5.7
CHF ₃	CF ₃ ⁺ + CHF ₃ → CHF ₂ ⁺ + CF ₄	2.1	-	- 8.1
	CHF ₂ ⁺ + CHF ₃ → CF ₃ ⁺ + CH ₂ F ₂		NR	+15.1
CH ₄ and CH ₂ F ₂	CH ₃ ⁺ + CH ₂ F ₂ → CH ₂ F ⁺ + CH ₃ F	6.4	-	- 8.4
	CH ₃ ⁺ + CH ₂ F ₂ → CHF ₂ ⁺ + CH ₄		+ ^e	-28.3
	CHF ₂ ⁺ + CH ₄ → CH ₃ ⁺ + CH ₂ F ₂		NR	+28.3
	CH ₂ F ⁺ + CH ₄ → CH ₃ ⁺ + CH ₃ F		NR	+ 8.4
CH ₄ and CHF ₃	CH ₃ ⁺ + CHF ₃ → CF ₃ ⁺ + CH ₄		NR	-13.2
	CH ₃ ⁺ + CHF ₃ → CHF ₂ ⁺ + CH ₃ F	7.6	-	- 8.1
	CF ₃ ⁺ + CH ₄ → CH ₃ ⁺ + CHF ₃		NR	+13.2
	CHF ₂ ⁺ + CH ₄ → CH ₃ ⁺ + CH ₂ F ₂		NR	+28.3
CH ₄ and CF ₄	CH ₃ ⁺ + CF ₄ → CF ₃ ⁺ + CH ₃ F		-	+ 4.5 ^(f)
	CF ₃ ⁺ + CH ₄ → CH ₃ ⁺ + CHF ₃		NR	+13.2
CH ₂ F ₂ and CHF ₃	CHF ₂ ⁺ + CH ₂ F ₂ → CH ₂ F ⁺ + CHF ₃	2.2	-	- 0.3
	CH ₂ F ⁺ + CHF ₃ → CHF ₂ ⁺ + CH ₂ F ₂	1.4	-	+ 0.3
CH ₃ F and CF ₄	CF ₃ ⁺ + CH ₃ F → CH ₃ ⁺ + CF ₄		+	- 4.5 ^(f)
	CH ₃ ⁺ + CH ₃ F → CH ₂ F ⁺ + CH ₄		-	-22.6
	CH ₂ F ⁺ + CF ₄ → CF ₃ ⁺ + CH ₂ F ₂		+	+12.9
	CH ₃ ⁺ + CF ₄ → CF ₃ ⁺ + CH ₃ F		-	+ 4.5 ^(f)

Table 3 Footnotes

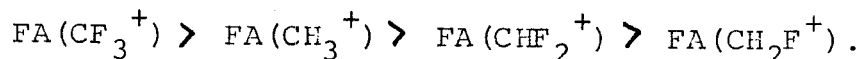
- ^a Not every reaction observed in the mixture is reported. Only those processes pertinent to determining relative fluoride and hydride affinities were examined.
- ^b Rate Constants measured using trapped ion techniques.
- ^c ΔH calculated using thermochemical data summarized in Table V.
- ^d NR (no reaction) indicates process was examined using double resonance techniques and not observed.
- ^e Even though exothermic, this process gave a positive double resonance response. This likely results from the competition of exothermic fluoride and hydride transfer reactions, suggesting that the latter process is more favorable only at high ion kinetic energies.
- ^f There is some experimental evidence to indicate that the reaction



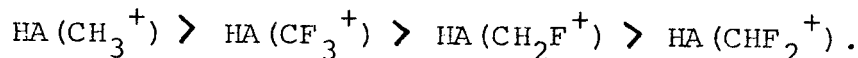
is exothermic. However, existing thermochemical data indicate that $\text{FA}(\text{CF}_3^+) > \text{FA}(\text{CH}_3^+)$. The experimental result is adopted for our purposes, although no attempt has been made to readjust other thermochemical quantities since it is not clear which of the existing values should be readjusted.

exothermic fluoride transfer reactions occur to the virtual exclusion of hydride transfer even when the latter process is significantly exothermic. The rationale for this is that the carbonium ion will interact strongly with the C-F bond dipole so as to favorably approach and bind to fluorine, forming a fluoronium ion intermediate of the type shown in equation (24). Alignment of the C-H bond dipole is not nearly so favorable an occurrence nor are two carbonium ions likely to be bound as strongly by a hydride ion as by fluoride.

From the results summarized in Table 3, it is apparent that the relative order of fluoride affinities of fluoromethyl cations is



Similarly the relative hydride affinities may be ordered as



All thermochemical data used and arrived at in this study are summarized in Table 4. The present data in conjunction with available literature data permit construction of Table 4 for the thermochemical properties of fluoromethyl cations. For a reference point, the determination of the photoionization threshold for production of CH_2F^+ from CH_3F which gives $\Delta H_f(\text{CH}_2\text{F}^+) = 200.3$ kcal/mole was chosen (31). Combining this with $\Delta H = -0.3$ kcal/mole for reaction (25) gives $\Delta H_f(\text{CHF}_2^+) = 142.4$ kcal/mole. This is in good agreement with $\Delta H_f(\text{CHF}_2^+) = 142.1$ kcal/mole derived from

TABLE 4
Summary of Thermochemical Data Used in this Study^a

Neutral Species	ΔH_f	Reference	Ionic Species	ΔH_f	Reference
CH_4	-17.89	b	CH_4^+	276.1	h
CH_3F	-55.9	b	CH_3F^+	233.3	h
CH_2F_2	-108.1	b	CH_2F_2^+	185.2	h
CHF_3	-166.3	b	CHF_3^+	151.9	h
CF_4	-223.0	c	CF_4^+	131.0	h
CH_3	34.0	b	CH_3^+	260.9	i
CH_2F	-4.9	d	CH_2F^+	200.3	d
CHF_2	-59.2	b	CHF_2^+	142.4	d
CF_3	-112.2	b	CF_3^+	99.3	j
CF_2	-39.0	e	CF_2^+	223.7	k
HF	-65.3	f	F^-	-61.3	f
F	18.72	f	H^-	33.39	g
H	52.09	g	H^+	365.7	g

Table 4 Footnotes

- ^a All data in kcal/mole at 298^o K.
- ^b J. A. Kerr and D. M. Timlin, Int. J. Chem. Kinet. III, 427 (1971).
- ^c J. R. Lacher and H. A. Skinner, J. Chem. Soc. A, 1034 (1968).
- ^d See text for discussion.
- ^e J. Heicklen, Advan. Photochem. 7, 57 (1969).
- ^f W. A. Chupka and J. Berkowitz, J. Chem. Phys. 54, 5126 (1971).
- ^g D. D. Wagman, W. H. Evans, V. B. Parker, I. Halow, S. M. Bailey, and R. H. Schumm, NBS Tech. Note 270-3, U. S. Government Printing Office, Washington, D.C. 20401 (1968).
- ^h Calculated using the neutral heats of formation and the adiabatic ionization potentials given by C. R. Brundle, M. B. Robin and H. Basch, J. Chem. Phys. 53, 2196 (1970).
- ⁱ G. Herzberg and J. Shoosmith, Can. J. Phys. 34, 523 (1956).
- ^j T. A. Walter, C. Lifshitz, W. A. Chupka and J. Berkowitz, J. Chem. Phys. 51, 3531 (1969).
- ^k T. Su, L. Kevan, and T. O. Tiernan, J. Chem. Phys. 54, 4871 (1971).

TABLE 5
Thermochemical Properties Related to Fluoromethyl Cation Stabilities^a

R	$\Delta H_f(R)$	$\Delta H_f(RH)$	$\Delta H_f(RF)$	$D(R-H)$	$D(R-F)$	$IP(R)$	$\Delta H_f(R^+)$	$D(R^+-H^+)$	$D(R^+-F^+)$
CH ₃	34.0	- 17.89	- 55.9	104.0	108.6	9.84 ^b	260.9	312.2	255.5
CH ₂ F	- 4.9	- 55.9	-108.1	103.1	121.9	8.90 ^c	200.3	289.6	247.1
CHF ₂	- 59.2	-108.1	-166.3	101.0	125.8	8.74 ^d	142.4	283.9	247.4
CF ₃	-112.2	-166.3	-223.0	106.2	129.5	9.17 ^e	99.3	299.0	260.0

^a All thermochemical data in kcal/mole at 298°K except ionization potentials which are given in eV. Except as noted all data is taken from Table V.

^b G. Herzberg and J. Shoosmith, Can. J. Phys. 34, 523 (1956).

^c F. P. Lossing, Bull. Soc. Chim. Belges 81, 125 (1972).

^d Calculated from $IP(R) = \Delta H_f(R^+) - \Delta H_f(R)$ (see text).

^e T. A. Walker, C. Lifshitz, W. A. Chupka and J. Berkowitz, J. Chem. Phys. 51, 3531 (1969).

Lossing's study of the fragmentation processes in CH_2F_2 using monoenergetic electron impact techniques (32). The ionization potential of the radical R is related to the heat of formation of R^+ by the relation

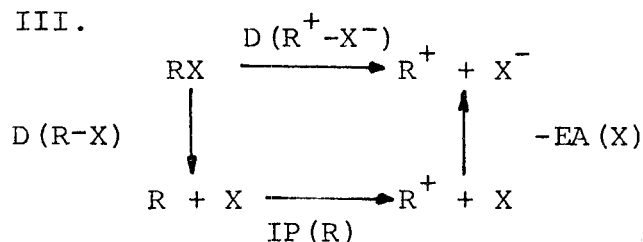
$$\text{IP(R)} = \Delta H_f(\text{R}^+) - \Delta H_f(\text{R}) \quad (26)$$

Lossing has determined the adiabatic ionization potential of CH_2F to be 8.90 eV (32). Although he was able to observe only upper limits for the ionization potentials of CHF_2 and CF_3 , Lossing provides evidence from competitive mass spectral fragmentation processes that $8.45 \leq \text{IP}(\text{CHF}_2) \leq 8.80$ eV. Combining our value of $\Delta H_f(\text{CHF}_2^+)$ with $\Delta H_f(\text{CHF}_2) = -59.2 \pm 2$ kcal/mole reported by Kerr and Timlin (33), equation (26) gives $\text{IP}(\text{CHF}_2) = 8.74$ eV consistent with the limits determined by Lossing. Using the value $\Delta H_f(\text{CH}_2\text{F}^+) = 200.3$ kcal/mole adopted in this work and $\text{IP}(\text{CH}_2\text{F}) = 8.90$ eV gives $\Delta H_f(\text{CH}_2\text{F}) = -4.9$ kcal/mole which is somewhat higher than the value -7.8 ± 2 kcal/mole reported by Kerr and Timlin (33). There are obvious uncertainties on the order of ± 2 kcal/mole in much of this data; however it is to be emphasized that the techniques used are capable of yielding differences in fluoride affinities accurate to within ± 0.1 kcal/mole.

Several criteria may be used in conjunction with data of Table 5 to evaluate the effects of fluorine substituents on carbonium ion stabilities. These include, in addition to relative fluoride and hydride affinities, the effect of

successive fluorine substitution on ionic heats of formation and the ionization potentials of the corresponding radicals. A much smaller decrease (20 kcal/mole) in ionic heat of formation is observed in proceeding from CHF_2^+ to CF_3^+ and CH_2F^+ to CHF_2^+ . Relative radical ionization potentials decrease in the same order, $\text{CH}_3 > \text{CF}_3 > \text{CH}_2\text{F} > \text{CHF}_2$ as the hydride affinities of the corresponding carbonium ions. The different order of fluoride and hydride affinities may be understood with the thermochemical cycle of Scheme III, described by equation (27). Unlike the

Scheme III.

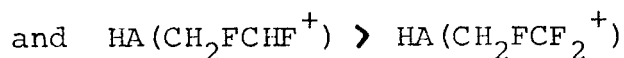
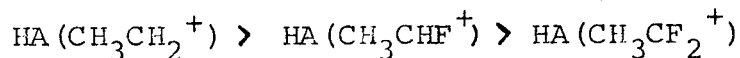


$$\text{D(R}^+ - \text{X}^-) = \text{D(R - X)} + \text{IP(R)} - \text{EA(X)} \quad (27)$$

relatively constant C-H bond dissociation energies, the C-F bond dissociation energies in the fluoromethanes vary considerably with the number of fluorines present (Table 5). Hence, only the hydride affinities parallel the changes in the radical ionization potentials. A reasonably consistent picture of the effects of fluorine substituents on carbonium ion stabilities emerges from the data presented here. The general effect of fluorine is to stabilize the carbonium ion relative to hydrogen. Dative π bonding is apparently

most significant in CH_2F^+ relative to CH_3^+ and to a lesser extent in CHF_2^+ and CF_3^+ relative to CH_2F^+ . Destabilization of the carbonium ion by electron withdrawal increases with increasing fluorine substitution causing CF_3^+ to be less stable than CH_2F^+ and CHF_2^+ .

Extension of the methodology developed for the fluoromethanes to fluorine substituted ethanes resulted in confirmation of the trends for substituent effects of fluorosubstituted methyl cations (34,35). For instance the increased carbonium ion stability resulting from replacement of fluorine for hydrogen on the carbonium ion center is reflected by the order of relative hydride affinities of fluoroethyl cations



analogous to the ordering determined for fluoromethyl cations. Also, in direct analogy to the fluoromethane results, the fluoride affinities of the mono and di fluoro substituted ethyl carbonium ions were found to be within 2 kcal/mole of each other with the difluoro cation favored slightly. This trait is illustrated in Fig. 8 for equilibrium between the $\text{CH}_2\text{FCF}_2^+$ and CH_2FCHF^+ ions in a mixture of CH_2FCF_3 and CH_2FCHF_2 . The equilibrium constant obtained for the reaction

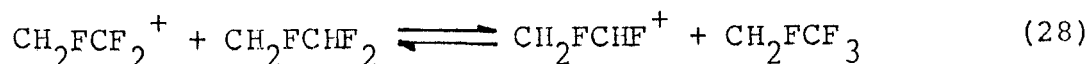
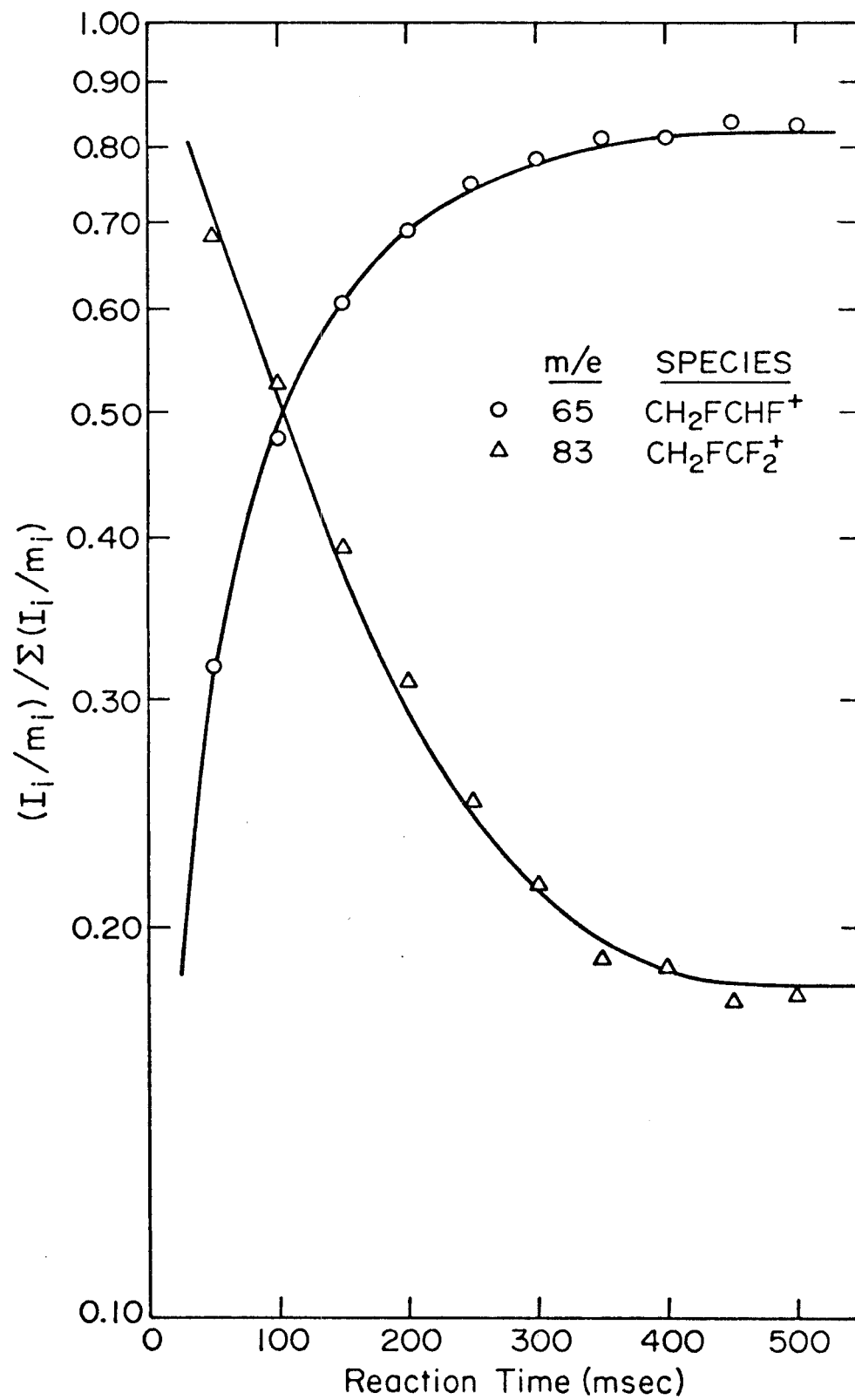
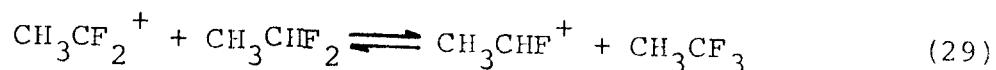


Figure 8

Variation of relative ion abundances with time of CH_2FCHF^+ and $\text{CH}_2\text{FCF}_2^+$, in a 3.7:1 mixture of CH_2FCF_3 and CH_2FCHF_2 . Other conditions are 5 msec, 70 eV electron beam pulse, total pressure 2.5×10^{-6} torr.



is 16.9 resulting in a free energy change of $\Delta G = -1.7$ kcal/mole for the reaction proceeding to the right. Due to a lack of existing entropy data for these species no attempt was made to evaluate the ΔS change for this reaction and the fluoride affinity difference was taken to be roughly equal to the measured ΔG . Similarly the difference in fluoride affinities of $\text{CH}_3\text{CHF}_2^+$ and CH_3CHF^+ obtained from the reaction



was found to be -1.4 kcal/mole. These combined results infer that the effect of one and two fluorines substituted for hydrogen on the carbonium ion center is similar in methyl and ethyl cations. In addition, it has recently observed that the fluoride affinity of $\text{CH}_3\text{CFCH}_3^+$ is approximately equal to that for $\text{CH}_3\text{CHCH}_3^+$.

The effects of β fluoro substituents in ethyl cations are less ambiguous in that they exhibit only destabilizing properties. This destabilization arises from the strong inductive electron withdrawing ability of fluorine substituents. While it is possible that a bridged fluoronium ion structure could provide some stabilizing effect through π donation, the experiment results indicate only destabilizing effects of β fluorines and hence the bridged structure is not a very probable one. The difference in hydride affinities of R_1^+ and R_2^+ , where R_2^+ has the same number of α fluorines as R_1^+ , but no β fluorines, may be taken as a

quantitative measure of the destabilization of β fluoro substituents. In this manner the destabilization of $\text{CH}_2\text{FCF}_2^+$, $\text{CHF}_2\text{CF}_2^+$, and CF_3CF_2^+ relative to CH_3CF_2^+ are determined to be 18, 23 and 42 kcal/mole, respectively. Recently Pople and co-workers³⁶ carried out ab initio MO calculations on similar ions and determined destabilization energies of 10.3, 26.6 and 41.0 kcal/mole, respectively, for $\text{CH}_2\text{FCH}_2^+$, $\text{CHF}_2\text{CH}_2^+$, and CF_3CH_2^+ relative to CH_3CH_2^+ .

Using both equilibrium and double resonance ICR techniques outlines above combined with existing thermochemical data and in some cases estimates of heats of formation by group equivalent methods the relative fluoride affinities, hydride affinities, and ionic heats of formation of a wide variety of substituted cations have been determined. The results are summarized in Table 6. The relative fluoride of two cations may be determined without knowledge of the appropriate neutral heats of formation by ICR experiments. The ordering of fluoride affinities is illustrated graphically in Fig. 9. In cases where the heat of formation of the corresponding hydride are also available the fluoride affinities have been converted to hydride affinities according to the relation

$$D(\text{R}^+-\text{H}^-) - D(\text{R}^+-\text{R}^-) = \Delta\text{H}_f(\text{RF}) - \Delta\text{H}_f(\text{RH}) - \Delta\text{H}_f(\text{F}^-) - \Delta\text{H}_f(\text{H}^-) \quad (30)$$

The hydride affinities thus obtained are summarized in Fig. 10. It is on the basis of this ordering that intrinsic relative

TABLE 6

Thermochemical Properties Related to Fluoro Carbonium Ion Stabilities

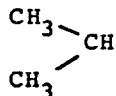
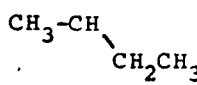
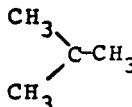


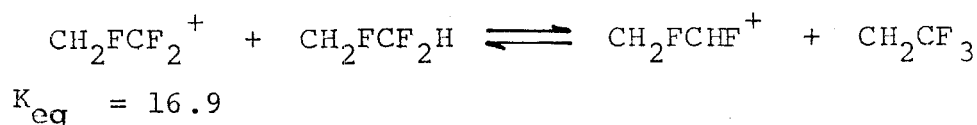
R	$\Delta H_{f298}^{\circ}(\text{RF})$	$\Delta H_{f298}^{\circ}(\text{RH})$	$\Delta H_{f298}^{\circ}(\text{R}^+)$	FA (R ⁺) = D (R ⁺ -F ⁻) ^(b)	HA (R ⁺) = D (R ⁺ -H ⁻) ^(b)
CH ₃ CH ₂	- 62.5 (c)	- 20.24 (d)	219.1 (e)	220.3	297.8
CH ₃ CHF	-118.0 (c)	- 62.5 (c)	172.9 (h)	230.4 (g)	268.8
CH ₃ CF ₂	-178.2 (c)	-118.0	114.1 (d, f)	231.8	265.5
CH ₂ FCHF	-158.9 (c)	-109.0 (i)	139.9 (j)	238.3	282.3
CH ₂ FCF ₂	-210.2 (i)	-158.9 (c)	91.1 (l)	240.0 (k)	283.4
CHF ₂ CF ₂	-265.8 (m)	-209.0 (n)	46.5 (h)	251.0 (o)	288.9
CF ₃ CF ₂	-318.2 (m)	-265.8 (m)	8.1 (m)	265.0	307.3
CH ₃ CH ₂ CH ₂	- 67.2 (p)	- 24.8 (d)	209.0 (d)	214.9	267.2
	- 69.0 (p)	- 24.8 (d)	190.0 (d)	197.7	248.2
	- 73.5 (i)	- 30.15 (d)	192.0 (d)	204.2	255.6
	- 74.1 (i)	- 32.2 (d)	176.0 (d)	188.8	241.6
	- 26.5 (d)	19.8 (d)	270.0	235.2	283.6
H-C≡C-CF ₂	-103.9 (i)	- 47.8 (i)	260.2 (s)	217.6 (s)	245.8 (s)
CH ₂ =CH-CF ₂	-154.0 (d)	- 87.5 (d)	134.0 (d)	226.7	254.9
CH ₂ =CH-CH ₂	- 37.0 (i)	4.9 (d)	226.0 (q)	201.7	254.5
 -CF ₂	-138.9 (d)	- 96.8 (i)	115.7 (t)	193.3 (t)	245.9 (t)
 -CH ₂	- 29.7 (r)	12.0	216.0	184.4	237.4

Table 6 Footnotes

- ^a All values in kcal/mole.
- ^b Calculated using $\Delta H_{f298}^{\circ}(\text{H}^-) = 33.4$ kcal/mole and $\Delta H_{f298}^{\circ}(\text{F}^-) = -61.3$ kcal/mole (W. A. Chupka and J. Berkowitz, J. Chem. Phys. 54, 5126 (1971)).
- ^c J. R. Lacher and H. A. Skinner, J. Chem. Soc. (1), 1034 (1968).
- ^d J. L. Franklin, J. G. Dillard, H. M. Rosenstock, J. T. Herron, K. Draxl and F. H. Field, "Ionization Potentials, Appearance Potentials and Heats of Formation of Gaseous Positive Ions," NSRDS-NBS, 26, (1969).
- ^e F. P. Lossing and G. P. Semeluk, Can. J. Chem. 48, 955 (1970).
- ^f Calculated from $\text{AP}(\text{R}^+)$ from $\text{RH} = 12.3$ eV.
- ^g Obtained from the equilibrium constant for the reaction
- $$\text{CH}_3\text{CF}_2^+ + \text{CH}_3\text{CHF}_2 \rightleftharpoons \text{CH}_3\text{CHF}^+ + \text{CH}_3\text{CF}_3 \quad K_{\text{eq}} = 16.5$$
- ^h Calculated from the experimentally observed $\text{D}(\text{R}^+-\text{F}^-)$.
- ⁱ Estimated using group equivalent methods of Benson (Thermochemical Kinetics, Wiley, New York, New York (1968)).
- ^j Based on the observation of $\text{FA}(\text{CH}_3\text{CF}_2^+) < \text{FA}(\text{CH}_2\text{FCHF}^+) < \text{FA}(\text{CH}_2\text{F}^+)$ Error = ± 5.7 kcal/mole.
- ^k Obtained from the equilibrium constant for the reaction



- ^l Calculated from (i), (j), and (k).
- ^m Calculated using $D(\text{C}_2\text{F}_5\text{-H}) = 103.0 \pm 1.0$ kcal/mole
(J. E. Bassett and E. Whittle, J. Chem. Soc. Farad. I 68, 492 (1972) and $\Delta H_{\text{f}298}^{\text{O}}(\text{C}_2\text{F}_5) = 214.9$ (R. E. Marcotte and T. O. Tiernan, J. Chem. Phys. 54, 3385 (1971)).
- ⁿ G. E. Millward, R. Hartig and E. Tschuikow-Roux, J. Phys. Chem. 75, 3195 (1971).
- ^o Estimated from $\text{FA}(\text{CHF}_2^+) < \text{FA}(\text{CHF}_2\text{CF}_2^+) < \text{FA}(\text{CF}_3^+)$
Error = ± 3 kcal/mole.
- ^p J. R. Lacher, J. Phys. Chem. 60, 1454 (1956).
- ^q F. P. Lossing, Can. J. Chem. 49, 357 (1971).
- ^r Estimated from methods of substitution constants in The Chemical Thermodynamics of Organic Compounds, Wiley, New York, N.Y. (1969).
- ^s Estimated from $\text{FA}(\text{CH}_3\text{CH}_2\text{CH}_2^+) < \text{FA}(\text{H-C}\equiv\text{C-CF}_2^+) < \text{FA}(\text{C}_2\text{H}_5^+)$
Error = ± 3 kcal/mole.
- ^t Estimated from $\text{FA}(\text{tBu}^+) < \text{FA}(\phi\text{-CF}_2^+) < \text{FA}(\text{i-Pr}^+)$
Error = ± 5 kcal/mole.

Figure 9

Table of heterolytic bond dissociation energies, $D(R^+-F^-)$ or fluoride affinities for a variety of fluorine substituted alkyl, allyl and aromatic compounds. The basis for assignment of these quantities is outlined in Table 6.

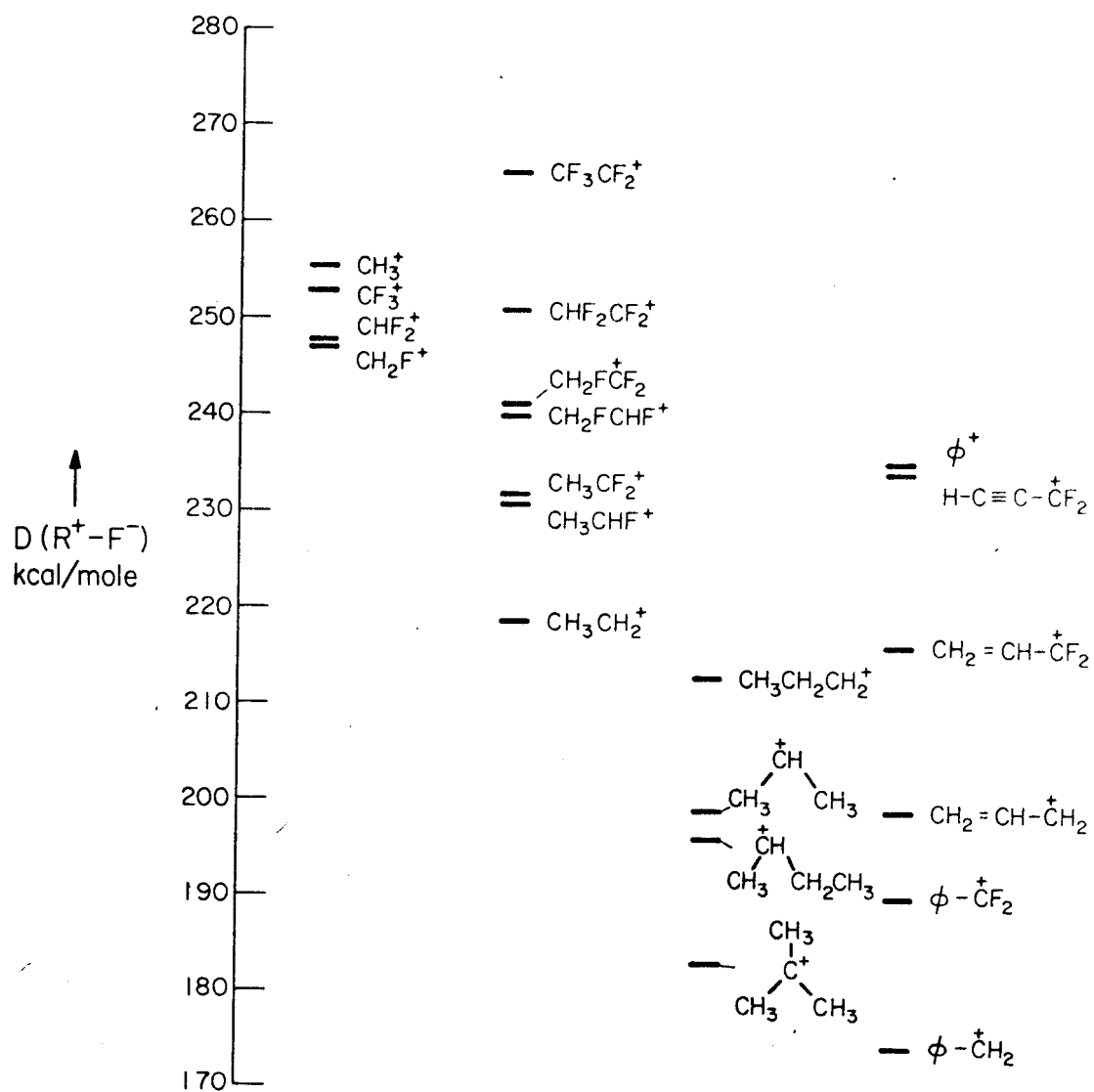
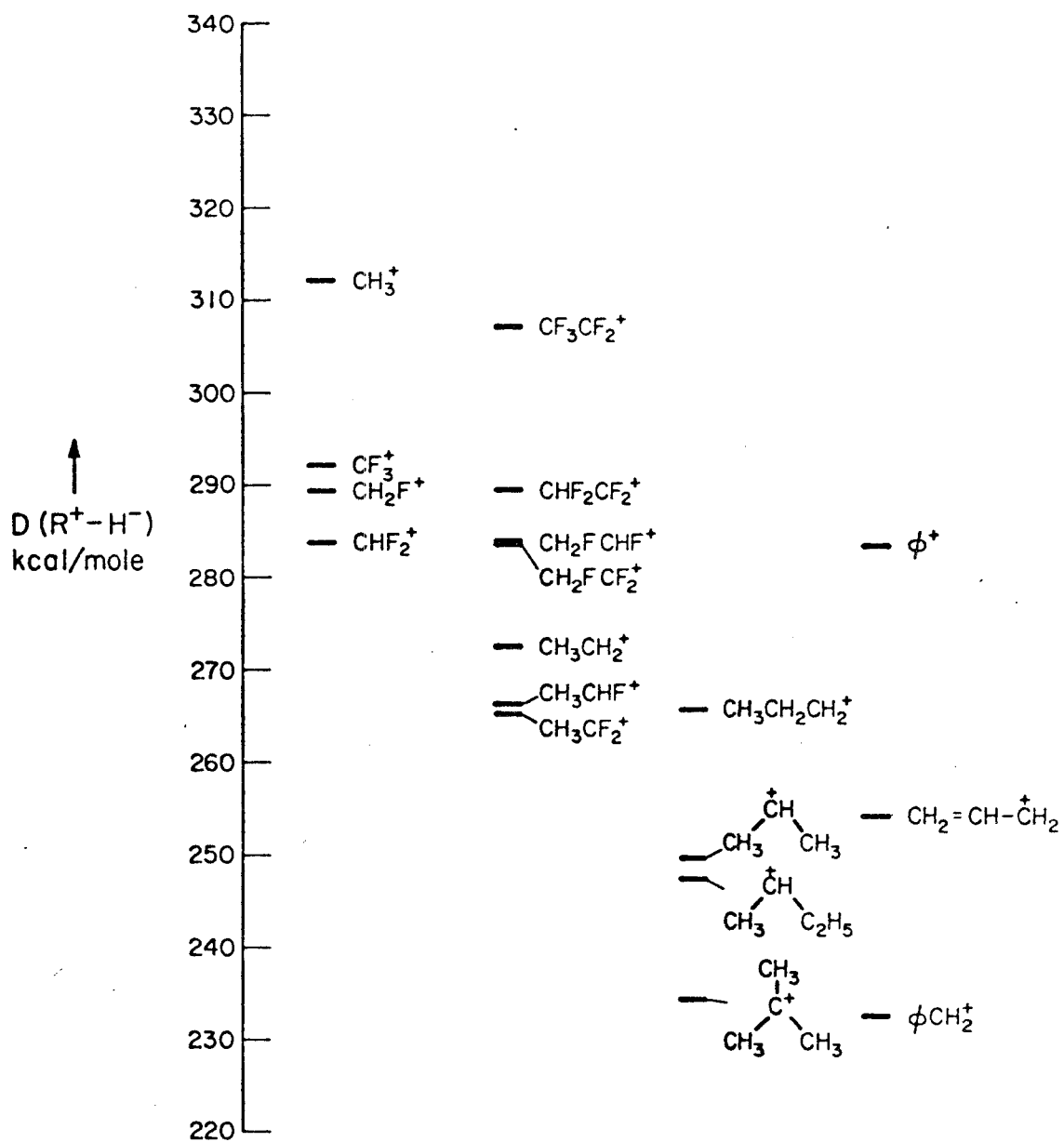


Figure 10

Table of heterolytic bond dissociation energies, $D(R^+-H^-)$ or hydride affinities for a variety of fluorine substituted alkyl, allyl and aromatic compounds. It is this quantity that is used as a basis for determination of relative intrinsic carbonium ion stabilities.



carbonium ion stabilities may be inferred with a lower hydride affinity implying a more stable carbonium ion.

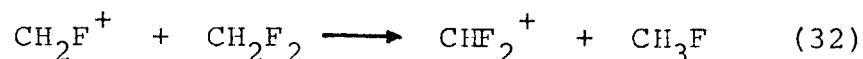
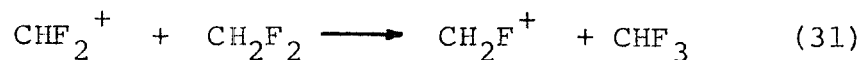
Based on the measurements conducted in the course of this study a number of interesting conclusions may be drawn regarding existing thermochemical data and in generalization of fluorine substituent effects.

In attempting to assess the fluoride affinity of phenyl cation, it was found that if the currently accepted heat of formation of fluorobenzene is used (37), the heat of formation of phenyl cation must be taken to be 270 ± 5 kcal/mole which is considerably below the value of 285 kcal/mole quoted by the NBS tabulation of ionic heats of formation (37). Recently, Rosenstock has re-examined benzene mass spectrometrically and has assigned a preferred heat of formation of phenyl cation of 270 kcal/mole. In addition, a recent measurement of the ionization potential of phenyl radical combined with Benson's value for $D(\phi-H)$ also gives $\Delta H_{f298}^{\circ}(\phi^{+}) = 270$ kcal/mole (38).

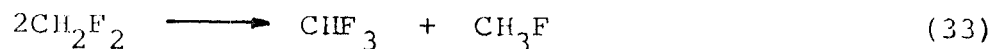
Unlike the combination of stabilizing and destabilizing effects of fluorine substituents observed for carbonium ions derived from saturated systems only destabilization is evident for unsaturated hydrocarbon ions when hydrogen is replaced by fluorine on the carbonium ion center. This may be regarded as being due to the diminished contribution of the π donation from fluorine to the carbon charge center since this resonance structure which delocalizes charge onto

fluorine prevents the delocalization of charge throughout the carbon skeleton. Hence it is the adverse electron withdrawing inductive effect of fluorine which dominates, destabilizing the carbonium ion. For example, of the allyl cations $\text{CH}_2\text{CHCF}_2^+$ is observed to be less stable than $\text{CH}_2\text{CHCH}_2^+$ and the fluorine substituted benzyl cation $\text{C}_6\text{H}_5\text{CF}_2^+$ is less stable than $\text{C}_6\text{H}_5\text{CH}_2^+$.

Considering carbonium ions as Lewis acids, it is to be emphasized that there is no absolute scale of carbonium ion stabilities. As in acid-base interactions, the scale is dependent on the reference base. In several cases, it has been observed that different orders of stability are derived for the reference bases H^- and F^- . This observed reversal of relative binding energies of H^- and F^- has interesting consequences. For example, in methylene fluoride, fluoride transfer (reaction 31) and hydride transfer (transfer 32) reactions are observed.



Both reactions are exothermic and even though the hydride transfer reaction is much slower than fluoride transfer, the net result of the two processes is a chain reaction (reaction 33) which is exothermic overall by 6 kcal/mole.



Such situations in which chain reactions are induced by

ionizing radiation could prove to be useful in synthesis of polyfluorinated species.

The important result of this study is the ability to use relatively fast fluoride transfer reactions to determine carbonium ion stabilities. With a sufficiently large number of reference species, it should be possible to accurately determine the stability of many carbonium ions of chemical interest. This method directly complements other techniques such as electron impact and photoionization mass spectrometry of neutrals and free radicals for determination of ion thermochemical properties. These latter methods suffer from difficulties associated with mass spectrometric experiments such as the inability to accurately identify ionization thresholds, to assess the contribution of thermal energy to ionization and fragmentation and the problems arising from kinetic shifts. The present adiabatic method of examining anion transfer reactions is especially well-suited for measuring small differences in carbonium ion stability and hence accurately assessing substituent effects.

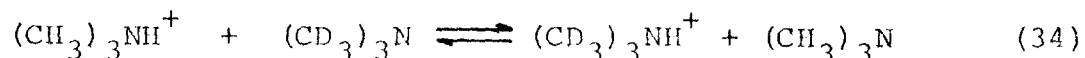
D. Deuterium Isotope Effects in Ion-Molecule Reactions

Kinetic isotope effects have proven to be extremely useful in mechanistic studies of solution reactions of organic molecules (39). The observed rate variations with isotopic substitution lead to important information regarding

the structural features of transition states involved in reaction. Theories rationalizing deuterium isotope effects have been developed by Bigeleisen (40) and by Melander (41) to explain these effects within a transition state theory formalism. In addition to this, examination of isotope effects on equilibrium constants leads to an understanding of how molecular structures are influenced by isotopic substitution (42).

Ionic intermediates have frequently been invoked in solution mechanisms but to date no systematic study of isotope effects in gas phase ion-molecule reactions has been undertaken. Using the trapped ion techniques developed for ICR, it is possible to make accurate assessments of both kinetic and equilibrium isotope effects. Such studies, carried out in the gas phase free from complicating solvent effects have the potential to supply facilely more detailed and accurate information regarding deuterium isotope effects than analogous experiments carried out in solution.

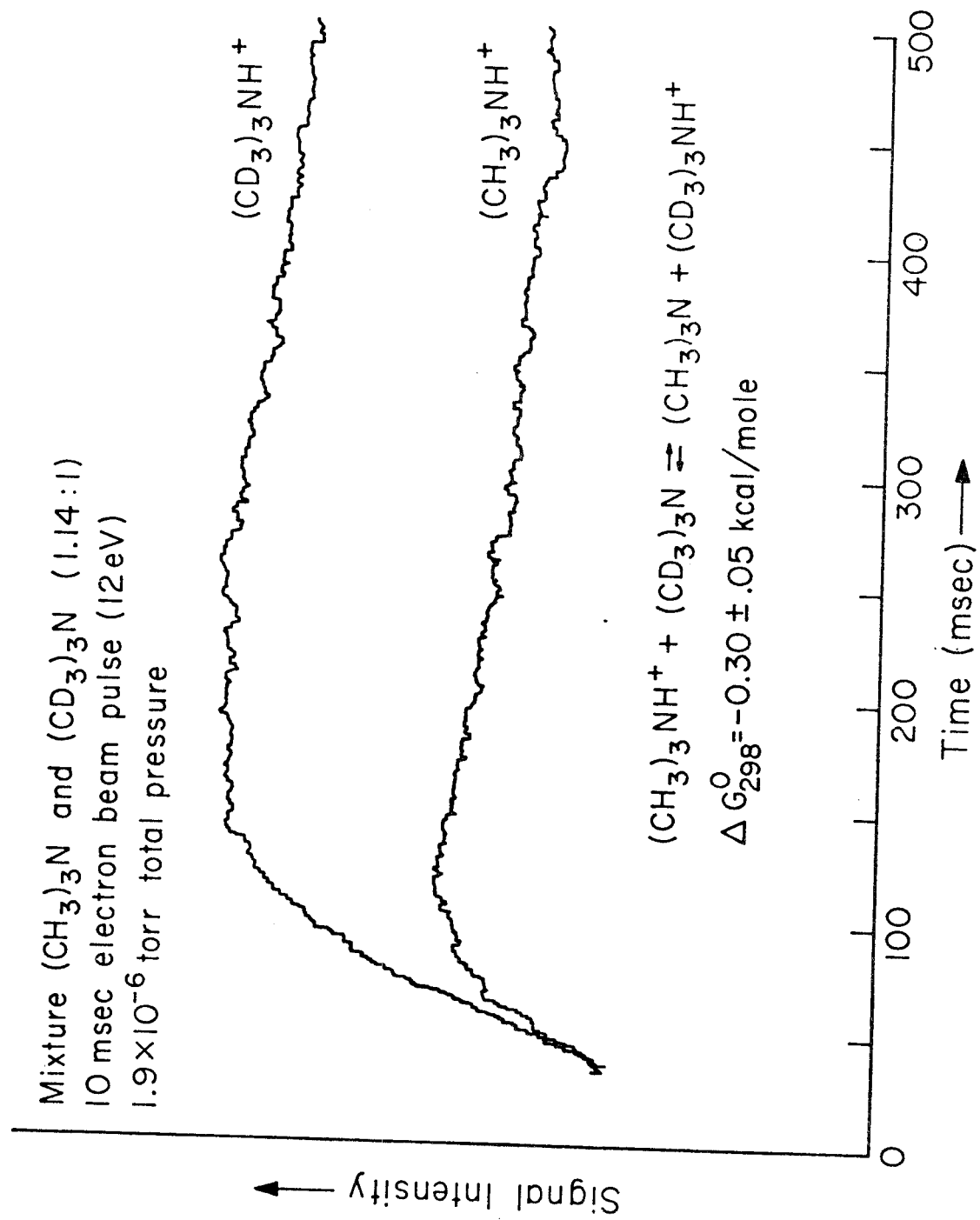
In the course of study of basicities of alkyl amines, it was observed that the proton affinity of trimethylamine-d₉ was approximately 300 ± 50 cal/mole greater than that of the undeuterated species. This result is illustrated in Fig. 11 for a 1.14:1 mixture of (CH₃)₃N and (CD₃)₃N. The equilibrium constant of 1.65 obtained for the reaction



was corroborated by the ratio of forward ($k_f = 3.1 \times 10^{-10}$

Figure 11

Trace of ion intensities of $(\text{CH}_3)_3\text{NH}^+$ and $(\text{CD}_3)_3\text{NH}^+$ vs. time in a 1.14:1 mixture of $(\text{CH}_3)_3\text{N}$ and $(\text{CD}_3)_3\text{N}$. Other conditions are 5 msec, 12 eV electron beam pulse, total pressure 1.9×10^{-6} torr.



$\text{cm}^3 \text{ molecule}^{-1} \text{ sec}^{-1}$) and reverse ($k_r = 1.9 \times 10^{-10} \text{ cm}^3 \text{ molecule}^{-1} \text{ sec}^{-1}$) rate constants measured using the time delayed ion ejection technique described earlier in this thesis.

The origin of such secondary isotope effects has been the subject of much speculation (43). It is generally accepted that the potential energy surfaces of isotopic molecules are essentially identical and that isotope effects arise from different energies of nuclear motions which are dependent on masses of the isotopic nuclei (44). The most significant difference is in the vibrational energy levels and the vibrational zero point energy which may be expressed as

$$\Delta \text{ZPE} = \frac{hc}{2} (\omega_H - \omega_D) \quad (35)$$

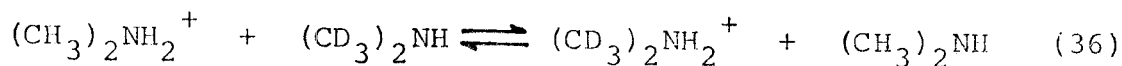
where ω_H and ω_D are the frequencies of H and D bonds in cm^{-1} , h is Planck's constant and c is the speed of light.

Since the mean square amplitude of vibration of the C-D bond is less than the C-H bond, the C-D bond will be on the average, closer to the equilibrium bond distance, r_e (45).

Halevi (46) has made the prediction that because a C-D bond is on the average shorter than a C-H bond, the electron density on carbon involving a C-D bond will be greater than that for a C-H bond. More simply stated, it might be assumed that D is a more inductively electron donating substituent than H. Therefore, introduction of a positive charge near carbon will be stabilized by a C-D bond more than

a C-H bond and favor the deuterated species in rate and equilibrium measurements of secondary isotope effects. This is exactly the effect observed in this experiment with trimethylamine-d₉. A temperature dependent study of the relative solution basicities of trimethylamine and trimethylamine-d₉ has been carried out by Robertson (47) who also found a ΔG for proton transfer which was constant with temperature of 300 cal/mole.

In order to test the generality of the deuterium isotope effect and to test the cumulative effects of deuterium substitution on amine basicity a similar experiment was carried out for dimethylamine. The observed equilibrium, shown in Fig. 12,

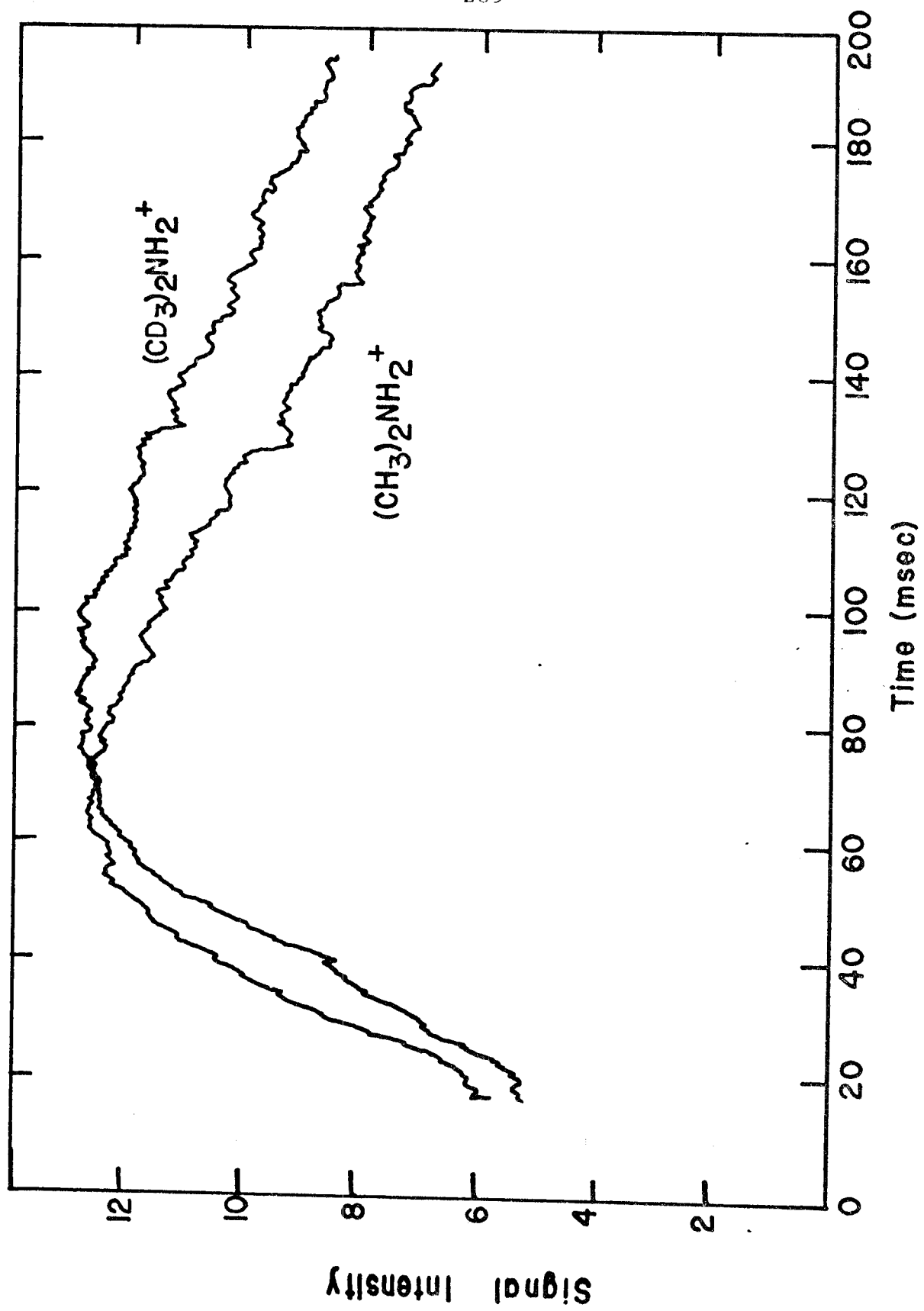


was found to favor the deuterated ion by 110 ± 50 cal/mole. The relative error in this measurement is rather large since the measured equilibrium constant is so close to unity. If the effects of deuterium substituents were additive the difference between basicities of deuterated and undeuterated dimethylamine would be expected to be two-thirds of that for trimethylamine. Considering experimental errors, this may be the case.

The number of systems on which measurements of β deuterium might be made is many. Further studies on alkyl amines should be carried out. In addition, the effect of deuterium substituents on different hetero atoms might be examined by

Figure 12

Trace of ion intensities of $(\text{CH}_3)_2\text{NH}_2^+$ and $(\text{CD}_3)_2\text{NH}_2^+$ vs. time in a 1:1 mixture of $(\text{CH}_3)_2\text{NH}$ and $(\text{CD}_3)_2\text{NH}$. Other conditions are 5 msec, 10.5 eV electron beam pulse, total pressure 1.8×10^{-6} torr.



studies of relative gas phase basicities between such pairs of molecules as CD_2O , CH_2O and $(\text{CD}_3)_2\text{O}$ and $(\text{CH}_3)_2\text{O}$.

REFERENCES

1. M. T. Bowers, D. H. Aue, H. M. Webb and R. T. McIver, Jr., J. Amer. Chem. Soc. 93, 4314 (1971).
2. R. T. McIver, Jr., and J. R. Eyler, *ibid*, 93, 6334 (1971).
3. J. P. Briggs, R. Yamdagni, and P. Kebarle, *ibid*. 94, 5128 (1972).
4. T. B. McMahon, R. J. Blint, D. P. Ridge and J. L. Beauchamp, *ibid*. 94, 8934 (1972).
5. J. J. Solomon and F. H. Field, *ibid*. 95, 4483 (1973).
6. T. L. Hill, An Introduction to Statistical Thermodynamics, Addison-Wesley, Reading Mass., 1960.
7. G. L. Pratt, Gas Kinetics, Wiley, New York, N.Y., 1969.
8. J. Hine, Physical Organic Chemistry, McGraw-Hill, New York, N. Y., 1962.
9. K. J. Laidler, Theories of Chemical Reaction Rates, McGraw-Hill, New York, N.Y., 1969.
10. H. Eyring, J. O. Hirschfelder and H. S. Taylor, J. Chem. Phys. 4, 479 (1936).
11. P. Langevin, Ann. Chim. Phys. 5, 245 (1905).
12. G. Gioumousis and D. P. Stevenson, J. Chem. Phys. 29, 294 (1958).
13. S. K. Gupta, E. G. Jones, A. G. Harrison and J. J. Myher, Can. J. Chem. 45, 3107 (1967).
14. R. T. McIver, Jr., Rev. Sci. Instrum. 41, 555 (1970).

15. T. B. McMahon and J. L. Beauchamp, *ibid.* 43, 509 (1972).
16. J. L. Beauchamp and S. E. Buttrill, Jr., *J. Chem. Phys.* 48, 1783 (1968).
17. J. L. Beauchamp, *Ann. Rev. Phys. Chem.* 22, 527 (1971).
18. W. G. Henderson, M. Taagepera, D. Holtz, R. T. McIver, Jr., J. L. Beauchamp, and R. W. Taft, *J. Amer. Chem. Soc.* 94, 4728 (1972).
19. E. M. Arnett, F. M. Jones III, M. Taagepera, W. G. Henderson, J. L. Beauchamp, and R. W. Taft, *ibid.* 94, 4724 (1972).
20. D. H. Aue, H. M. Webb and M. T. Bowers, *ibid.* 94, 4726 (1972).
21. R. Yamdagni and P. Kebarle, *ibid.* 95, 3504 (1973).
22. R. Yamdagni and P. Kebarle, *ibid.* 95, 4050 (1973).
23. D. K. Bohme, R. S. Hemsworth, G. I. MacKay and H. I. Schiff, presented at the 21st Ann. Conf. Mass Spectrom. Allied Top., San Francisco, Calif., 1973.
24. R. T. McIver, Jr., J. A. Scott, and J. H. Silvers, *ibid.* 1973.
25. P. Ausloos and S. G. Lias, *J. Amer. Chem. Soc.* 92, 5037 (1970).
26. J. L. Beauchamp, D. Holtz, S. D. Woodgate and S. L. Patt, *ibid.* 94, 2798 (1972).
27. R. J. Blint, T. B. McMahon, and J. L. Beauchamp, *ibid.* submitted for publication.
28. S. W. Benson, Thermochemical Kinetics, Wiley, New York,

- N.Y., (1968).
29. N. C. Baird and R. K. Datta, Can. J. Chem. 49, 3708 (1971).
 30. P. G. Miasek, Ph.D. Dissertation, California Institute of Technology, 1973.
 31. M. Krauss, J. A. Walker, and V. H. Diebler, J. Res. Nat. Bur. Stand., Sect. A, 72, 281 (1968).
 32. F. P. Lossing, Bull. Soc. Chim. Belg. 81, 125 (1972).
 33. J. A. Kerr and D. M. Timlin, Int. J. Chem. Kinet. 3, 427 (1971).
 34. D. P. Ridge, Ph.D. Dissertation, California Institute of Technology, 1973.
 35. D. P. Ridge, J. Y. Park, T. B. McMahon, and J. L. Beauchamp, to be published.
 36. L. Radom, J. A. Pople and P. von R. Schleyer, J. Amer. Chem. Soc., 94, 5935 (1972).
 37. J. L. Franklin, J. G. Dillard, H. M. Rosenstock, J. T. Herron, K. Draxl, and F. H. Field, "Ionization Potentials, Appearance Potentials and Heats of Formation of Gaseous Positive Ions," NSRDS-NBS, 26, (1969).
 38. (a) H. M. Rosenstock, private communication.
(b) Y. Sergev, M. Akopyan, F. I. Vilesov, and V. I. Kleimenov, Opt. Spectrosc. 29, 63 (1970).
 39. L. Melander, Isotope Effects on Reaction Rates, Ronald Press, New York, N.Y. (1960).
 40. J. Bigeleisen and M. G. Mayer, J. Chem. Phys. 15, 261 (1947).

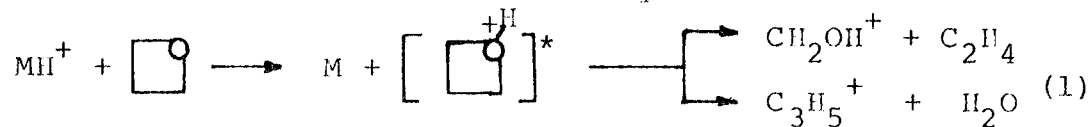
41. L. Melander, Arkiv. Kemi, 2, 211 (1950).
42. M. Wolfsberg and M. J. Stern, Pure Appl. Chem. 8, 225 (1964).
43. E. R. Thornton, Ann. Rev. Phys. Chem. 17, 349 (1966).
44. R. E. Weston, Jr., Tetrahedron, 6, 31 (1959).
45. L. S. Bartell, J. Amer. Chem. Soc. 83, 3567 (1961).
46. E. A. Halevi, Prog. Phys. Org. Chem. 1, 109 (1963).
47. D. Northcott and R. E. Robertson, J. Phys. Chem. 73, 1559 (1969).

Gas Phase Ion Chemistry of Trimethylene Oxide. Unimolecular
Decomposition of Excited Intermediates in Ion-Molecule Reactions

A. Introduction

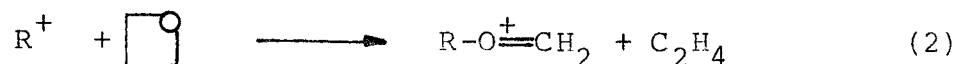
The qualitative study of the gas phase ion chemistry of individual molecules or homologous series of molecules has been a major application of ion cyclotron resonance spectroscopy (1-5). As a result, the mechanisms of many solution organic reactions, postulated by more classical physical organic techniques to proceed via ionic intermediates, have been elucidated. In addition, the reactions of certain classes of organic ions with a variety of functional groups have been generalized.

In contrast to simple alkyl ethers, trimethylene oxide has an exceedingly rich ion chemistry, exhibiting a wide variety of ion-molecule processes. Of particular interest are proton transfer reactions from acidic species to the parent molecule. Chemically activated protonated trimethylene oxide, thus formed, subsequently decomposes by ring opening followed by either direct bond cleavage to yield protonated formaldehyde and ethylene or formation of $C_3H_5^+$ by rearrangement and loss of water (equation 1).



A number of associative fragmentation processes have

also been observed in which reaction of various cations with trimethylene oxide induces decomposition involving loss of ethylene with formaldehyde remaining bound to the cation (equation 2)



Based on observations of subsequent reactions of the adducts of these associative fragmentations with both trimethylene oxide and other neutrals it is possible to make inferences about the structures of R^+ and $R-O^+=CH_2$.

In addition to the delineation of the ion chemistry and ion structures derived from trimethylene oxide a number of thermochemically oriented studies were undertaken.

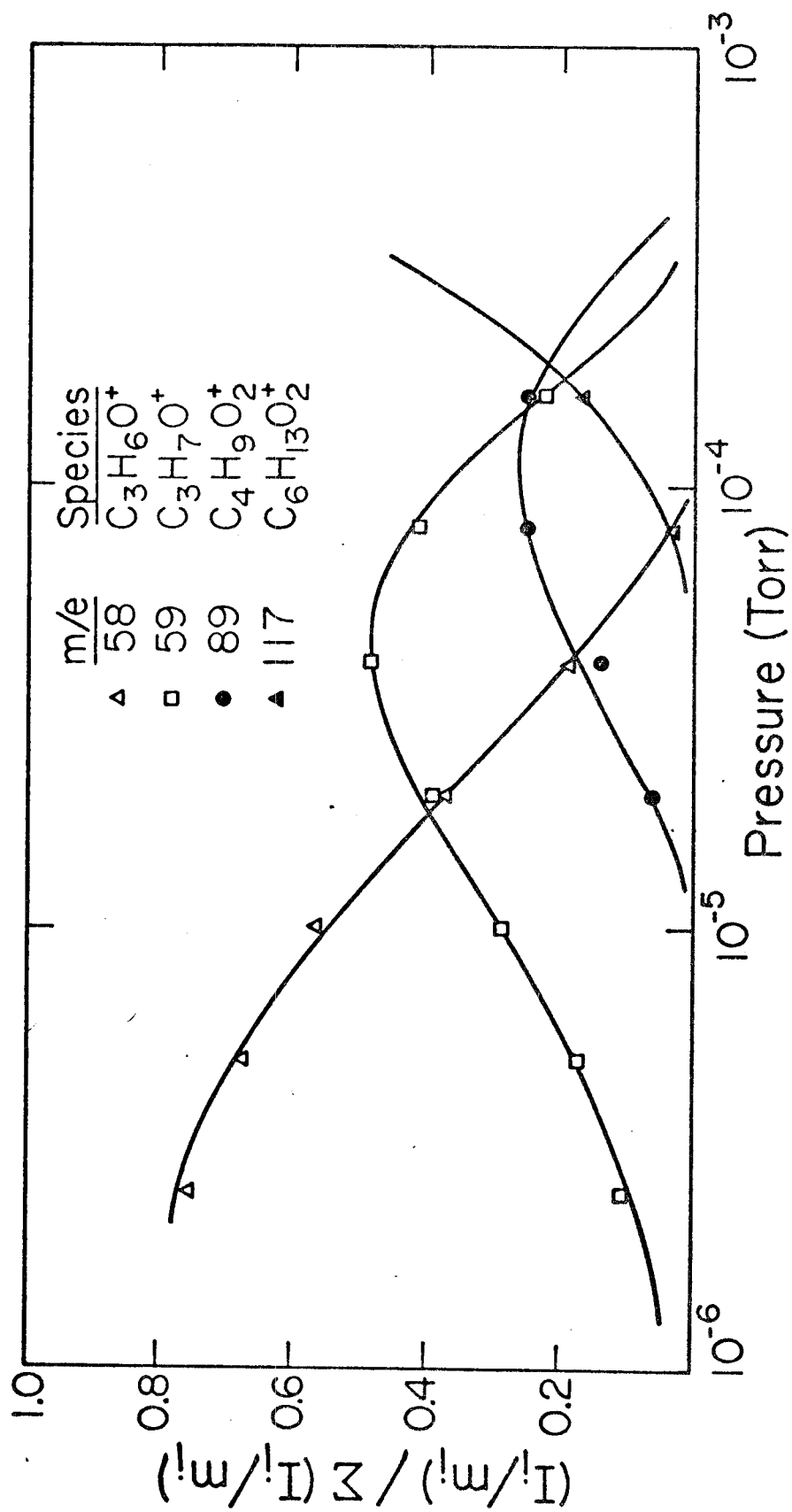
B. Ion-Molecule Reactions of Trimethylene Oxide

The reported ionization potential of trimethylene oxide is 9.667 eV (6). On electron impact at 10.0 eV in the ICR spectrometer the only ion observed was the parent ion at m/e 58. The ion-molecule reactions arising from the parent ion are illustrated in the plot of relative ion abundances vs. pressure shown in Figure 1. Since the lowest ionization potential of trimethylene oxide corresponds to removal of a non-bonding electron from oxygen, it is likely that the parent ion retains a cyclic structure near threshold.

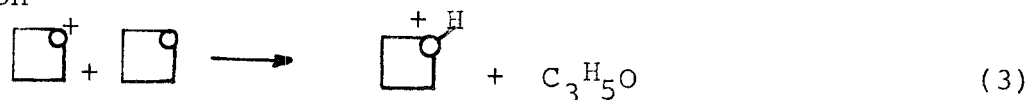
An examination of the ion-molecule reactions of trimethylene oxide α, α' -d₄ (7) at the same electron energy showed that the deuterated parent was formed in a 5 to 1

Figure 1

Variation of relative ion abundances with pressure for trimethylene oxide at 10.0 eV.

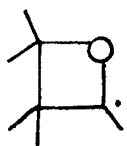


preference over protonated parent indicating that the most likely mechanism for formation of protonated parent involves either proton transfer or hydrogen abstraction from the α position

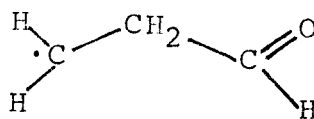


The actual structures of $\text{C}_3\text{H}_7\text{O}^+$ and $\text{C}_3\text{H}_5\text{O}$ are open to question but they may be postulated on the basis of further observations.

In studies of competitive proton transfer in binary mixtures of trimethylene oxide and other neutrals the proton affinity (PA) was found to be bracketed by acetone and dimethyl ether and on this basis was assigned to be 189 ± 5 kcal/mole. Using this value for the proton affinity a heat of formation of the protonated parent ion, $\Delta H_f^0(\text{C}_3\text{H}_7\text{O}^+)$, is determined to be 153 kcal/mole. The reasonable structures of $\text{C}_3\text{H}_5\text{O}$ resulting from the protonation reaction are



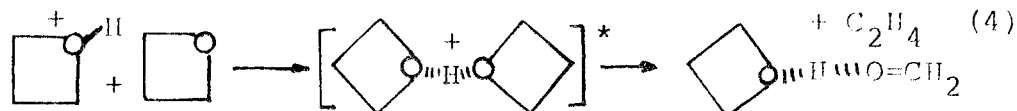
and



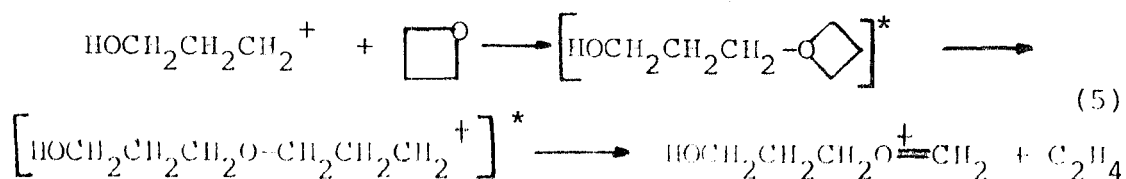
Using group equivalent methods (8) the heat of formation of the cyclic radical is estimated to be 23 kcal/mole while that for the linear structure is estimated as -5 kcal/mole.

Reaction (3) is thus predicted to be endothermic by 1 kcal/mole for cyclic $\text{C}_3\text{H}_5\text{O}$ and exothermic by 27 kcal/mole for linear $\text{C}_3\text{H}_5\text{O}$ indicating that the linear structure may be more probable.

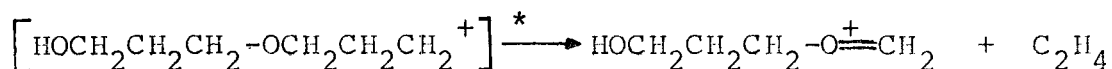
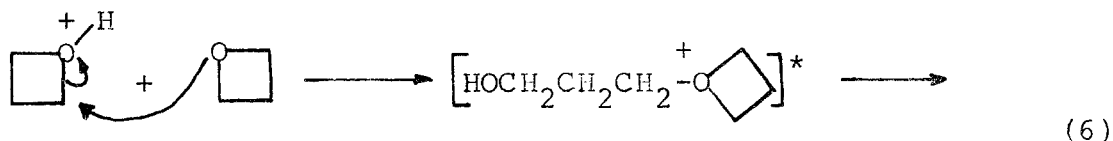
Double resonance experiments show that an ion at m/e 89 results from reaction of the protonated parent ion in undeuterated trimethylene oxide. Based on observations of ion-molecule reactions of other species containing heteroatoms the immediate tendency is to postulate the reaction as proceeding via a proton bound dimer intermediate which decomposes losing ethylene to leave a proton bound dimer of trimethylene oxide and formaldehyde (reaction 4).



However, in studies of binary mixtures of trimethylene oxide with methanol and acetone it was found that these molecules would not displace a molecule of formaldehyde from the m/e 89 complex. Since the proton affinities of both methanol and acetone are greater than that of formaldehyde it was expected that this reaction should occur. Since it does not, it seems apparent that the m/e 89 ion does not have the proton bound dimer form. This result may be interpreted as indicating that on protonation the m/e 59 ion undergoes ring opening to a 3 hydroxy propyl cation. Formation of the m/e 89 ion would then result from an associative fragmentation reaction in which the carbonium ion center associates with trimethylene oxide to form an oxonium ion which subsequently eliminates C_2H_4 (reaction 5).

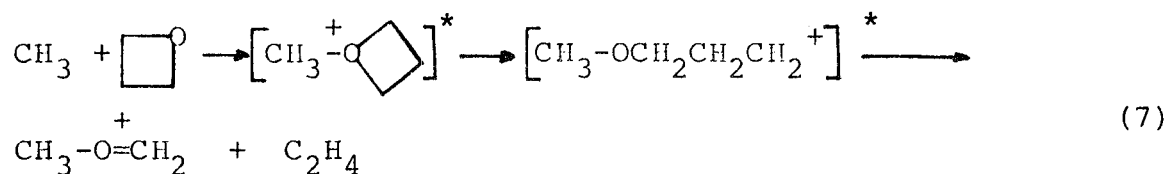


Alternatively, m/e 59 may retain a cyclic structure and m/e 89 could be formed by nucleophilic attack at the carbon (reaction 6) followed by elimination of ethylene.



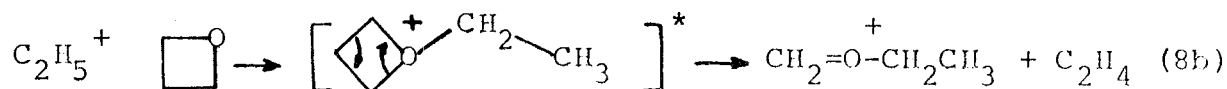
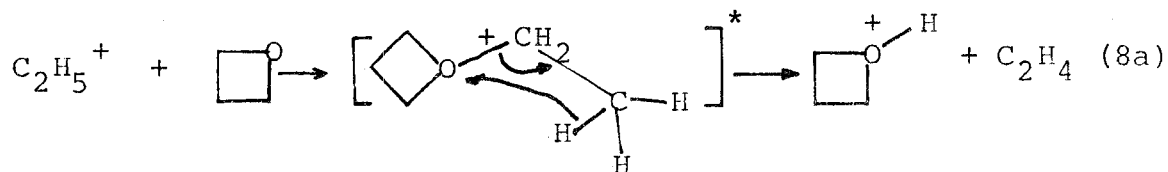
Such a reaction would result in the same products as the carbonium ion mechanism.

Evidence for an associative fragmentation reaction between carbonium ions and trimethylene oxide exists. The reaction of carbonium ions with trimethylene oxide to bind formaldehyde and eliminate ethylene, was shown to be general by reaction of a number of alkyl cations. In a mixture of methane and trimethylene oxide methyl cation was observed to undergo the reaction

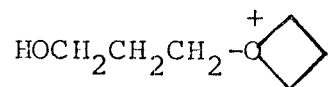


In addition, ethyl cation was observed by double resonance experiments to react to give m/e 59. This reaction may be regarded as either proton transfer or an associative fragmentation reaction. Reaction of ethyl cation with trimethylene oxide-d₄ proved that both of these reactions occur with proton transfer being favored by about 3 to 1. These

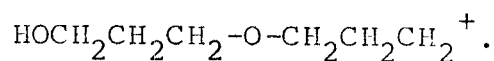
two reactions may be postulated to occur via a common intermediate (reaction 8).



At higher pressures an ion at m/e 117 is observed. Double resonance experiments show that this ion results from reactions of m/e 59 and m/e 89. The ion at m/e 117 formally corresponds to the proton bound dimer of trimethylene oxide. However, in addition to this, an ion of m/e 117 may be postulated to result from the collisionally stabilized intermediate of the reaction producing m/e 89. This ion may have either a cyclic oxonium structure,



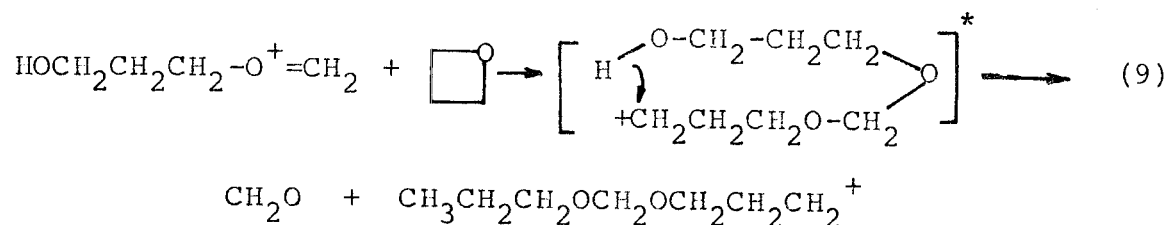
or an acyclic carbonium ion form,



At still higher pressures, an ion of m/e 175 corresponding to addition of another molecule of trimethylene oxide is observed. Thus a pattern of reaction becomes evident in which an oxonium ion or carbonium ion reacts with trimethylene oxide to cause ring opening. At low pressures, ring opening is followed by fragmentation to lose ethylene.

However, at pressure sufficiently high for collisional stabilization to compete with fragmentation the ring opened oxonium carbonium ion is the final product. This sequence of reactions is thus a chain reaction, much like that observed in the acid catalyzed polymerization of ethylene oxide in solution (9).

The formation of the m/e 117 adduct resulting from m/e 89 is less clear. However, the internal hydride transfer mechanism of reaction (9) for its formation is a feasible one.

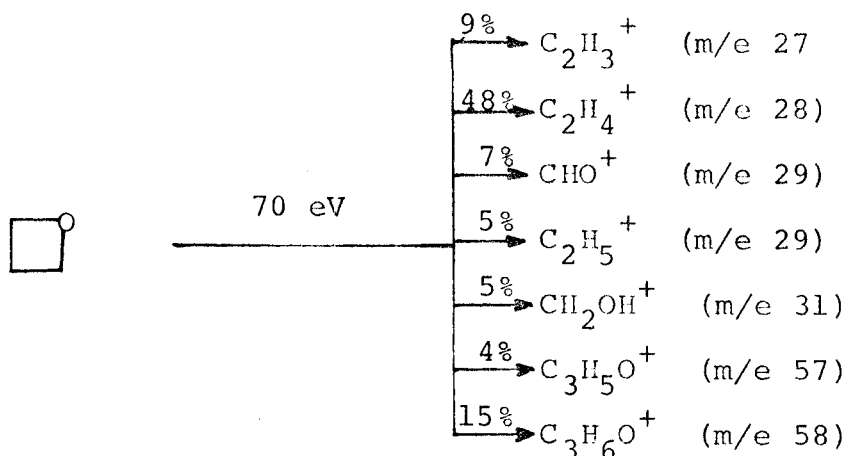


This mechanism predicts that there will be two different species of m/e 117, one formed by termolecular kinetics from m/e 59 and the other formed in bimolecular reaction from m/e 89. This prediction is verified by the observation of an ion of m/e 117 in a trapped-ion study of trimethylene oxide resulting from reaction of m/e 89. Under normal operating conditions for trapped-ion experiments only bimolecular processes are observable. At higher pressures in drift mode experiments termolecular processes are also possible and hence under these conditions two different forms of m/e 117 will be observed.

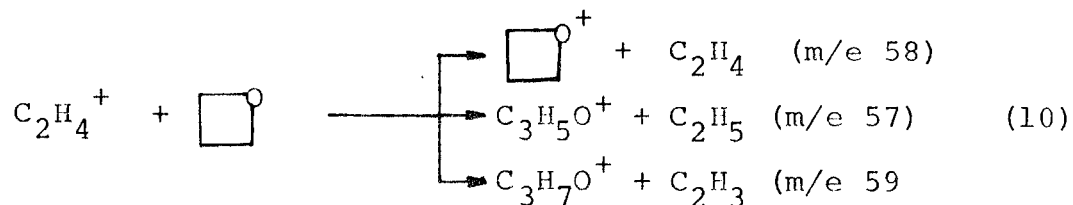
According to the above mechanisms the ion-molecule reactions arising from the molecular ion of trimethylene

oxide are summarized in Figure 2.

At higher electron energies a number of fragment ions are formed. The principle fragments are listed in Scheme 1 along with their relative abundances for electron impact at 70 eV. In cases where more than one ion structure is possible the assignment has been made on the basis of the high resolution mass spectrometric study by Beynon (10).



The variation of ion abundance with pressure for the ions derived from trimethylene oxide is shown in Figure 3. The most prominent fragment, $C_2H_4^+$, reacts via three reactions, charge exchange, hydride abstraction and proton transfer (equation 10)



Experiments with trimethylene oxide α , α' - d_4 have shown that hydride abstraction occurs from both the α and β positions to produce ions at m/e 61 and m/e 60, respectively. On

Figure 2

Ion-molecule reactions resulting from the parent ion of trimethylene oxide formed by electron impact at 10.0 eV.

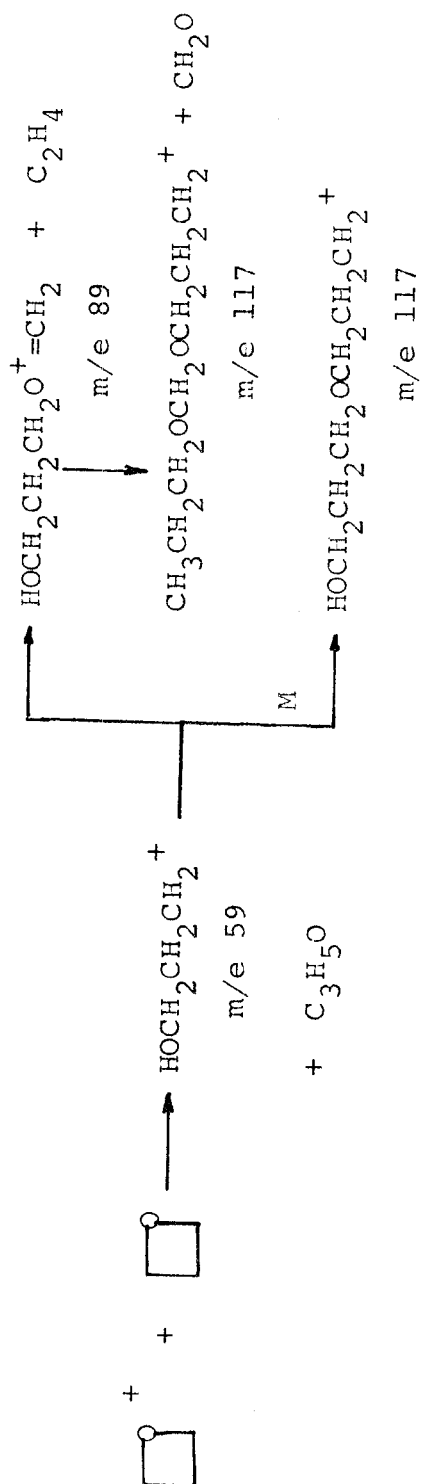
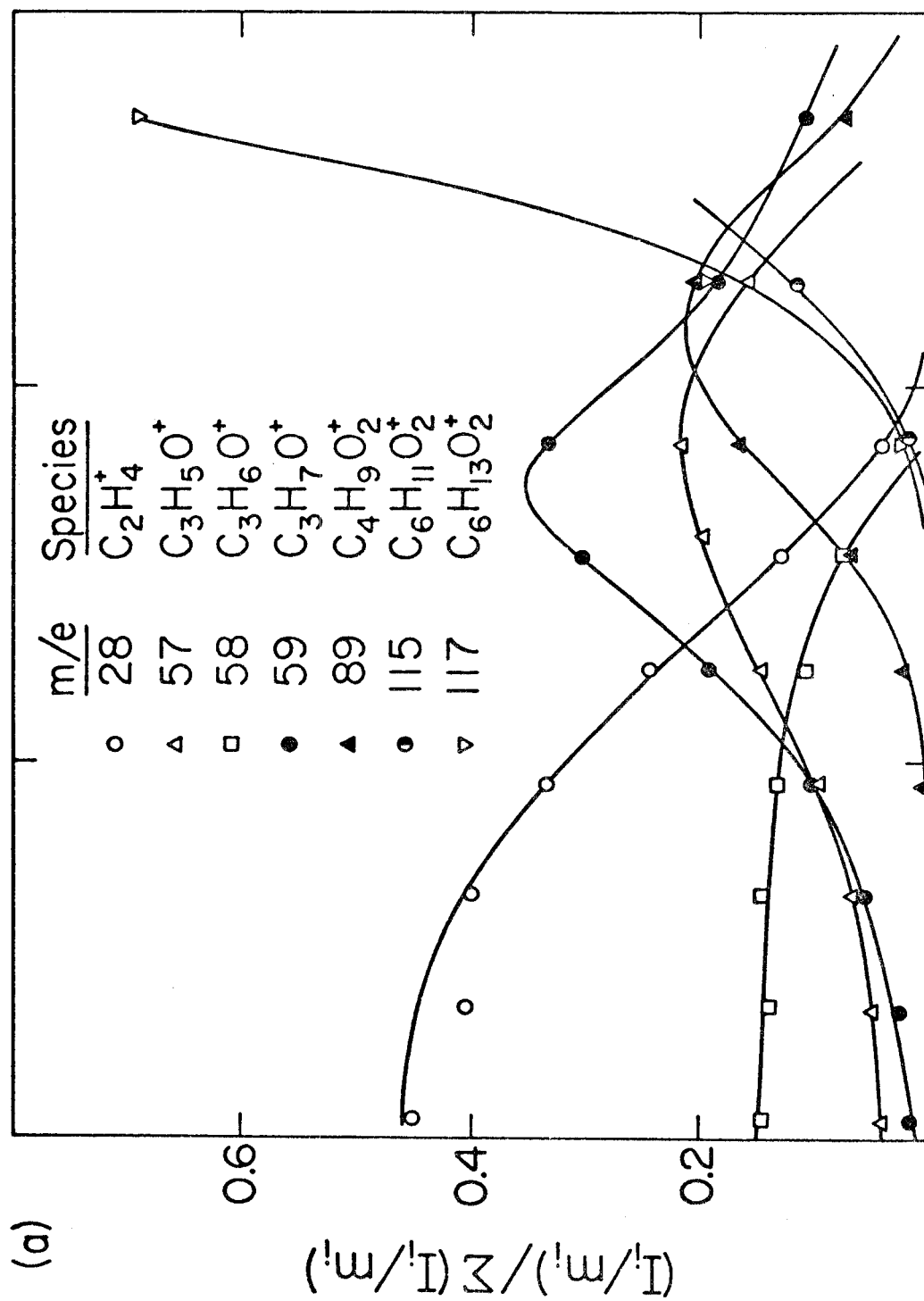
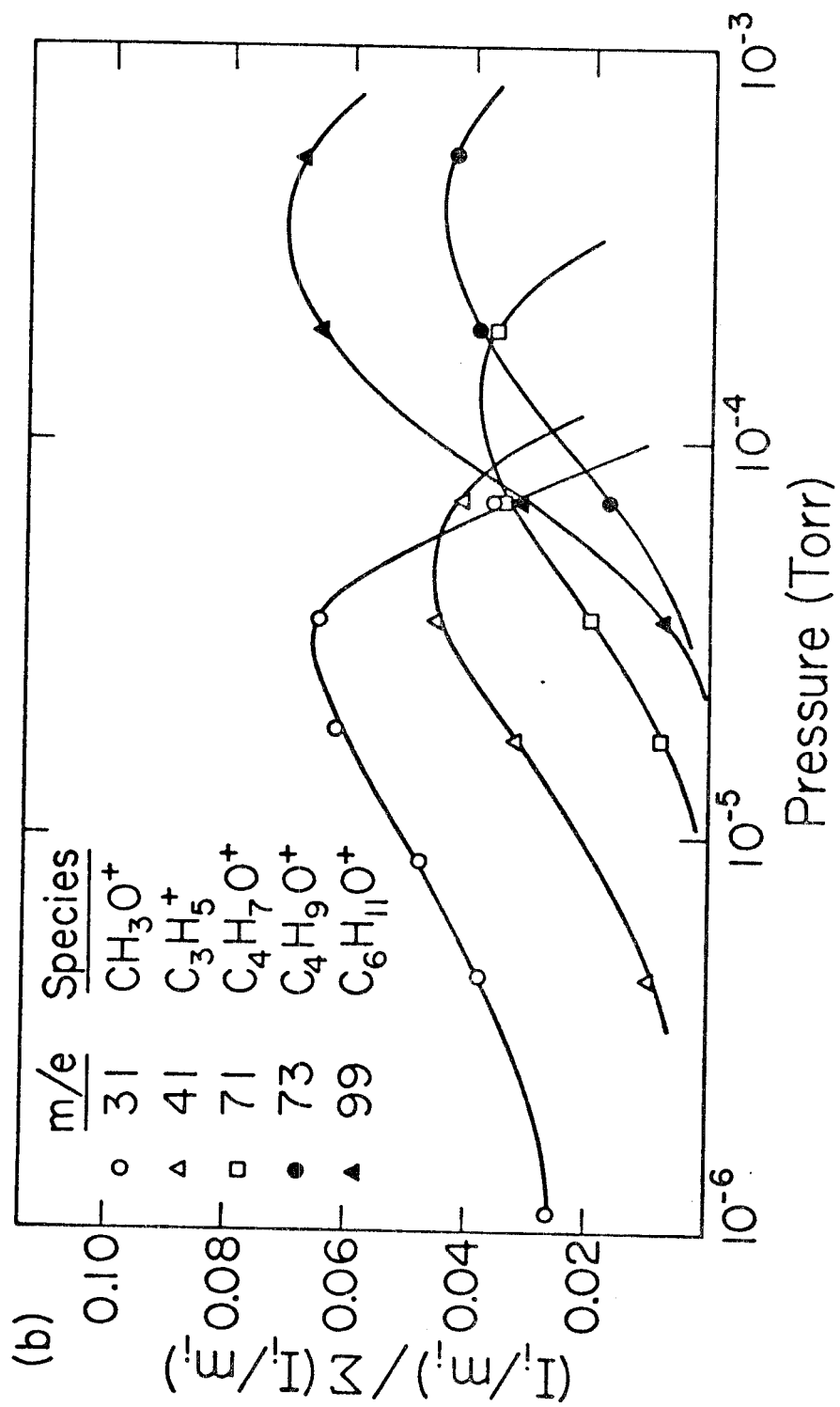


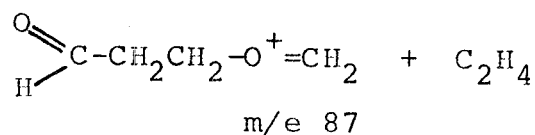
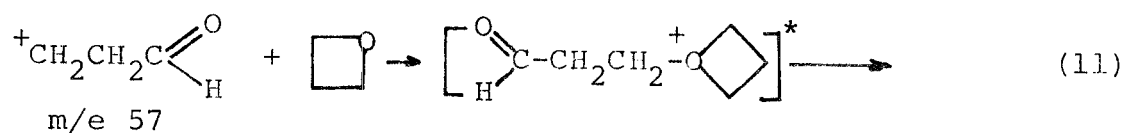
Figure 3

Variation of relative ion abundances with pressure for trimethylene oxide at 70 eV. Figure 3(a) shows the major ionic species while Figure 3(b) shows minor contributions to the total ion abundance.





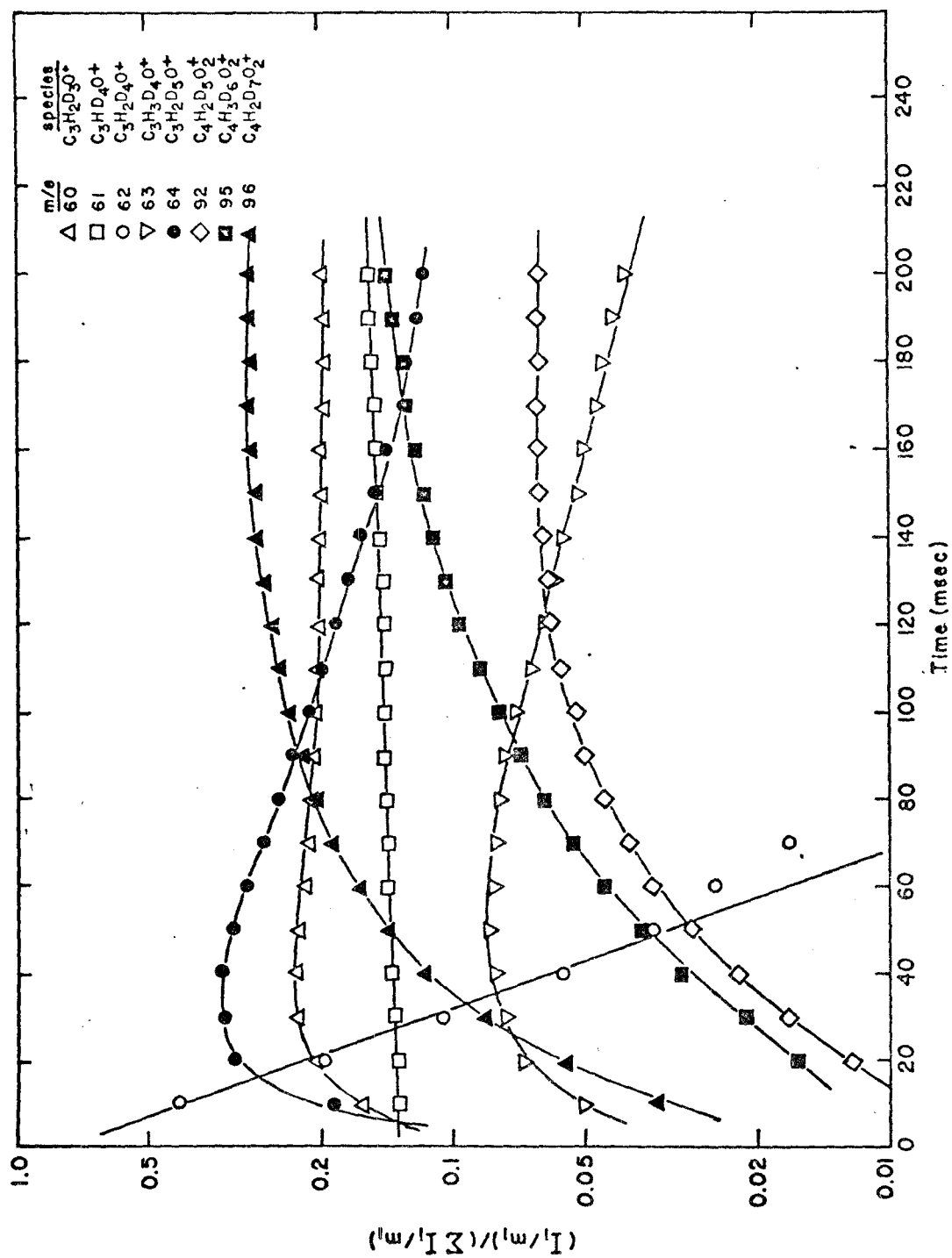
electron impact at 70 eV the loss of deuterium is favored by about 3:2 over loss of hydrogen. Hence in ordinary trimethylene oxide there will be two distinctly different forms for the m/e 57 ion. The only observed bimolecular reaction of this ion is the production of an ion at m/e 87. This may be associative fragmentation reaction much like that postulated for the m/e 59 ion and hence it seems likely that one possible mechanism producing m/e 87 would be reaction (11)



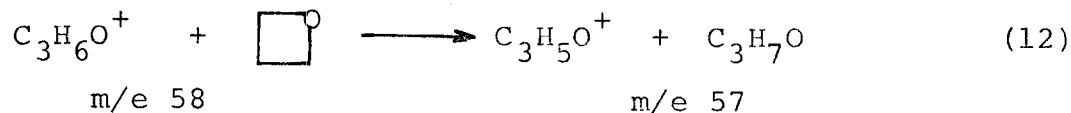
corresponding to reaction of the ion resulting from loss of H from the α position followed by ring opening. A trapped ion study of trimethylene oxide α, α' -d₄ at 11 eV, is shown in Figure 4. At this electron energy the only primary ions present are the molecular ion and fragments resulting from loss of H and loss of D. As can be seen the m/e 61 ion resulting from loss of H from the β position is unreactive, while after an initial increase the m/e 60 ion reacts slowly to produce an ion at m/e 92 which is analogous to m/e 87 in the undeuterated system. The initial rise in the m/e 60 ion intensity was shown by double resonance experiments to be due to the reaction of the m/e 62 molecular ion. This

Figure 4

Variation of relative ion abundances with time for trimethylene oxide at 11.0 eV. Ion formation was by a 5 msec, electron beam pulse at a total pressure of 1.5×10^{-6} torr.



reaction corresponds to reaction (12) for the undeuterated system.



This may be taken to indicate that at this electron energy ring opening of the molecular ion has occurred since in studies just above threshold (10 eV) reaction (12) does not occur.

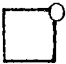
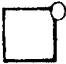
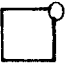
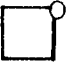
The ions at m/e 95 and 96 in Figure 4 are the products of associative fragmentation reactions analogous to reactions (5) and (6).

The ion at m/e 115 shown in Figure 3 is the collisionally stabilized intermediate of reaction (11). In contrast to the m/e 117 ion, double resonance experiments revealed no bimolecular production of m/e 115 from m/e 87.

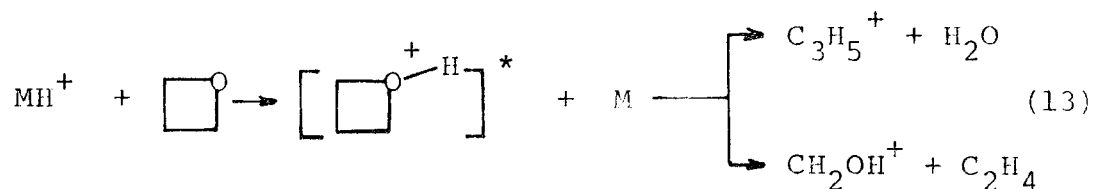
The most common observed reaction at 70 eV is proton transfer from the fragment ions C_2H_3^+ , CHO^+ , C_2H_5^+ , and CH_2OH^+ , all of which possess a labile proton. These reactions have varying degrees of exothermicity which may appear as internal excitation of the protonated trimethylene oxide. These reactions and the exothermicity of each are summarized in Table 1. If a sufficient amount of the exothermicity of these proton transfer reactions becomes internal excitation of the protonated molecule unimolecular decomposition may occur. Double resonance experiments indicated that the m/e 41 ion, C_3H_5^+ , resulted from reaction of each of the ions

TABLE 1

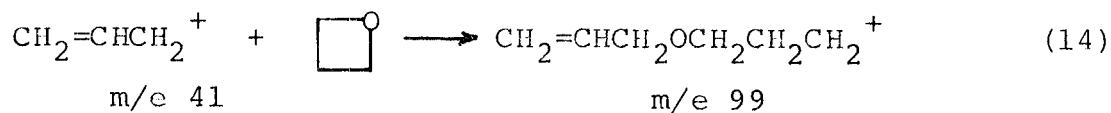
Exothermic Proton Transfer Reactions
Occurring in Trimethylene Oxide at 70 eV

<u>Reaction</u>			<u>ΔH (kcal/mole)</u>
CH_2OH^+ m/e 31	+ 	$\longrightarrow \text{C}_3\text{H}_7\text{O}^+ + \text{CH}_2\text{OH}$	-24
C_2H_5^+ m/e 29	+ 	$\longrightarrow \text{C}_3\text{H}_7\text{O}^+ + \text{C}_2\text{H}_4$	-28
C_2H_3^+ m/e 27	+ 	$\longrightarrow \text{C}_3\text{H}_7\text{O}^+ + \text{C}_2\text{H}_2$	-36
HCO^+ m/e 29	+ 	$\longrightarrow \text{C}_3\text{H}_7\text{O}^+ + \text{CO}$	-46

having labile protons. This result implies that the exothermicity of proton transfer may contribute to the unimolecular decomposition of the $C_3H_7O^+$ species to produce $C_3H_5^+$. In addition, it was observed that CH_2OH^+ , m/e 31, was also a product of these exothermic proton transfer reactions. From these observations, it is concluded that excited protonated trimethylene oxide may undergo unimolecular decomposition by two modes. One of these involved simple bond cleavage while the other requires rearrangement loss of water (reaction 13).



The m/e 41 ion resulting from unimolecular decomposition was observed to react further to produce an ion of m/e 99. Assuming the $C_3H_5^+$ species to be allyl cation the reaction is likely another involving association of a carbonium ion with the ether linkage (reaction 14).

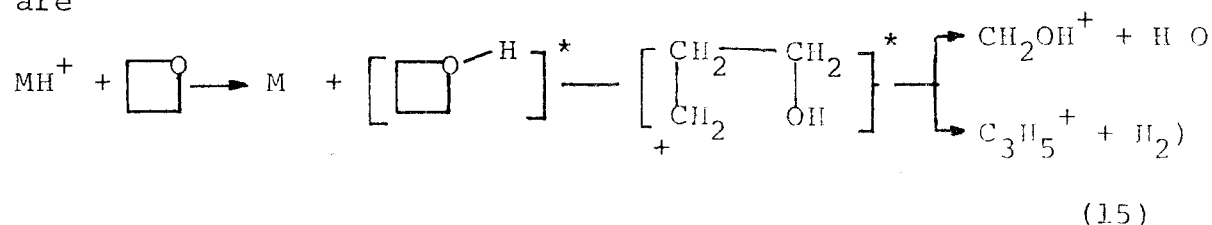


No fragmentation to lose C_2H_4 was observed indicating that this reaction is not sufficiently exothermic to induce bond breakage following ring opening.

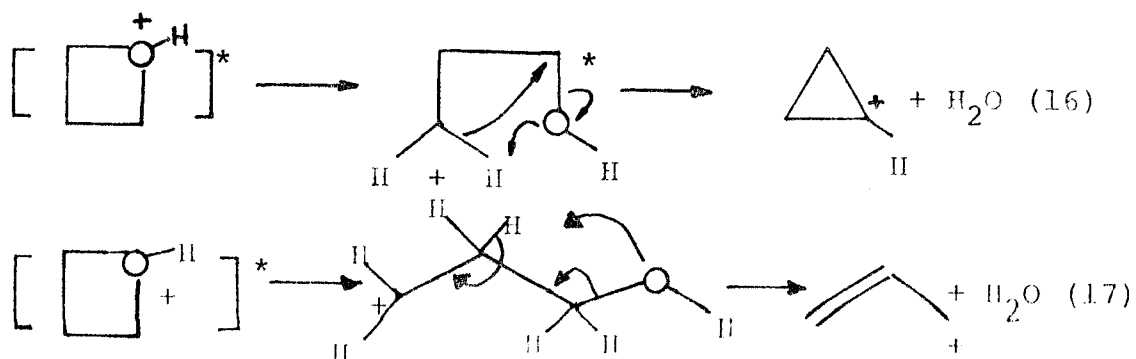
C. Unimolecular Decomposition of Chemically Activated Trimethylene Oxide

Following the observation that exothermic proton transfer reactions from acidic species to trimethylene oxide could induce unimolecular decomposition of the resulting ion a number of experiments involving binary mixtures of trimethylene oxide with other neutrals were carried out. Reagent ions were chosen to provide a wide range of possible excitation energies of the protonated trimethylene oxide.

The possible decomposition pathways of the excited ion are



In order to determine the theoretical threshold for decomposition it is necessary to know the structure of C_3H_5^+ . This ion may result from a migration of hydrogen from an carbon in which case a cyclopropyl cation is more likely (reaction 16) or migration from a α carbon which results in an allyl cation (reaction 17).

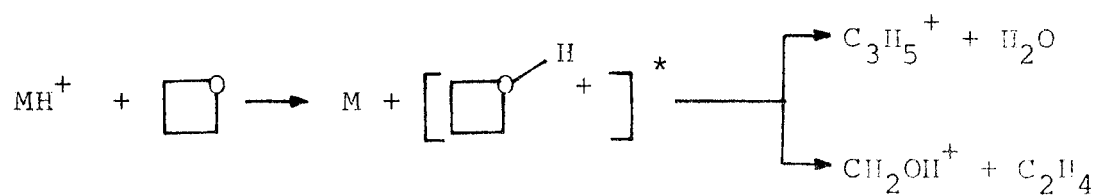


An examination of analogous decomposition processes in trimethylene oxide α, α' -d₄ showed that hydrogen migration took place predominantly from the β carbon. Therefore the majority of $C_3H_5^+$ is allyl cation.

Based on a heat of formation of 153 kcal/mole for protonated trimethylene oxide decomposition to produce allyl cation and water is endothermic by 15 kcal/mole which production of protonated formaldehyde and ethylene is endothermic by 31.5 kcal/mole. A number of proton transfer reagents, together with the maximum amount of excitation energy such a reaction would impart to protonated trimethylene oxide are listed in Table 2. The experimental variation of the product distribution with internal excitation energy of the protonated molecule is shown in Figure 5. It can be readily seen that at higher excitation energies $CH_2OH^+ + C_2H_4$ are clearly the favored reaction products. Although production of $C_3H_5^+ + H_2O$ is thermodynamically more favorable it involves a rearrangement process. The $CH_2OH^+ + C_2H_4$ products, however, involve only simple bond cleavage and are thus kinetically favored. As the internal energy of the protonated molecule is increased, its lifetime will decrease. If the lifetime of the ion is shorter than the time scale involved in the rearrangement process, no $C_3H_5^+ + H_2O$ will be observed. However, at low internal excitation energies the activated ion will have a lifetime sufficient to allow internal rearrangement and the thermodynamically more

TABLE 2

Proton Transfer Reagents for Producing
Chemically Activated Trimethylene Oxide

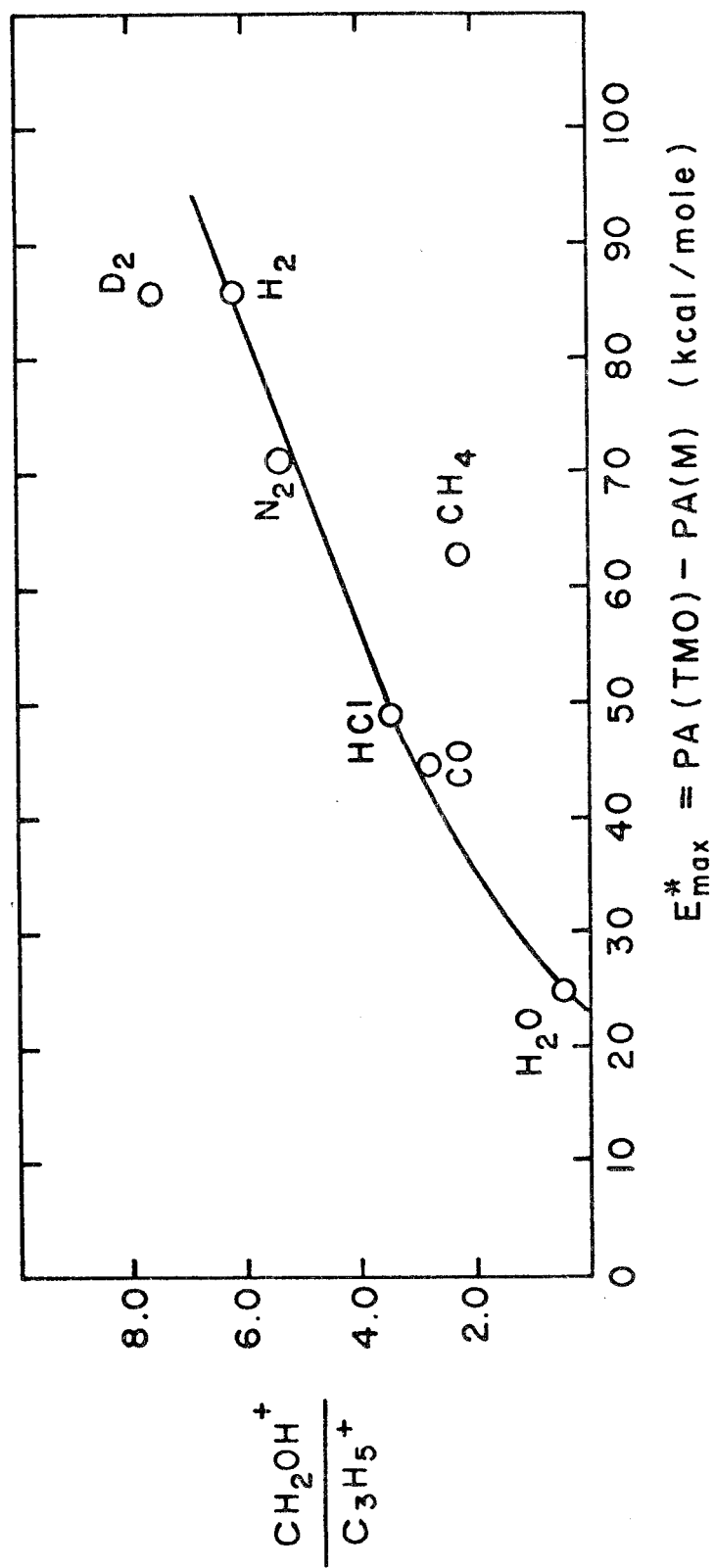


$$E^*_{\text{max}} = \text{PA} \left(\text{[Trimethylene Oxide]} \right) - \text{PA}(\text{M})$$

<u>Species M</u>	<u>E*_{max} (kcal/mole)</u>
H ₂	85
N ₂	71
CH ₄	63
HCl	49
CO	46
H ₂ O	24

Figure 5

Experimental variation of the $\text{CH}_2\text{OH}^+:\text{C}_3\text{H}_5^+$ product ratio arising from exothermic proton transfer from a variety of proton transfer reagents.



favorable allyl cation channel will predominate.

The notable exception to the smooth curve of Figure 5 is CH_5^+ as proton transfer agent. It appears that the neutral product, CH_4 , of the proton transfer reaction has sufficient vibrational modes to carry off a considerable amount of the exothermicity of reaction as internal excitation itself. This observation provides a useful technique for determining the partitioning of energy between the products of reactions. In the CH_5^+ case, the exothermicity of proton transfer is 63 kcal/mole. However, the product distribution is more compatible with an internal excitation of 38 kcal/mole in the protonated trimethylene oxide. This means that roughly 25 kcal/mole of excess energy appears as internal excitation of the neutral product CH_4 or as relative translational energy of the products. Such experimental observations on the basis of product distributions might be usefully compared with predictions of more complex theories of unimolecular decomposition.

REFERENCES

1. D. Holtz, J. L. Beauchamp, and J. R. Eylar, J. Amer. Chem. Soc. 92, 7045 (1970).
2. J. M. S. Henis, J. Amer. Chem. Soc. 90, 844 (1968).
3. M. T. Bowers, D. D. Elleman, and J. L. Beauchamp, J. Phys. Chem. 72, 3599 (1968).
4. J. L. Beauchamp and M. C. Caserio, J. Amer. Chem. Soc. 94, 2638 (1972).
5. J. L. Beauchamp, D. Holtz, S. D. Woodgate and S. L. Patt, J. Amer. Chem. Soc. 94, 2798 (1972).
6. G. J. Hernandez, J. Chem. Phys. 38, 2233 (1963).
7. The author is extremely grateful to Professor H. Wieser of the University of Calgary for generously supplying a sample of trimethylene oxide, α, α' -d₄.
8. J. L. Franklin, J. Chem. Phys. 21, 2029 (1953).
9. D. J. Cram and G. S. Hammond, Organic Chemistry, McGraw-Hill, New York, N.Y. (1959).
10. J. H. Beynon, Mass Spectrometry and its Application to Organic Chemistry, Elsevier, Amsterdam, 1960).

APPENDIX

```

FORTRAN IV G LEVEL 19          MAIN          DATE = 2/08/71 12:58
C
0001      DIMENSION DENS(20),SIZE(20),MASS(20),NPREC(20),TAU(20),
      CTAU(20),RATE(20,20,20),RATEI(20,20),RATEJ(20,20),
      CSIZE(20,20),FACT(20),NCON(20),HWIDTH(20,20),COLF(20)
C INPUT CELL DIMENSIONS,GAMU,DRIFT VOLTAGES,NO. SPECTRA
0002      READ(5,101) T,ALEN1,ALEN2
0003      31 READ(5,102) GAMU,VSCUR,VRES,NSPEC,CMAMU
0004      IF(GAMU*CMAMU) GO TO 30
C INPUT SPECTRA CARDS,-NO.,PRESSURE,,INTENSITIES,LINE WIDTH
0005      51 CONTINUE
0006      READ(5,103) NUMBER,DENS(NUMBER),NPEAKS,(SIZE(I,NUMBER),
      CI=1,NPEAKS),HWIDTH(I,NUMBER),I=1,NPEAKS)
0007      WRITE(6,722) HWIDTH(I,NUMBER),I=1,NPEAKS)
0008      IF(DENS(NUMBER).LT.1.DENS(NUMBER)/DENS(NUMBER)*3.23E16
0009      IF(NUMBER.NE.NSPEC) GO TO 51
C INPUT NO. OF EACH TYPE OF ION,ION MASSES,PRECURSORS
0010      READ(5,104) NPRIM,NSC,CV,TENT,(MASS(I),I=1,NPEAKS)
0011      C,(NPREC(I),I=1,NPEAKS)
0012      NPRIM=NPRIM+1
0013      NSC=NSEC+1
C CALCULATE T-SOURCE,T-ANALYZER FOR EACH ION
0014      BLAT=(1.6E-19)*(6.02E23)*(1.CE-21)
0015      DO 1 I=1,NPEAKS
0016      TAU(I)=ALEN1*GAMU*MASS(I)*C/(VSCUR*10**8)
0017      TAU(I)=TAU(I)+ALEN2*GAMU*MASS(I)*C/(VRES*10**8)
0018      WRITE(6,112) GAMU,VSCUR,VRES,TAU(I),TAUP(I)
0019      DO 25 NUMBER=1,NSPEC
0020      DO 10 I=1,NPEAKS
0021      COLF(I)=GAMU*HWIDTH(I,NUMBER)/CMAMU*BLAT/MASS(I)
      ACCN(NUMBER)=1
C CALCULATE INITIAL RATE CONSTANTS
0022      DO 2 J=NPRIM,TERT
0023      DO 3 I=1,NPEAKS
0024      COLF(I)=GAMU*HWIDTH(I,NUMBER)/CMAMU*BLAT/MASS(I)
0025      RATE(I,J,NUMBER)=0
0026      3 PI=TAU(NPREC(J))+TAUP(NPREC(J))
0027      IF(SIZE(NPREC(J),NUMBER).EQ.0.0.AND.SIZE(J,NUMBER).EQ.0.0)
      GO TO 47
      RATE(NPREC(J),J,NUMBER)=2.*MASS(NPREC(J))*SIZE(J,NUMBER)
      C/DENS(NUMBER)*PI*(MASS(NPREC(J))*SIZE(J,NUMBER)+MASS(J)*
      CSIZE(NPREC(J),NUMBER)))
0028      GO TO 2
0029      40 RATE(NPREC(J),J,NUMBER)=0.0
0030      2 CONTINUE
C INITIALIZE ITERATION COUNTER
0031      ITER=1
C CALCULATE I AND JSUBI
0032      50 DO 41 I=1,NPRIM
0033      RATEI(I,NUMBER)=0
0034      DO 4 J=NPRIM,NSC
0035      RATEJ(I,NUMBER)=RATE(I,NUMBER)+RATE(I,J,NUMBER)
0036      IF(SIZE(I,NUMBER).EQ.0.0) RATEI(I,NUMBER)=RATEI(I,NUMBER-1)
0037      WRITE(6,986) I,RATEI(I,NUMBER)
0038      4 NORMALIZE OBSERVED INTENSITIES
0039      DO 6 N=1,NPRIM
0040      SUM7=0

```

```

FORTRAN IV G LEVEL 19          MAIN          DATE = 2/08/71 12:58:
0041      DO 5 IB=1,NPEAKS
0042      IF(NPREC(IB).EQ.0.AND.NPREC(NPREC(IB)).EQ.0) SUM2=SUM2+
          C SIZE0(IB,NUMBER)
0043      5      CONTINUE
0044      DO 6 IB=1,NPEAKS
0045      IF(NPREC(IB).EQ.0.AND.NPREC(NPREC(IB)).EQ.0) SIZE0(IB,NUMBER)=
          C SIZE0(IB,NUMBER)/SUM2
0046      6      CONTINUE
          C BRANCH IF NO TERTIARIES
0047      IF(NTERT.EQ.NSEC) GO TO 8
0048      DO 7 J=NPRIM,NSEC
0049      RATEJ(J,NUMBER)=0
0050      DO 7 K=NSEC,NTERT
0051      RATEJ(J,NUMBER)=RATEJ(J,NUMBER)+RATE(J,K,NUMBER)
0052      7      WRITE(6,999)J,RATEJ(J,NUMBER)
          C CALCULATE PREDICTED INTENSITIES
0053      8      DO 9 I=1,NPRIM
0054      A1=EXP(-DENS(NUMBER)*RATEI(I,NUMBER)*TAU(I))
0055      A2=EXP(-DENS(NUMBER)*RATEI(I,NUMBER)*TAUP(I))
0056      IF(COLF(I).EQ.0) GO TO 200
0057      A3=EXP(-COLF(I)*TAUP(I))
0058      A4=EXP(-COLF(I)*TAU(I))
0059      SIZE(I,NUMBER)=((A1-A2)/(DENS(NUMBER)*RATEI(I,NUMBER)+EXP(COLF
          C (I)*TAU(I))*(A2-A3-A1*A4)/(DENS(NUMBER)*RATEI(I,NUMBER)+COLF(I))
          C (MASS(I)*COLF(I))
0060      IF(SIZE(I,NUMBER).LT.0.0) SIZE(I,NUMBER)=SIZE(I,NUMBER)*(-1.0)
0061      GO TO 9
0062      200      SIZE(I,NUMBER)=(A1-A2-DENS(NUMBER)*RATEI(I,NUMBER)*(TAUP(I)-TAU(I)
          C 1)*A2)/(MASS(I)*RATEI(I,NUMBER))
0063      IF(SIZE(I,NUMBER).LT.0.0) SIZE(I,NUMBER)=SIZE(I,NUMBER)*(-1.0)
0064      9      CONTINUE
0065      WRITE(6,801)A1,A2,A3,A4
0066      WRITE(6,800)I,SIZE(I,NUMBER)
0067      DO 12 J=NPRIM,NSEC
          C BRANCH IF NO TERTIARIES
0068      S1=EXP(-DENS(NUMBER)*RATEI(NPREC(J),NUMBER)*TAU(J))
0069      S2=EXP(-DENS(NUMBER)*RATEI(NPREC(J),NUMBER)*TAUP(J))
0070      S10=DENS(NUMBER)*RATEI(NPREC(J),NUMBER)
0071      S11=TAUP(J)-TAU(J)
0072      S13=EXP(COLF(J)*TAU(J))
0073      S16=S10-COLF(J)
0074      S17=RATEI(NPREC(J),NUMBER)
0075      IF(COLF(J).EQ.0.0.AND.NTERT.EQ.NSEC) GO TO 202
0076      IF(NTERT.EQ.NSEC) GO TO 11
0077      S2=EXP(-DENS(NUMBER)*RATEJ(J,NUMBER)*TAU(J))
0078      S3=1.0/S2
0079      S4=EXP(-DENS(NUMBER)*RATEJ(J,NUMBER)*TAUP(J))
0080      S5=DENS(NUMBER)*RATEJ(J,NUMBER)
0081      S6=S5-COLF(J)
0082      S7=DENS(NUMBER)*(RATEJ(J,NUMBER)-RATEI(NPREC(J),NUMBER))
0083      S9=S7-COLF(J)
0084      S12=RATEJ(J,NUMBER)-RATEI(NPREC(J),NUMBER)
0085      S14=S6*TAUP(J)
0086      S15=S6*TAU(J)
0087      S18=RATEJ(J,NUMBER)
0088      IF(S18.EQ.0.0.AND.COLF(J).EQ.0.0) GO TO 202

```

```

FORTRAN IV G LEVEL 19          MAIN          DATE = 2/06/71    12:55:00

0089          IF(S18.EQ.0.0) GO TO 11
0090          IF(COLF(J).EQ.0.0) GO TO 201
0091          SIZE(J,NUMBER)=(S1-S2)*S3*((S4-S2)/S5+S13*(EXP(-S14)-EXP(-S15))/  

1561/S12+S1*((S4/S2-1.0)/(S5*S7)-(S8/S1-1.0)/(S10*S7))+TS8/S1-1.0)/(  

2510*S9)-(EXP(-S6*S11)-1.0)/(S6*S9))*DENS(NUMBER))*RATE(NPREC(J),J,  

3NUMBER)/(MASS(J)*COLF(J))
0092          IF(SIZE(J,NUMBER).LT.0.) SIZE(J,NUMBER)=SIZE(J,NUMBER)*(-1.0)
0093          WRITE(6,800)J,SIZE(J,NUMBER)
0094          GO TO 12
0095          201 SIZE(J,NUMBER)=(RATE(NPREC(J),J,NUMBER)*S1/(MASS(J)*S18**2*(S17-S1  

18)**2))*((S16**2+S17*S18*S4/S2-S19**2*S5/S1+S17*(S17-S18)*EXP(-S7*  

2TAU(J))-S17*(S17-S18)*(1+S5*(TAU(J)-TAU(J)))*S4/S1-S17*S18)  

IF(SIZE(J,NUMBER).LT.0.) SIZE(J,NUMBER)=SIZE(J,NUMBER)*(-1.0)
0096          WRITE(6,800)J,SIZE(J,NUMBER)
0097          GO TO 12
0098          202 SIZE(J,NUMBER)=RATE(NPREC(J),J,NUMBER)/(MASS(J)*S17**2)*(S10**2*(  

1TAU(J)-TAU(J))*2/2-S10*(TAU(J)-TAU(J))*S1+S1-S9)
0100          IF(SIZE(J,NUMBER).LT.0.) SIZE(J,NUMBER)=SIZE(J,NUMBER)*(-1.0)
0101          WRITE(6,800)J,SIZE(J,NUMBER)
0102          GO TO 12
0103          11 SIZE(J,NUMBER)=RATE(NPREC(J),J,NUMBER)*((S1-1.0)*(1.0-EXP(COLF(J)  

1*T-S11)))/(COLF(J)-S11/S10*S11*S7/S10*S5-S17/S10**2)-(S5-S11/(S  

210*S16)*EXP(-COLF(J)*TAU(J))*S1*S13/(COLF(J)*S1)-S17/(COLF(J)*S1  

3)*DENS(NUMBER))/(MASS(J)*COLF(J))
0104          IF(SIZE(J,NUMBER).LT.0.) SIZE(J,NUMBER)=SIZE(J,NUMBER)*(-1.0)
0105          WRITE(6,800)J,SIZE(J,NUMBER)
0106          12 CONTINUE
C BRANCH IF NO TERTIARIES
0107          IF(INTER.EQ.NSEC) GO TO 314
0108          DO 13 K=NSECP,INTER
0109          T1=EXP(-DENS(NUMBER)*RATE(NPREC(NPREC(K)),NUMBER)*TAU(K))
0110          T2=DENS(NUMBER)*RATE(NPREC(NPREC(K)),NUMBER)
0111          T3=-1.0*(1.0-EXP(-T2*TAU(K)))/(1.0/T1)
0112          T4=TAU(K)-TAU(K)
0113          T5=EXP(-DENS(NUMBER)*RATE(NPREC(K),NUMBER)*TAU(K))
0114          T6=EXP(-DENS(NUMBER)*RATE(NPREC(K),NUMBER)*T4-1.0)
0115          T7=DENS(NUMBER)*RATE(NPREC(K),NUMBER)
0116          T8=T7-COLF(K)
0117          T9=EXP(COLF(K)*TAU(K))
0118          T10=T2-COLF(K)
0119          T11=EXP(-COLF(K)*TAU(K))-EXP(-COLF(K)*TAU(K))
0120          T12=RATE(NPREC(NPREC(K)),NPREC(K),NUMBER)
0121          T13=RATE(NPREC(K),K,NUMBER)
0122          T14=RATE(NPREC(NPREC(K)),NUMBER)
0123          T15=RATE(NPREC(K),NUMBER)
0124          IF(COLF(K).EQ.0.0) GO TO 203
0125          897 WRITE(6,988) COLF(K),T2,T7,T6,T10,RATE(NPREC(NPREC(K)),NUMBER),  

CRATE(NPREC(K),NUMBER),RATE(NPREC(NPREC(K)),NPREC(K),NUMBER),  

0126          SIZE(K,NUMBER)=T12*T13/(T14-T15)*(((T14-T15)*T15*T1-T14*T5)*(T4  

1EXP(-COLF(K)*T4)-1.0/COLF(K))/T11+T14*T17*DENS(NUMBER)*T5*T6/(T7  

2**2)+T4*T5/T7-T5*T6/(T7*T8)-T1*T3/(T2**2)-T1*T4/T2+T5*T9*T11/(COL  

3(K)*T8)+T1*T3/(T2*T10)-T1*T9*T11/(COLF(K)*T10))/((MASS(K)*COLF(K)  

IF(SIZE(K,NUMBER).LT.0.0)SIZE(K,NUMBER)=SIZE(K,NUMBER)*(-1.0)
0127          GO TO 13
0128          203 SIZE(K,NUMBER)=T12*T13/(MASS(K)*T14*T15**3*(T14-T15))*(((T14**3-J  

1S(NUMBER)*T14**3*T15*T4)*T5-(T15**3-T2*T4*T15**3)*T1*T15**3)*EXP(-

```

```

FORTRAN IV G LEVEL 19          MAIN          DATE = 2/06/71 12:56:
2 T2*TAUP(K))-T14**3*EXP(-T7*TAUP(K))+T2**2*T15**2*(T14-T15)*T4**2/2
3)/T14
0130      IF(SIZE(K,NUMBER).LT.0)SIZE(K,NUMBER)=SIZE(K,NUMBER)*(1.0)
0131      13      CONTINUE
0132      WRITE(6,800)(K,SIZE(K,NUMBER))
C NORMALIZE CALCULATED INTENSITIES
0133      314      DO 15 I=1,NPRIM
0134      SUM1=0
0135      DO 14 IA=1,NPEAKS
0136      IF(INPREC(IA).EQ.0.0)NPREC(INPREC(IA)).EQ.0)SUM1=SUM1+
C SIZE(IA,NUMBER)
0137      14      CONTINUE
0138      DO 15 IA=1,NPEAKS
0139      IF(INPREC(IA).EQ.0.0)NPREC(INPREC(IA)).EQ.0)SIZE(IA,NUMBER)=
C SIZE(IA,NUMBER)/SUM1
0140      15      CONTINUE
0141      WRITE(6,120)
0142      WRITE(6,105)(SIZE(I,NUMBER),I=1,NPEAKS)
0143      WRITE(6,105)(SIZE(I,NUMBER),I=1,NPEAKS)
0144      DO 16 J=NPRIMP,NTEPT
0145      16      WRITE(6,106)NPREC(J),NPREC(J),NUMBER,DATE(INPREC(J),J,NUMBER)
C COMPARE CALCULATED INTENSITIES TO OBSERVED INTENSITIES AND COMPUTE
C RATE CONSTANTS
0146      IF(NSEC.EQ.NTEPT) GO TO 18
0147      DO 17 J=NSECP,NTEPT
0148      FACT(J)=SIZE(J,NUMBER)*SIZE(INPREC(J),NUMBER)/SIZE(J,NUMBER)*
C SIZE(INPREC(J),NUMBER)
0149      FACT(J)=SQRT(ABS(FACT(J)))
0150      IF(FACT(J).GT.2.0)FACT(J)=2.0
0151      IF(FACT(J).LT.0.5)FACT(J)=0.5
0152      RATE(INPREC(J),J,NUMBER)=RATE(INPREC(J),J,NUMBER)*FACT(J)
0153      17      CONTINUE
0154      18      DO 20 J=NPRIMP,NSEC
0155      IF(SIZE(J,NUMBER).EQ.0.0) GO TO 600
0156      IF(SIZE(INPREC(J),NUMBER).EQ.0.0)SIZE(INPREC(J),NUMBER)
C =SIZE(INPREC(J),NUMBER)
0157      IF(SIZE(INPREC(J),NUMBER).EQ.0.0) GO TO 20
0158      FACTP=1.
0159      DO 19 K=NSECP,NTEPT
0160      IF(INPREC(K).EQ.0.0)FACTP=SIZE(K,NUMBER)/SIZE(K,NUMBER)
0161      19      CONTINUE
0162      FACT(J)=(SIZE(J,NUMBER)/SIZE(J,NUMBER))**2*FACTP*
C SIZE(INPREC(J),NUMBER)/SIZE(INPREC(J),NUMBER)
0163      FACT=ABS(FACT(J))
0164      IF(FACT.GT.4.0)FACT(J)=4.0
0165      IF(FACT.LT.0.25)FACT(J)=0.25
0166      RATE(INPREC(J),J,NUMBER)=RATE(INPREC(J),J,NUMBER)/SQRT(ABS(FACT(J)))
0167      GO TO 20
0168      600      RATE(INPREC(J),J,NUMBER)=0.
0169      20      CONTINUE
C IF ITERATIONS EXCEED 30, PROCEED TO NEXT RUN
0170      IF(ITER.EQ.30) GO TO 22
0171      ITER=ITER+1
C IF CONVERGENCE HAS OCCURRED PROCEED TO NEXT RUN
0172      DO 21 I=1,NPEAKS
0173      CT=ABS(SIZE(I,NUMBER)-SIZE(I,NUMBER))

```

```

FORTRAN IV G LEVEL 19          MAIN          DATE = 2/06/71 12:56:
0174          IF(SI280(1,NUMBER).EQ.0.) GO TO 21
0175          IF(CT>GT.I.CE=4) GO TO 50
0176          21 CONTINUE
0177          GO TO 23
0178          22 WRITE(6,107)
0179          NCON(NUMBER)=2
0180          GO TO 24
0181          23 WRITE(6,108)
0182          24 WRITE(6,110)
0183          25 CONTINUE
0184          26 DO 27 NUMBER=1,NSPEC
0185          27   DENS(NUMBER)=DENS(NUMBER)/((3.23E10)
0186          GO 29 J=NP*(MP,INTERT
0187          WRITE(6,109)MADS(INPREC(J)),MASS(J)
0188          WRITE(6,111)
0189          DO 28 NUMBER=1,NSPEC
0190          IF(INCON(NUMBER).EQ.1) WRITE(6,113)MASS(INPREC(J)),MASS(J),NUMBER,
CRATE(INPREC(J)),J,NUMBER,DENS(NUMBER)
0191          IF(INCON(NUMBER).EQ.2) WRITE(6,115)MADS(INPREC(J)),MASS(J),NUMBER,
CRATE(INPREC(J)),J,NUMBER,DENS(NUMBER)
0192          28 CONTINUE
0193          WRITE(6,120)
0194          29 CONTINUE
0195          WRITE(6,110)
0196          GO TO 31
0197          30 CONTINUE
0198          722 FORMAT(13F6.2)
0199          800 FORMAT(12,E9.2)
0200          801 FORMAT(4E9.2)
0201          988 FORMAT(5E8.1)
0202          999 FORMAT(12,E9.2)
0203          986 FORMAT(12,E9.2)
0204          101 FORMAT(F4.2,2F5.2)
0205          102 FORMAT(F5.1,2F5.2,13,F5.2)
0206          103 FORMAT(12,E9.2,13,11F6.2/(13F6.2/1)
0207          104 FORMAT(12,2E13/(13E13/1)
0208          105 FORMAT(' ',15F6.4)
0209          106 FORMAT(' K(','13',' ',13,' ',12,' ','1E14,')
0210          107 FORMAT(' THIS RUN DID NOT CONVERGE')
0211          108 FORMAT(' THIS RUN HAS CONVERGED')
0212          109 FORMAT(' RATE CONSTANTS FOR A/E=' ,13,' ' GOING TO M/E=' ,13)
0213          110 FORMAT(1H1)
0214          111 FORMAT(1H1)
0215          112 FORMAT(' RATES FOR RUNS WITH G/GV0=' ,F5.1,' ',V=,' ,F5.2,' ',V*R=,' ,
C F5.2,' ,TAUP=' ,1PE11.3,' , TAUP-PRIME=' ,511.5/1)
0216          113 FORMAT(' K(' ,13,' ',13,' ',12,' ' ,1PE11.5,10X,' P=' ,E6.3,
C ' TOXR',20X,'CONVERGED')
0217          115 FORMAT(' K(' ,13,' ',13,' ',12,' ' ,1PE11.4,10X,' P=' ,E6.3,
C ' TOXR',20X,'NOT CONVERGED')
0218          120 FORMAT(1H1)
0219          STOP
0220          END

```